1992

Crustal Structure Of The Kapuskasing Uplift From Lithoprobe Near-vertical/wide-angle Seismic Reflection Data

Jianjun Wu

Crustal Structure of the Kapuskasing Uplift from LITHOPROBE Near-Vertical/Wide-Angle Seismic Reflection Data

by

Jianjun Wu

Department of Geophysics

Submitted in partial fulfillment

of the requirement for the degree of

Doctor of Philosophy

Faculty of Graduate Studies

The University of Western Ontario

London, Canada

June, 1992

ISBN 0-315-75351-X

Canada

ABSTRACT

The Kapuskasing uplift (KU), located in the central Canadian shield, is believed to be an exposed cross-section of the Archean middle to lower crust, which was uplifted to the surface along the northwest-dipping Ivanhoe Lake fault zone (ILFZ), a boundary separating the high-grade gneisses of the KU from the low-grade Abitibi greenstone to the east. As one of the first targets of the LITHOPROBE project, the KU has been subjected to extensive geological and geophysical studies for the last decade. A regional seismic refraction survey indicates that the rocks in the upper crust of the KU possess a higher P-wave velocity (6.5-6.6 km/s) than their counterparts in the adjacent regions (6.2-6.3 km/s). Deep seismic reflection profiling suggests that the KU is a thin thrust sheet which may flatten at a depth of 12 km. Both refraction and reflection data provide further support to the uplifted nature of the KU. However, its subsurface geometry, particularly the shallow structure of the ILFZ, is still poorly defined by the seismic reflection data partially due to originally insufficient processing. As a result, the tectonic process creating the KU remains to be clarified.

To better delineate the crustal structure across the KU, we have reprocessed some of the seismic reflection data. By carefully applying standard seismic processing techniques such as first arrival muting, F-K filtering, refraction and residual static corrections, we have enhanced seismic images significantly. Our tests indicate that the full data set should be used without stacking two adjacent shot gathers into one in order to preserve dipping reflections and to keep high fold coverage.

Our processing provides a wealth of new information on the nature of the KU. For the first time, the shallow structure of the ILFZ is clearly imaged on a seismic section as a series of prominent northwest-dipping reflections

with listric geometry. It appears that the ILFZ is a steep fault (~50°) at the surface but quickly flattens out to ~20° at shallow depths. 2-D tomographic inversion of multiple coverage first arrivals, picked from the seismic reflection data, was also performed to reconstruct P-wave velocity structure of the ILFZ near the surface. The most striking aspect of the inversion is that it reveals a northwest-dipping high-velocity zone, in excellent agreement with the seismic reflection images. It shows that the west-dipping reflectors mark the boundary juxtaposing high-velocity against low-velocity rocks, providing additional and firm support for the interpretation of the seismic reflection images. Direct correlation with geological observations indicates that the high reflectivity associated with the fault zone most likely originates from mylonites.

The least expected yet most important finding of the reprocessing is a pronounced northwest-dipping midcrustal reflector, originating from the Abitibi belt and plunging under the KU. The existence of such a reflector is independently confirmed by wide-angle reflection data from a cross-profile. This reflector is also detected by two other reflection profiles crossing the ILFZ about 80 km to the southwest. Its concave-down shape and broad lateral extent, in conjunction with the present geological and other geophysical data, suggest that it represents underthrusting of the Abitibi greenstone rocks beneath the KU. With the overthrust (KU) and underthrust (Abitibi) defined, it becomes evident that the KU is a product of intra-plate collision. The large-scale underthrusting of the Abitibi rocks may not only be primarily responsible for the emplacement of the KU, but also act as a means to balance the overloaded Kapuskasing dense rocks in the upper crust. Neither the seismic refraction nor reflection data show conclusive evidence for a thick crustal root under the KU.

To the memory of my grandparents, Shifu He and Mourong Xie. They never had a chance to get an education, but had always encouraged me to get one and provided financial support for my education when my family had difficulty to do so.

Also to my parents, Benyou Wu and Hongming He. They have ingrained in me that an education is most important, and have done everything they can to support my education.

ACKNOWLEDGEMENTS

I would like to express my sincere thanks and deepest appreciation to Dr. Robert F. Mereu, my thesis supervisor for his close guidance and encouragement.

Discussions with, and/or comments by Dr. John Percival of the Geological Survey of Canada, Dr. Gordon West of the University of Toronto, Dr. Zoli Hajnal of the University of Saskatchewan, Dr. Larry Brown of Cornell University, Drs. Lalu Mansinha, Currie Palmer, Helmuth Schloessin of the University of Western Ontario are gratefully acknowledged.

I also thank Dave Hamilton for his assistance with the tomographic velocity analysis across the Ivanhoe Lake fault zone; Mike Cyze for his help with color plotting; Dr. Po Yu Shen and Anthony P. Yapp for their help with English writing; John Brunet, Bernie Dunn, Berry Price, and Kris Vasudevan for their technical assistance with the SUN/ITA seismic processing system.

Special thanks to my wife, Xiaoju (Julia) Wang, and my son, Mengbing (Alex) Wu, for their patience and understanding.

None of this work would be possible if not for my parents, who have always encouraged and supported my education.

This work was funded by the research grants from NSERC (A-1793), LITHOPROBE, and EMR Canada, a visa bursary from the University of Western Ontario, and three Canadian Society of Exploration Geophysicists Scholarships. I came to Canada under an overseas graduate scholarship from the People's Republic of China, my motherland.

TABLE OF CONTENTS

LIST OF TABLES

LIST OF FIGURES

CHAPTER 1 INTRODUCTION

1.1 Why study the Kapuskasing Uplift

The northwest trending Kapuskasing Uplift (KU) cuts obliquely across the east-west trend of the Wawa-Abitibi and Quetico-Opatica greenstone belts in the central Archean Superior Province of the Canadian shield (Fig. 1.1). It is distinguished from the adjacent belts by high-grade metamorphic rocks producing broad positive gravity and aeromagnetic anomalies. Regions of high-grade metamorphic rocks are commonly assumed to be representative of the deep crust because of their metamorphic grade. The Ivrea zone of the southern Alps, the Pikwitonei belt of northern Manitoba, the Musgrave block of central Australia, the Limpopo belt in southern Africa, the Dharwar craton in the southern India are some well-documented examples (Fountain and Salisbury, 1981 and 1990; Coward and Fairhead, 1980; Raase et al., 1986). Largely by analogy, Percival and Card (1983) interpreted the KU as an oblique exposure of the Archean middle to lower crust (Fig. 1.2), which was uplifted to the surface along the northwest-dipping Ivanhoe Lake fault zone (ILFZ). Thus, the KU may provide a rare window for study of the Archean middle to lower crust.

The Archean is the period from 4.5 Ga ago, when the Earth was formed, to approximately 2.5 Ga ago, and records almost 45% of the total history of the Earth. It is during the Archean time that life began (Nisbet, 1987). More than 50% of the present volume of the continental crust was formed by the end of the Archean (Moorbath and Taylor, 1981; Dewey and Windley, 1981; Armstrong, 1981). Yet there is no accepted theory to explain how the Archean Earth worked and no understanding of how it came to be inhabited by life. The question as to how the lower continental crust was constructed has been intensely debated for many years, mainly due to the lack of knowledge of the

deep crust. In order to gain a full understanding of processes of crustal genesis, it is crucial to identify and study any relics of deep crust which are exposed at the surface. Obviously the study of the KU is of great scientific interest. Fundamental questions concerning the structure, composition and evolution of the Archean deep crust can be addressed by studying the KU. For example, the tectonic processes associated with the KU may be useful in clarifying the argument as to whether the tectonic processes which operated on the Archean crust resemble those that are active today.

Although many features typical of the deep crust, such as dense, high-grade metamorphic rocks and ductile shear zones, have been recognized within the Kapuskasing zone, none of these is conclusive. A rigorous test for the hypothesis of a tilted crust section is the ability to trace the rock units of the KU to their normal position in the deep crust with seismic reflection profiling. By determining the geometry of the Uplift at depth and by examining the background crustal architecture around it, seismic reflection profiling would provide critical information on the nature and evolution of the Uplift.

1.2 Why Seismic Reflection Profiling

Our ability to observe crustal structures is largely limited to the surface of the Earth, essentially a two-dimensional observation platform. Without a complete three-dimensional picture, it is impossible to fully understand the origin and evolution of the structures. In order to visualize the third-dimension of the structures, we must rely on geophysical techniques, such as gravity, magnetics, seismic reflection, seismic refraction, and earthquake seismology, which are capable of mapping the subsurface formations of the structures. Among these techniques, seismic reflection profiling is probably

the most precise in terms of resolution and imaging capability and is, by far, the most widely used. Whereas seismic reflection profiling produces a vertical seismic section similar to a geologic cross-section showing detailed structures at many levels at once, the measurement from gravitational and magnetic prospecting is a composite of contributions from all depths and such contributions can be individually resolved only in special cases.

Seismic reflection profiling has long been employed by the petroleum industry to explore for hydrocarbon-trapping structures in sedimentary basins. Its adoption for deep crustal studies began in the 1950s (Junger, 1951; Dohr, 1957; Robertson, 1963; Dohr and Fuchs, 1967; Kanasewich et al., 1969). Since the mid-1970s it has been used worldwide for detailed studies of selected geologic structures (see for example, Barazangi and Brown, 1986a and b; Mereu et al., 1990a; Meissner et al., 1991), partly due to the early success of the Consortium for Continental Reflection Profiling (COCORP) (Oliver et al., 1976).

LITHOPROBE, the largest earth science research program ever undertaken in Canada, is Canada's national collaborative, multidisciplinary earth science research program (Clowes, 1984). The program is created to address fundamental questions on the nature and evolution of the lithosphere (the solid Earth's outermost shell) beneath the country and its surrounding oceans. It integrates modern geophysical, geological and geochemical concepts and technology to extend knowledge of the lithosphere, in various key areas across Canada, into the third-dimension - depth. Among its targets are the Kapuskasing Uplift, the Southern Cordillera, the Abitibi-Grenville, the Trans-Hudson Orogen, and the Alberta Basement.

1.3 Thesis Objectives

Because of its tectonic significance in understanding the evolution of the Archean crust, the KU was selected by LITHOPROBE as one of the first targets. A long range seismic refraction survey was conducted over the KU and its surrounding regions in 1984 to obtain information on its velocity structure. 2-D ray-tracing modeling studies by Wu (1987), Boland and Ellis (1989, 1991), and Wu and Mereu (1990) show that the rocks near the surface of the KU possess a higher P-wave velocity (6.5-6.6 km/s) than their counterparts in the Wawa and Abitibi belts (6.2-6.3 km/s). Several deep seismic reflection profiles were surveyed across the KU during 1987-88 to map the subsurface structure. The deep seismic reflection data were originally processed by an industry contractor. The initial results indicate that the KU is a thin thrust sheet which may flatten at a depth of 12 km (Percival et al., 1989; Geis, et al., 1990).

Undoubtedly, both refraction and reflection data add firm support to the tectonic model of Percival and Card (1983). It appears certain that the KU represents a piece of the Archean middle crust. Yet the structure beneath the Uplift was poorly constrained by the reflection data, partly due to inadequate processing (Hajnal et al., 1991; Wu et al., 1992). Particularly, the shallow structure of the ILFZ, believed to be the basal thrust carrying the high-grade gneisses of the KU over the low-grade greenstone of the Abitibi, was poorly imaged. In addition, the underthrust involved in the tectonic process, which produced the KU, was never mapped. Therefore, the tectonic mechanism associated with the KU was not fully resolved (Percival et al., 1989).

The primary objectives of this thesis are: (1) to find out what can be done to improve the quality of the seismic sections by processing two

reflection profiles, worst and best in terms of quality of commercially processed seismic sections. The processing was implemented by utilizing the state-of-the-art seismic processing facility: the Inverse Theory and Application Ltd. (ITA) seismic interactive processing package based on a SUN workstation, provided by Lithoprobe; (2) to define the shallow structure of the ILFZ through the processing; (3) to determine in situ seismic velocity of crystalline bedrock within the ILFZ by performing a 2-D seismic tomography inversion of multiple coverage first arrivals, picked from the seismic reflection data; (4) to define the underthrust associated with the Kapuskasing overthrust by processing the seismic reflection data and reanalyzing wide-angle reflection data from the 1984 seismic refraction survey; (5) to construct a more complete structural cross-section beneath the Uplift by combining the seismic refraction and reflection results; and following from this (6) to elucidate the nature and evolution of the uplift.

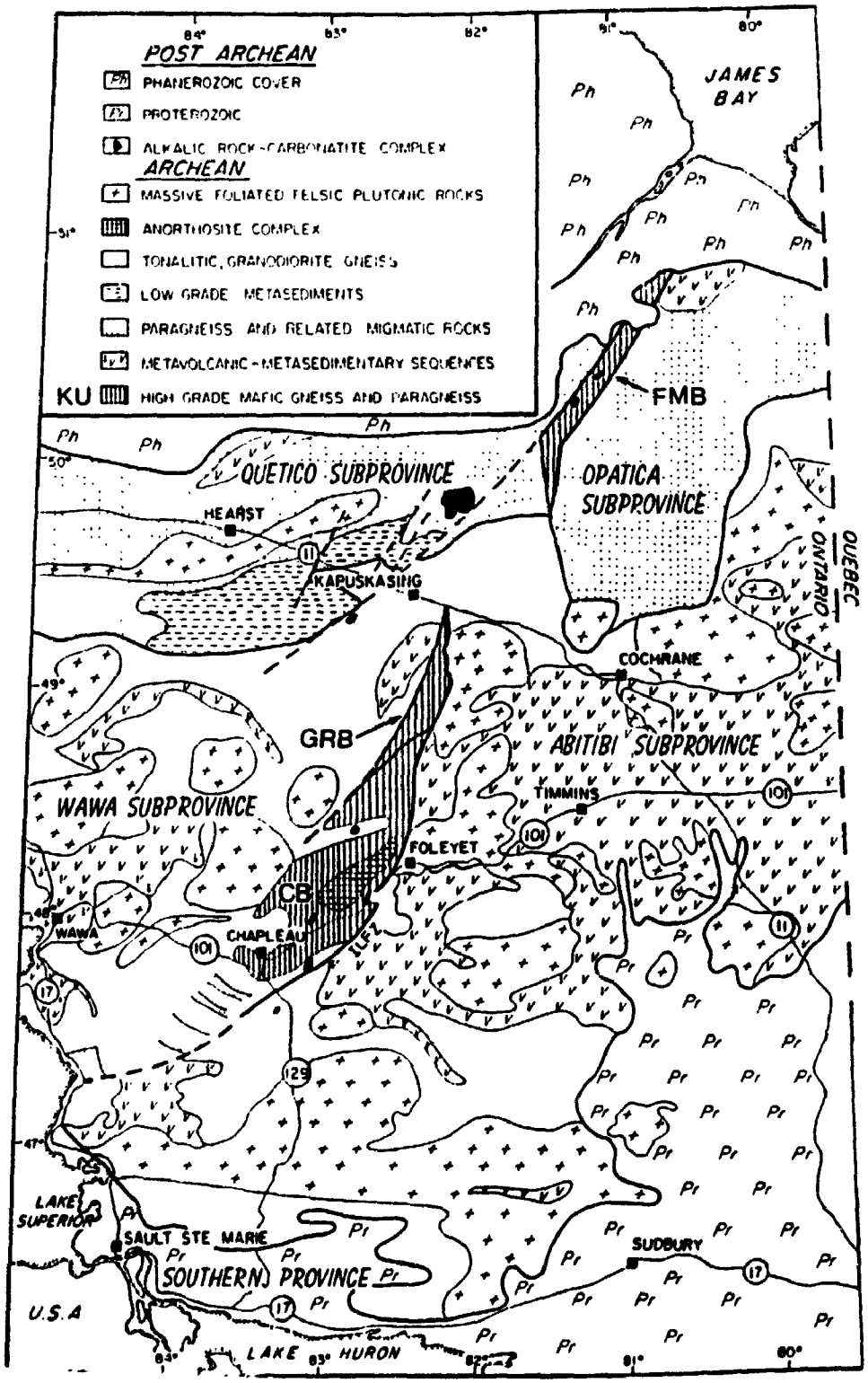

Fig. 1.1 General geology of northeastern Ontario (modified from Northey and West, 1985). FMB=the Fraserdale-Moosonee block, GRB=the Groundhog River block, CB=the Chapleau block.

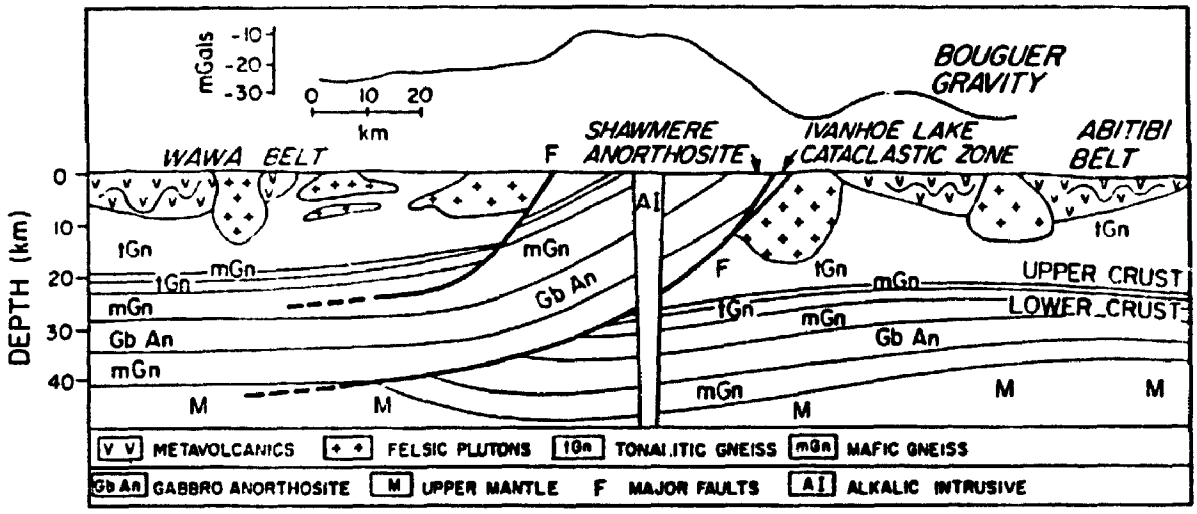

Fig. 1.2 Schematic W-E geological cross-section of the Kapuskasing Uplift near Foleyet, proposed by Percival and Card (1983) and adopted from Northey and West (1985).

CHAPTER 2 GENERAL REVIEW

2.1 Geological and Geophysical Setting

The Superior Province, one of the world's largest preserved Archean cratons, is well known for its greenstone belts, which contain a large proportion of Canada's mineral resources. Easterly trending structures are typical of the province. In contrast, the Kapuskasing Uplift (KU) is a north-northeast trending belt, extending over a distance of approximately 500 km from the Proterozoic margin near Lake Superior and disappearing beneath the Phanerozoic sedimentary rocks of the James Bay Lowland (Fig. 1.1).

The KU was first recognized as a remarkable positive anomaly on a gravity traverse along the Trans-Canada Highway (Garland, 1950) and was outlined by later regional gravity and aeromagnetic surveys (Innes, 1951; Innes, 1960; MacLaren, 1968). The Bouguer gravity map shows a broad, north-northeast trending high along the axis of the KU, only 50 km wide in the south and widening to approximately 240 km to the north (Fig. 2.1). The most striking feature on the aeromagnetic map (Fig. 2.2) is the northeast-trending anomaly that runs from James Bay to Fraserdale, where it disappears abruptly and then resumes south of Kapuskasing. Percival (1985) divides the KU into three tectonic blocks according to their distinct geological and geophysical characters. They are, from north to south, the Fraserdale-Moosonee, Groundhog River and Chapleau blocks (Fig. 1.1). These three blocks are characterized by high-grade granulitic rocks and fault-bounded on both the east and west sides (Bennett et al., 1967; Thurston et al., 1977). The Fraserdale-Moosonee and Chapleau Blocks have coaxial positive gravity and aeromagnetic anomalies. Along the Groundhog River block, the aeromagnetic anomaly coincides with the strike of the Kapuskasing zone, but the gravity anomaly does not. Rather, the

gravity high runs along the Val Rita block of the Wawa subprovince, diverging up to 30 km to the west of the Grounghog River block (Innes, 1960). Between the Fraserdale-Moosonee and Groundhog River blocks is a 60-km-wide gap of lower-grade rocks, typical of the Wawa subprovince. Percival and McGrath (1986) consider that later normal faulting is responsible for dissecting the once-continuous Kapuskasing Uplift into discrete blocks with different subsurface configurations.

A systematic eastward increase in metamorphic grade and paleopressure is observed over a 120-km-wide zone, from the low-grade Michipicoten greenstone belt near Wawa (2-3 Kbar), through the intermediate-grade Wawa domal gneiss terrain (5-6 Kbar), and to the high-grade granulitic rocks (7-9 Kbar) of the Chapleau block of the KU (Percival and Card, 1983). To the east, the granulite gneiss of the KU is separated from the greenschist- to amphibolite-facies metavolcanic rocks of the Abitibi greenstone belt by the Ivanhoe Lake cataclastic zone, a 1-2 km wide zone of cataclasis and faulting (Bennett, 1969; Thurston et al., 1977, Percival and Card, 1983; Bursnall, 1989), now known as Ivanhoe Lake fault zone (ILFZ) (Percival et al., 1989; Geis et al., 1990). Because of irregularly and poorly distributed outcrop, this fault zone is defined mainly on a large scale based on pieces of evidence of faulting such as: (1) aeromagnetic lineaments; (2) presence of shearing, brecciation or mylonites; (3) abrupt discontinuities in metamorphic grade; and so on (Bennett, 1969; Thurston et al., 1977). North of the Chapleau block, the fault zone coincides with the steep gravity gradients between the Kapuskasing high and Abitibi low (Fig. 2.1), typical of some well-documented large-scale thrust faults (Smithson et al., 1978; Fountain and Salisbury, 1981).

On the basis of these observations, Percival and Card (1983) propose that the KU represents the exposure of an oblique cross-section through the

upper two-thirds of the Archean Superior Province crust, which was uplifted to the surface along the low-angle east-verging thrust fault, the ILFZ.

2.2 Tectonic Models

As more and more geological and geophysical information on the KU has been gained, its tectonic interpretations have evolved from a band of thinned granitic crustal layer (Garland, 1950), through a fracture zone extending to great depth (Innes, 1960), an upwarp in the Conrad discontinuity (Wilson and Brisbin, 1965), a complex horst (Bennett et al., 1967; Thurston et al., 1977), a graben associated with a mid-Proterozoic rifting (Innes et al., 1967), a Proterozoic suture (Wilson, 1968; Gibb, 1978), a failed arm of the Keweenawan rift structure (Burke and Dewey, 1973), a broad sinistral transcurrent fault zone (Watson, 1980; Goodings and Brookfield, 1992), to an exposed oblique cross-section of Archean middle to lower crust (Percival and Card, 1983). It is of interest to note that all of these models have one thing in common, this being that the high-density deep crustal rocks must have been uplifted to explain the broad positive gravity anomaly. At present, it is the model of Percival and Card (1983) that is generally accepted for the reasons given above.

2.3 LITHOPROBE Investigations

Since 1984, the KU has been the subject of a wide variety of geophysical and geological investigations sponsored by LITHOPROBE. These include a pilot seismic reflection survey (Cook, 1985), a regional seismic refraction survey (Wu, 1987; Boland and Ellis, 1989; Wu and Mereu, 1990), 380 km of deep seismic reflection profiling (Percival et al., 1989; Geis et al., 1990; Green et al., 1990; Hajnal et al., 1991; Milkereit et al., 1991; Percival et al., 1991; Wu and Mereu, 1991; Wu et al., 1992; Wu and Mereu, 1992), geological

and structural mapping (Leclair and Nagerl, 1988; Bursnall, 1989), paleomagnetic studies (Halls and Palmer, 1990; Lewchuk and Symons, 1990); petrological studies (Percival and McGrath, 1986), electromagnetic soundings of conductivity structure (Woods and Allard, 1986; Bailey et al., 1989; Kurtz et al., 1989; Mareschal, 1990), and aeromagnetic studies (West and Ernst, 1991). The main results may be summarized as follows:

1. The seismic refraction data show that, near the surface, the high-grade granulites of the KU possess a higher P-wave velocity (6.5-6.6 km/s) than their counterparts in the Wawa and Abitibi belt (6.2-6.3 km/s). The Moho, the boundary separating the crust from the upper mantle, under the KU is a wide transition zone rather than a sharp boundary. There is limited evidence that the crust under the KU is thicker than the surrounding areas.

2. The KU appears to be a thin thrust sheet bounded by the ILFZ, which is traceable to ~15 km depth at an average dip of 15° NNW on the commercially processed high-resolution seismic section of line 2. To account for the 20 km of inferred uplift along the ILFZ, crustal shortening of the order of 55-70 is required.

3. The Archean structural history includes production and folding of gneissic layering, followed by extensional collapse. The ILFZ has a complex history involving early mylonite, cut by cataclasite, pseudotachylite and brittle faults, representing components of thrust, normal and transcurrent movement.

4. Major uplifting of the KU must have taken place before 2.45 Ga, when the huge Matachewan mafic dyke is believed to have been emplaced.

5. Unlike in situ lower crust, the Kapuskasing granulites have normal upper crustal conductivity. The ILFZ has no electrical signature. Zones of weak conductivity were mapped at depths of 2 and 5 km by a UTEM electromagnetic survey, showing no correlation with the seismic reflection images.

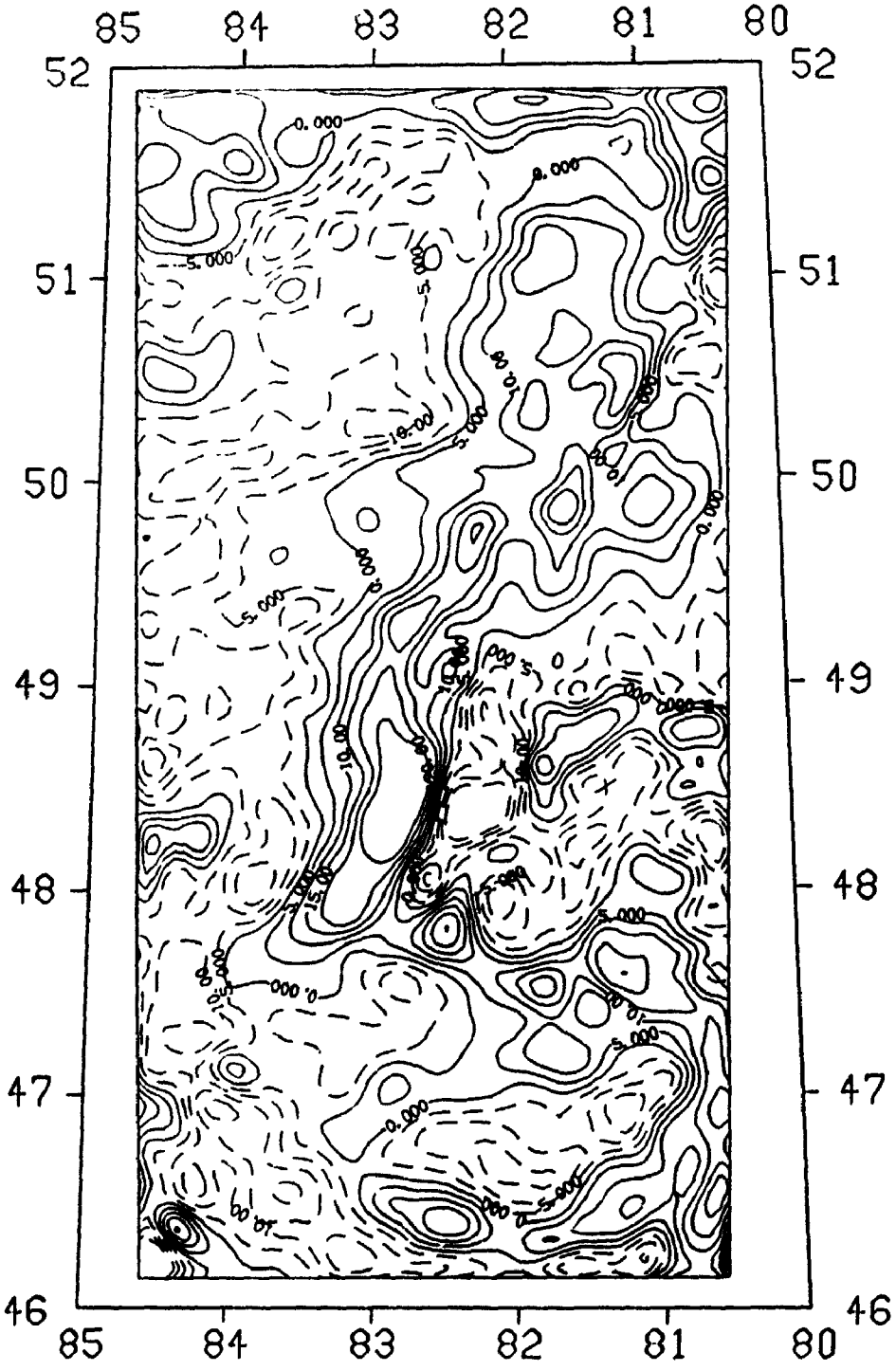

Fig. 2.1 The residual component of the Bouguer gravity around the Kapuskasing Uplift (after Wu and Mereu, 1990).

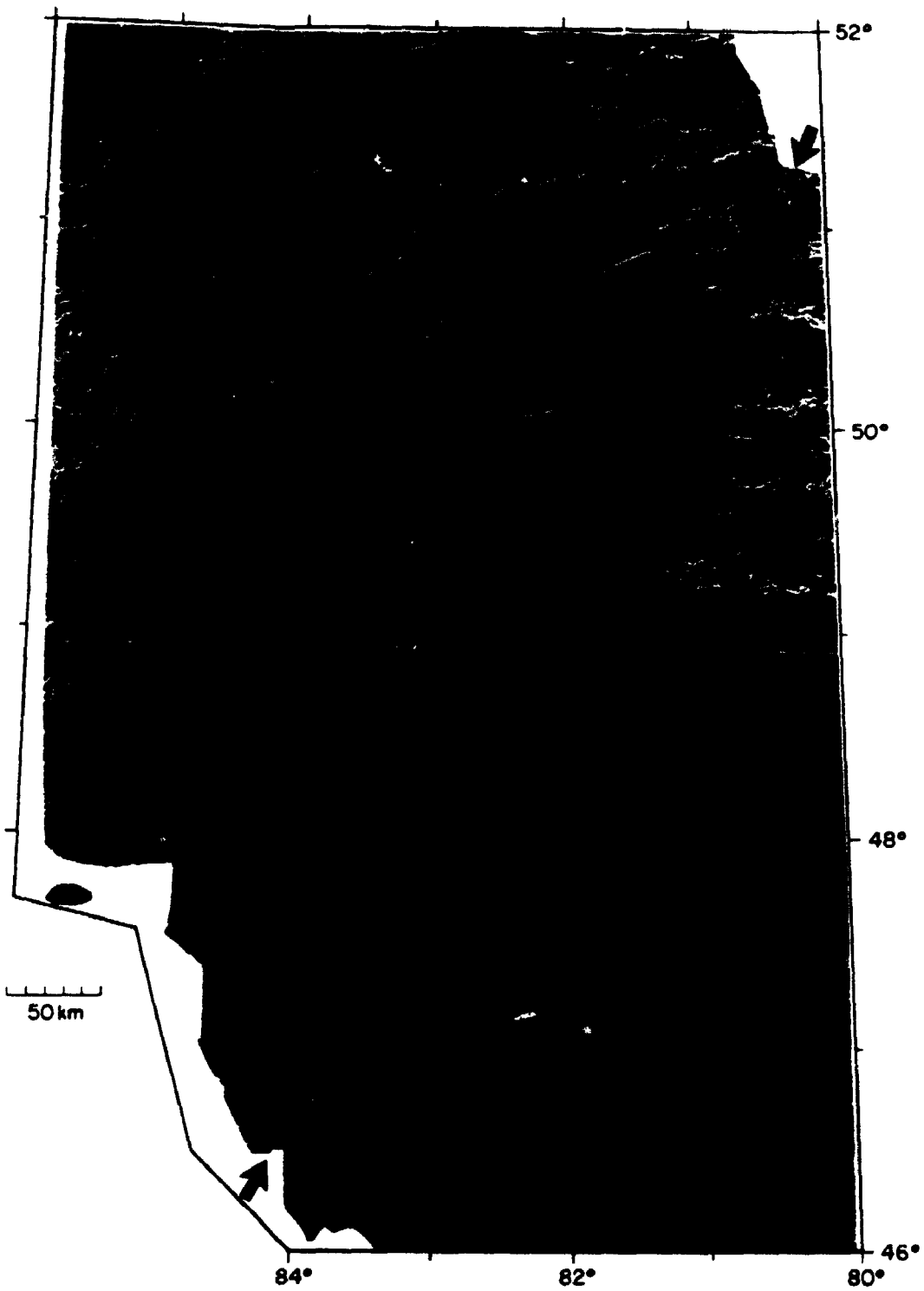

Fig. 2.2 Aeromagnetic map of the Kapuskasing Uplift (after West and Ernst, 1991). Red is high and blue is low.

CHAPTER 3 NEAR-VERTICAL INCIDENT SEISMIC REFLECTION DATA

3.1 Data Acquisition

During the winter of 1987-88, a deep seismic reflection survey was conducted over the Kapuskasing uplift as part of the LITHOPROBE project. Approximately 380 km of vibroseis data were collected along 9 profiles with 6 covering the Chapleau block and 3 crossing the Val Rita block (Figs. 3.1, 3.2). All profiles were recorded with regional-resolution parameters (Table 3.1) designed to penetrate the whole crust. An attempt to fill the gaps between lines 2, 3, and 4, caused by no road access, was made by collecting data with the vibrators and geophones located on opposite sides of the gap (undershooting). In addition, line 2 was resurveyed with high-resolution parameters (Table 3.2), with the aim of focusing on the upper crustal features.

3.2 Commercial Data Processing

The reflection data were initially processed by an industry contractor, Veritas Seismic of Calgary. Due to limited funding, the data had to be reduced by summing two adjacent shot gathers into one prior to processing in order to reduce the amount of data to be processed to half, therefore reducing cost significantly. The details of the commercial processing are given in Tables 3.3 and 3.4. Obviously, only rudimentary seismic processing techniques were applied to the data. Many sophisticated or advanced, but time-consuming and expensive techniques, such as refraction statics, F-K filtering, and surface-consistent residual statics, were not yet tried, partly due to lack of funding. Some of the commercially processed seismic sections will be discussed in chapters 7 and 8.

3.3 Lithoprobe Seismic Processing Facility

LITHOPROBE installed its own seismic data processing facility, Lithoprobe Seismic Processing Facility (LSPF), at the University of Calgary in early 1988, after years of meetings and negotiations. Initially, the LSPF consisted of a Control Data Corporation (CDC) CYBER 835 CPU with an attached MAP_V array processor and other peripherals (4 tape drives, 3 disks, 1 Versatec plotter). The software included CDC's NOS/VE operating system, and CogniSeis DISCO seismic processing system. Although the DISCO processing software is well-known in the seismic industry, the CYBER/DISCO combination was the first in the world (also the last). As one could expect, the system broke down quite often due to technical problems.

For remote site users, communications to the LSPF were accomplished through DATAPAC with a baud rate of 1200. The LSPF offered its first introductory DISCO-seismic data processing course to all remote site users at the end of May 1989, after the CYBER/DISCO system more or less reached its maturity. After taking this course, I began some seismic processing by using the system. Since the CYBER/DISCO was a batch processing system, users were not able to see processing results from computer terminals. All outputs had to be sent to the Versatec plotter. This was not too bad for local users, but very time-consuming for remote site users like myself. Remote site users had to wait for at least two days to see the outputs delivered by courier which sometimes were lost during travelling. It was sort of blind and non-productive processing. For example, even for a small bandpass filtering test, I had to wait for two days to see the results, before I went on to the next processing step. I must say that it was a very frustrating experience. This experience was apparently shared by most remote site users, as a number of

professors from universities across Canada expressed their frustration, concerning the batch processing, in the Lithoprobe seismic group meeting held in Calgary in 1990.

3.4 The SUN/ITA Interactive Processing System

The problem with batch processing from remote sites was recognized by LITHOPROBE, and a decision was made to equip six universities, selected from across Canada, with new interactive seismic data processing workstations. The University of Western Ontario was one of the universities and received its workstation in February 1990. The initial hardware consisted of a SUN Sparc 330 workstation with 240M-byte internal hard disk, an Exabyte tape drive, a CG6 color monitor (17 inch), , and 8M-byte random memory (RAM). companioned with INSIGHT/1, the interactive processing software developed by Inverse Theory and Applications Inc. (ITA). Exabyte tape, 8 mm digital audio tape, provides a 2.4G-byte capacity. Since the ITA software took most of the internal hard disk, 750M-byte external hard disk was purchased through Dr. R.F. Mereu's own research grant. Recently two 1.2G-byte external hard disks and 24M-byte RAM were also purchased by Dr. R.F. Mereu. A color printer, provided by LITHOPROBE, was attached to the SUN/ITA system in March 1992. A super processing card is expected to arrive soon, which shall make the system run 5 time faster. The SUN/ITA is run under UNIX, a multi-user multitasking operating system, allowing users to do more than one job at the same time.

INSIGHT/1, a complete pre- and post-stack seismic processing package, is a standalone, workstation designed, interactive seismic processing system. Job decks that contain the desired interactive processes to be applied to the data are accessed through the interactive processing routines. All prestack processing functions offered by INSIGHT/1 are available for use during

interactive analysis. These job decks can be updated and modified with new processing parameters or algorithm choices and applied to the data interactively for direct review and analysis of results. These same job decks can also be easily submitted for batch processing control for off hours processing. Some examples of the job decks are provided in appendix A.

As parameters are modified and the data are processed, it becomes necessary to make comparisons between processing outputs for full parameter effectiveness to be analyzed. This is accomplished by mapping subsequent pipe processing flows to alternate graphics planes on the graphic advice. A simple toggling of the graphics planes permits in-depth scrutiny of several processing flows for review of parameter effectiveness. Once the analysis is complete, the pipe processing job deck can then easily be used with all parameters intact for further interactive or batch processing. It is the high speed processing and powerful graphics capabilities of the SUN/ITA system that make interactive seismic data processing a reality.

A two-day ITA interactive seismic processing course was given at the ITA headquarters in Calgary in May 1990. Among attenders were Dr. R.F. Mereu and myself. The first Exabyte tape with the Kapuskasing line 5 seismic reflection data did not arrived until August 1990. The delay occurred because special equipment at the LSPF was required to transfer the data from nine track tape to Exabyte tape. For unknown reasons, the first version of the ITA software, which we received, did not have the program to read the SEGY format tape. In October 1990, after a new version of the ITA software arrived, we were finally able to read the Exabyte tape. Real seismic processing was started!

It is interesting to note that by February 1992 the CYBER/DISCO system was entirely phased out. In comparison with the CYBER/DISCO batch processing

system, the SUN/ITA interactive processing system is highly efficient and therefore productive. If I had had the SUN/ITA system at the beginning, I would have finished my thesis at least one year earlier. Some of my experiences with the SUN/ITA system is provided in appendices B and C.

3.5 The University of Western Ontario Printer-Plotter Program

In the early stage of the LSPF, one of the major problems facing remote site users was that their processing results on the LSPF CYBER/DISCO system could only be seen after the courier delivered their plots. This was very inconvenient and slowed down one's research. The plotting problem still faces users of the SUN/ITA interactive system, which has drives for only the electrostatic plotters. In order to overcome the problem, a special project was carried out at the University of Western Ontario by Dr. R.F. Mereu. An efficient method for sending the data set, from any mainframe computer or workstation such as the SUN to a small PC computer with a modem and a dot matrix printer, was developed. The details of the method are given by Mereu et al. (1990b). Briefly, the method works primarily with two FORTRAN programs. The first, residing on the mainframe computer, strips the data set of all non-essential bits, partially rasterizes the set and converts it into a simple ASCII character set sequence. The second program, residing on the PC computer, obtains the compressed data file from the mainframe, and completes the rasterizing process by creating the bit map for the printer. Since the method does not require the use of a hard disk on the PC, any size data can be plotted. Both programs are very easy to use. All seismic sections shown in this thesis were plotted on an Epson LQ2550 printer by utilizing the printer-plotter program. A typical plot table and instructions as to how a user may plot a seismic section using the program is given in appendix D.

TABLE 3.1 REGIONAL RESOLUTION ACQUISITION PARAMETERS

SOURCE SETTINGS	
VIBRATOR:	4 Mertz 18 Buggy style 20,072 vibrators
SWEEP FREQUENCY:	12-52 Hz (Linear)
SWEEP LENGTH:	14 s
NUMBER OF SWEEPS:	8 per vibration point
VIBRATION SPACING:	100 m
RECORDING SETTINGS	
GEOPHONE:	OYO 14 Hz, 0.7 damping
	Vertical motion sensitive
GROUP DESIGN:	12 geophones distributed evenly over 50 m
GROUP SPACING:	50 m
NUMBER OF CHANNELS:	240
COVERAGE:	60 fold
SAMPLE INTERVAL:	4 ms
SPREAD DESIGN:	Asymmetric split spread
	60 stations north or west
	13 stations gap
	180 stations south or east
RECORDING LENGTH:	18 s
CORRELATED RECORD	16 s

TABLE 3.2 HIGH RESOLUTION ACQUISITION PARAMETERS

SOURCE SETTINGS	
VIBRATOR:	2 Mertz 18 Buggy style 20,072 vibrators
SWEEP FREQUENCY:	20-130 Hz (Linear)
SWEEP LENGTH:	8 s
NUMBER OF SWEEPS:	8 per vibration point
VIBRATION SPACING:	20 m
RECORDING SETTINGS	
GEOPHONE:	OYO 14 Hz, 0.7 damping
	Vertical motion sensitive
GROUP DESIGN:	12 geophones distributed evenly over 25 m
GROUP SPACING:	20 m
NUMBER OF CHANNELS:	120
COVERAGE:	60 fold
SAMPLE INTERVAL:	2 ms
SPREAD DESIGN:	End on, 8 station gap
	Source on west end
RECORDING LENGTH:	8 s
CORRELATED RECORD	8 s

TABLE 3.3 COMMERCIAL REGIONAL RESOLUTION DATA PROCESSING

DEMULTIPLEX	
ADJACENT RECORD SUMMATION	2:1
AMPLITUDE RECOVERY	2000 ms AGC
GEOMETRY	Crooked line
ELEVATION CORRECTIONS	Datum - 400 m above sea level
	Replacement Velocity - 5000 m/s
CMP GATHER	~35 fold
VELOCITY ANALYSIS	
NORMAL MOVEOUT CORRECTION	
FIRST BREAK MUTE	
TRIM STATICS	Correlation Window: 800 - 12,000 ms
STACK	~35 fold
BANDPASS FILTER	8/12 - 52/62 Hz
TRACE EQUALIZATION	Time variant

TABLE 3.4 COMMERCIAL HIGH RESOLUTION DATA PROCESSING

DEMULTIPLEX	
AMPLITUDE RECOVERY	2000 ms A C
GEOMETRY	Crooked line
ELEVATION CORRECTIONS	Datum - 400 m above sea level
	Replacement Velocity - 5000 m/s
CMP GATHER	~60 fold
VELOCITY ANALYSIS	
NORMAL MOVEOUT CORRECTION	
FIRST BREAK MUTE	
TRIM STATICS	Correlation Window: 400 - 6000 ms
STACK	~60 fold
BANDPASS FILTER	15/20 - 100/110 Hz
TRACE EQUALIZATION	Time variant

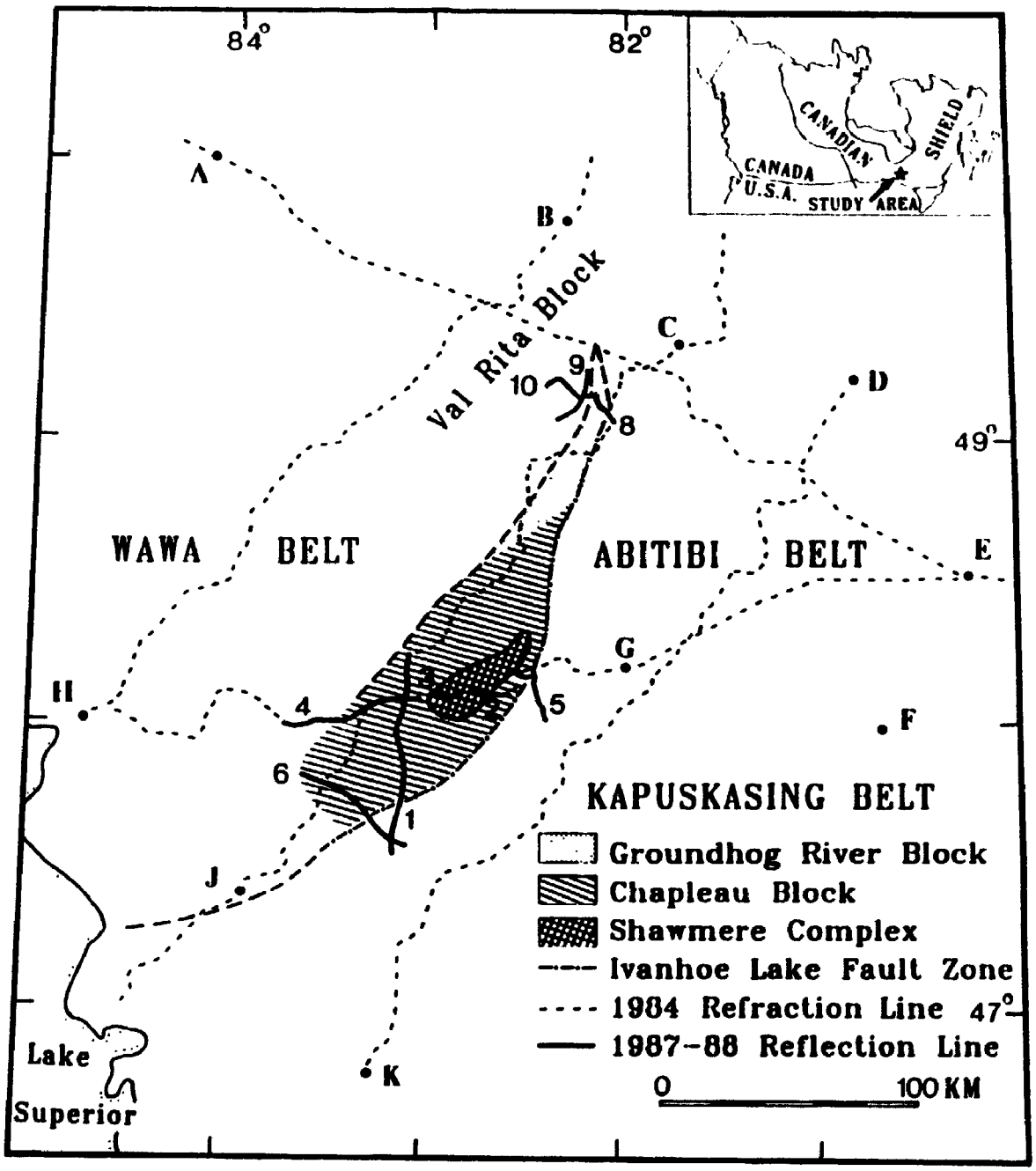

Fig. 3.1 Location of Lithoprobe seismic reflection and refraction profiles and main geological features of the Kapuskasing Uplift. Letters are shot points for the seismic refraction survey.

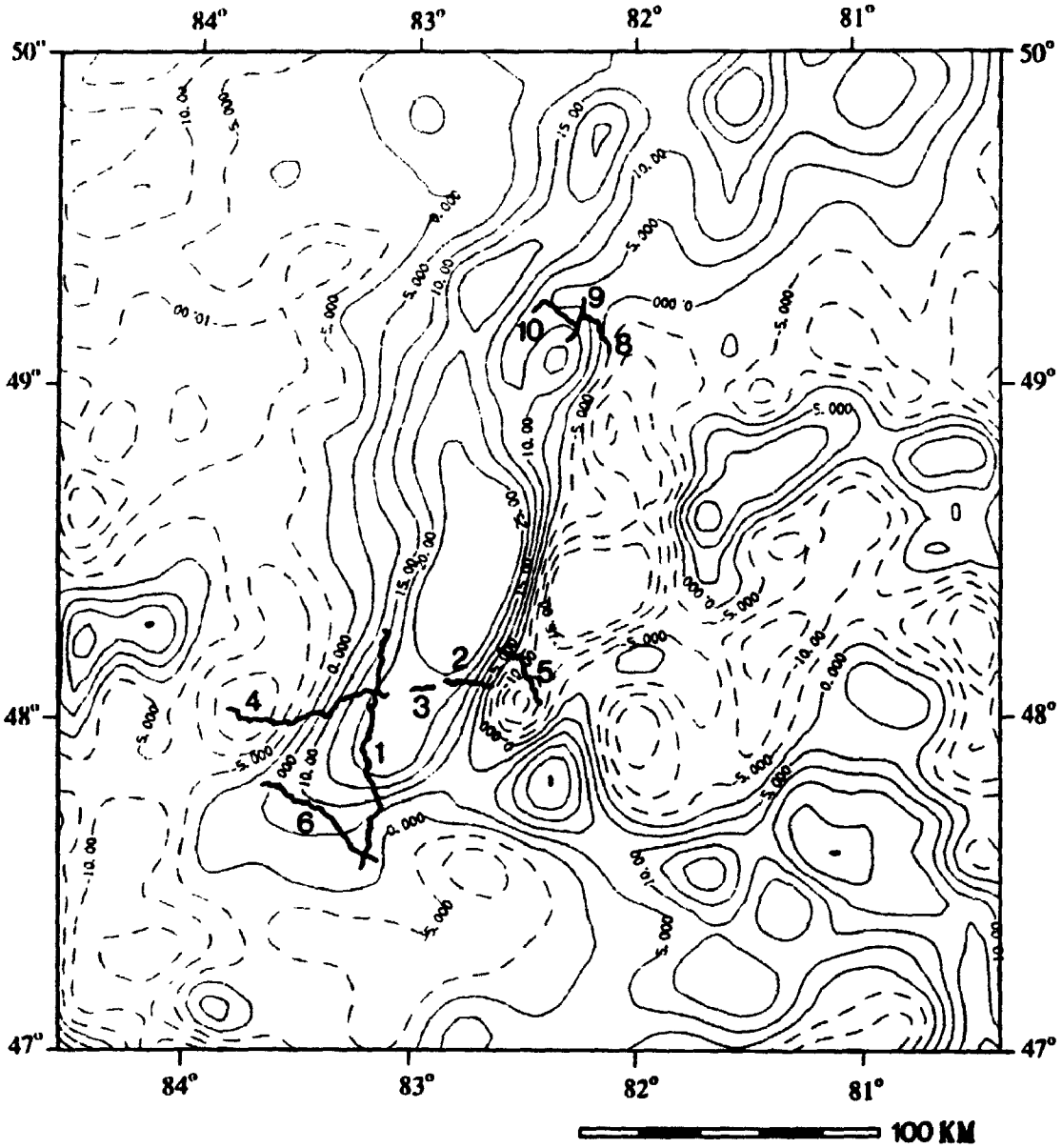

Fig. 3.2 The residual component of the Bouguer gravity around the Kapuskasing Uplift with seismic reflection profiles superimposed.

CHAPTER 4 INTERACTIVE PROCESSING OF REFLECTION LINE 5

4.1 Why Choose Line 5

As a principal target of the seismic reflection survey, the Ivanhoe Lake fault zone (ILFZ) was crossed by four profiles, lines 1, 5, 6 and 8, whereas line 2 approached the fault zone from the west (Fig. 3.1). Surprisingly, none of the commercially processed seismic sections of these lines, surveyed with the regional resolution parameters (Table 3.1), shows the image of the fault (Percival et al., 1989). Three distinct west-dipping reflectors are identified on the high-resolution (Table 3.2) seismic section of line 2, and may be followed to the vicinity of the ILFZ (Geis et al., 1990). Since line 2 does not extend far enough eastward to cross the fault zone, these reflectors cannot be traced to the surface and positively identified. Therefore, it is difficult to determine which reflector corresponds to the fault zone (Geis et al., 1990). As a result, the ILFZ remains poorly defined.

Among all of the 9 reflection profiles, the original image of line 5 was the worst as virtually no distinct reflections are recognizable throughout the whole section. As a consequence, line 5 was completely ignored in the earlier interpretations (Percival et al., 1989; Geis et al., 1990). However, according to the Bouguer gravity data the fault zone was best developed in the area covered by lines 2 and 5 (Fig. 2.1). To find out what can be done to improve the images of the regional resolution data and to define the shallow structure of the fault zone, we have processed line 5 (Fig. 4.1) by utilizing the SUN/ITA interactive seismic processing system (see chapter 3). Most techniques used in our processing are well established and clearly explained in many seismic exploration textbooks such as those by Dobrin and Savit (1988) and Yilmaz (1987).

4.2 Analysis of the Field Data

The original poor image of line 5 may be attributed to a number of causes such as: (1) absence of reflective structures in the crust; (2) poor ground conditions; (3) high ambient noise; (4) inadequate processing; and so on. In order to resolve this uncertainty, the field data were analyzed as they contain basic information about the earth crust. The importance of such an analysis has been demonstrated by Johnson and Smithson (1986), who, through a careful field data analysis, detected a processing artifact previously interpreted to be a geological boundary.

Line 5 was surveyed using a 4-ms sampling rate, 50-m station spacing, 100-m source spacing, and 240 channel recording system to provide 60 fold coverage (Table 3.1). A total of 299 common shot gathers was collected along line 5. The stations along the line were numbered from 101 to 713 as shown in Fig. 4.1. Every raw shot gather was visually inspected on our SUN workstation. A constant 16 ms time delay on the far-offset channels (121-240) was recognized on all shot gathers (Fig. 4.2a). This delay, also seen on other data sets (Hajnal et al., 1991), was presumably introduced by the recording system. Two recording trucks were used in the field with one recording channels 1-120 and the another channels 121-240. Due to some technical problems, the two trucks did not start recording synchronously. A constant 16 ms time adjustment was therefore made to correct for the delay (Fig. 4.2b). It is not known whether the contractor made such correction prior to the commercial processing.

It has been found that the data quality is highly variable from one shot gather to another due to variations in vibrator coupling with the surface. Illustrated in Fig. 4.3 are the shallow parts of two field shot gathers acquired only 100 m apart with one showing some good shallow reflections

between 0.6 and 0.8 s and the another showing no such shallow reflections at all. This difference is clearly due to the coupling rather than subsurface geology. However, the data are not as poor as one would assume from the commercially processed section. Two selected shot gathers are shown in Figs. 4.4 and 4.5. Distinct shallow reflections, most likely from the fault-plane of the ILFZ, are clearly visible on some shot gathers collected with the source over the fault zone (Fig. 4.4). Perhaps the most impressive observation is the prominent continuous reflections seen between 4 and 6 s two-way-traveltime (TWT) beneath the Abitibi belt, dipping north-northwest (Fig. 4.5). The fact that neither of these features could be identified on the commercial section suggests that the commercial processing was not sufficiently adequate and new processing is necessary. Fig. 4.5 also indicates that the most part of the upper crust is seismically transparent. It is clear that this transparency is due to geological reality rather than the variation in the surface conditions, as the midcrustal reflections have been detected. It should be mentioned that Figs. 4.4 and 4.5 represent a few of the best shot gathers acquired along the entire survey line.

One of the most interesting observations on the field data is that almost all of the shallow dipping reflections were apparently recorded on the receivers located on the west side of the recording spread while the source was directly over the surface trace of the fault zone (Figs. 4.3a and 4.4). No single shot gather, collected with the source located on the west end of line 5 and the receivers on the east side of the source, shows such continuous shallow reflections (Fig. 4.6).

4.3 Interactive Processing

Line 5 is very crooked, as road access across the ILFZ in the area is

extremely limited (Fig. 4.1). In fact, the north portion of line 5 follows an old fire-tower road. An abrupt bend, occurring in the line between stations 247-310 running along Highway 101, caused the arrival time reversal seen between channels 150 and 170 (Fig. 4.4). As a consequence of the bend, the distribution of common-midpoint (CMP), especially those with long offsets, scatters widely instead of focusing within a narrow bin (Fig. 4.7). The maximum CMP bin height is about 3000 m while CMP bin width is only 25 m (half of receiver spacing). The first effort in the processing was therefore made to define crooked line geometry. Two different but natural choices were tested. Firstly, line 5 was treated as a continuous line and a scattergram of CMP was computed from all field data (Fig. 4.7). An average CMP line was selected on the basis of the CMP distribution. The CMP swath was then divided into a set of bins perpendicular to the CMP line with a length equal to the CMP interval and a width varying from 50 m to 3000 m. This process is illustrated in Fig. 4.8. All traces falling within a bin were considered to belong to that CMP (Fig. 4.9a) and would be summed together, after normal moveout (NMO) correction (Fig. 4.9b), to form a single stacked trace (Fig. 4.9c). Secondly, line 5 was divided into two segments: north part between stations 101-247 and south part between stations 310-713, and processed separately (Fig. 4.10). Data collected between stations 247-310 were largely omitted from processing because their CMPs were widely scattered. Pilot processing was then carried out in the same manner following each of these two CMP geometries. The difference shown in the final stacked sections (Fig. 4.11) suggests that the second geometry is certainly a better choice, which has been adopted thereafter.

At first, the revelation of the 16 ms delay on the far offset channels (Fig. 4.2) might lead one to believe that it would make a significant

difference to the final stacked section. A fellow-up test, however, indicated that this was not the case. Shown in Fig. 4.12 are the final stacked sections prepared with and without the correction. For the north part of line 5, this can be easily explained by the fact that all the shallow dipping reflections were recorded on the near-offset receivers (Figs. 4.3a, 4.4, 4.9). In other words, the dipping reflections were recorded on the first 120 channels, thus on the same recording truck. For the south part of line 5, this may be due to the application of trim statics, which align the reflections within a CMP gather if the reflections fall within a small time window.

To find out how stacking two adjacent shot gathers into one, which was done prior to the commercial processing to reduce the amount of data to be processed by 50%, affects the seismic image, the line was first processed by choosing exactly the same procedure as the contractor's (Table 3.3). Fig. 4.13 compares the three sections processed with the same procedure but from three different data sets: the data with the mixing, the data composed of every second shot gathers only, and the data including all shot gathers without the mixing. It is clear that the second data set produces a better image than the first data set, while the third data set generates the best image, indicating the data mixing cancels out dip reflections and higher fold is important for signal-to-noise enhancement.

Therefore, all of the following processing was done with the full data set without any mixing to provide the best seismic image possible. A variety of pre-stack processing techniques was applied to the data, with emphasis on techniques which had not been explored in the commercial processing. These techniques included velocity (F-K) filtering to reduce ground-roll noise, deconvolution to remove short-period multiples, interactive first arrival muting to maximally preserve shallow reflections, interactive refraction

statics to correct time differences caused by the near-surface weathering layer, surface-consistent residual statics to account for extra time shifts related with the surface locations, velocity analysis, offset-limited stacking to eliminate far-offset traces often characterized by low signal-to-noise ratio, and stacking with artificially high velocity to search for steeply dipping events. Further details on some of these techniques and examples of the ITA job decks are given in appendix A.

It is discovered that first arrival muting makes a notable impact on the shallow seismic images. Shown in Fig. 4.14 are two seismic sections processed with identical procedures and parameters except that first arrivals were muted differently. In one case, only every fifth shot gathers were viewed on the screen and muted interactively. For the remaining shot gathers, first arrivals were muted by interpolation. In the other case, every shot gather was interactively muted. The final stacked sections look astonishingly different. Evidently the better muting has two effects on the image. Firstly, it gets rid of large amplitude first arrivals more completely, which will depress the reflections if left behind. Secondly, the better muting can maximally preserve the very shallow reflections, which otherwise could be muted.

It is found that refraction and surface-consistent residual static corrections are particularly effective in enhancing the signal-to-noise ratio and improving the continuity of reflections throughout the whole seismic section (Figs. 4.15 and 4.16). It appears that refraction statics are not very effective in improving the shallow section of the north part of line 5 (Fig. 4.15), but are highly effective in improving the deep section of the south part of line 5 (Fig. 4.16). This performance difference is caused by thickness variations of the weathered layer. Shown in Fig. 4.17 are the

variations of elevation, refraction statics, and thickness of overburden along line 5. Overall, there is little overburden along line 5, except between stations 341 to 501, where overburden thickens up to ~100 m. By removing travel time delays produced by the overburden, refraction statics effectively align reflection energy and yield a greatly improved section (Fig. 4.16). In addition, Figs 4.15 and 4.16 also demonstrate that surface-consistent residual static corrections always perform better following the application of refraction static corrections. One immediate implication of these results is that the application of refraction statics is necessary in this part of the Canadian shield, consistent with the findings of Hajnal et al. (1991) and Milkereit et al. (1991). This indicates that little overburden and small elevation variations in most parts of Canadian shield do not necessarily mean that refraction statics are always negligible.

F-K filtering proves to be instrumental in suppressing ground-roll noise (Fig. 4.18). High-amplitude ground-roll noise is clearly seen on most field gathers and the shallow dipping reflections are severely contaminated by this noise (Figs. 4.2-4.6). This noise, because of its broad spectrum, cannot be simply attenuated by applying a high-pass filter. Due to the factors such as the crooked line and varying surface conditions, the apparent velocity for ground-roll may vary from one shot gather to another, even within the same shot gather (see Fig. 4.18b). This means that a F-K filter, designed on the basis of one shot gather or several, will not work equally well for the whole data set. Fortunately, the updated ITA software, received by us on February 13, 1991, has a module called "FKSURG", which allows users to interactively design F-K filters. For example, a F-K filter may be designed for every five shot gathers. The module will automatically save all F-K filters into a file, which can be applied to the whole data set anytime in the future. Our

experience tells that interactively designing the F-K filter is the key to the successful suppression of ground-roll (compare Figs. 4.19f and g). Without doubt, it is a very time-consuming process.

Velocity analysis is an important step in seismic data processing and often consumes more time than many other steps. Common approaches for determining stacking velocities are based on the fundamental assumption of CMP stacking method, that the earth's crust is composed of horizontal, homogeneous layers. Obviously the assumption is a crude approximation to reality. If it is valid, seismic rays whose travel times are plotted against source-receiver offset would show hyperbolas and stacking velocities could be precisely determined by flattening the hyperbolas (Fig. 4.20). Undoubtedly, the Kapuskasing data violate the assumption, as no hyperbola is observed anywhere (Figs. 4.2-4.6, and 4.18) because of its complex tectonic history. Like CMP 483 (Fig. 4.21), many CMP gathers do not contain recognizable reflections across the entire gather, thus providing no clue on crustal velocity. Where good reflections are present (Fig. 4.22a), they are mainly confined to near-offsets ($\leq$ 3 km). The NMO corrections, from which velocities are estimated, are small (Fig. 4.22b) because of high velocities in the Canadian shield and great depth of the deep reflections compared to relatively small source-receiver offsets. In order to demonstrate this quantitatively, the NMO correction at 6 s for each trace is plotted at the bottom of Fig. 4.22b. Shown in Fig. 4.22c is the velocity spectra of CMP 413. It is almost impossible to pick stacking velocities from it, implying that velocity spectra-type techniques are not suitable to the data set. Constant velocity stacking method was then tried. Fig. 4.23 illustrates this approach. Here, 48 successive CMP gathers from the northern line 5 are NMO-corrected and stacked with a set of constant velocities, ranging from 6000 m/s to 7750

m/s with an increment of 250 m/s. The resulting 48-trace CMP stacks are displayed side by side in Fig. 4.23 to allow a detailed comparison. It appears that stacking velocity of ~7000 m/s yields the best quality stack in terms of reflection amplitude and continuity. Although crustal velocities near the surface along the north part of line 5 are unlikely to exceed 6000 m/s as indicated from first arrivals (Fig. 4.24), artificially higher stacking velocity is necessary to search for dipping structures. Theoretically, the stacking velocity for a dipping reflector is equal to the medium velocity divided by the cosine of the dip angle (Levin, 1971). By proceeding in the same way, stacking velocities for the whole line can be built up. Our tests suggest that constant velocity stacking method is more useful in areas with complex structure.

Trace editing to remove noisy traces was also applied to the data, but no significant differences were observed between the final stacked sections processed with and without this technique. Marginal improvement after applying deconvolution suggests that multiple cyclicity is not a major problem (see Figs. 4.19g and h). The observation, that most reflections, shallow or deep, are confined to near-offsets (Figs. 9, 22), led to the processing which used near-offsets ($\leq$ 3 km) only. The output, produced from the processing, is as good as the one processed with all offsets, if not better. This may indicate that collecting of far-offset traces is not necessary.

It should be emphasized that to ensure correct identification of reflected events on the final stacked section, all coherent events observed on the field data were visually inspected on the SUN workstation after each step of the processing. The basic criterion is that any reflections seen on the final stack section must be observed on the raw shot and/or CMP gathers.

Most of the processing steps must be repeated several times in order to optimize the final stacked section, not to mention the parameterization of each module of the ITA software. For instance, to see how trace editing will affect the final stacked section, the whole processing flow has to be repeated. The constant 16 ms delay on far offset channels (Fig. 4.2), unfortunately, was recognized in the middle of the processing. The whole processing flow from first arrival picking to CMP stacking, therefore, had to be repeated after the 16 ms delay was corrected.

As inferred from geological, gravity, and aeromagnetic observations, the north part of line 5 covers the ILFZ (Figs. 3.1, 3.2). Since field shot gathers, collected over the surface trace of the fault zone, show some excellent shallow dipping reflections (Figs. 4.3a, 4.4, and 4.18a), considerable efforts have been made to enhance the shallow seismic images of this part of the line. Fig. 4.19 demonstrates how, step by step, the images can be improved utilizing the techniques discussed above. Fig. 4.19a was processed following the contractor's procedure and is identical with the commercial seismic section.

The final stacked section for the whole line is given in Fig. 4.25 and the processing sequence is tabulated in Table 4.1. Our processing has greatly improved the seismic image of line 5. The improvement is mainly seen in two areas: the top northwest and the middle center parts of line 5. These two areas are shown enlarged in Figs. 4.26 and 4.27 to allow a detailed comparison with the commercially processed section. Along the north portion of line 5, our processing brings to light a band of northwest-dipping reflections in the uppermost crust (Fig. 4.26b). These reflections can be followed from a depth of about 600 m (0.2 s), assuming P wave velocity of 6 km/s, to around 3 km. This feature was not discernible on the commercial

section. Our processing also reveals a major midcrustal reflector within the Abitibi belt, dipping northwest with a lateral continuity of more than 10 km (Fig. 4.27b). This reflector was essentially buried by noise on the commercial section. Its down-dip termination to the northwest resulted from a low fold coverage caused by the abrupt bend in the line, a low signal-to-noise ratio, and a sharp increase in dip. In addition, many other but less distinctive northwest-dipping reflections are also observed between 1 to 10 s TWT within the AGB (Fig. 4.25).

As the final step in seismic data processing, migration is crucial in mapping dipping geological structures, as it moves dipping reflections back into their true subsurface positions and collapses diffractions. In principle, all geological interpretations should be made on the basis of migrated seismic sections. However, appropriate migration requires the knowledge of accurate velocity information. As mentioned above, it is highly improbable to obtain such information in the study area. Warner (1987) has found that, even given accurate crustal velocities, migration of deep seismic reflections still generally produces poor results and that the best migration may be achieved at velocities of up to 50% less than directly derived from stacking velocities.

As illustrated in Fig. 4.25, the final stacked section shows two major dipping events, indicating that migration is necessary. A series of migration tests was therefore applied to the stacked data. A constant velocity of 6 km/s, derived from the first arrivals of shot gathers (Fig. 4.24), was used to migrate the shallow dipping reflections seen on the north uppermost part of line 5. Two different approaches were taken. Firstly, the stacked data were migrated directly (Fig. 4.28a). Secondly, the stacked data were initially coherency-filtered and then migrated (Fig. 4.28b). The latter

approach is obviously superior to the former as the reflections are much more continuous after migration. The migrated sections (Fig. 4.28) look very similar to the stacked section (Fig. 4.26b), except that all dipping reflectors moved a short distance in the updip direction, became shorter and slightly steeper after migration. This is exactly what migration is supposed to do to the dipping events. The dipping event seen between 2 and 2.5 s on the stacked section (Fig. 4.26b), showing hyperbolic curvature, was collapsed after migration (Fig. 4.28), suggesting that it is a diffraction. Smiling effects of migration are clearly seen and deteriorate with increasing travel time, the problem for the deep reflections (Warner, 1987). Figs. 4.29a, b, and c compare the migrated sections for the major midcrustal event with different constant velocities. The best migration result is apparently obtained with a velocity of 4.5 km/s, which is about 70% of the realistic crustal velocity 6-6.5 km/s. The apparent shortening of the major reflector after migration (Fig. 4.29a) is likely due to the limitation of the survey line. If line 5 extended straight further northwest beyond station 309, the reflector could be much longer.

TABLE 4.1 ACADEMIC PROCESSING of LINE 5

DEMULTIPLEX	
AMPLITUDE RECOVERY	2000 ms AGC
GEOMETRY	Crooked line
REFRACTION STATICS	One-layered Model
ELEVATION CORRECTIONS	Datum - 400 m above sea level
	Replacement Velocity - 5000 m/s
DECONVOLUTION	Predictive
F-K FILTERING	
CMP GATHER	~60 fold
VELOCITY ANALYSIS	
NORMAL MOVEOUT CORRECTION	
FIRST BREAK MUTE	
RESIDUAL STATICS	Surface-consistent
STACK	Offset $\leq$ 3 km
TRACE EQUALIZATION	Time variant
MIGRATION	

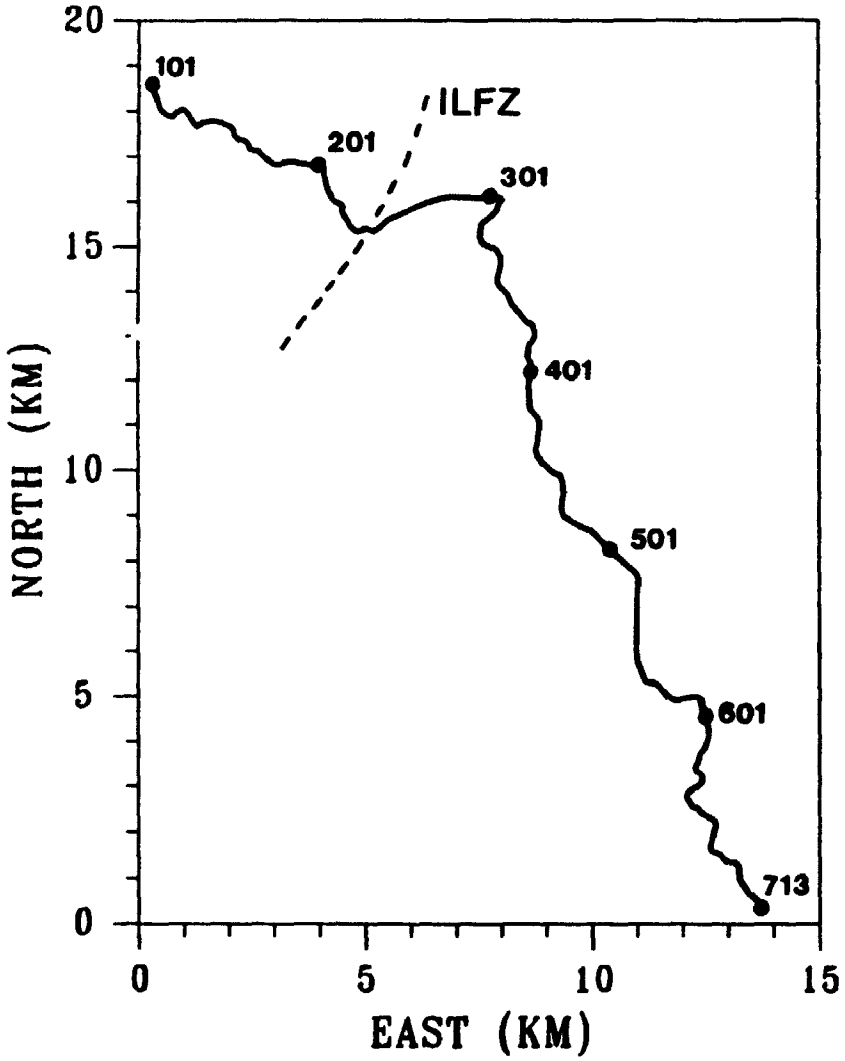

Fig. 4.1 Geometry of reflection profile 5 with station numbers labelled.

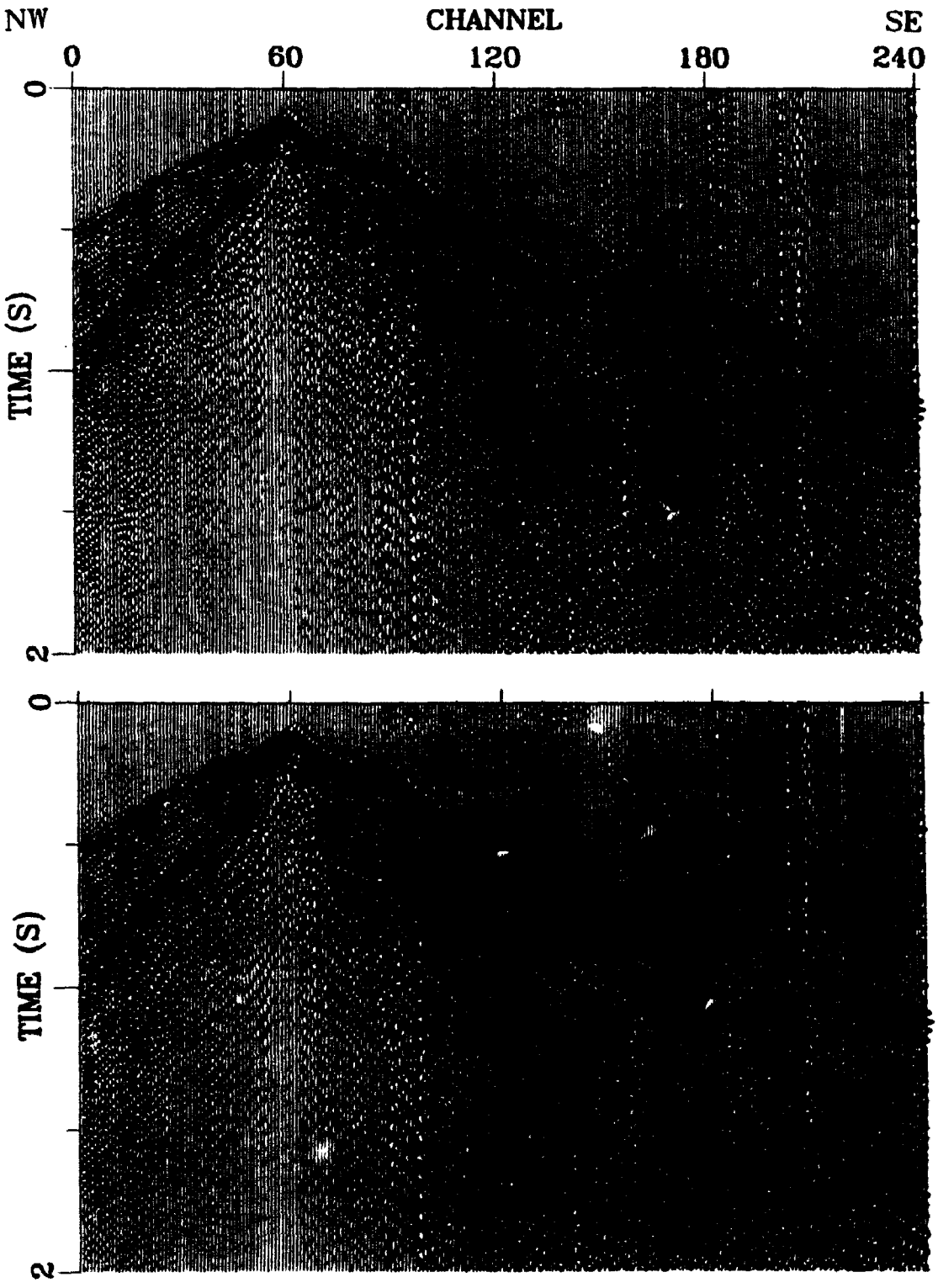

Fig. 4.2 Top: Example of field shot gathers collected with the source at station 221, showing 16 ms travel-time gap (marked by arrow) between channels 1-120 and 121-240, introduced by recording system. Bottom: the same shot gather after 16 ms correction applied to channels 121-240. The sections were plotted with trace normalization. No AGC gain was applied.

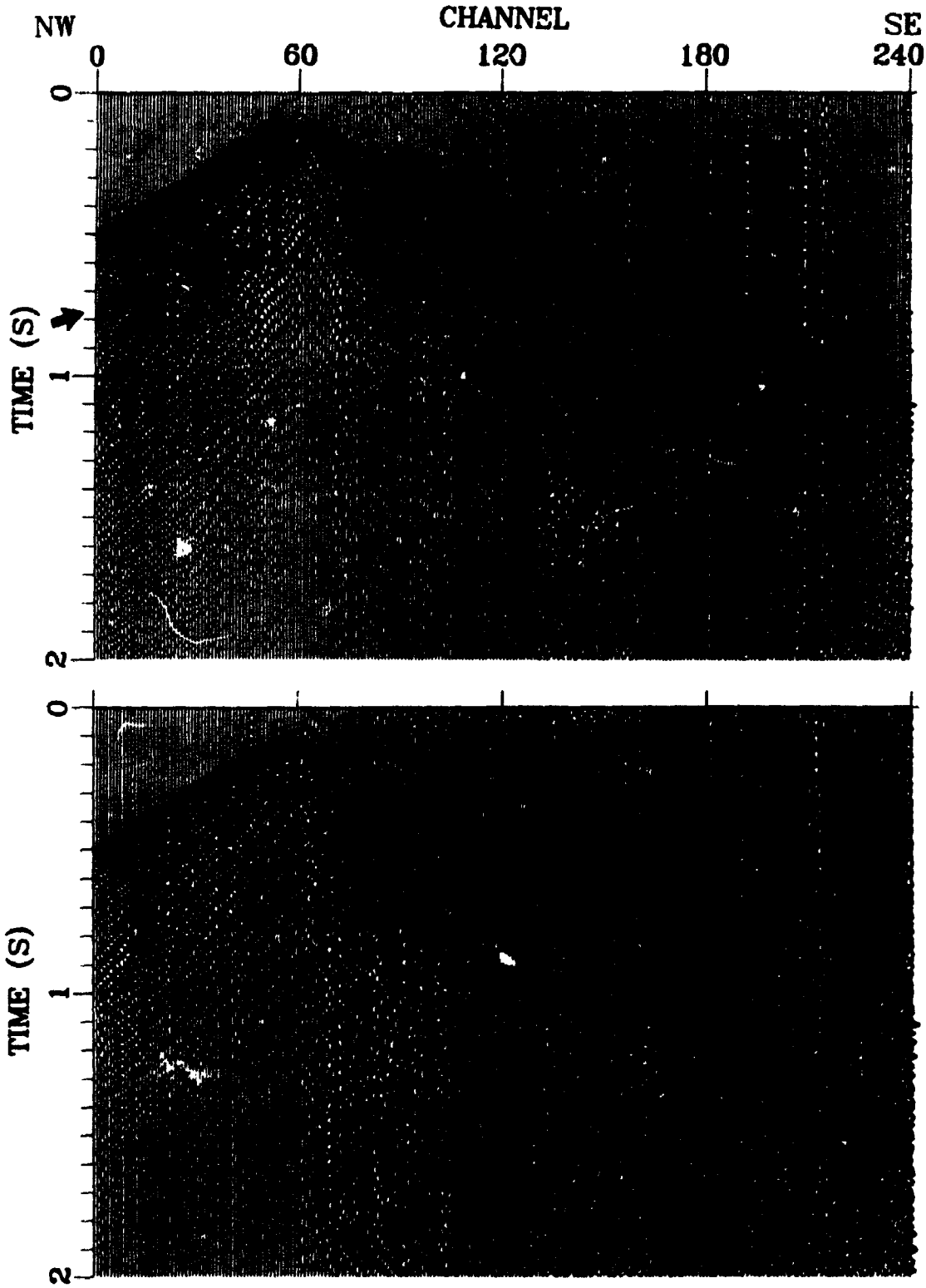

Fig. 4.3 Two shot gathers collected from shotpoints 100 m apart (top: station 213, bottom: station 215). Shallow dipping reflections, clearly observed on the top (marked by arrow), are not seen at all on the bottom, attributed to source-surface coupling variations. The sections were plotted with trace normalization. No AGC gain was applied.

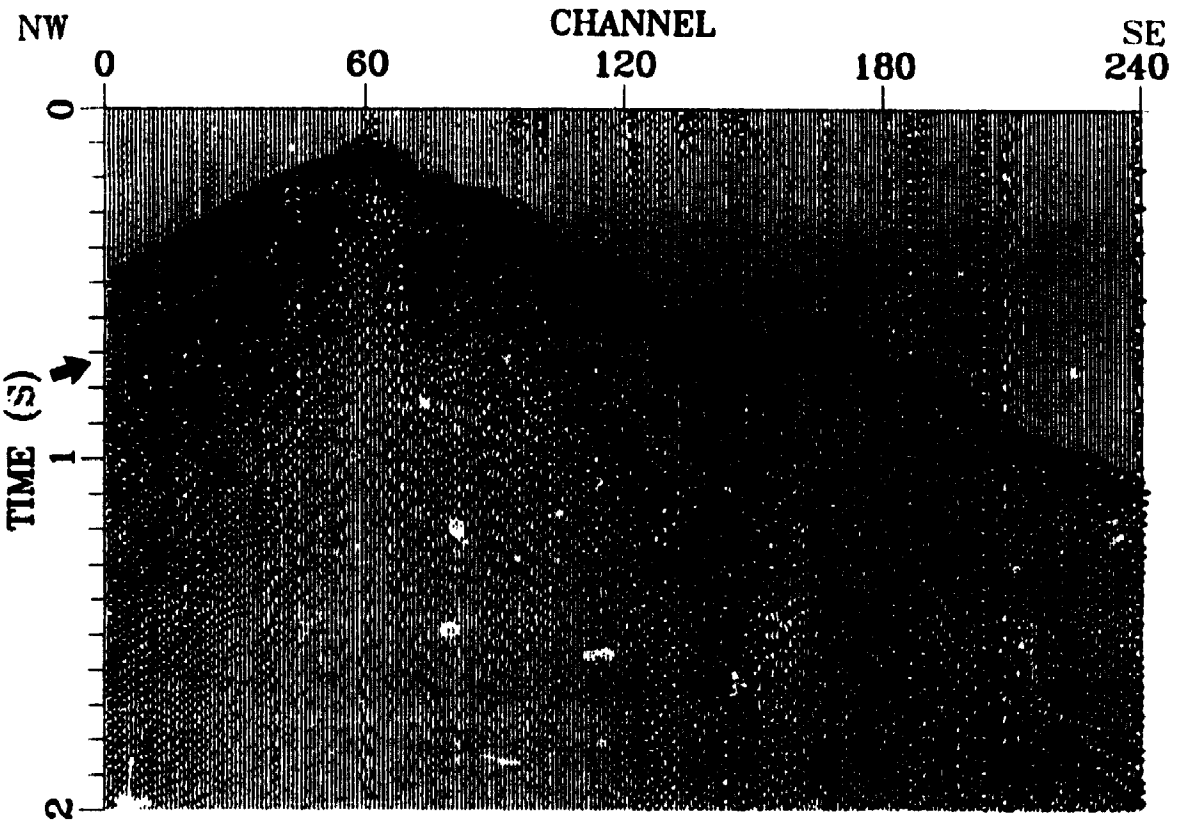

Fig. 4.4 A selected shot gather (VP 219, VP = vibrating point = source point) from the north part of line 5, showing west-dipping events near the surface (marked by arrow) that are interpreted as fault-plane reflections from the Ivanhoe Lake fault zone (ILFZ). The section was plotted with trace normalization. No AGC gain was applied.

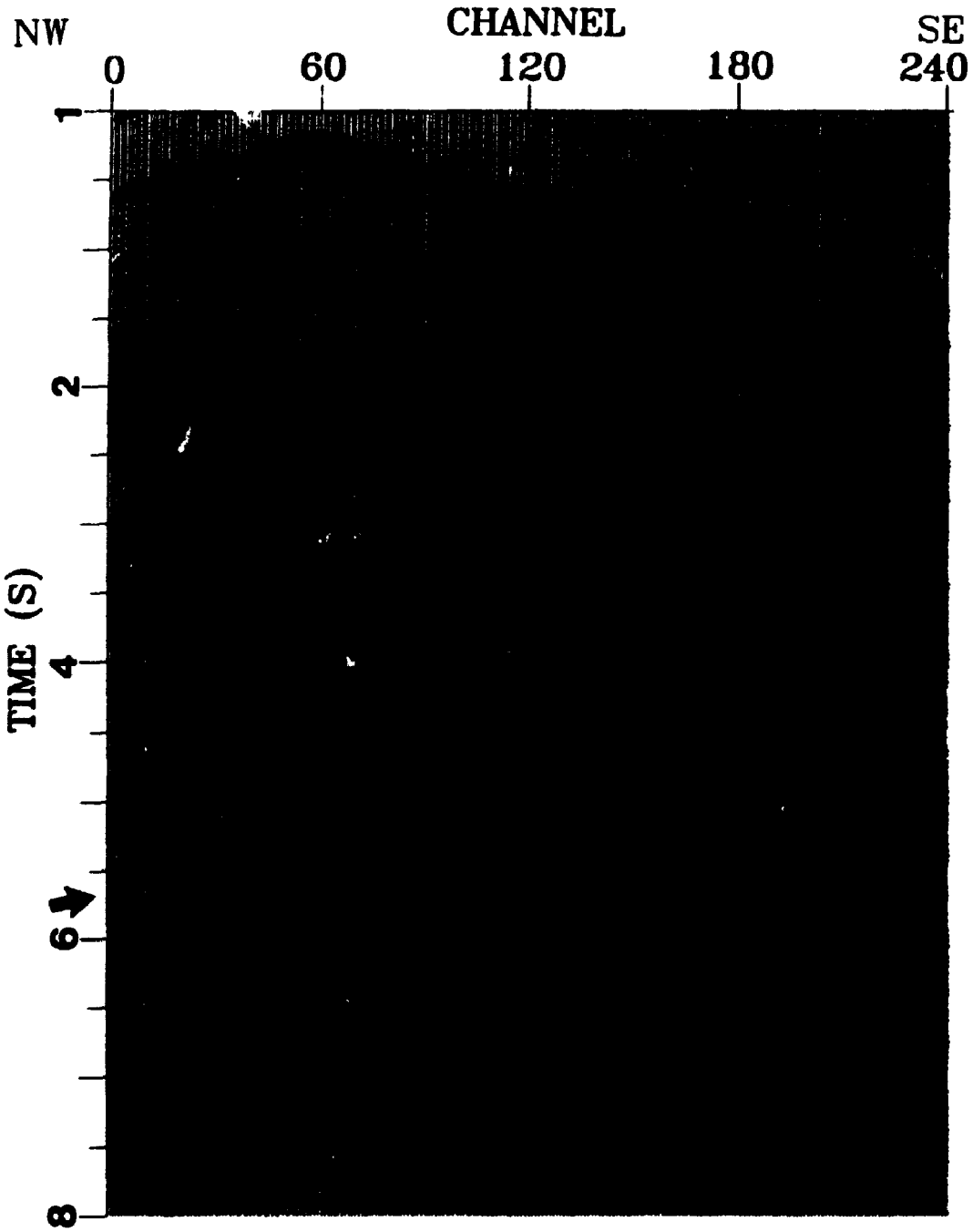

Fig. 4.5 A selection shot gather (VP 387) from the middle of line 5, showing west-dipping reflections (marked by arrow) across the whole gather between 4 and 6 s two-way travel time. The data were AGC-gained.

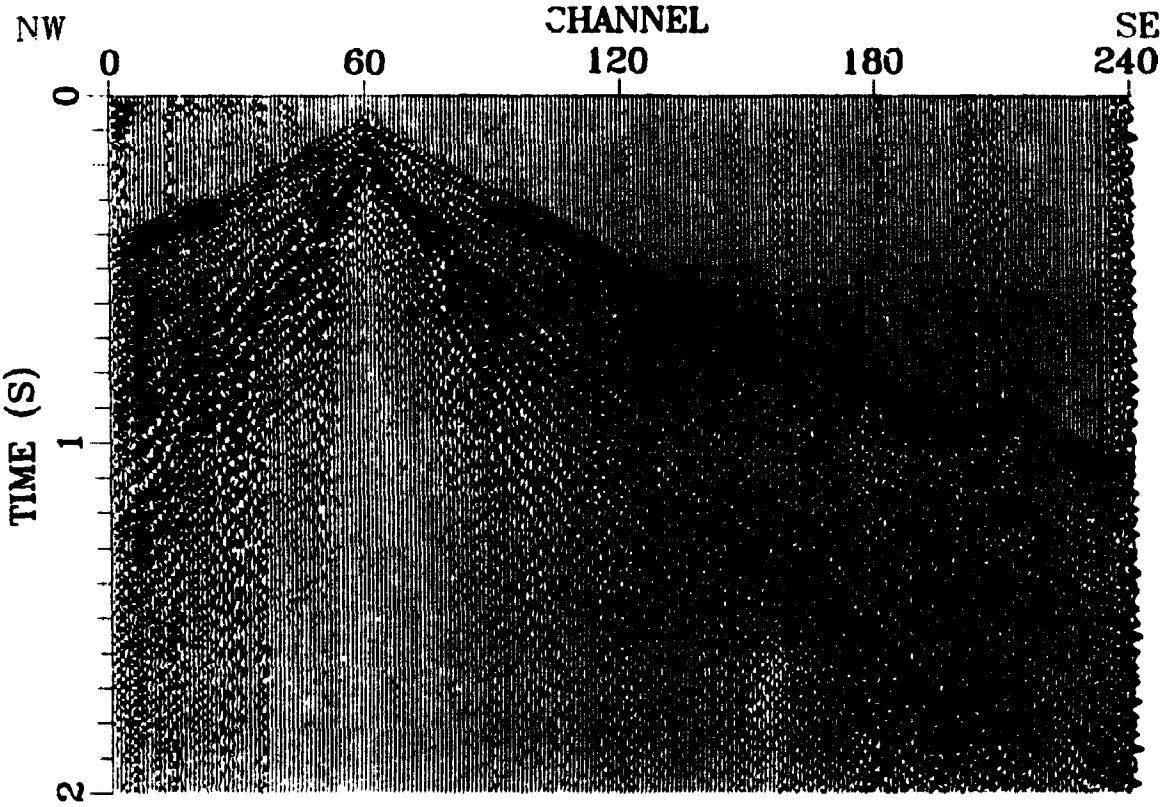

Fig. 4.6 A selected shot gather (VP 169). Note that no reflections are observed between channels 60-120. The section was plotted with trace normalization. No AGC gain was applied.

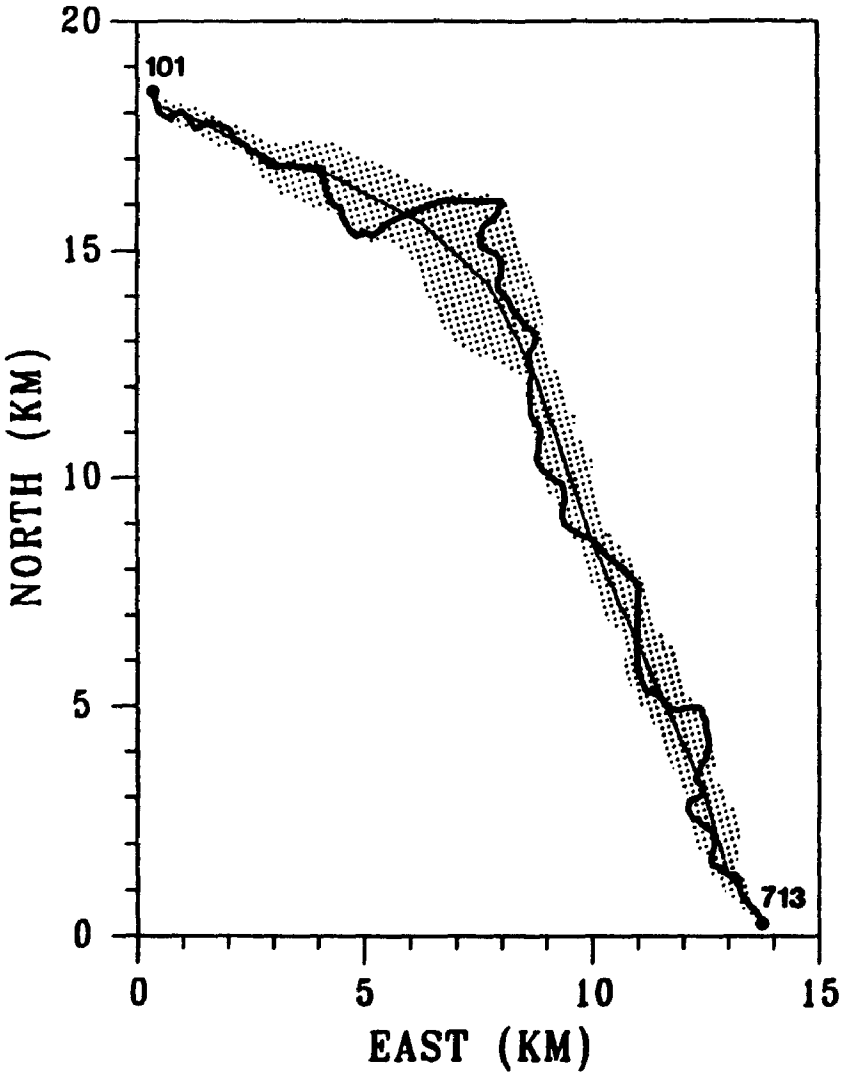

Fig. 4.7 Geometry of reflection line 5 with the distribution of common-midpoints (CMP) superimposed. Note that each dot does not necessarily represent only one CMP rather than tens or hundreds. The thin line corresponds to one possible CMP geometry.

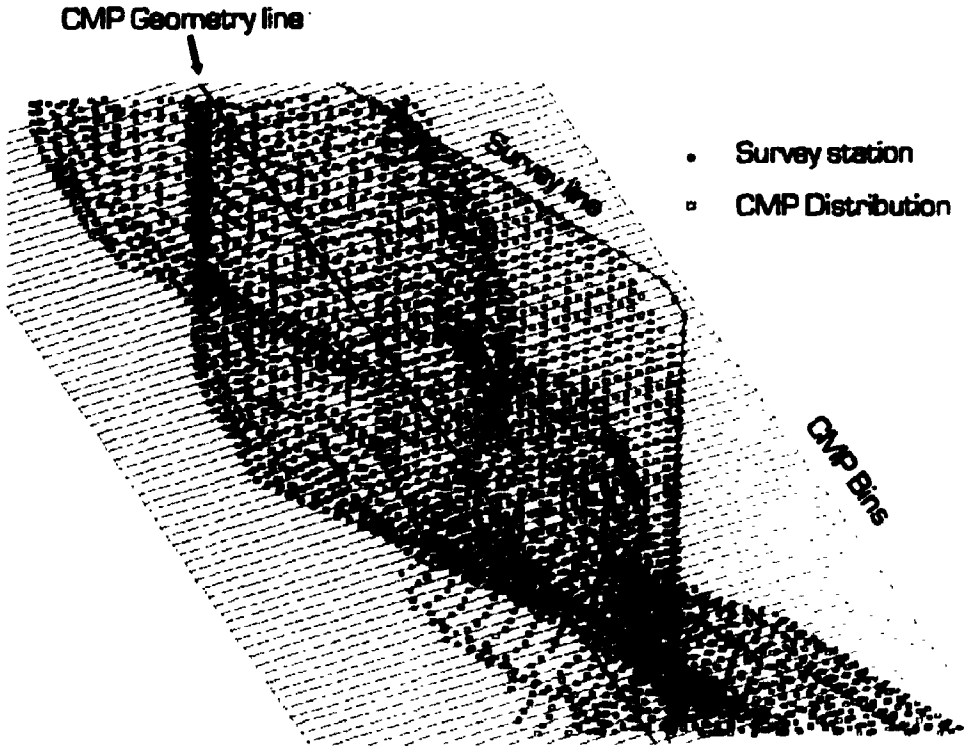

Fig. 4.8 Enlarged portion of line 5 CMP swath.

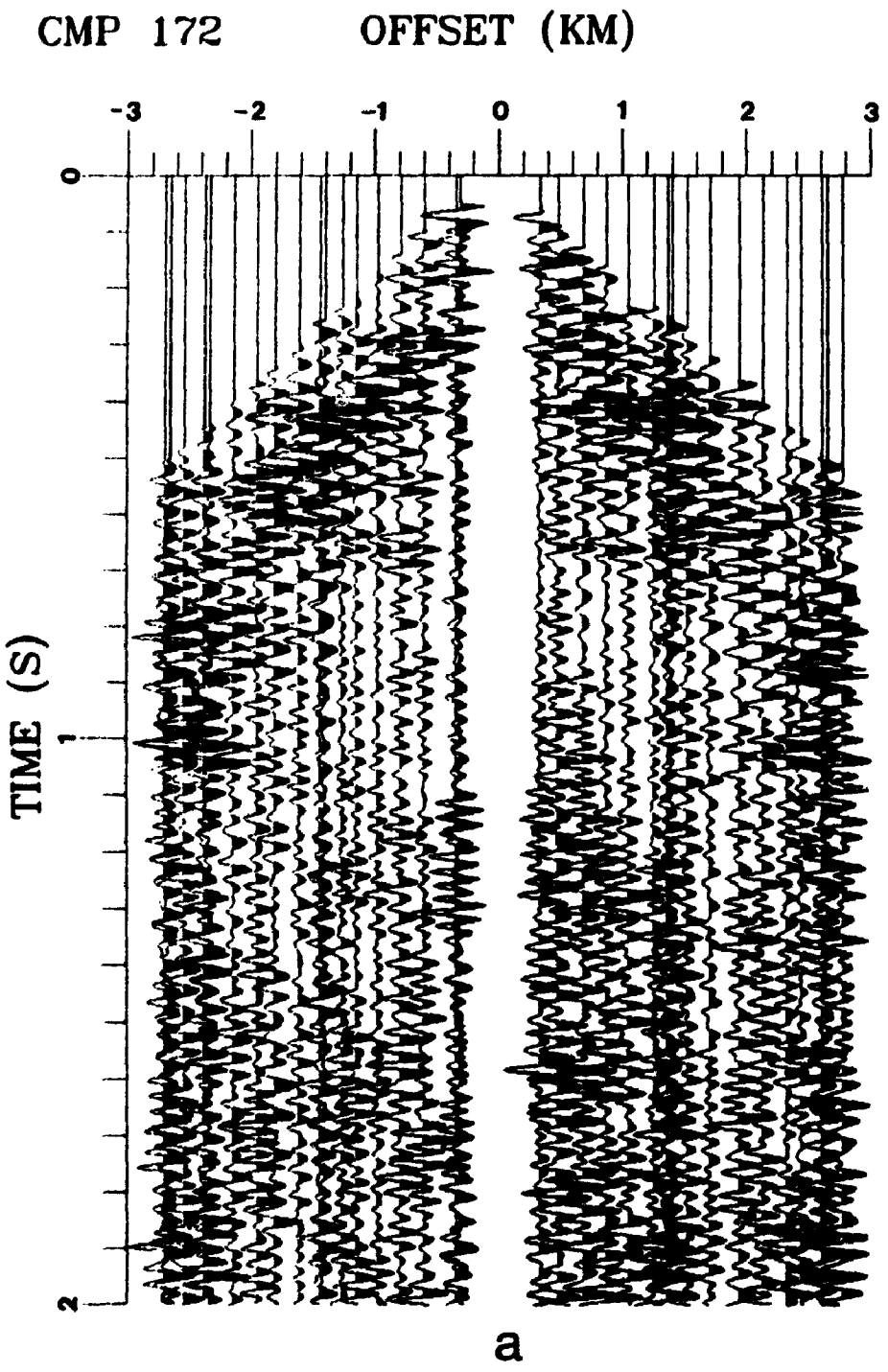

Fig. 4.9 (a) CMP gather 172 before NMO correction. The data were AGC-gained.

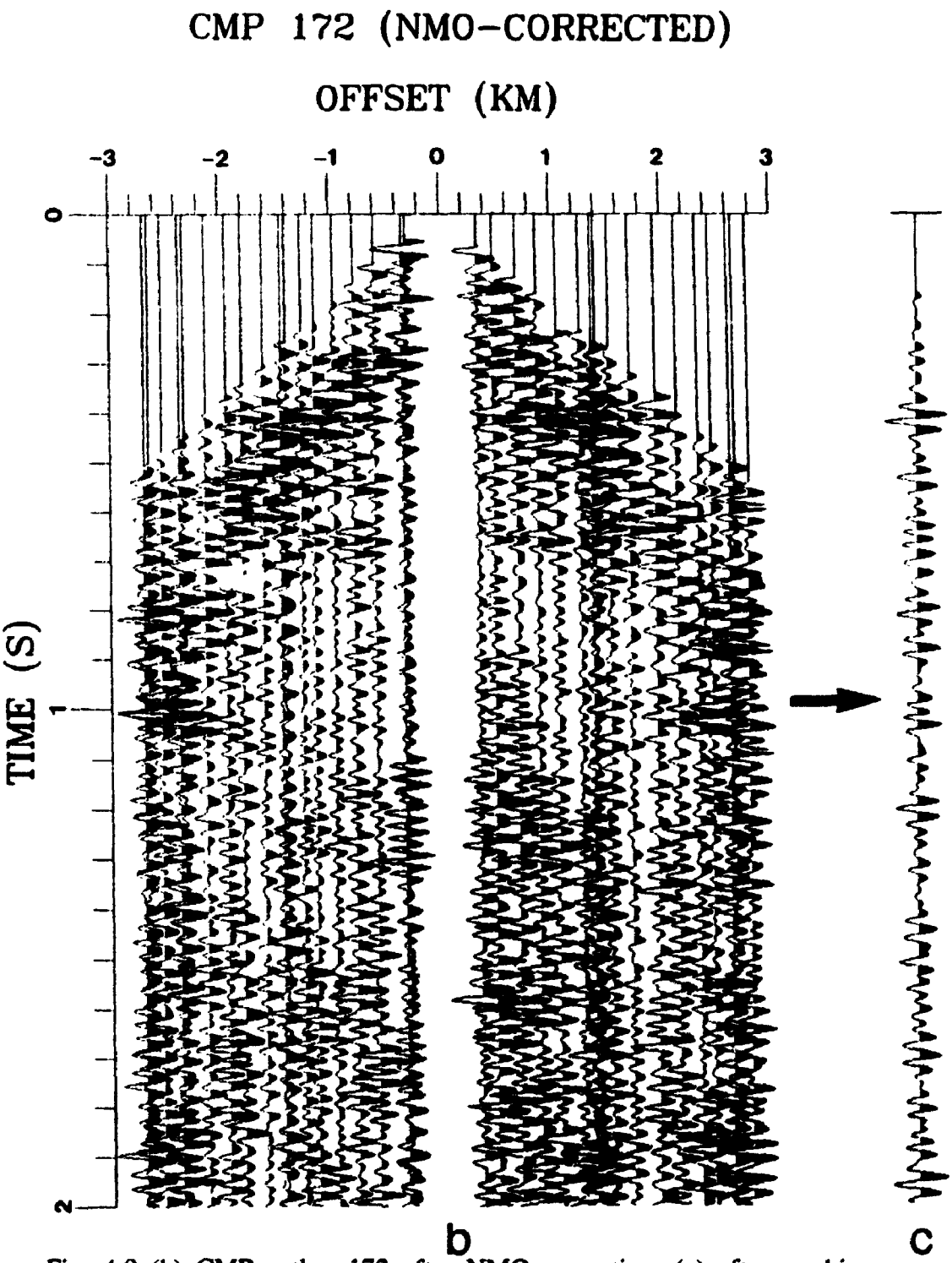

Fig. 4.9 (b) CMP gather 172 after NMO correction. (c) after stacking.

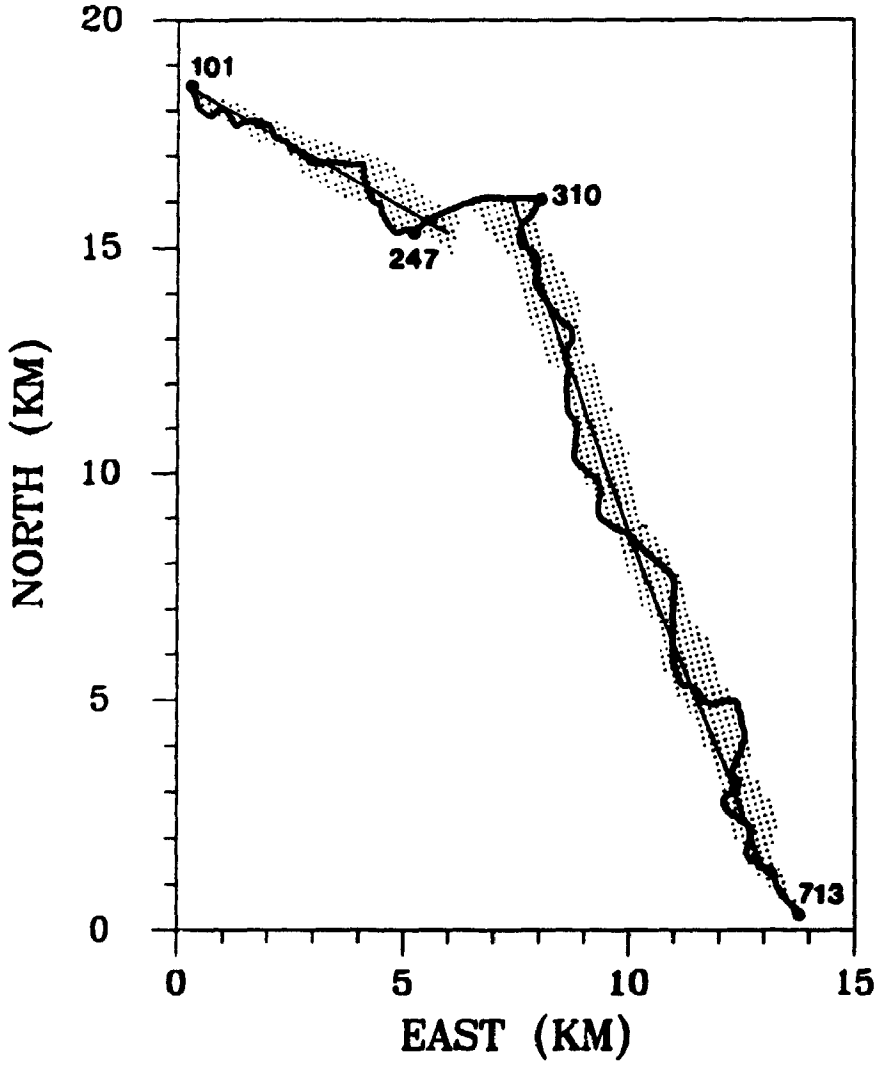

Fig. 4.10 Geometry of reflection line 5 with the distribution of common-midpoints (CMP) superimposed. Note that the data collected between stations 247 and 310 are largely omitted. The thin line corresponds to the second CMP geometry.

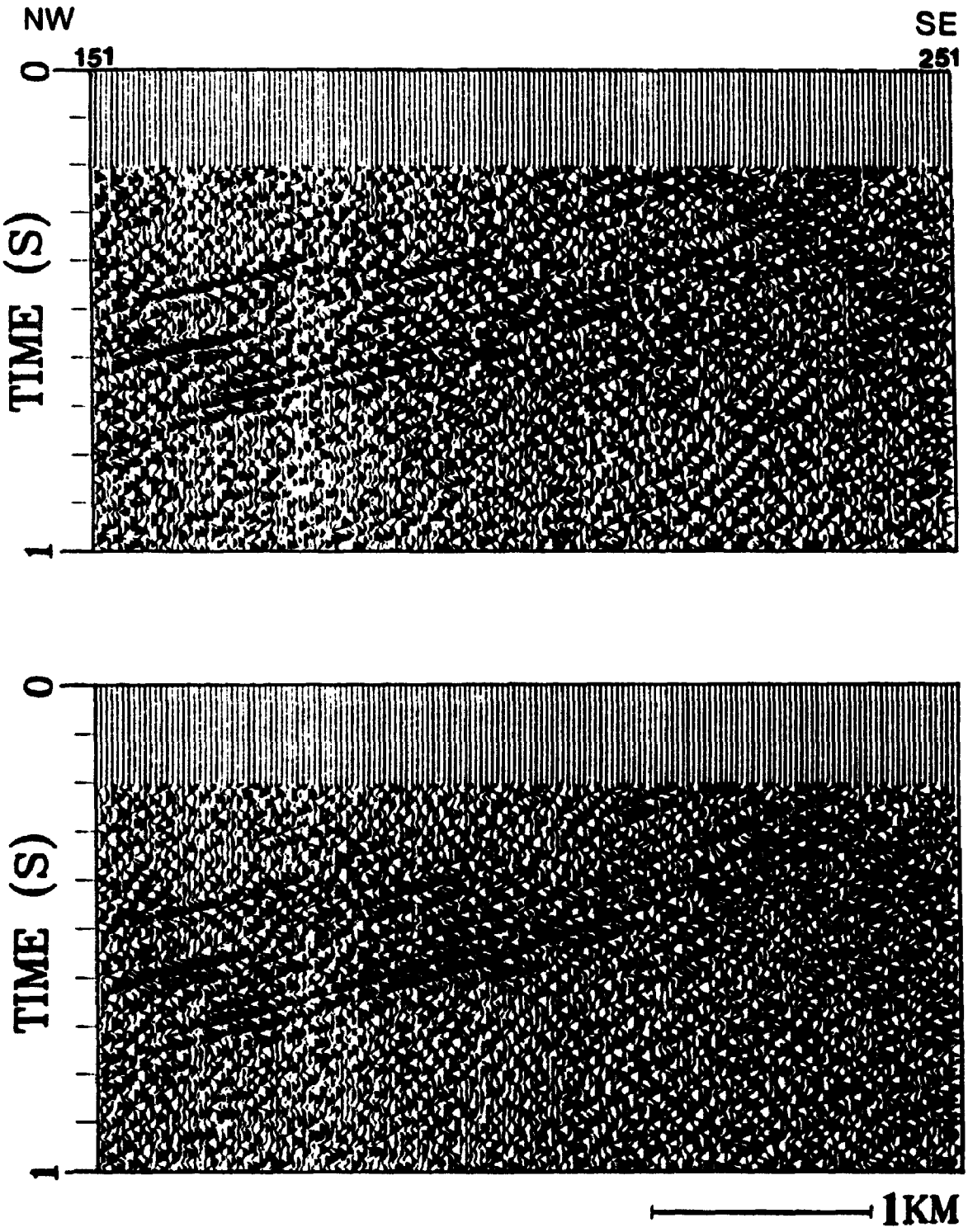

Fig. 4.11 Example to demonstrate the effect of the CMP geometry. Top: processed with the CMP geometry shown in Fig. 4.7. Bottom: the same section processed with the CMP geometry shown in Fig. 4.10.

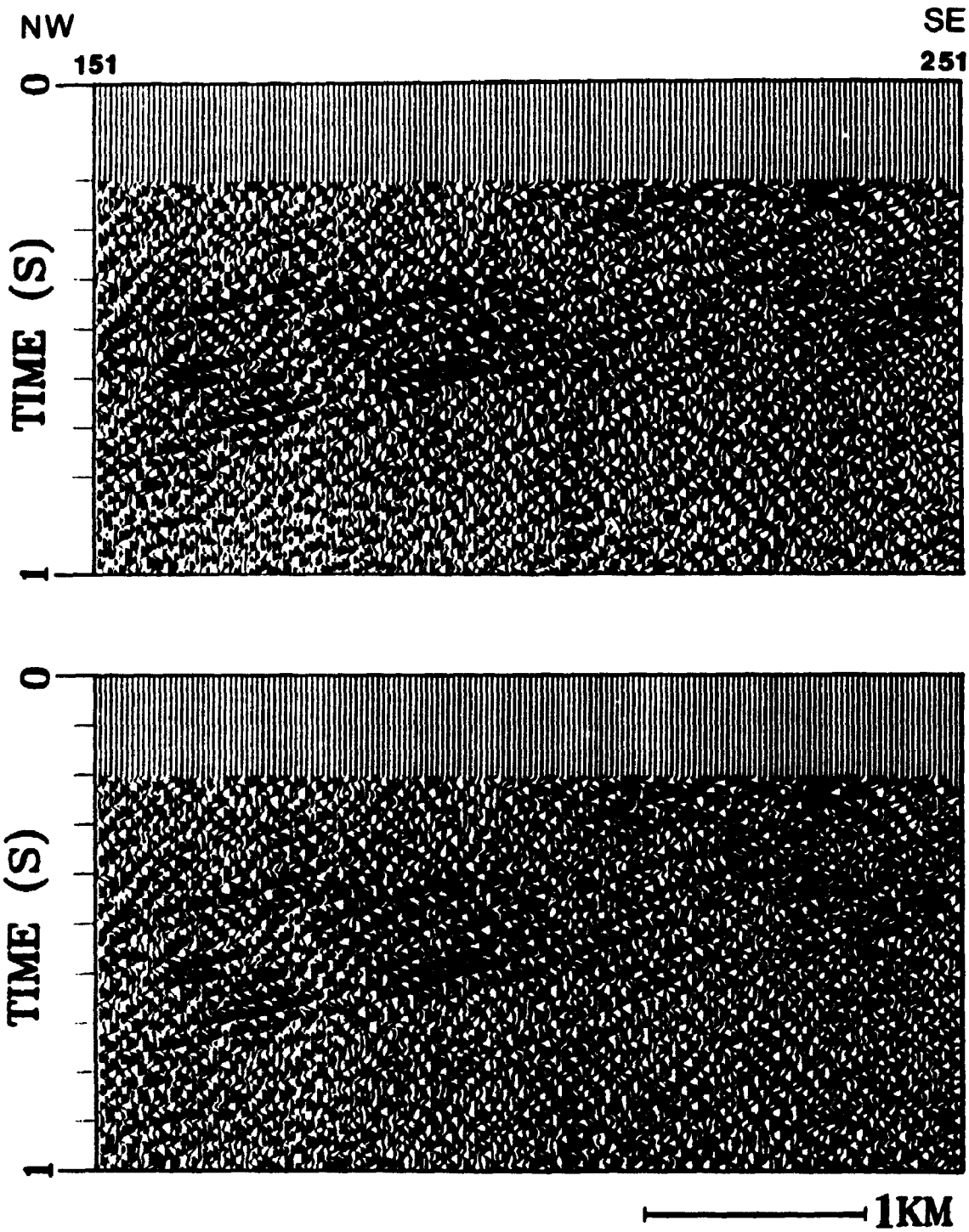

Fig. 4.12 Example to demonstrate the effect of the 16 ms recording gaps between channels 1-120 and 121-240 introduced by recording system (see Fig. 4.2). No difference is observed between the sections prepared without (top) and with (bottom) the 16 ms corrections.

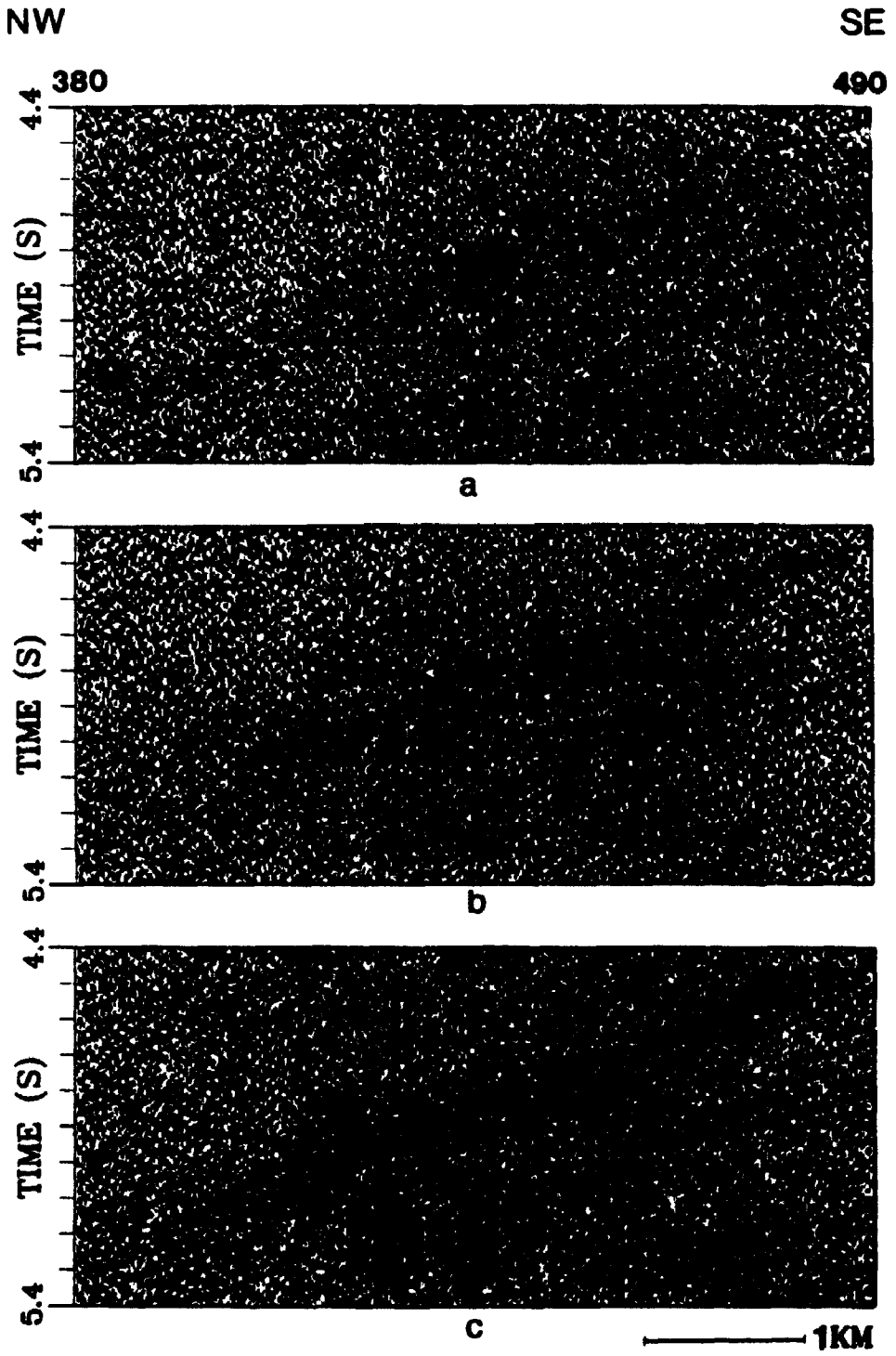

Fig. 4.13 Example to demonstrate the effect of the data mixing by summing two adjacent shot gathers into one. Top: the selected seismic section processed from the data set with mixing. Center: the same section processed from the data set composed of only every second shot gather. Bottom: the same section processed from the data set including every shot gather without the mixing.

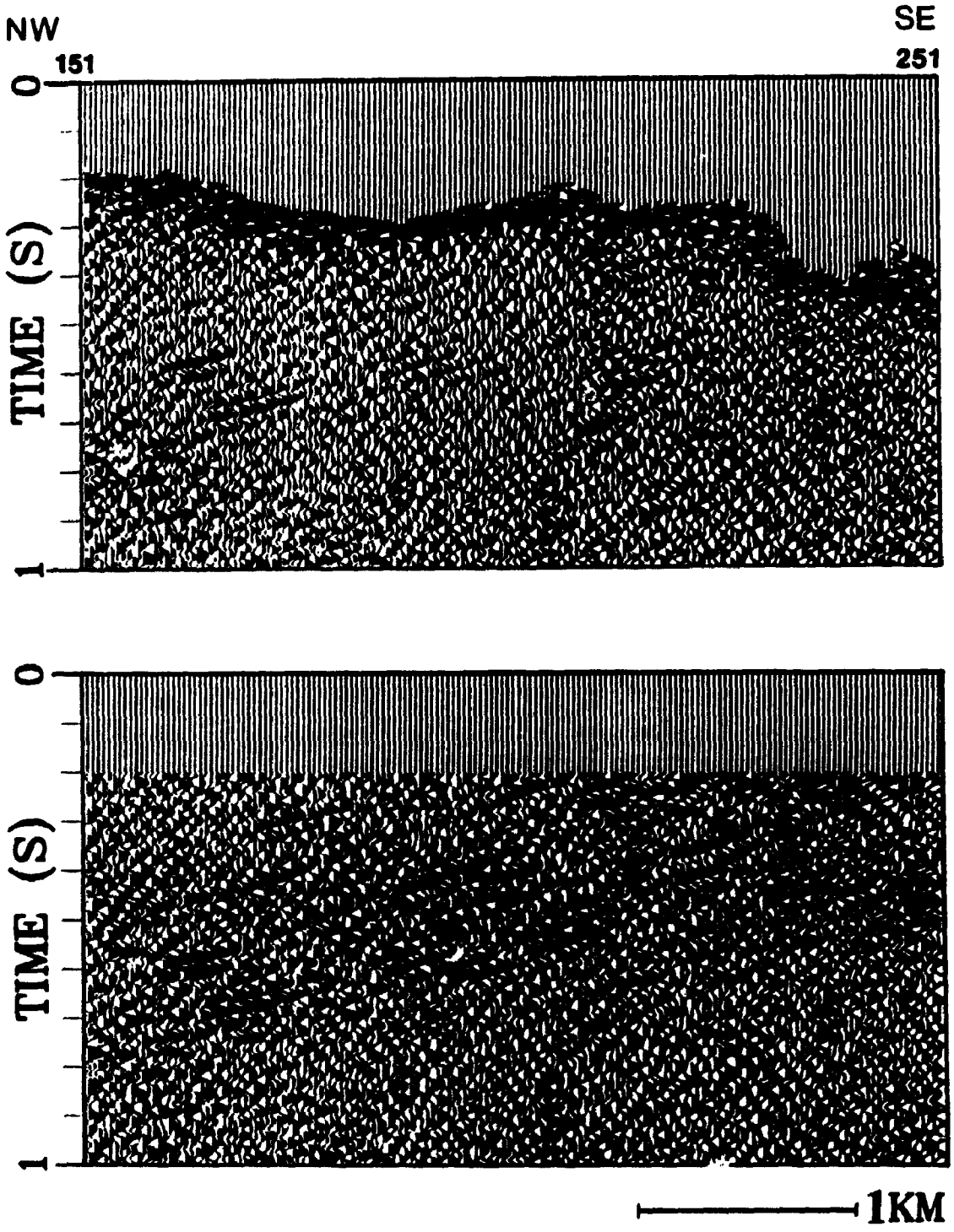

Fig. 4.14 Example to demonstrate the effect of different first arrival muting. Top: the selected seismic section processed with coarse first arrival muting. Bottom: the same section processed with careful first arrival muting.

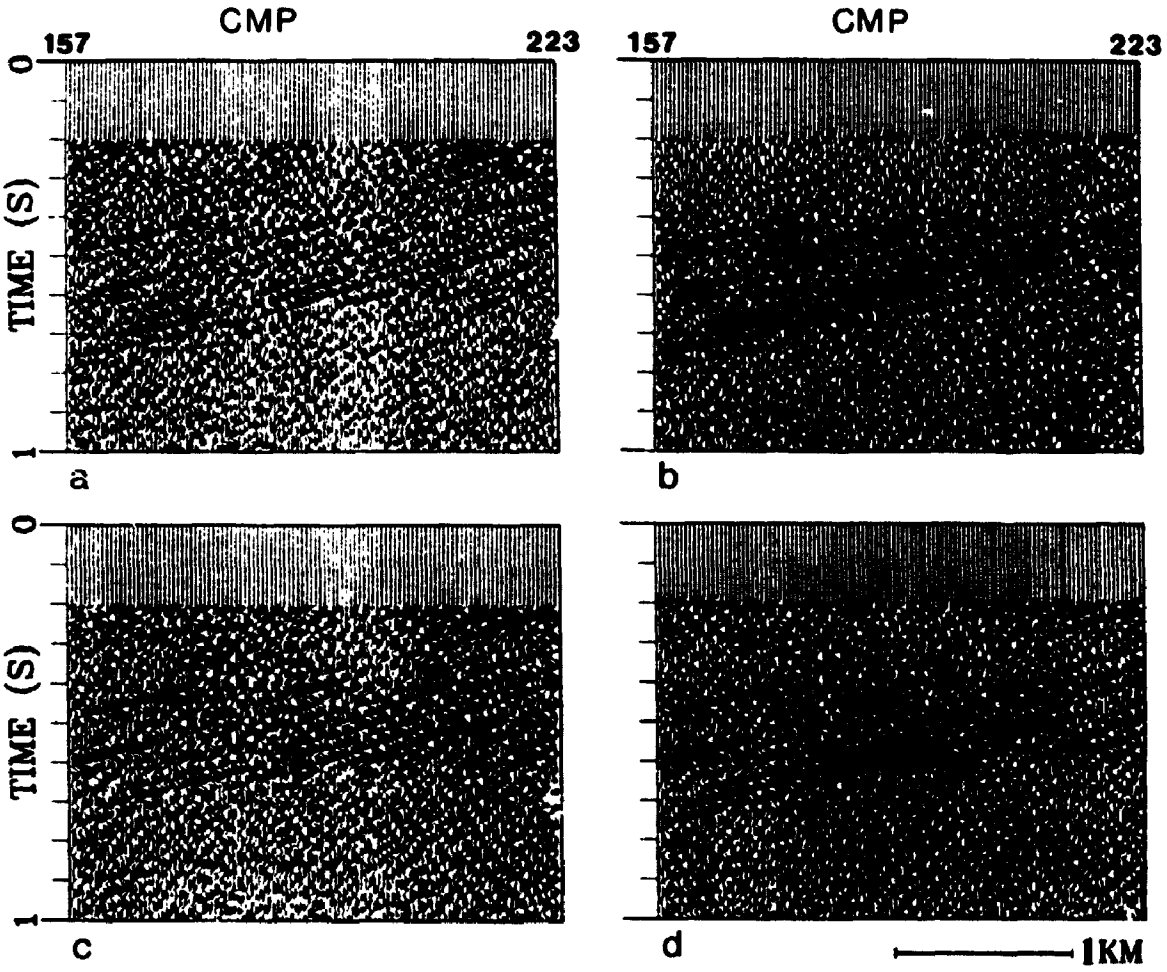

Fig. 4.15 Example to demonstrate the effects of refraction and surface-consistent residual static corrections for the north part of line 5: a) brute stack with elevation corrections only; b) brute stack with elevation and surface-consistent residual static corrections; c) brute stack with elevation and refraction statics; d) brute stack with elevation, refraction and surface-consistent residual statics.

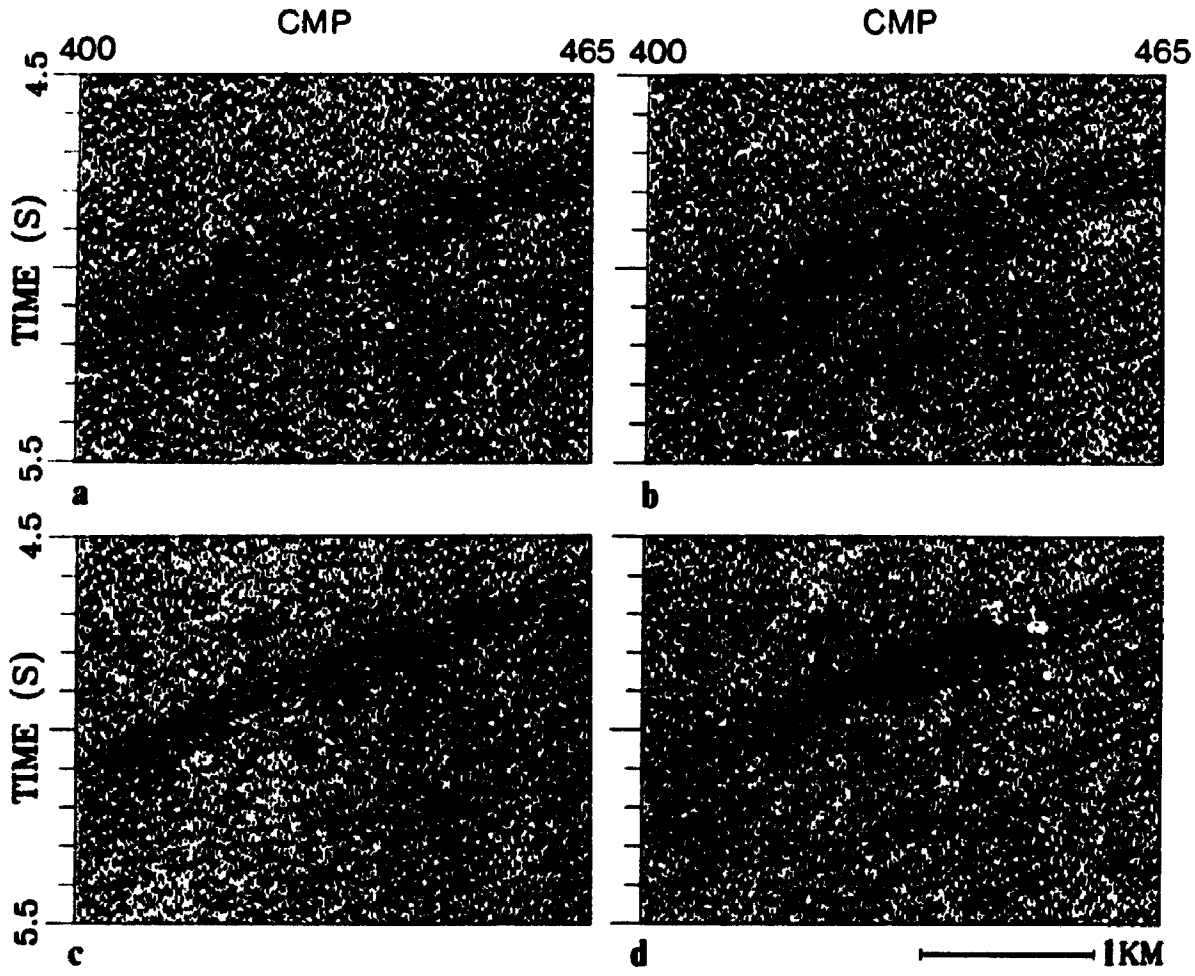

Fig. 4.16 Example to demonstrate the effects of refraction and surface-consistent residual static corrections for the south part of line 5: a) brute stack with elevation corrections only; b) brute stack with elevation and surface-consistent residual static corrections; c) brute stack with elevation and refraction statics; d) brute stack with elevation, refraction and surface-consistent residual statics.

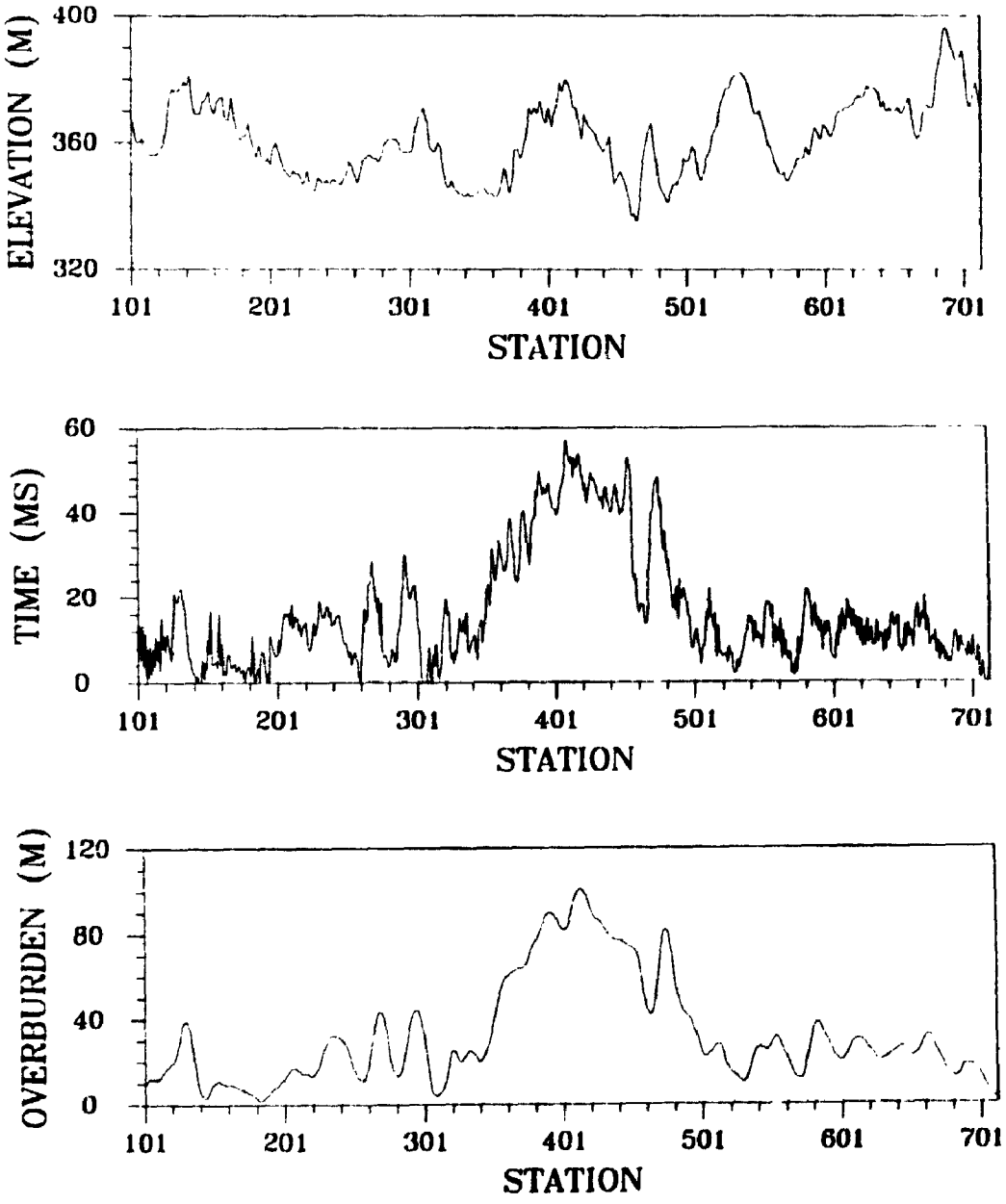

Fig. 4.17 Top: Elevation variations along line 5. Center: refraction static corrections along line 5. Bottom: overburden variations along line 5.

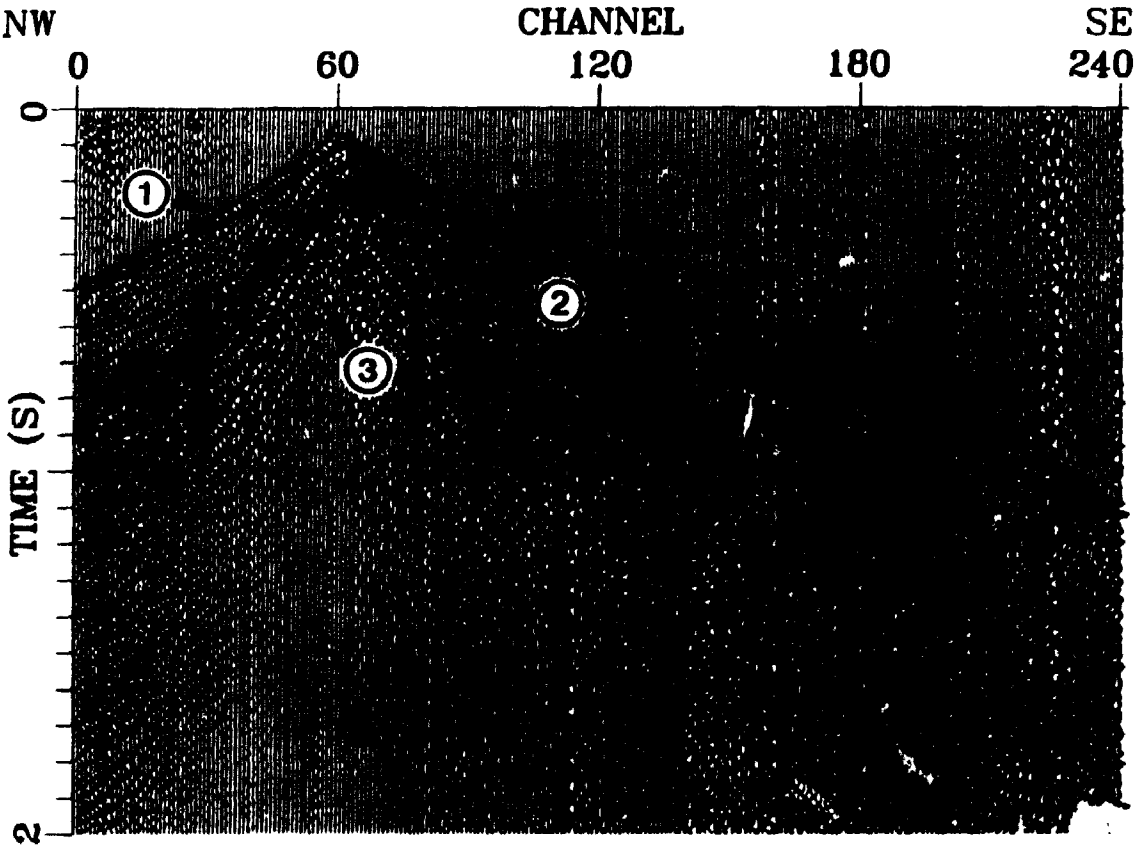

Fig. 4.18 The effect of F-K filtering (or velocity filtering) upon field data. a) A field shot gather (VP 203). 1 = first arrival, 2 = ground-roll noise, 3 = primary reflections. The section was plotted with trace normalization. No AGC gain was applied.

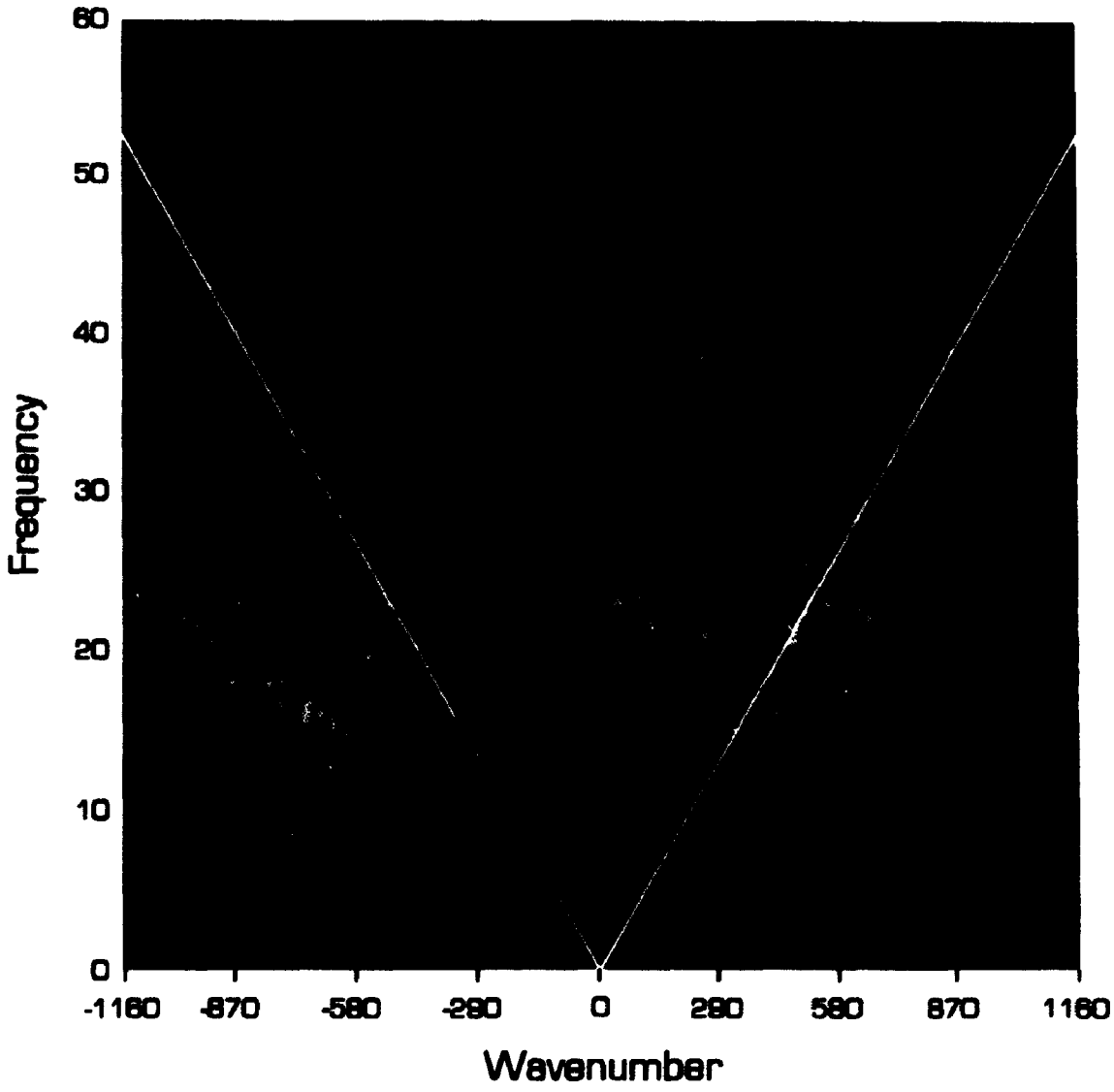

Fig. 4.18 b) 2-D F-K spectra of shot gather VP203.

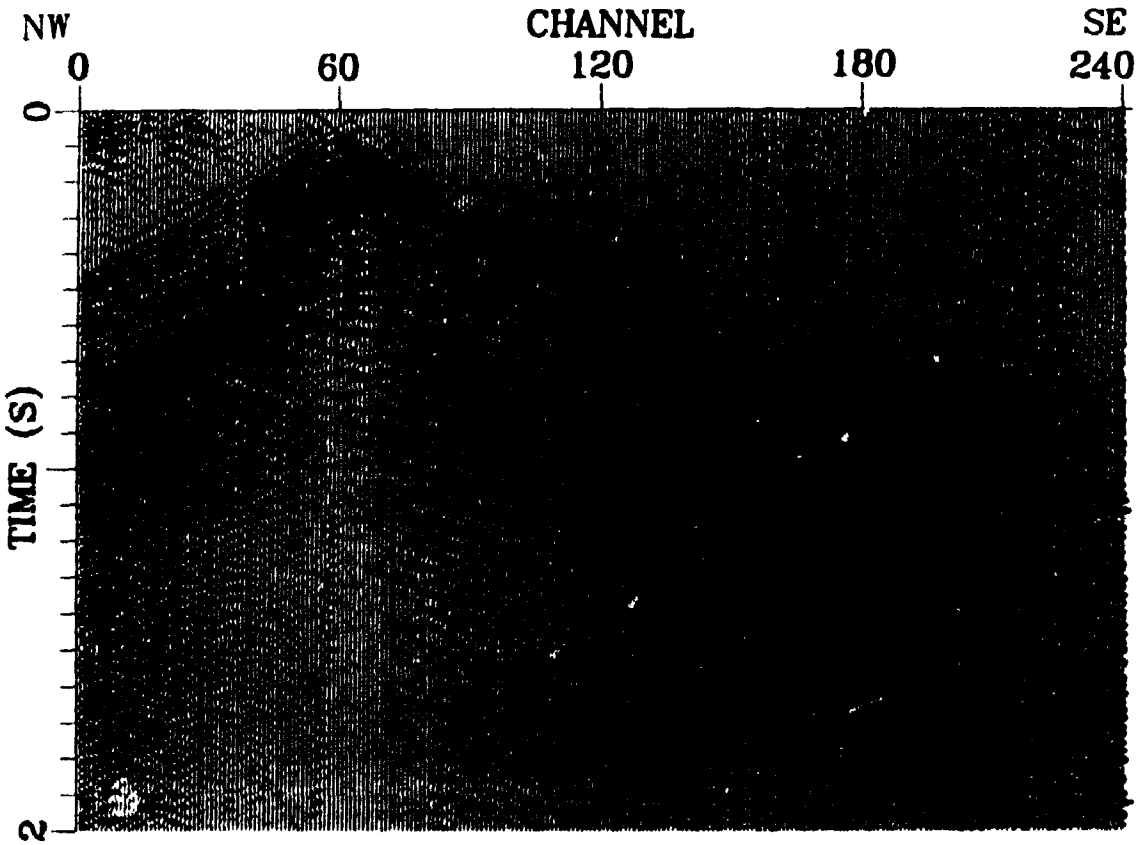

Fig. 4.18 c) The same shot gather with F-K filtering (the portions of F-K domain above the line). Note that most ground-roll noise is gone and more reflections are shown up.

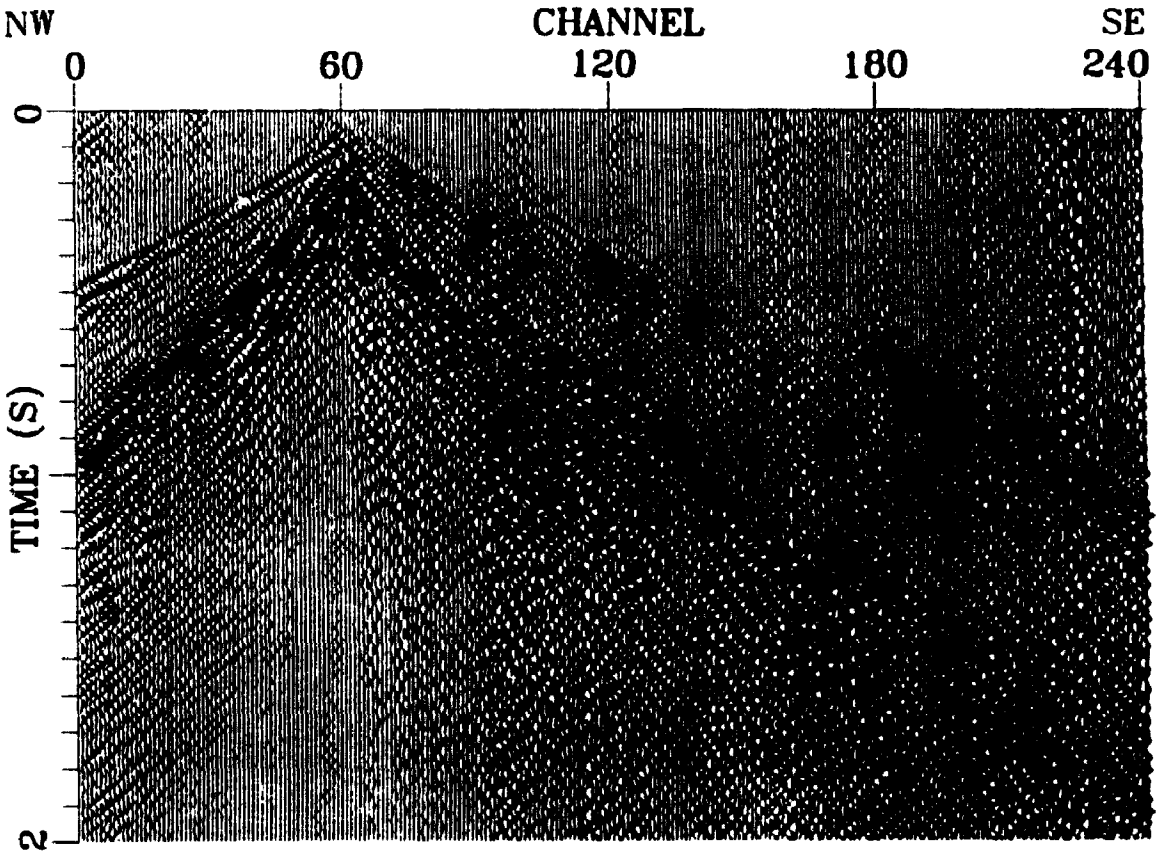

Fig. 4.18 d) The filtered portions of shot gather VP203 (the portions of F-K domain below the line). Note the strong ground-roll noise on the left side.

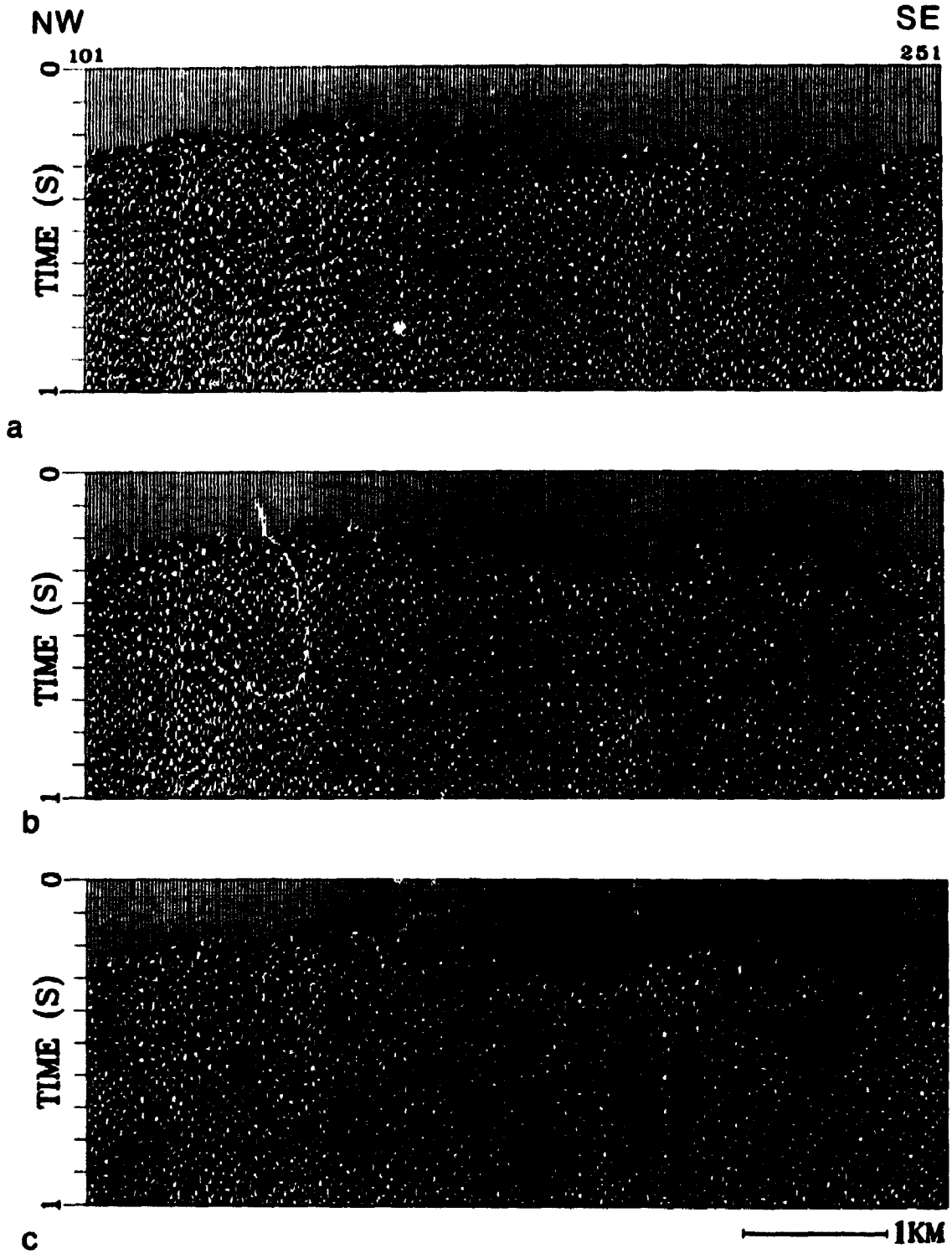

Fig. 4.19 Detailed comparison for the north part of line 5 where the Ivanhoe Lake fault zone is inferred from geological and aeromagnetic observations, illustrating step by step how the commercial image could be improved. a) The brute stack processed with the shot gather mixing 2:1. The processing flow is identical with the contractor's (see table 3.2). b) The brute stack processed from the data set consisting of every second shot gathers without any mixing. c) The brute stack processed from the whole data set without any mixing.

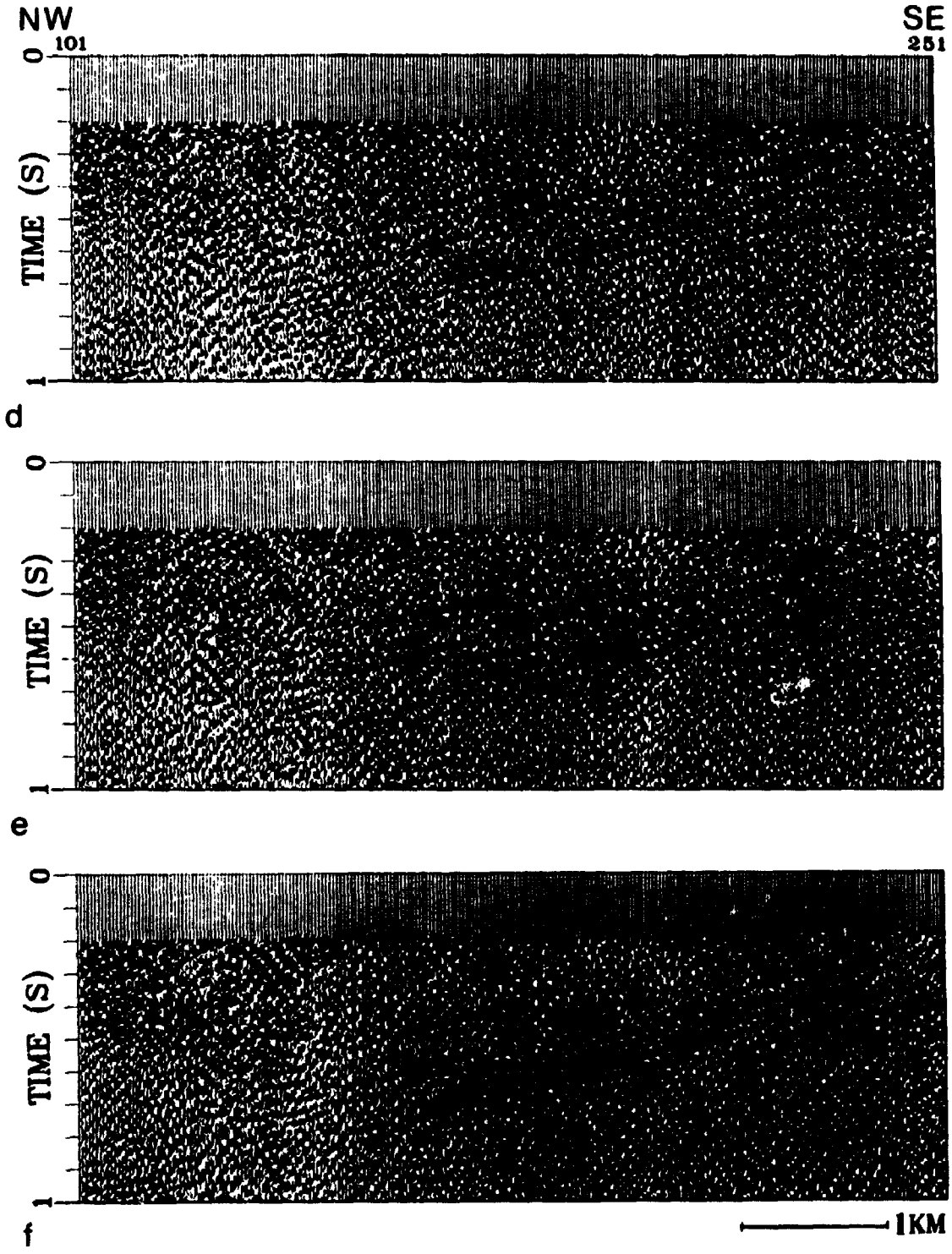

Fig. 4.19 d) The brute stack processed in the same way as (c) but with a more careful first arrival muting applied. e) The brute stack processed in the same way as (d) but with refraction statics applied. f) The brute stack processed in the same way as (e) but with surface-consistent residual statics applied.

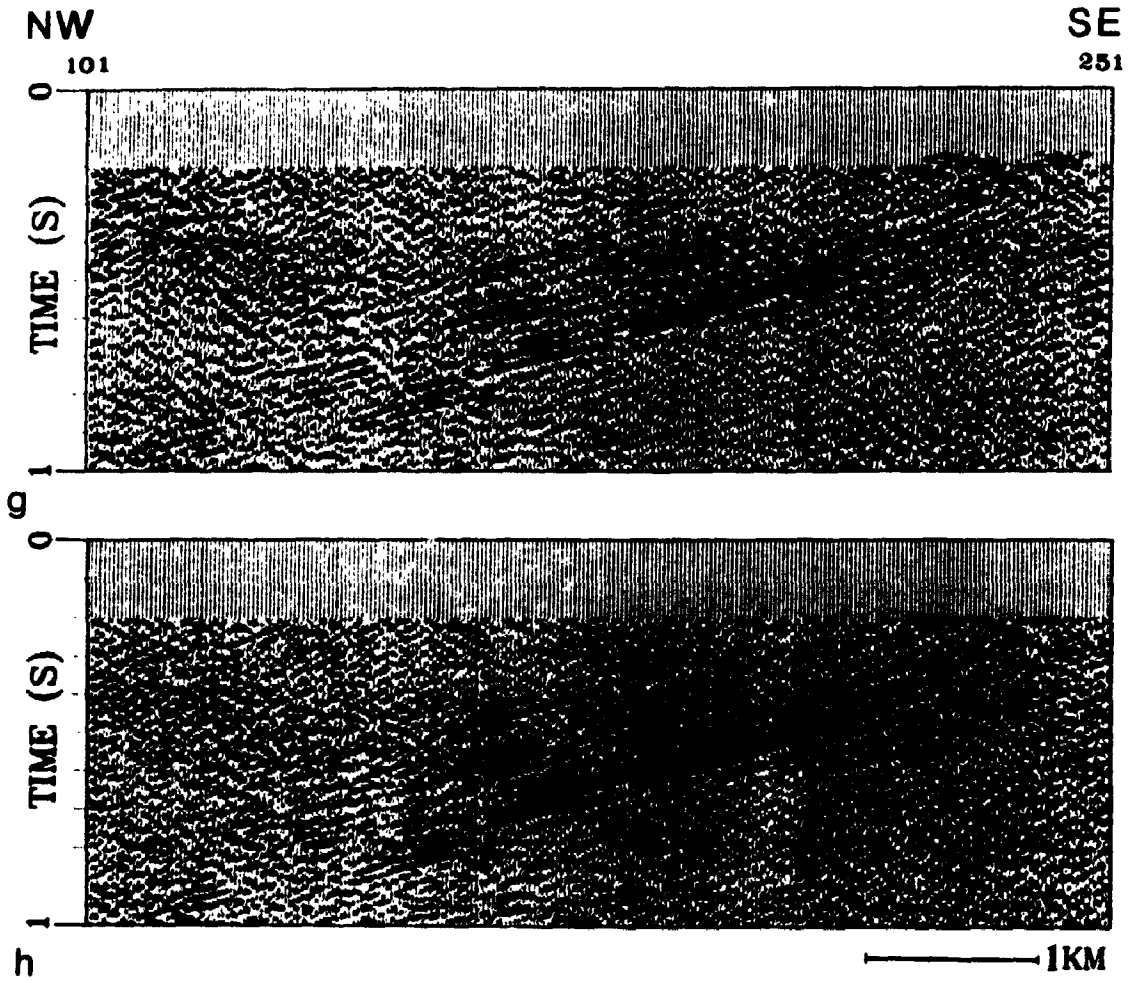

Fig. 4.19 g) The brute stack processed in the same way as (f) but with F-K filtering applied. h) The brute stack processed in the same way as (f) but with a deconvolution filtering applied.

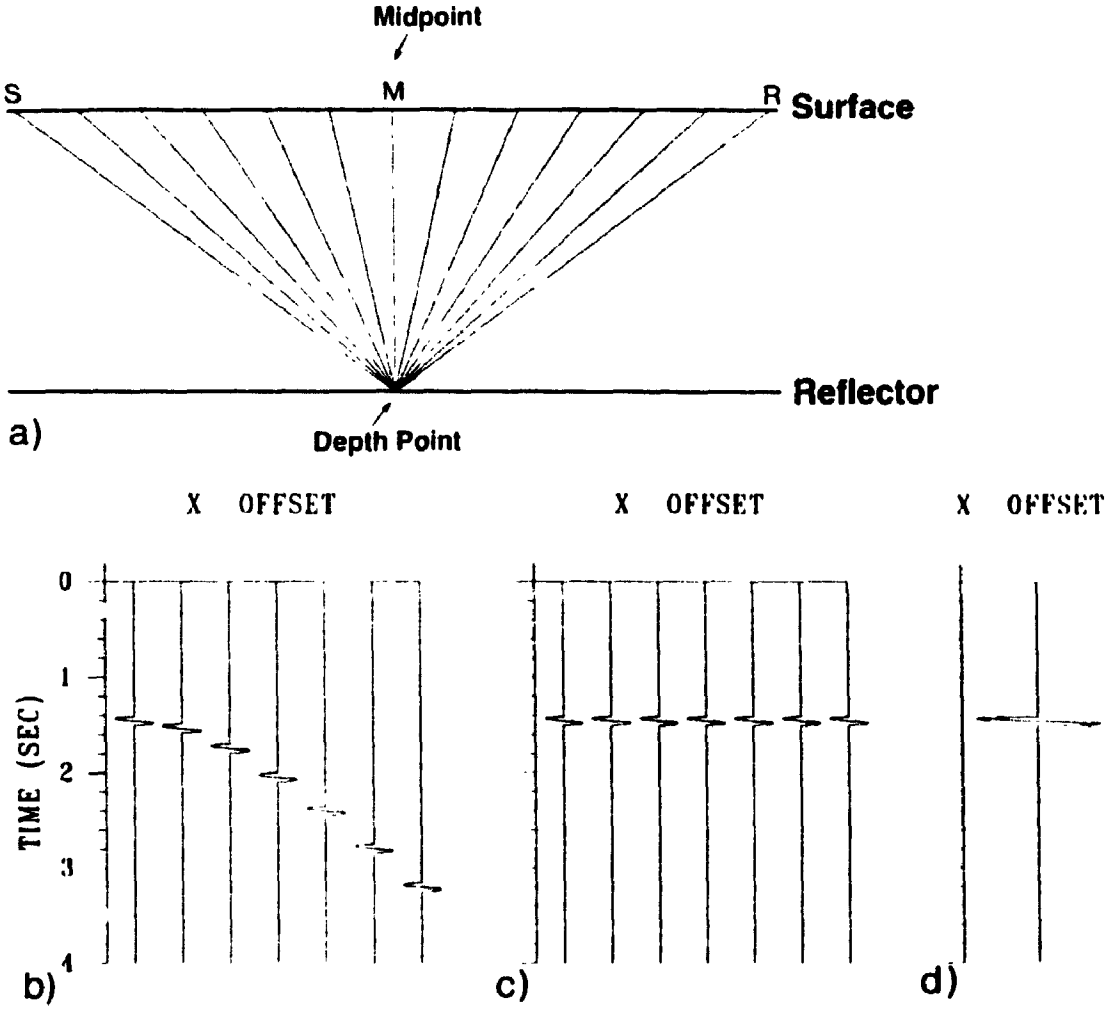

Fig. 4.20 a) Ray paths for reflections from a single point in common-depth-point shooting, assuming a constant velocity and horizontal interface. b) Synthetic CMP gather associated with the geometry in (a). Traveltime curve for a flat reflector is a hyperbola. c) The same CMP gather after NMO correction. By flattening reflections, stacking velocity can be precisely determined. c) After stacking to form a single CMP trace.

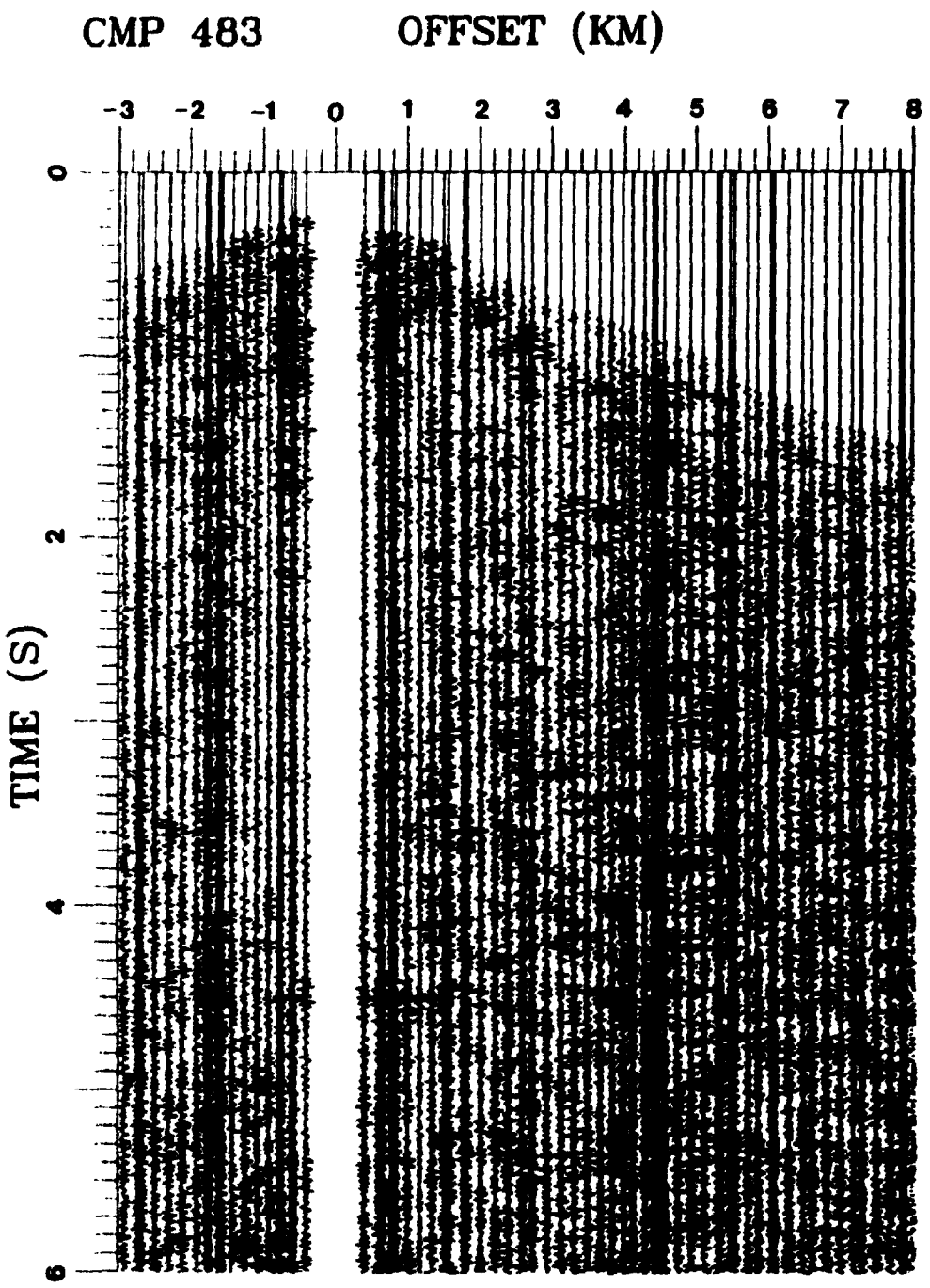

Fig. 4.21 A typical CMP gather (CMP 483) showing no reflections across entire gather. The data were AGC-gained.

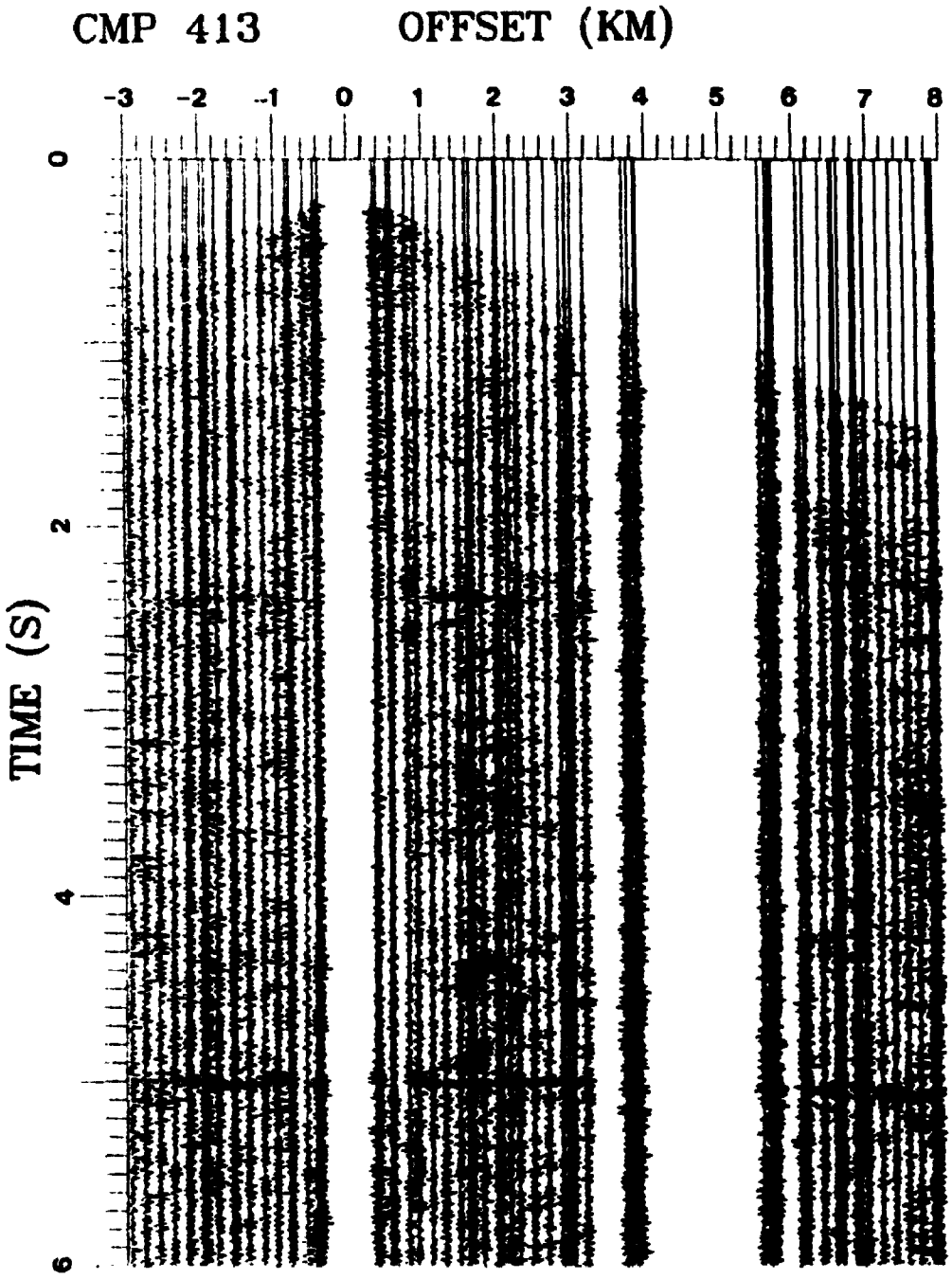

Fig. 4.22 a) CMP gather 413 showing good reflections. The data were AGC gained.

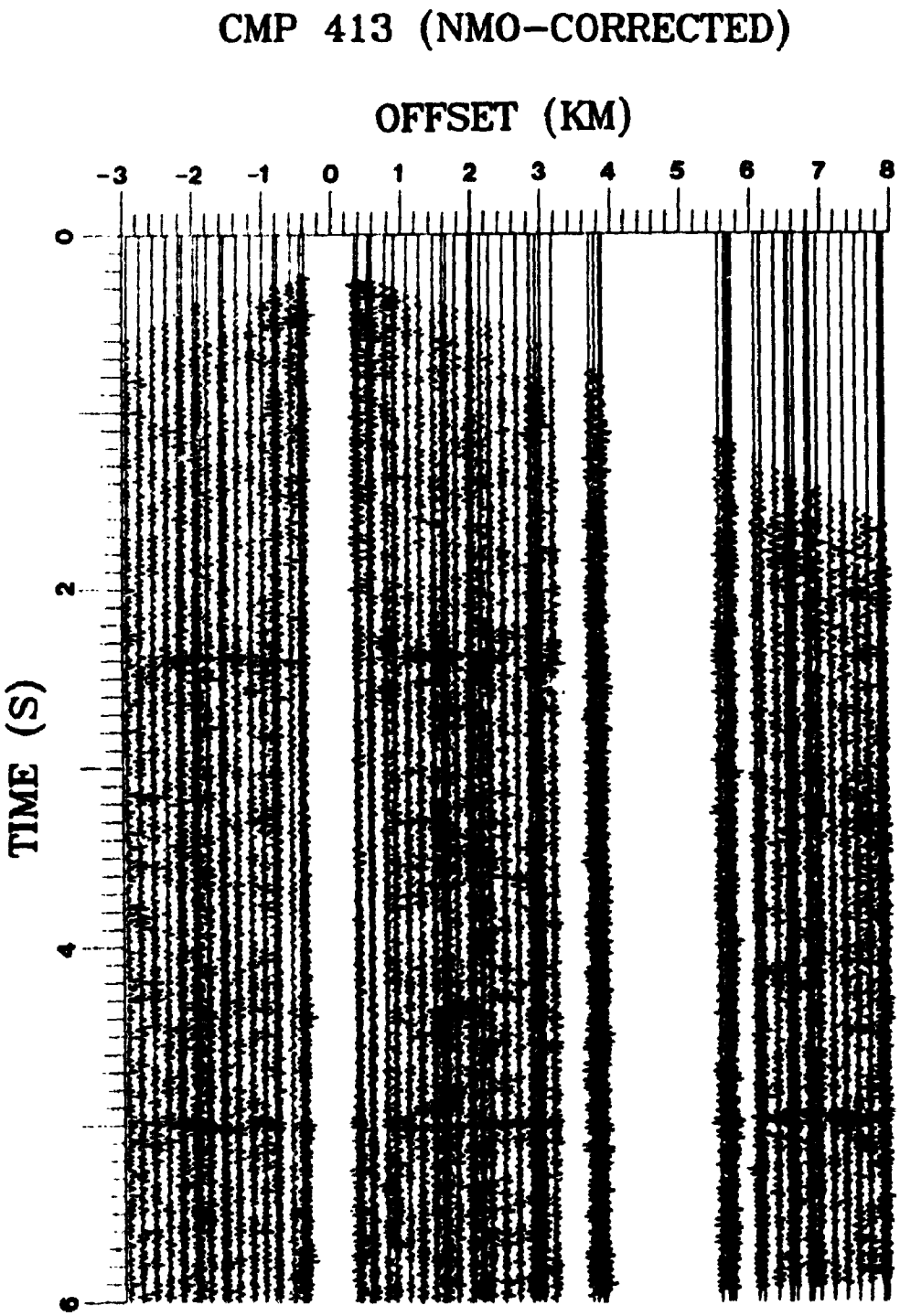

Fig. 4.22 b) CMP gather 413 after NMO correction. There is little correction for traces with offset < 3 km.

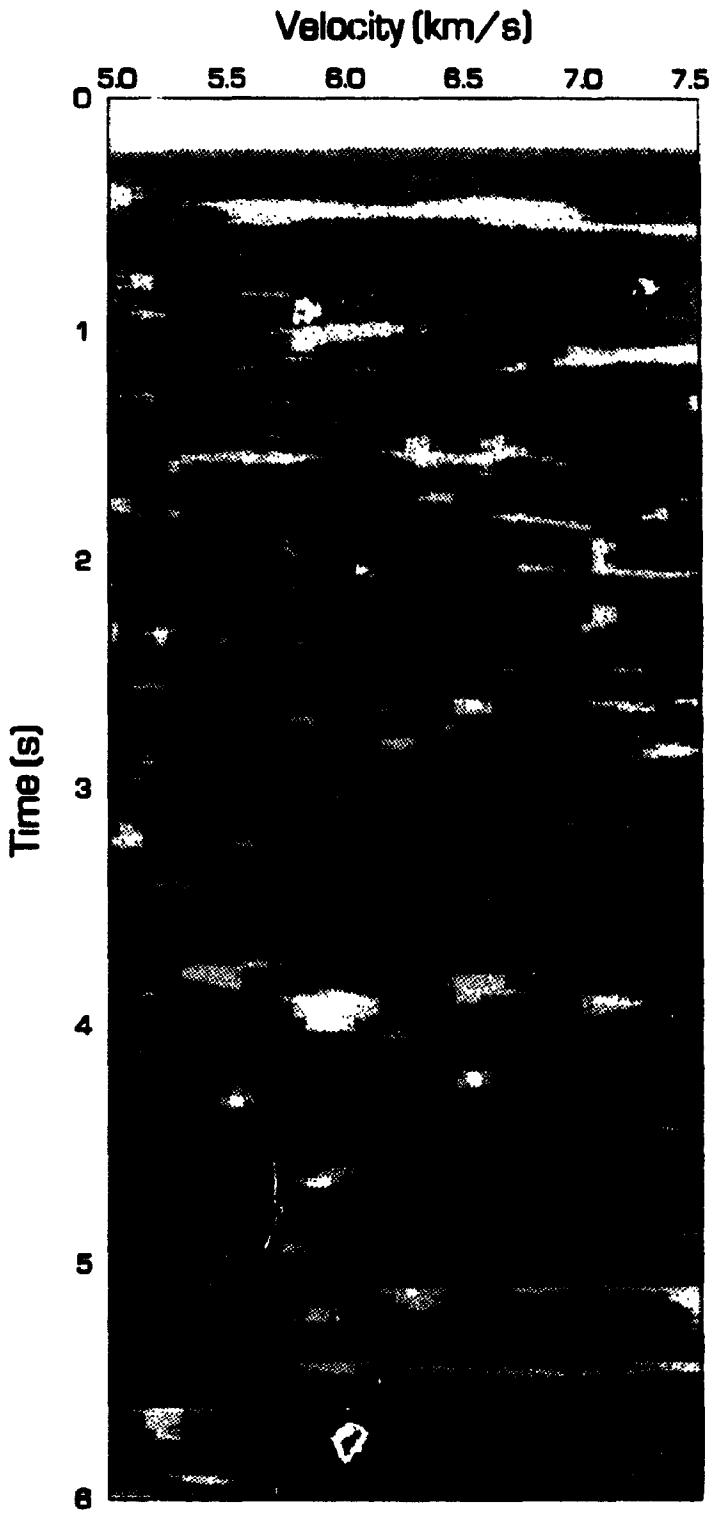

Fig. 4.22 c) Velocity spectra of CMP gather 413.

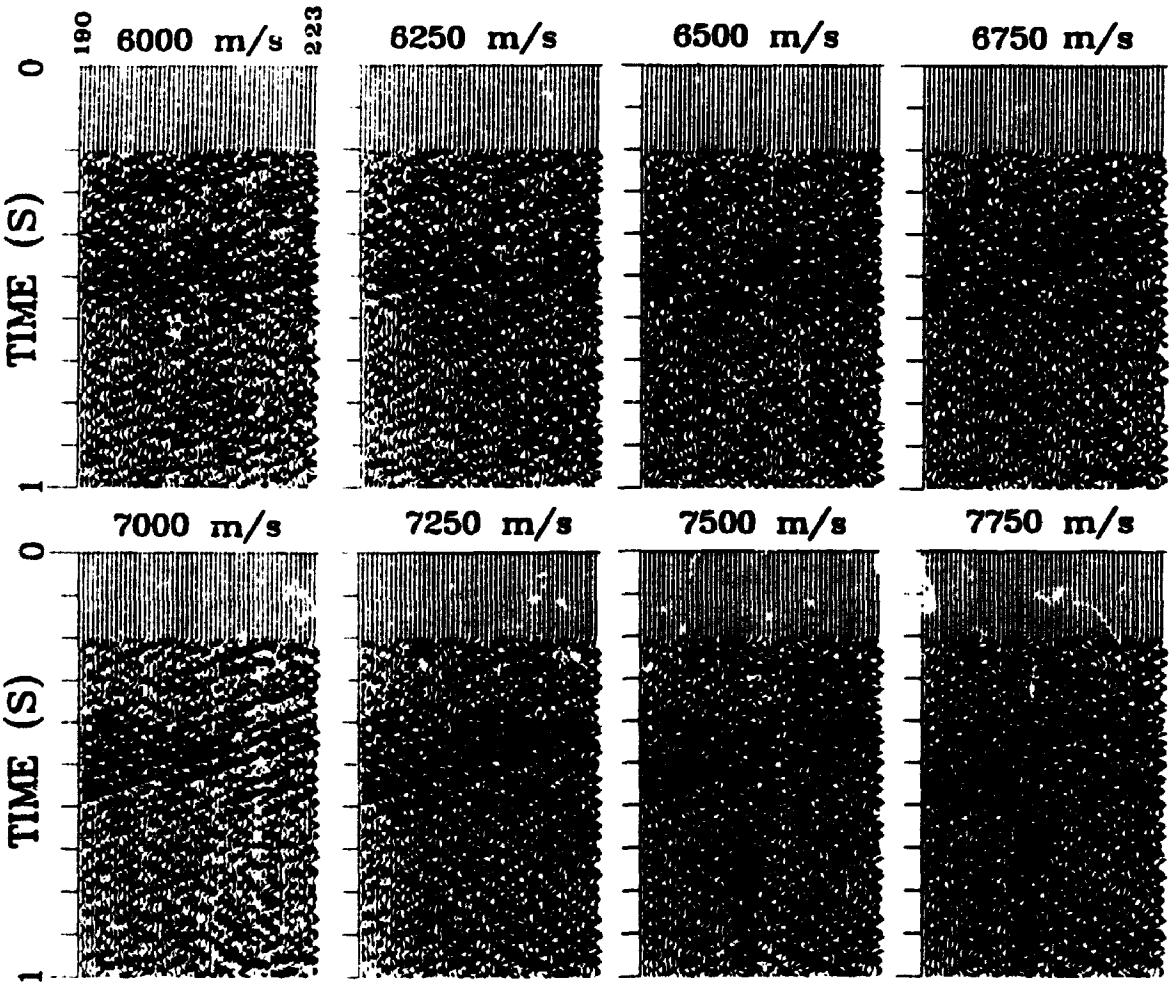

Fig. 4.23 An example to show the effect of stacking velocity. The brute stacks are processed with the constant velocities labelled at the top.

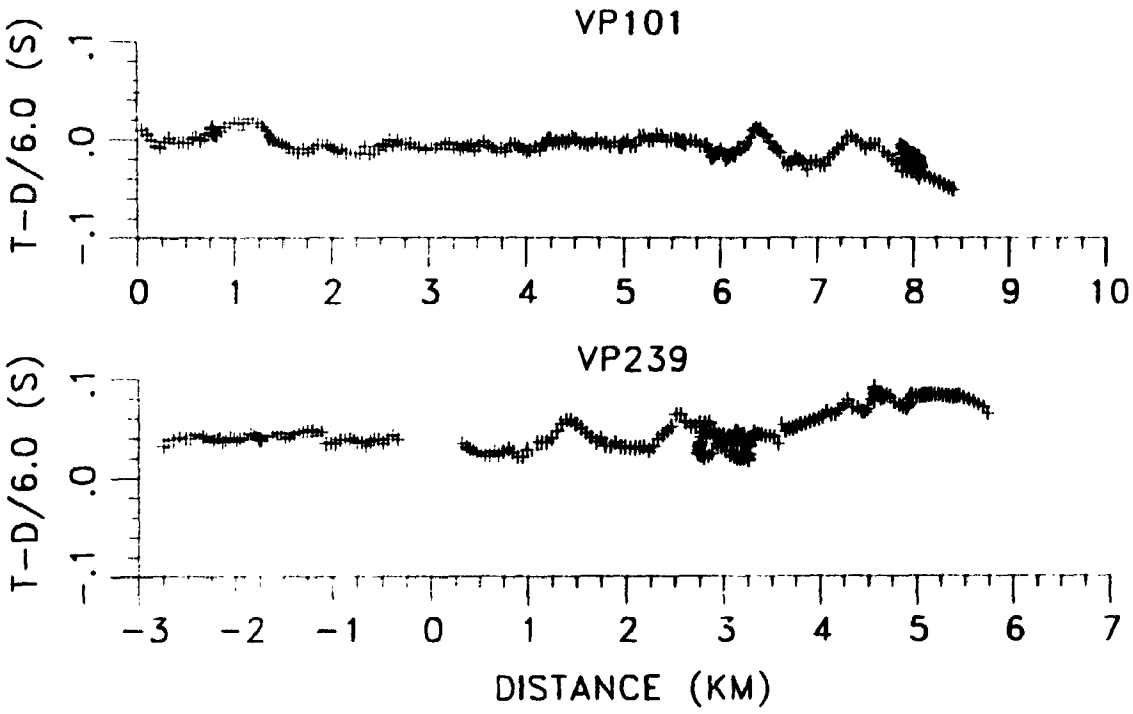

Fog. 4.24 Picked first arrivals from shot gathers VP 101 and VP 239 with a reducing velocity of 6 km/s used. Shotpoints are located at zero distance.

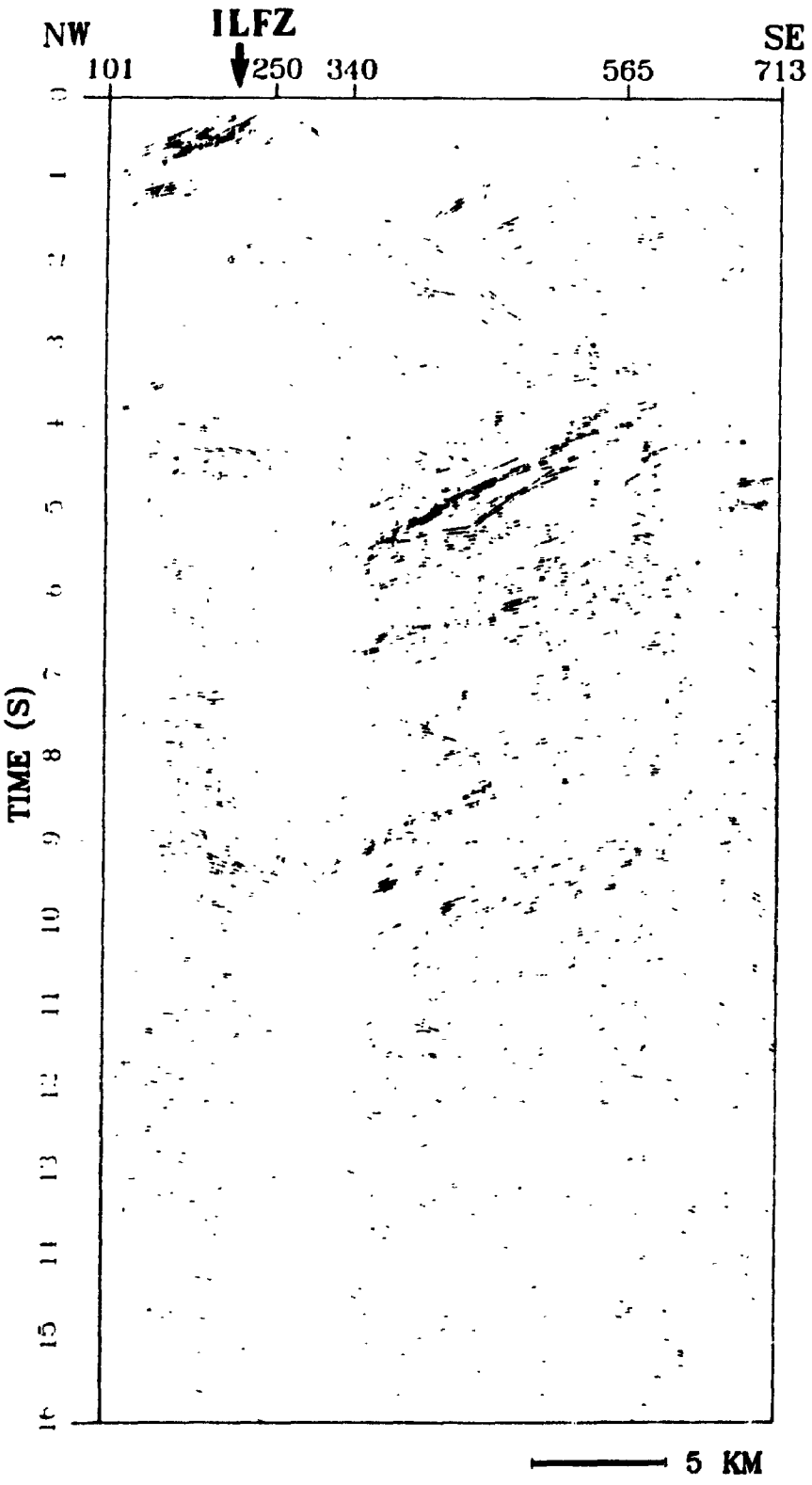

Fig. 4.25 The final brute stack of line 5 (coherence-filtered for display) with station numbers labelled at the top. The section is plotted 1:1 for average velocity of 6 km/s.

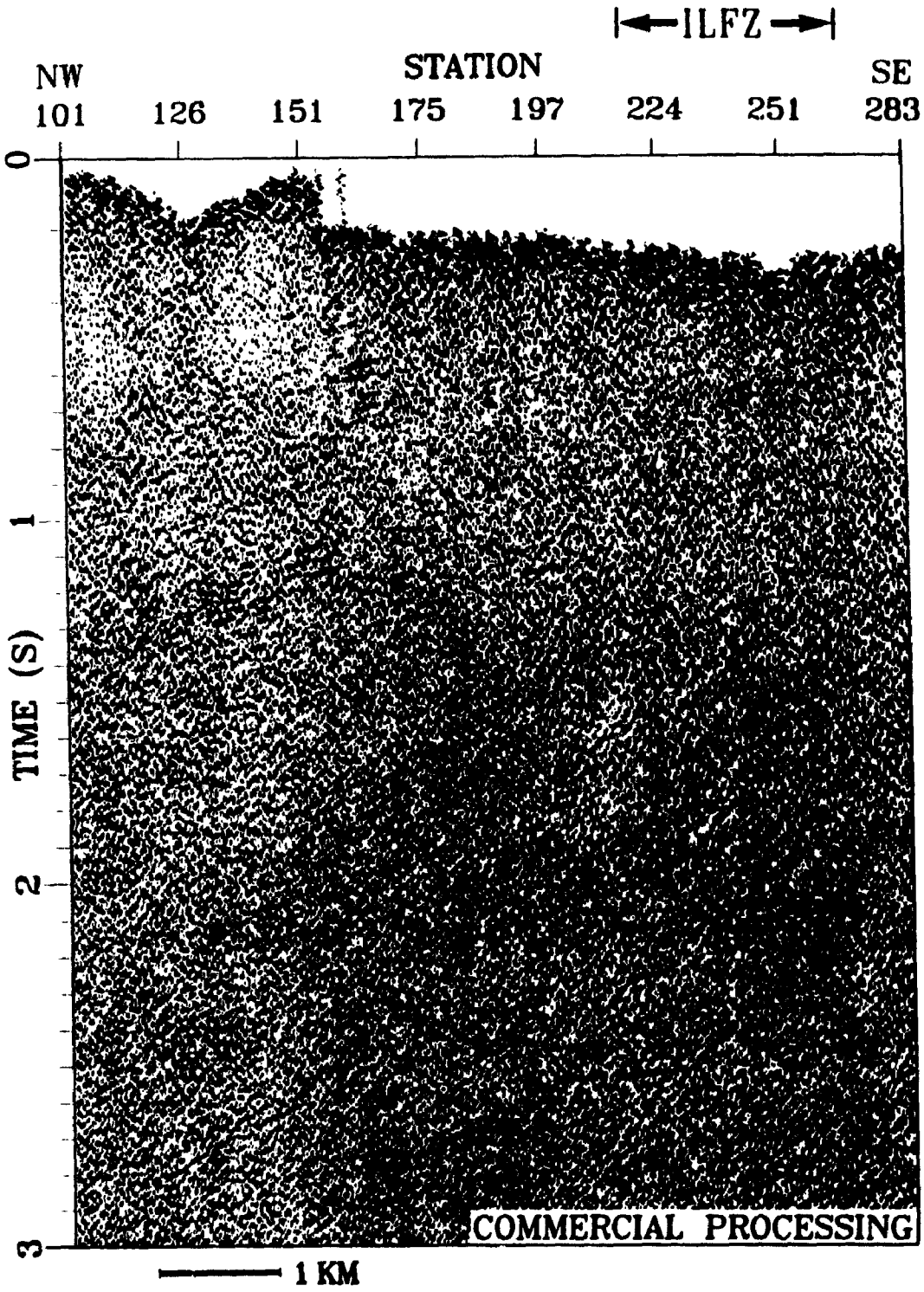

Fig. 4.26 a) The commercial image of the Ivanhoe Lake fault zone (ILFZ).

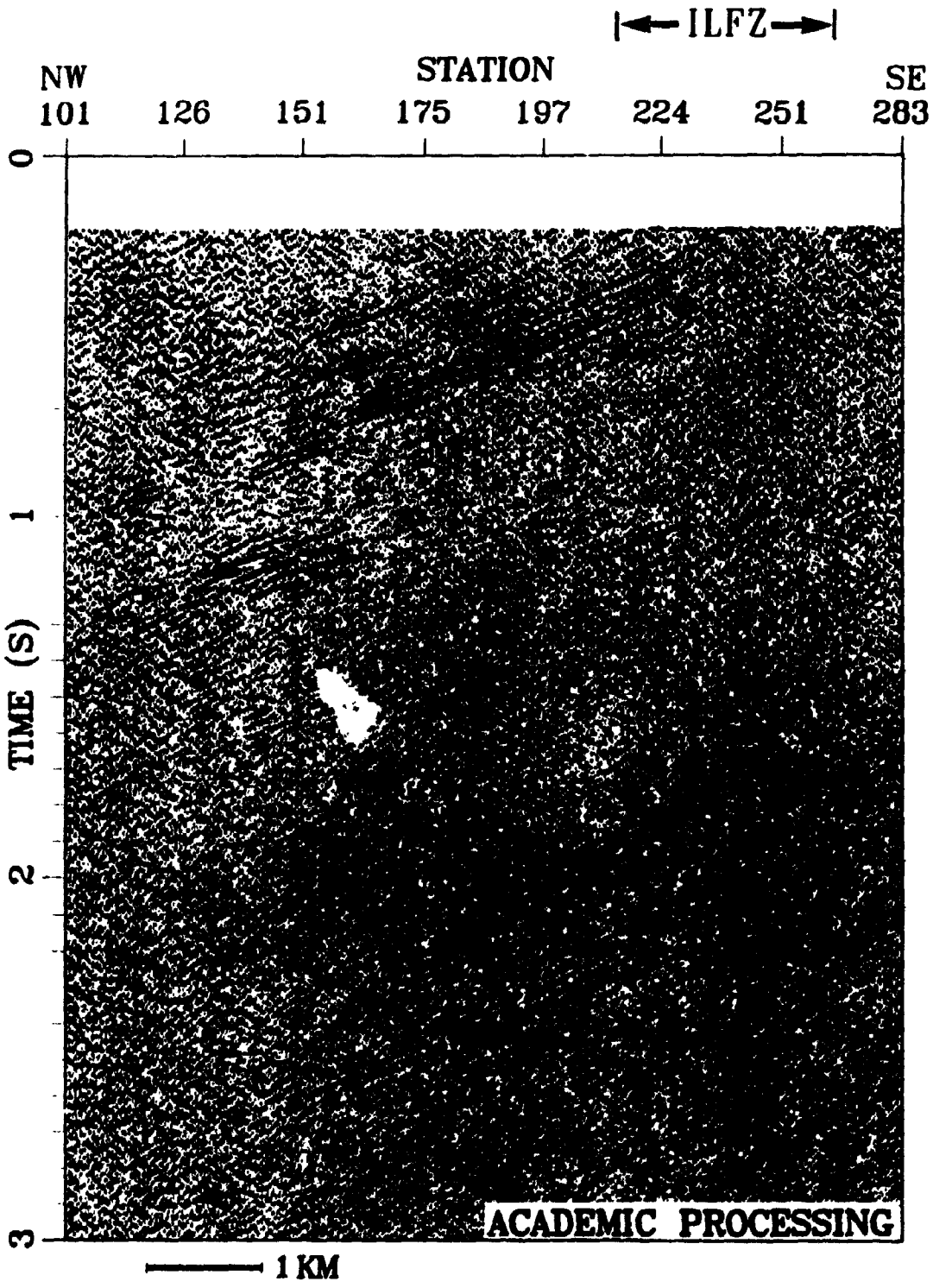

Fig. 4.26 b) The reprocessed image of the Ivanhoe Lake fault zone (ILFZ).

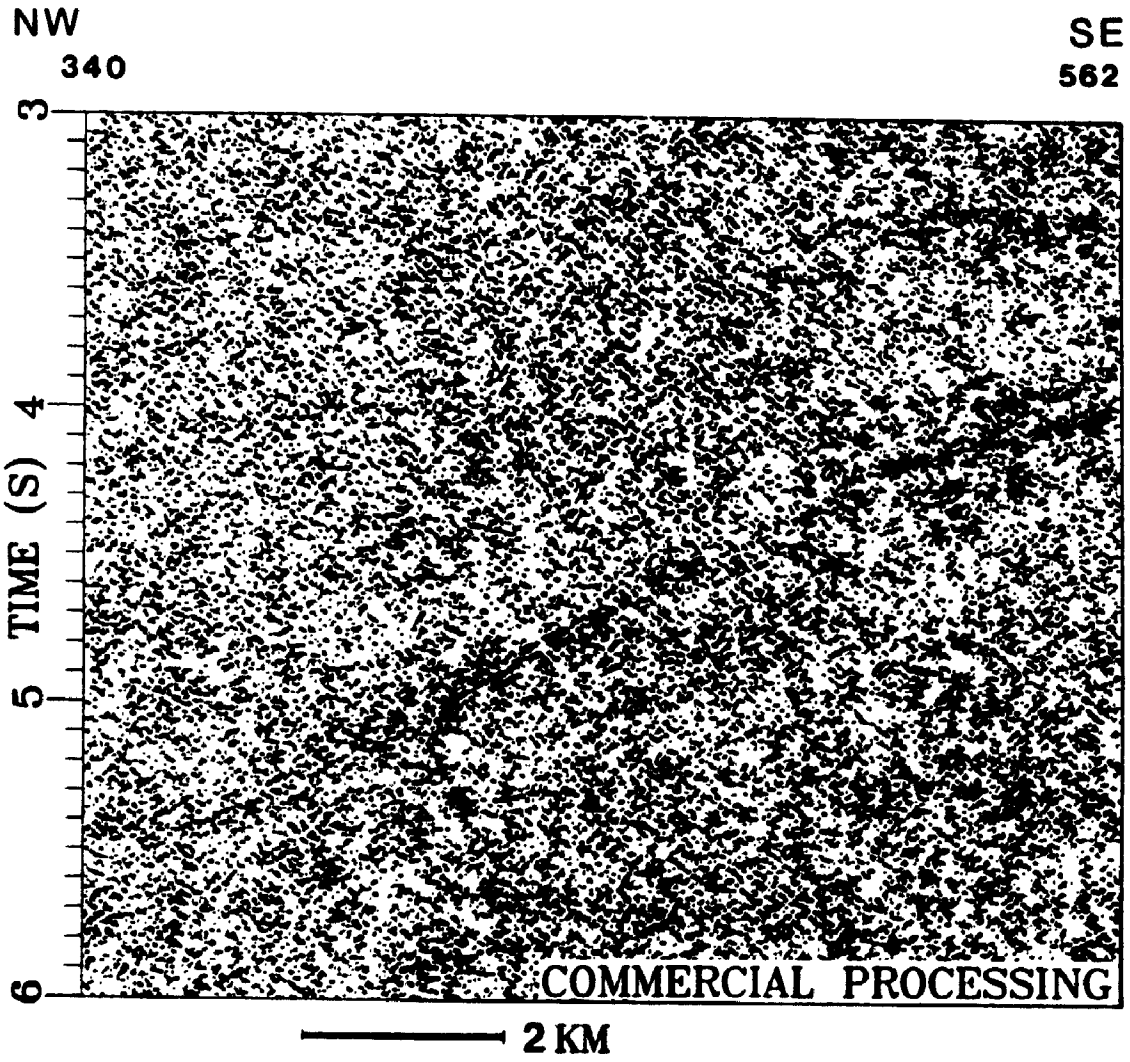

Fig. 4.27 a) The commercial image of the major midcrustal reflector.

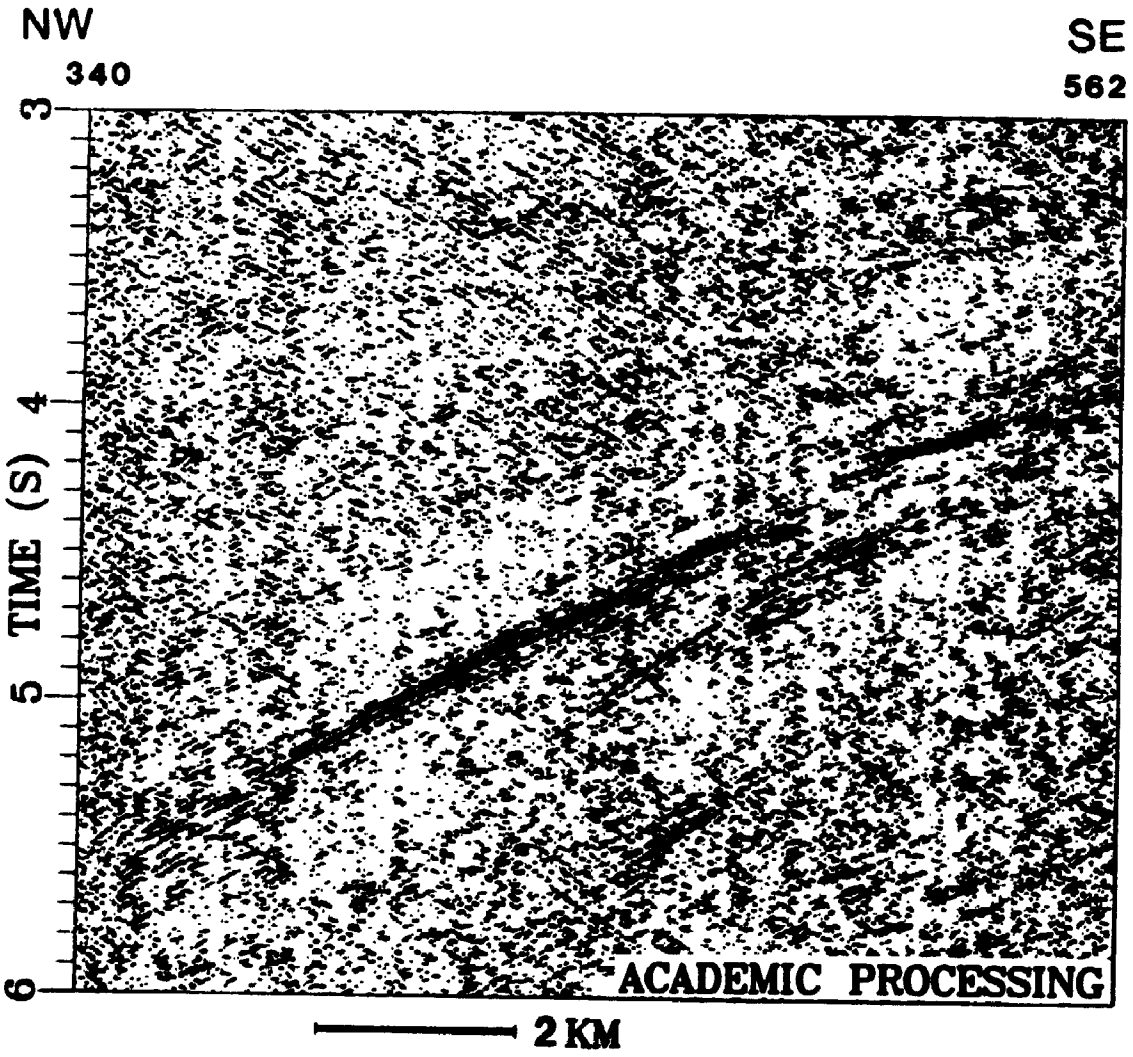

Fig. 4.27 b) The reprocessed image of the major midcrustal reflector.

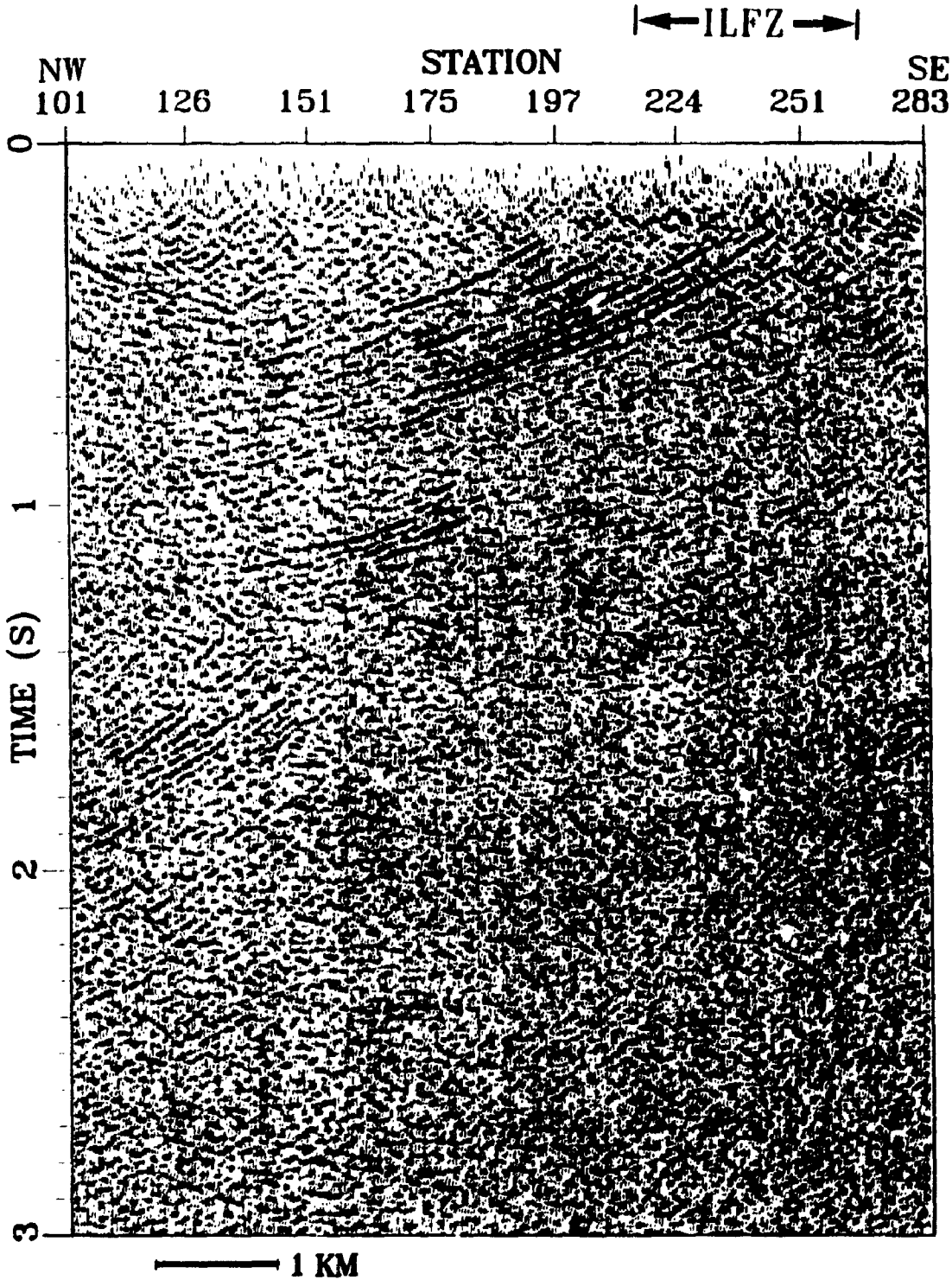

Fig. 4.28 The migrated images of the Ivanhoe Lake fault zone (ILFZ). a) migrated without coherence-filtering.

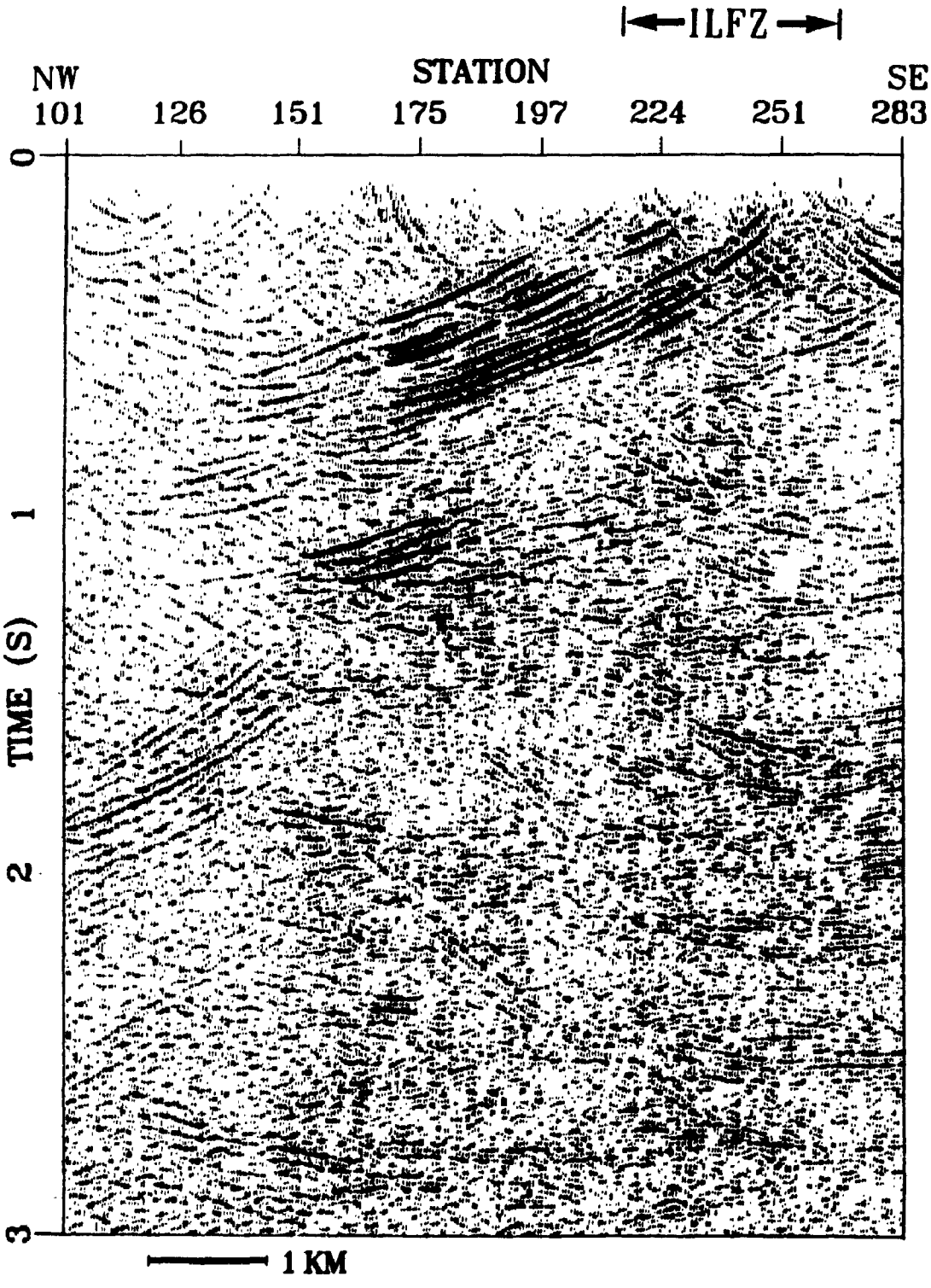

Fig. 4.28 b) migrated after coherence-filter applied.

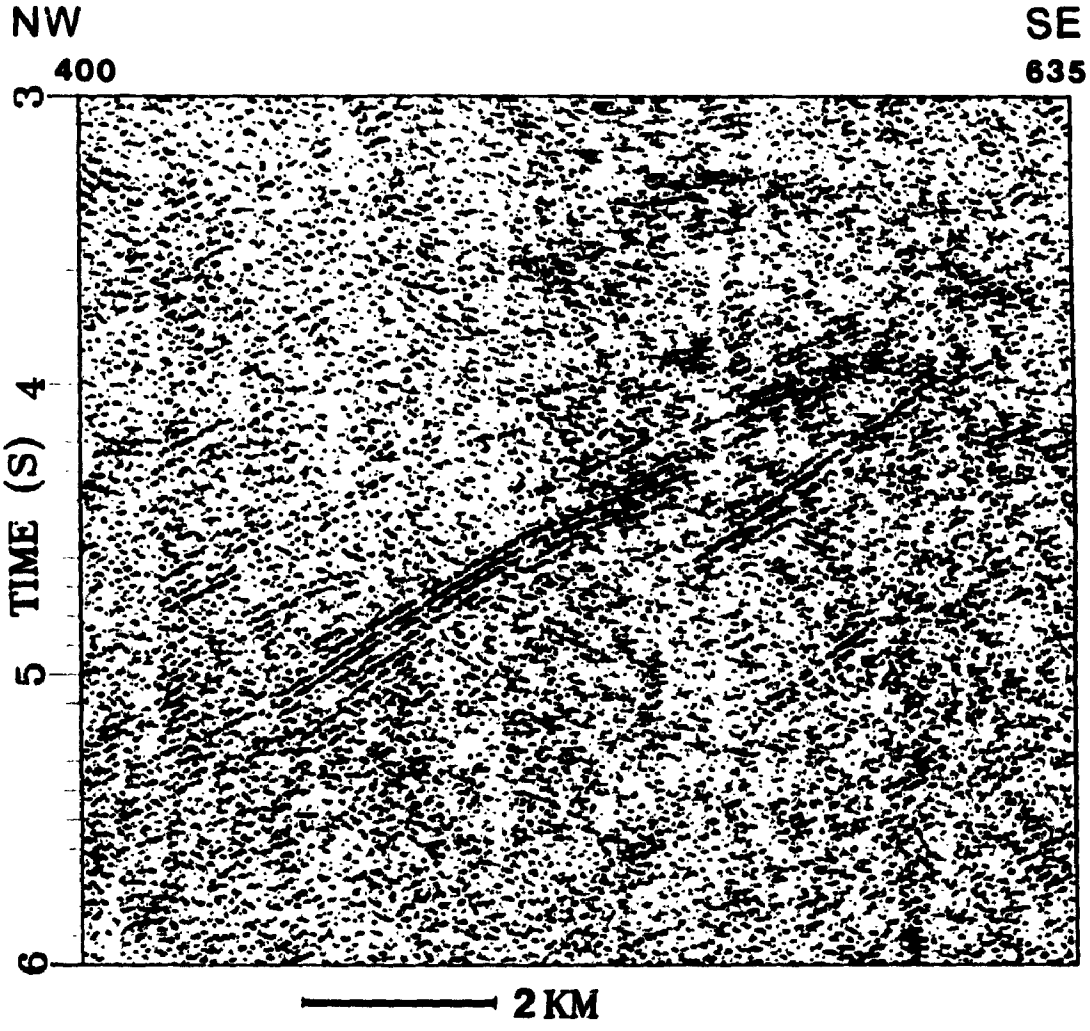

Fig. 4.29 The migrated images of the major midcrustal reflector. a) migrated with a constant velocity of 4.5 km/s.

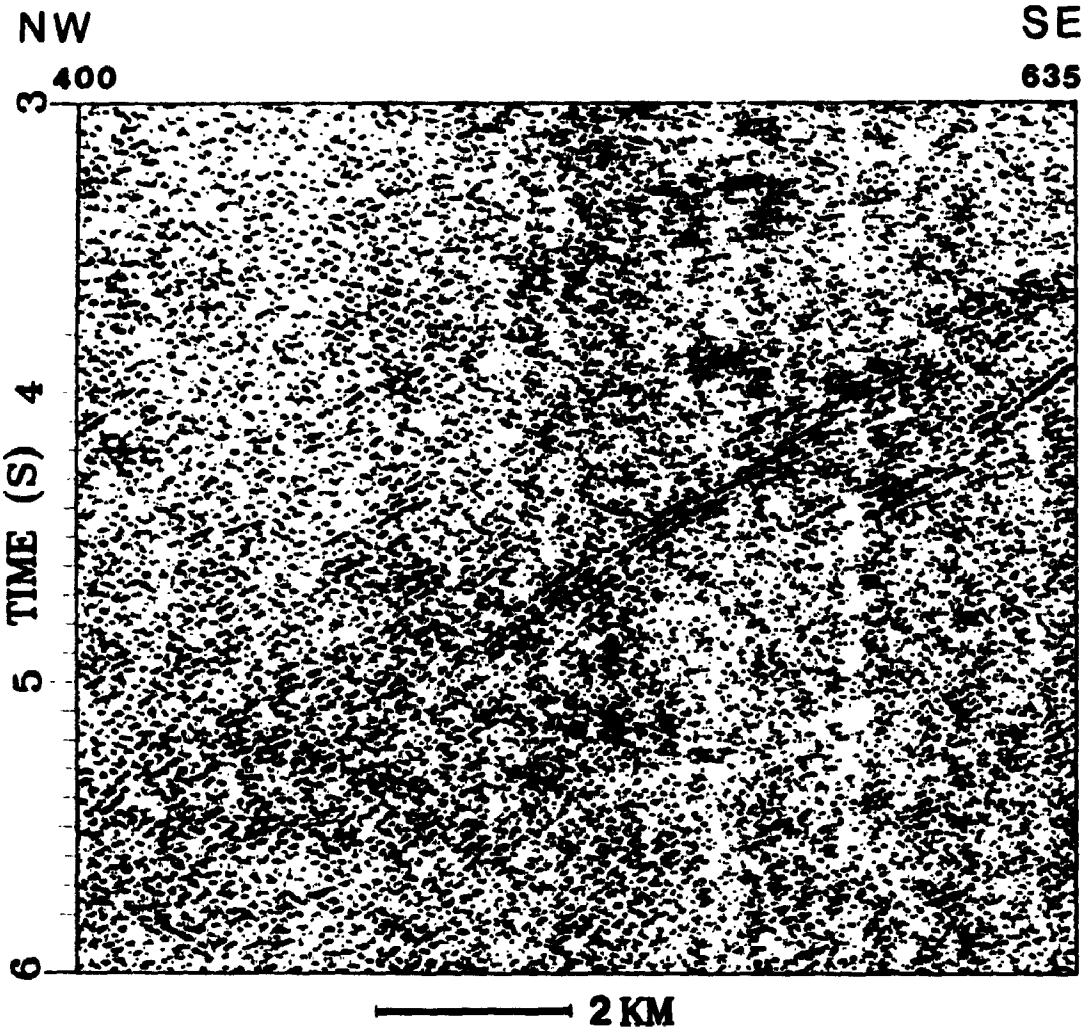

Fig. 4.29 b) migrated with a constant velocity of 5 km/s.

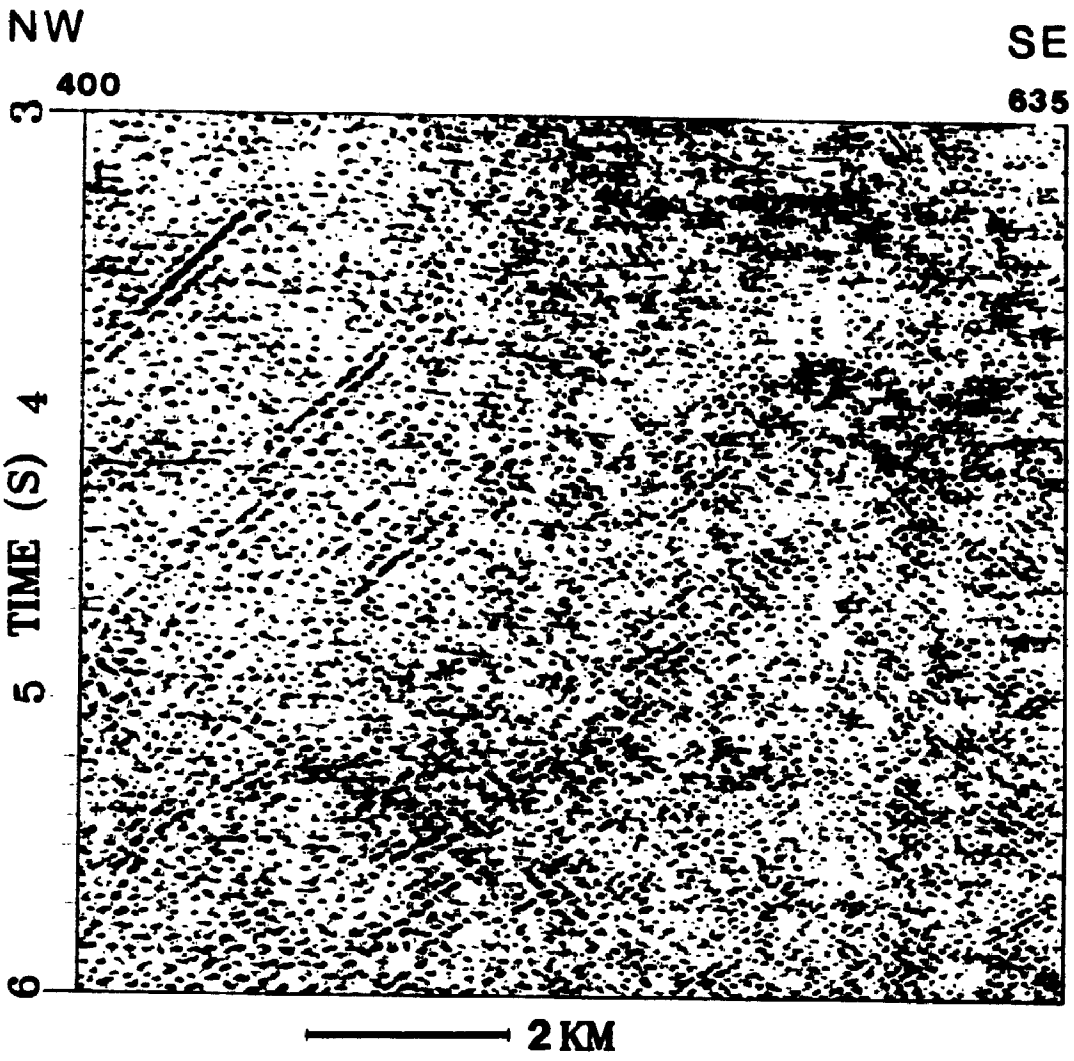

Fig. 4.29 c) migrated with a constant velocity of 6 km/s.

CHAPTER 5

2-D TOMOGRAPHIC IMAGING OF THE IVANHOE LAKE FAULT ZONE

5.1 Introduction

Multiple coverage seismic reflection data provide an important source of information on the shallow structure associated with the Ivanhoe Lake fault zone (ILFZ). However, seismic reflection data do not tell us a great deal concerning the seismic velocity of crystalline bedrock within the ILFZ, which may be crucial in correlating seismic reflection results with surface geology. First arrivals are known as an important source of in situ bedrock velocity, but they are usually muted in seismic reflection data processing due to stacking technique being applied. In an attempt to determine the shallow velocity structure of the ILFZ and to see how well it will correlate with the seismic reflection results, a 2-D tomographic inversion of multiple first arrivals picked from the field shot gathers was performed. In this case, the focus is the north part of line 5 (between stations 101-241, Fig. 4.1), where the ILFZ seems clearly mapped on the seismic section (Fig. 4.22b).

5.2 Tomographic Inversion

In general, the field shot gathers are of high quality (Figs. 4.2-4.6). First arrivals can be easily and accurately picked with an uncertainty of no more than 12 msec (three sampling points) for most traces. Technical details on first arrival picking are provided in appendix B. In order to eliminate weathered layer effect, first arrivals were initially corrected for refraction statics, calculated during the reprocessing of line 5. Two sets of corrected first arrivals are shown in Fig. 5.1. A total of 1500 first arrivals from 18 field shot gathers, every fifth shots between stations 101-

255, was used in the inversion. It is assumed that surface recording geometry could be approximated by a straight line for each common shot gather, if absolute offsets are used rather than nominal offsets. While the error, caused by crooked line geometry, is certainly present, it is believed to be minimized by utilizing multiple coverage first arrivals.

Seismic tomography is primarily a tool for processing transmitted seismic energy (seismic refractions) and is widely used for reconstructing the velocity structure of a desired target. The main advantage of tomographic inversion over trial-and-error forward modeling is that it is less subjective. The details of surface seismic refraction tomography have been discussed by Dines and Lytle (1979), Cassell (1982), Bishop et al. (1985), Bording et al. (1987), White (1989). The tomographic inversion method used in this study follows closely that of Hamilton (1991). Two main components of this method are ray tracing and the inversion algorithm.

Forward ray trace modeling is necessary because differences between observed and model times are used to infer nodal velocity updates in each triangular cell. Within a given cell, a velocity gradient is established in order that all ray paths traveling through it are arcs of circles. This modeling method is described fully by Mereu (1990).

The inversion algorithm used here is a damped singular value decomposition (SVD) routine. A matrix **A** of partial travel time derivatives is constructed such that the following system of equation is satisfied:

$$\mathbf{Ax} = \mathbf{b}$$

As such, A_{ij} is $\frac{\partial T_i}{\partial V_j}$, where ∂T_i is the travel time perturbation from the i^{th} ray observed when the j^{th} nodal velocity ∂V_j is perturbed. The travel time differences at each station ($t_{observed}$ - t_{model}) are contained in **b**, and the

velocity updates are found in **x**.

The initial velocity model is updated with the **x** solutions iteratively until the RMS travel time misfit is in the neighborhood of the anticipated uncertainty. As well, the nodal values are smoothed after each update. This allows for easier subsequent ray tracing. The final RMS value - once the updates have concluded - is divided by the number of rays traced, yielding an average model misfit.

Inversion of the first arrivals was performed in close collaboration with Dave Hamilton using a set of computer programs developed by him. In order to minimize any possible bias which may affect the final velocity model, the inversion was implemented without using any geological and/or geophysical constraints, including the seismic reflection images. A simple, three-layer model comprising 101 cells was used with starting velocities of 6.0 km/s at the surface and 6.5 km/s at a depth of 1200 m (Fig. 5.2). The surface layer was modeled first and fixed before proceeding to the deeper region. The RMS/ray misfit for the complete, final model was ~1 msec/ray, well within the anticipated uncertainty of ~5 msec/ray.

5.3 Near-Surface Velocity Structure

The final 2-D tomographic image of the Ivanhoe lake fault zone is shown in Fig. 5.3. Due to the lack of seismic ray coverage, the velocity below 1200 m cannot be determined with much confidence. Both ends of the velocity model lack reversed ray coverage and are therefore less reliable than the center part. The most prominent aspect of the tomographic model is the west-dipping high velocity (≥6.4 km/s) zone, traceable all the way from the west end of the line 5 upward to within 300 m beneath the surface. The field layout of recording spread was designed in such a way that, except for the two ends,

the major part of line 5 was surveyed with a six-station gap (~350 m) between the source and the first receivers on each side of the source to avoid source-generated noises. As a result, the final velocity structure of the top few hundred meters cannot be resolved. Instead, the velocity structure was smoothed out, giving a laterally homogeneous impression. It should be emphasized that the inversion was only driven by the data and the final model was achieved without using any constraints. The significance of the model lies in its overall picture, not its details.

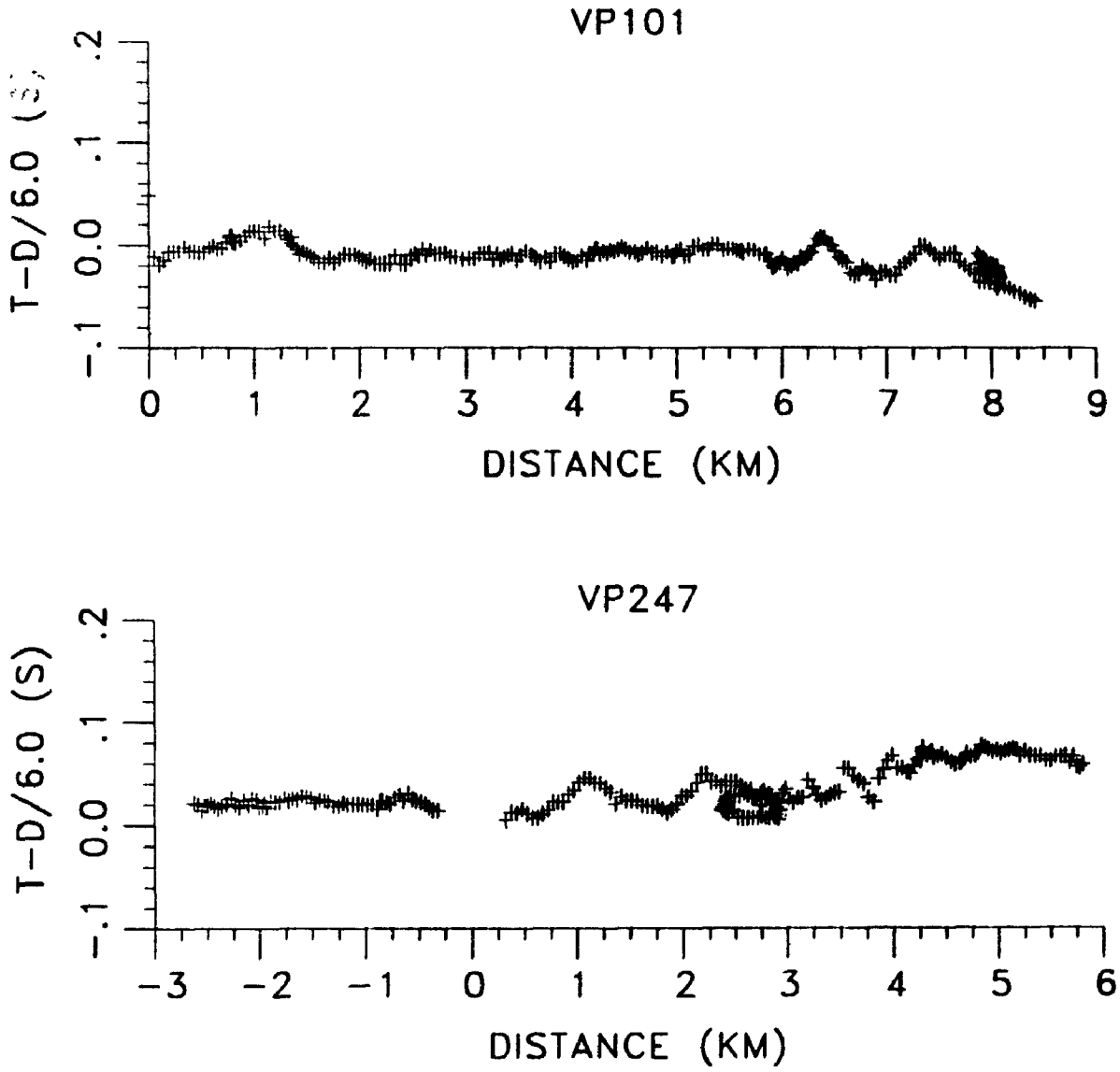

Fig. 5.1 Two sets of picked first arrivals with refraction static corrections applied to eliminate overburden effects.

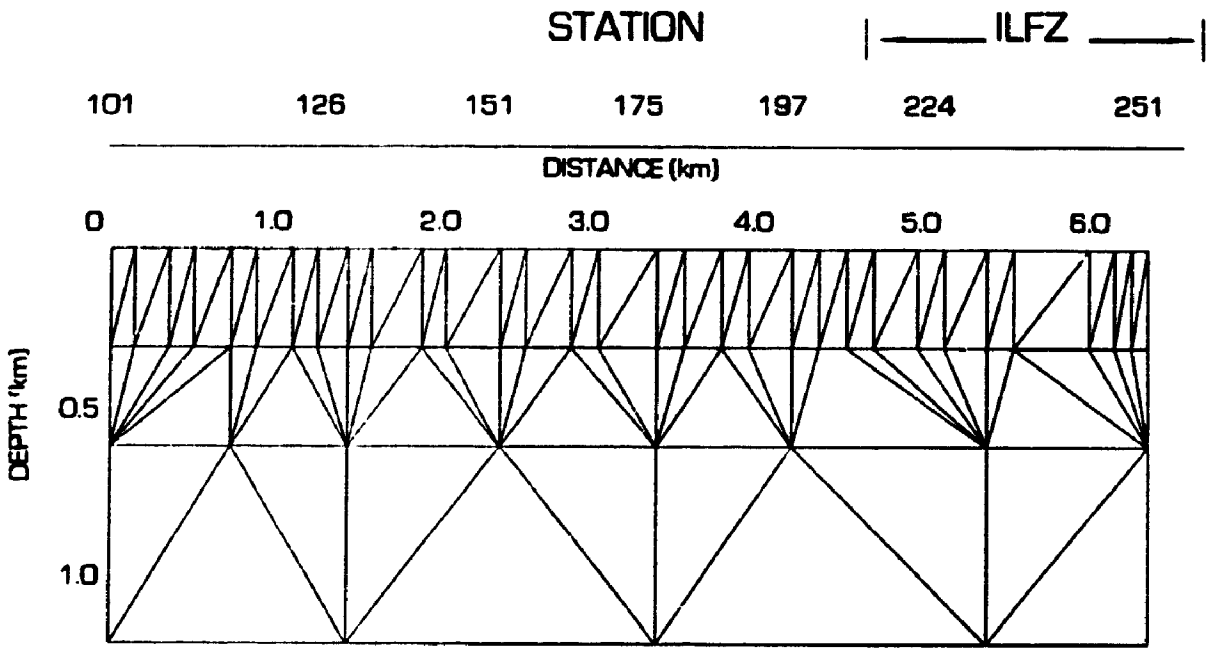

Fig. 5.2 Cell configuration of the shallow crust model. A total of 110 cells were used.

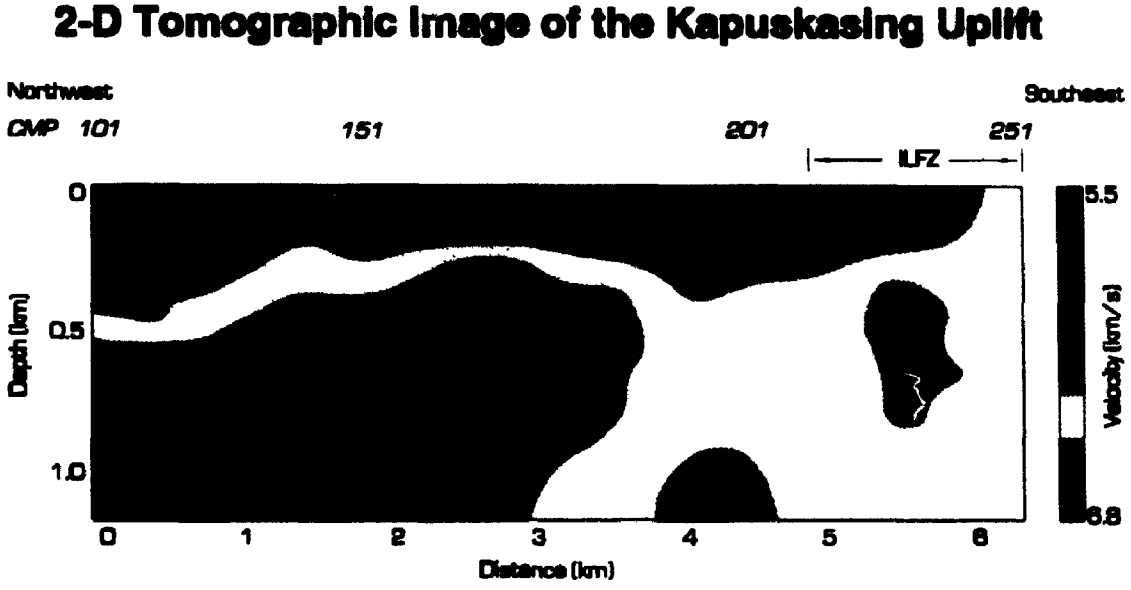

Fig. 5.3 2-D velocity structure across the Ivanhoe Lake fault zone (ILFZ).

CHAPTER 6 THE MIDCRUSTAL REFLECTOR: EVIDENCE FROM THE 1984 KAPUSKASING WIDE-ANGLE SEISMIC REFLECTION DATA

6.1 Observations

Reprocessing of line 5 has disclosed a major midcrustal dipping reflector (Fig. 4.27b). Although the reflector was clearly observed on the raw shot gather (Fig. 4.5), the existence of this reflector would be more convincing if it was also observed on a cross-profile. Unfortunately, there was no reflection profile nearby crossing line 5 or the fault zone. However, we do have a seismic refraction line crossing line 5 as well as the fault zone (Fig. 3.1). If the reflector does exist and has broad lateral extent, we should be able to see wide-angle reflections from the reflector along the refraction profile.

Refraction line GH begins within the Abitibi greenstone belt and crosses the Ivanhoe Lake fault zone obliquely along Highway 101 (Fig. 3.1). It intersects reflection line 5 and overlaps with reflection lines 2, 3 and 4. Owing to its location, only the seismic data acquired on the stations close to shot point G are considered in this analysis. An explosive shot of 800 kg hydromix was fired at the bottom of Reeves Pit (shot point G). Line GH was recorded by 66 geophones with a spacing of 2-5 km. A 10-km gap occurred along the line at a distance of 70 km from shot-point G due to road inaccessibility. The data were digitized at 60 samples per second. Fig. 6.1 displays both the P- and S-wave sections for this data set, plotted using a reduced travel-time with a reducing velocity of 6.5 km/s for the P-waves and 3.75 km/s for the S-waves. The reducing velocity and reduced time scale for the S-waves are chosen in such a way that if Poisson's ratio is close to 0.25, then P- and S-wave refractions and/or reflections from the same geological boundary will overlap

when P- and S-wave record sections are overlain with the zero reduced time lines coincident (El-Isa et al., 1987). Poisson's ratio, in turn, can provide information on lithologic variations (Holbrook et al., 1988), and on the presence of fluids (Hawman et al., 1990) within the crystalline crust. For example, Poisson's ratio is quite high in feldspar and very low in quartz.

Prominent large-amplitude secondary arrivals are clearly seen between 30 to 110 km from shot G on the P-wave section and between 70 to 110 km on the S-wave section (Fig. 6.1). These are believed to be wide-angle reflections from a midcrustal reflector, whose midpoints are plotted in Fig. 6.2. The S-wave data were bandpass-filtered in order to enhance the correlation between P- and S-wave wide-angle reflections. It should be stressed that, because of the poor spatial and temporal resolution, the long range seismic refraction data show no indication of the ILFZ. They do, however, show that there is a high velocity zone near the surface of the Kapuskasing structure.

6.2 NMO Correction

To facilitate comparison between wide-angle and near-vertical reflection data, the P-wave wide-angle data are corrected for normal-moveout (NMO) and plotted according to their midpoint locations (Fig. 6.3) in the same manner as the near-vertical reflection data. A simple crustal model with a constant P-wave velocity of 6.4 km/s and a constant depth of 15 km to the reflector, estimated from the T^2-X^2 display (Fig. 6.4), was used for the NMO correction. Here, X is the source-receiver offset for a common shot, while T is the travel time of the reflection at X. Strictly speaking, this approach is only valid for horizontally-layered, homogeneous media. Other possible velocities and depths have been tried for the NMO correction. Our tests show that the arrival times for the reflections will vary, but the main feature remains the same, that is,

a major west-dipping reflector is easily identified between 4 and 6 s TWT and can be traced laterally for up to 40 km within the AGB and under the KU.

6.3 Ray-Tracing Modelling

Forward modeling of the first and secondary P-wave arrivals was performed using the 2-D ray-tracing algorithm of Mereu (1990), which parameterizes the model with triangular blocks, each with a constant velocity gradient. The original 2-D velocity model of Wu and Mereu (1990) was chosen as the starting model, which was then altered using an iterative approach. The final model has a midcrustal reflector with an apparent westerly dip at depths of 12-16 km (Fig. 6.5). The reflector most likely extends further to the west with a steep dip. Theoretical traveltimes generated from this model are superimposed on the observations, showing a satisfactory fit for both the traveltime and the relative amplitude (Fig. 6.6). The new model is similar to the old one in that they both show a high velocity of 6.5 km/s near the surface of the KU. The same model can also fit the S-wave arrivals (Fig. 6.7), if an average Poisson's ratio of 0.25 is assumed.

6.4 More P- and S-wave Comparisons

An examination of all the S-wave record sections indicates that S-waves are in general of poor quality and often difficult to see clearly, because they are later arrivals and lie in the coda of P-waves. This is particularly true of Sn arrivals, refracted S-waves from the Moho, as no Sn arrivals can be identified with confidence. Two examples comparing P- and S-wave arrivals are provided in Figs. 6.8 and 6.9. On the whole, the S-wave sections do show great similarities with P-wave sections. Sg arrivals, refractions from the upper crust, are clearly observed near the shot points and often traceable for more than 100 km. Ray-tracing modeling shows that the same 2-D P-wave velocity

models can provide a good fit for S-waves assuming an average Poisson's ratio of 0.25. Detailed comparisons of P and S-wave studies for the 1984 Kapuskasing seismic refraction data were given by Wu and Mereu (1990) and Boland and Ellis (1991).

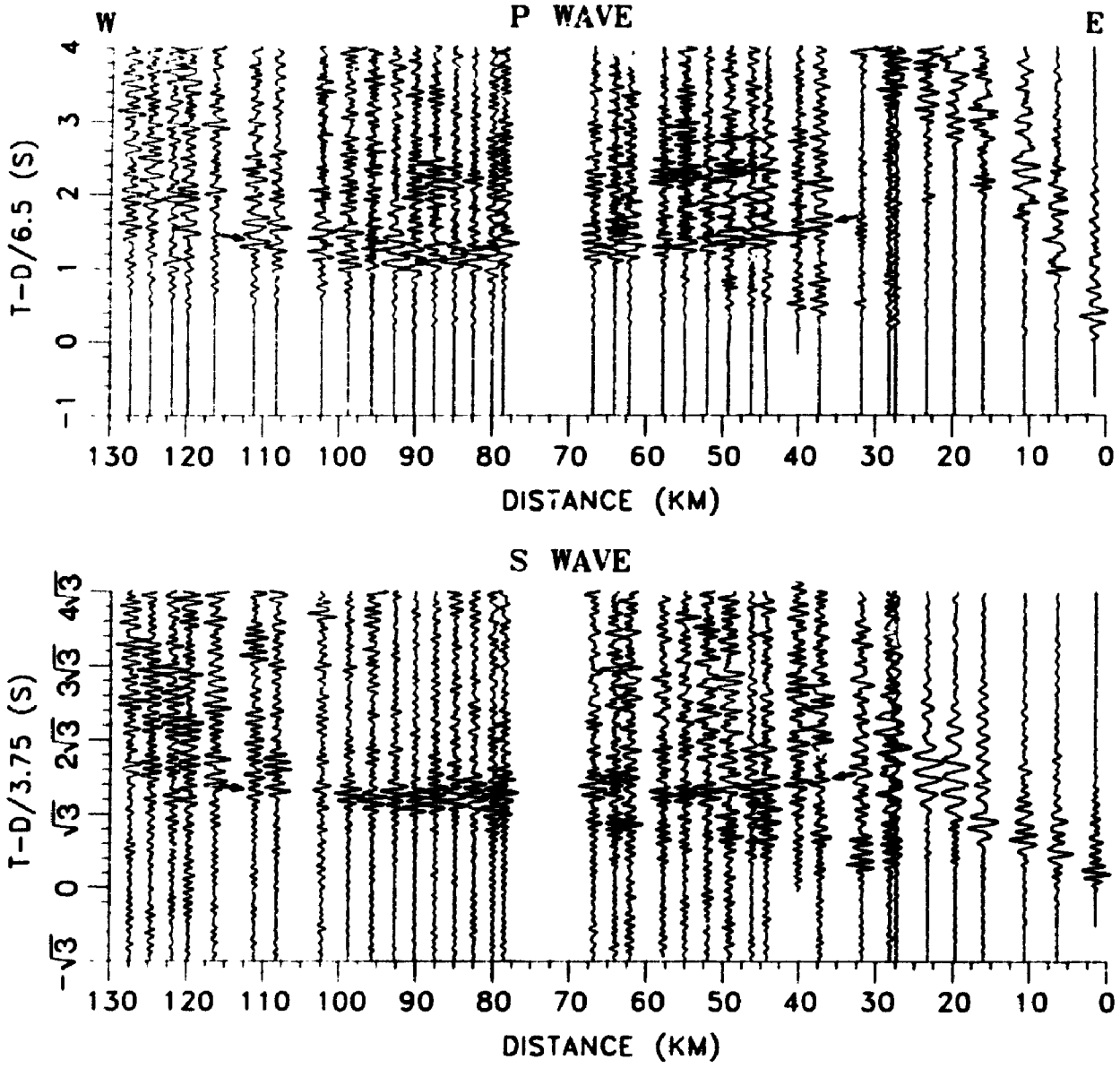

Fig. 6.1 P- and S-wave wide-angle reflections from shotpoint G along refraction line GH. The data are plotted using reduced travel-time and with trace-normalization. S-wave data are bandpass-filtered between 2 and 5 Hz.

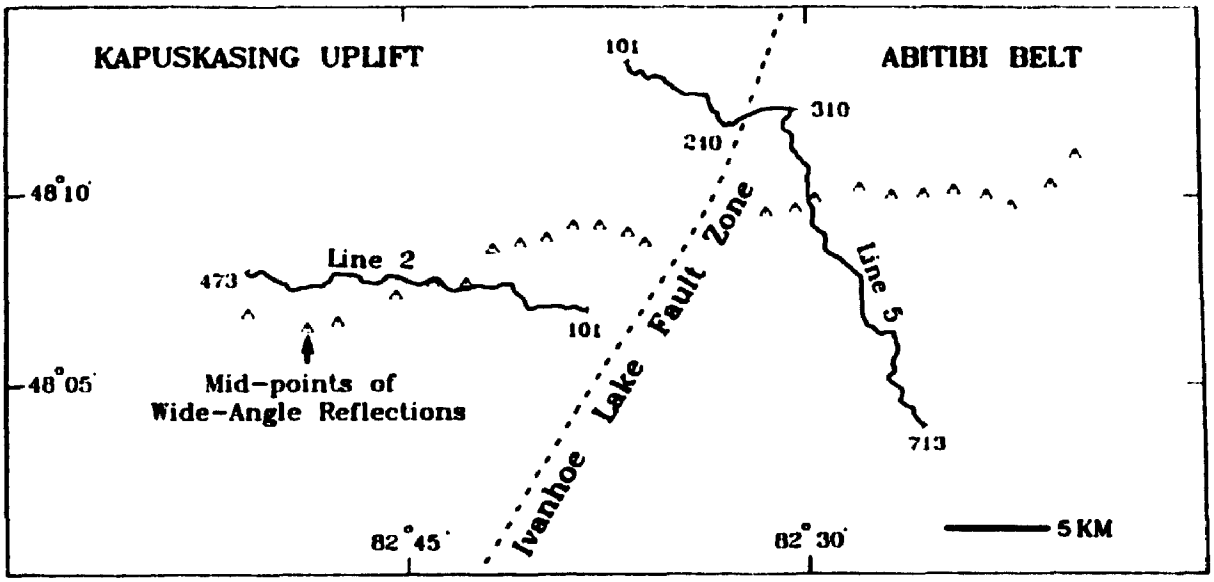

Fig. 6.2 Enlargement of reflection line 5 with mid-points of wide-angle reflections from shotpoint G along refraction line GH superimposed.

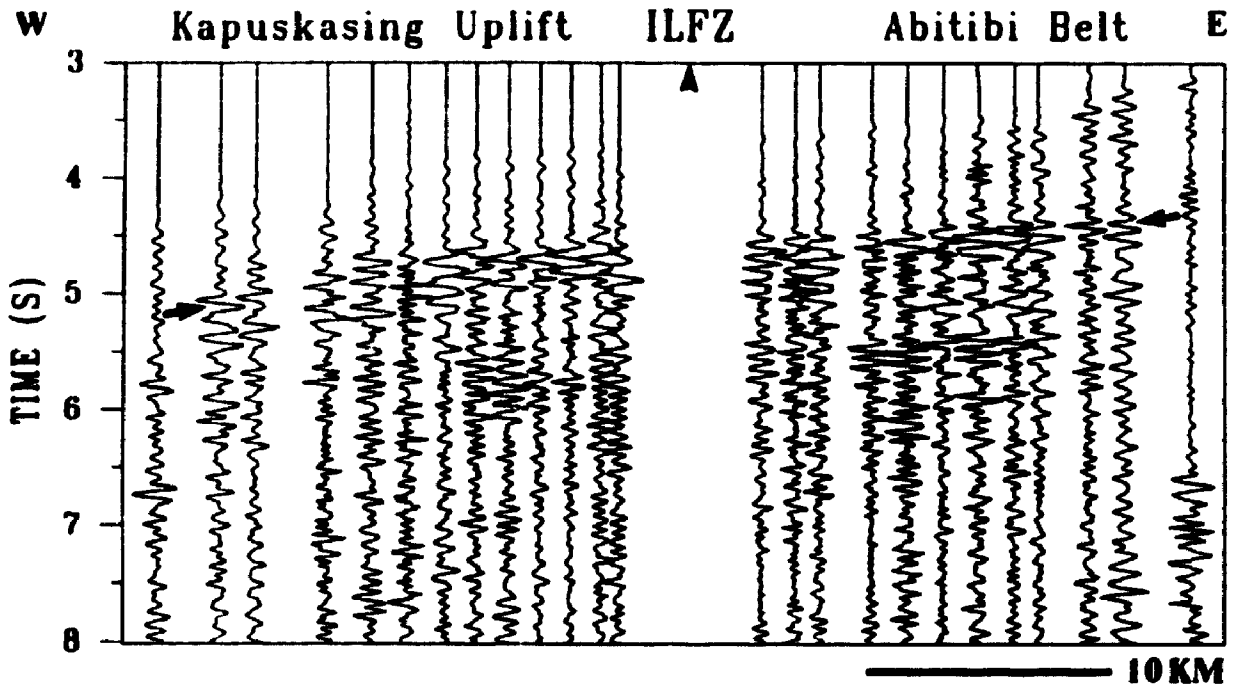

Fig. 6.3 P-wave wide-angle reflections (marked by arrows) with the normal moveout correction applied. The data are plotted at their common-midpoints (half way between receivers and shotpoint G).

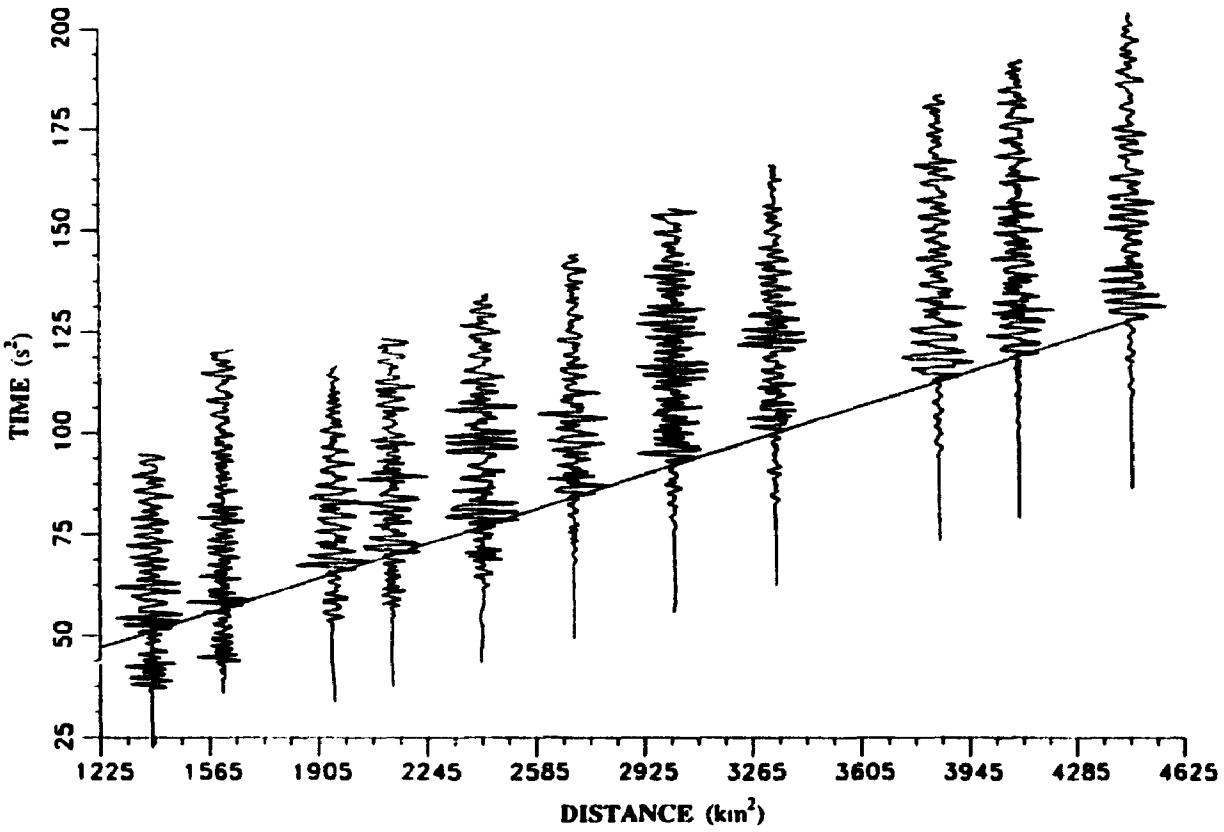

Fig. 6.4 The T^2 - X^2 display of the P-wave wide-angle reflections.

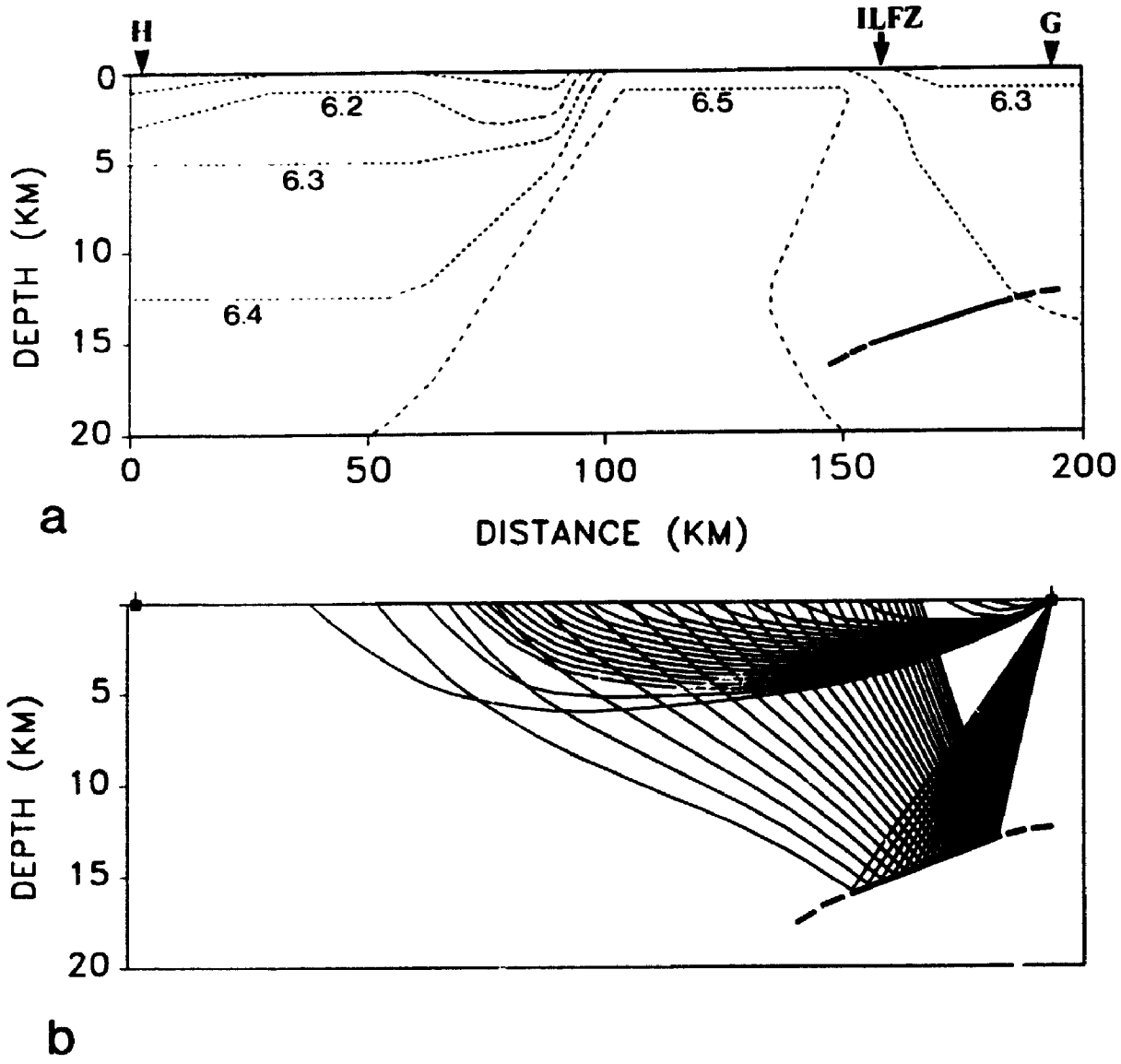

Fig. 6.5 a) 2-D velocity model for line GH derived from trial-and-error forward ray-tracing modeling. The thick line corresponds to the major midcrustal reflector. Note that the Ivanhoe Lake fault zone cannot be resolved by the refraction data due to the poor resolution. b) ray-tracing diagram.

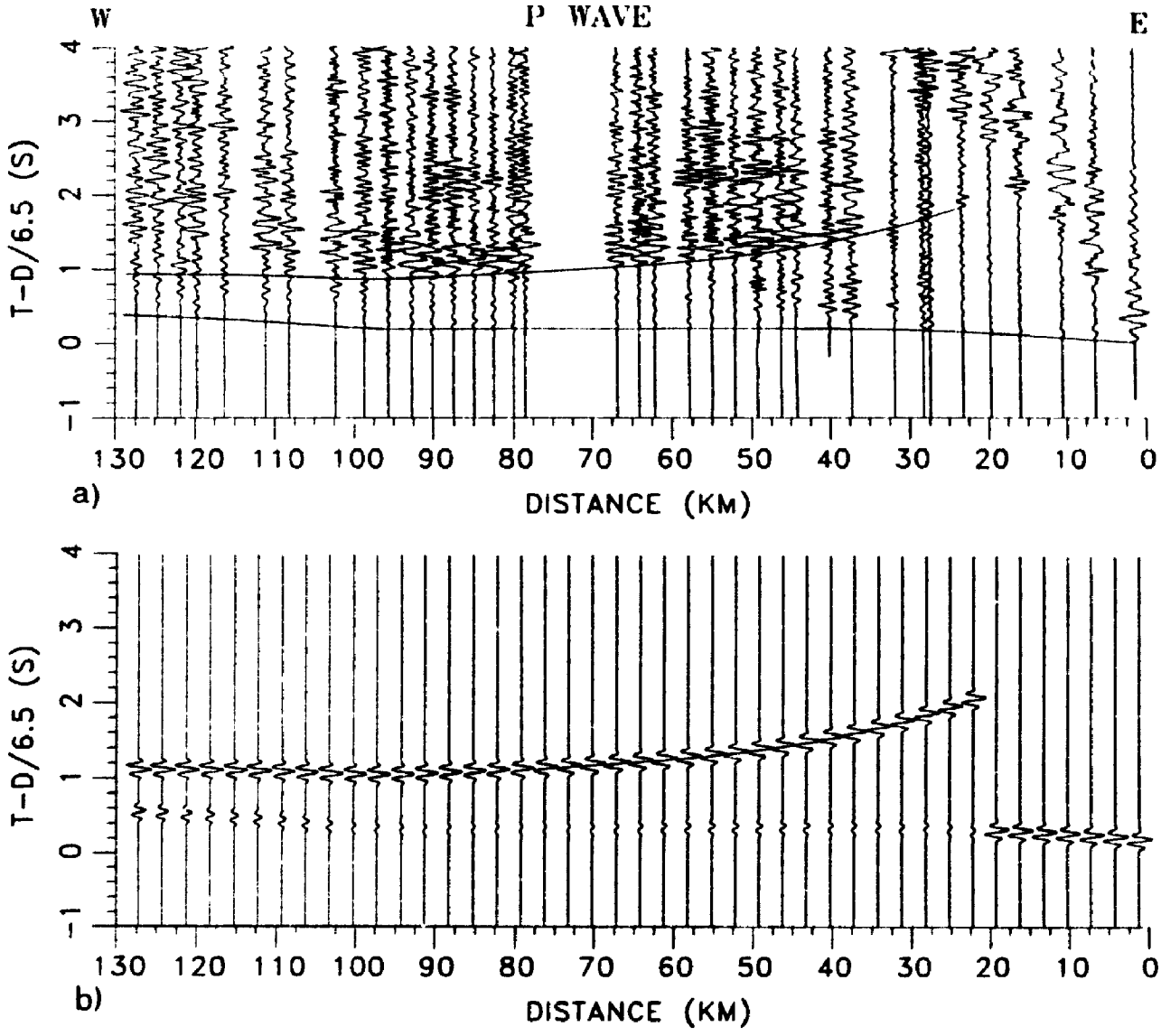

Fig 6.6 a) Theoretical P-wave travel-time curves are superimposed on the observations, plotted with trace-normalization. b) the corresponding synthetic seismogram plotted with trace-normalization.

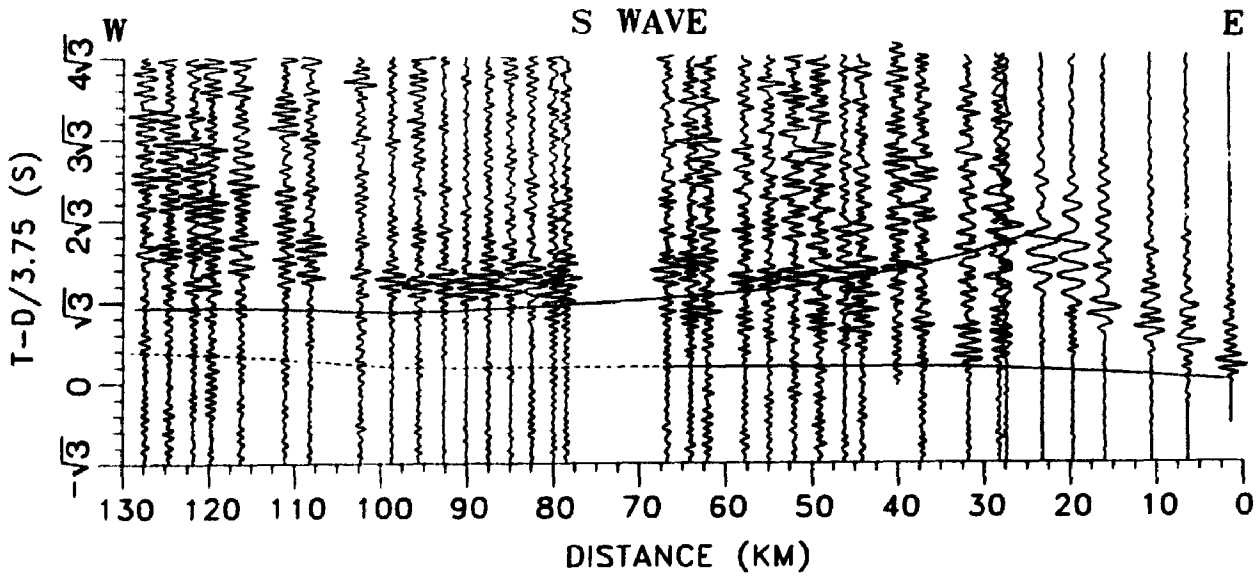

Fig. 6.7 Theoretical S-wave travel-time curves, generated from the same P-wave velocity model by assuming an average Poisson's ratio of 0.25, are superimposed on the observations. Dashed lines indicate where there is no clear S-wave observation.

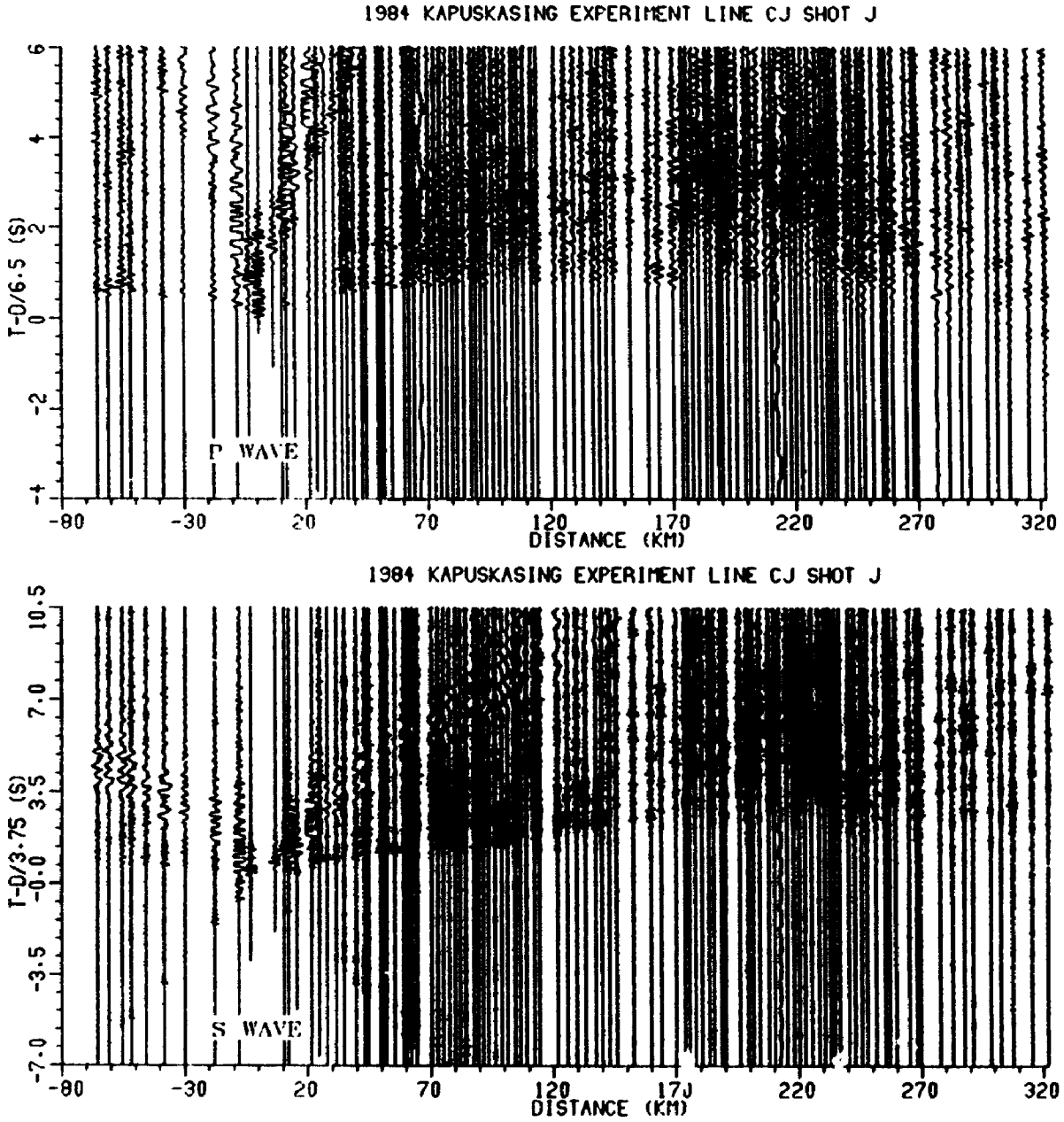

Fig. 6.8 P- and S-wave record sections acquired from Shot J along line CJ (see Fig. 3.1 for location).

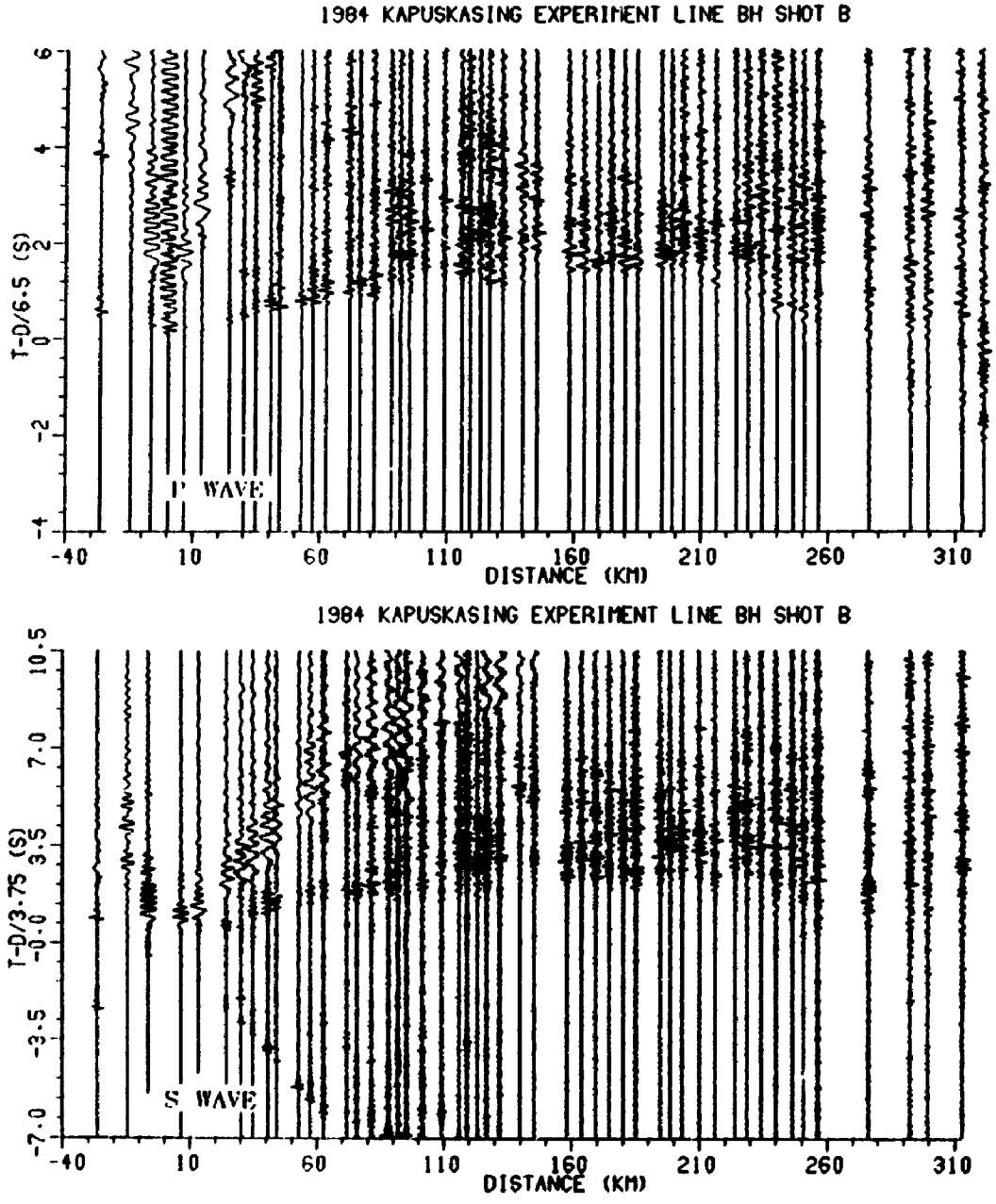

Fig. 6.9 P- and S-wave record sections acquired from Shot B along line BH (see Fig. 3.1 for location).

Chapter 7 INTERPRETATION

7.1 The Ivanhoe Lake Fault Zone

By far the most striking feature of the reprocessed section is the band of bright northwest-dipping reflections with a concave-up geometry, seen between 0.2-1.0 s TWT on the top north portion of line 5 (Fig. 4.26b) and most pronounced between stations 150-250. West of station 150, these reflections are much weaker and discontinuous. However, they are clearly traceable to the west end of line 5. The discontinuous and weak character is probably due to the surface conditions, as indicated by the field shot gathers. Where the reflections become prominent they have a low-angle dip ~20° (Fig. 4.28). They steepen upward when they approach the surface. They may have a maximum dip of as much as 50° if extended to the surface. They can be easily projected to the surface with a horizontal width of about 1.5 km, where they overlap with the surface trace of the Ivanhoe Lake fault zone (ILFZ) inferred from geological and aeromagnetic observations. The 2-D tomographic inversion reconstructs a west-dipping high-velocity (≥6.4 km/s) zone (Fig. 5.3). In combination with the reflection images, it indicates that rocks above the group of west-dipping reflections are of high P-wave velocity, further implying that these rocks represent deep crust. These observations strongly suggest that these reflections correspond to the fault zone, along which dense, high-velocity deep crustal rocks were uplifted. It should be kept in mind that many thrust faults tend to form in a concave-up geometry. This interpretation is broadly consistent with the geological interpretation of Percival and Card (1983 and 1985) in that the ILFZ is a northwest-dipping thrust fault. As well, it is consistent with the surface observation of Bursnall (1989) that rocks within the fault zone possess a dominant planar

fabric of > 45°, since the ILFZ is a steep fault near the surface.

The fault zone is poorly exposed in the area and is mainly defined on the basis of an aeromagnetic lineament (J. Percival, pers. commun.). It is clearly defined by a recent high-resolution aeromagnetic survey as a 4-km-wide band of positive aeromagnetic anomalies (West and Halls, 1991), lying approximately between stations 150-250 along line 5. The coincidence of the pronounced northwest-dipping reflections with the positive aeromagnetic anomalies is particularly intriguing. Evidently, the rocks within the fault zone are highly magnetic and reflective, indicating that they possess different petrological characteristics than rocks from either the Kapuskasing Uplift (KU) or the Abitibi greenstone belt (AGB). The positive aeromagnetic anomalies might be attributed to the high magnetic susceptibility of the rocks presently exposed (Gaucher, 1966). According to Bennett (1969), Thurston et al. (1977), and Bursnall (1989), narrow mylonite zones up to 70 m wide are frequently observed within or near the fault zone. Mylonites are also recorded by Thurston et al. (1977) along the north portion of line 5 and Highway 101 in this area. Since these mylonites are highly magnetic (Bennett, 1969; Thurston et al., 1977) and mylonites have been shown to be good reflectors (Hurich et al., 1985; Smithson et al., 1986; Christensen and Szymanski, 1988), the high reflectivity and high magnetism associated with the fault zone is likely to be of mylonite origin.

For the first time, the shallow structure associated with the ILFZ is clearly marked on a seismic section. Reflection lines 1, 6 and 8 also cross the ILFZ but provide no image on the fault zone (Percival et al., 1989). Three distinct west-dipping events are observed along line 2 (A, B, C, Fig. 7.1) and may be followed to the vicinity of the ILFZ (Percival et al., 1989; Geis et al., 1990; Green et al., 1990). Yet they cannot be traced to the

surface and positively identified, because line 2 does not extend far enough eastward to cross the fault zone (Figs. 3.1, 3.2, 6.2). At first glance, event A on line 2 looks very similar to the shallow reflections imaged on line 5 as both show laminated-reflections and may be attributed to the base zone of the Shawmere anorthosite (Geis et al., 1990). Close examination, however, indicates that they do not image the same geological feature for three reasons. First, the reflections of line 5 are of listric geometry suggesting a thrust fault, while event A (see Fig. 7.1) shows a linear geometry usually related with layering. Second, if the reflections of line 5 are projected downward ~10 km further west, equivalent to the west end of line 2, they would appear between 2 to 2.5 s TWT, too deep to be event A, but just right to be event B. Third, the juxtaposition of high-velocity rocks against low-velocity rocks across the west-dipping reflections, as shown on the 2-D velocity model (Fig. 5.3) makes it irrefutable that they do mark the fault zone. It appears more likely that the shallow reflections of line 5 are the continuation of the events B and C of line 2 (Fig. 7.1), as they share an identical geometry. This interpretation would suggest that the fault zone broadens at depth because the vertical separation of the two events is as much as 0.8 s, much greater than the vertical width (0.4 s) of the top northwest-dipping event on line 5.

One may still argue that the shallow reflectors imaged on line 5 look more similar to event A rather than B and C on line 2 (Fig. 7.1), because these latter are more discrete (few cycles) and more steeply dipping when they approach the surface. However, along most of line 2, especially the west end, these three events are clearly parallel to each other with a westerly dip of ~15° (Percival et al., 1991), in accord with the dip of the shallow reflectors seen on line 5. Events B and C also show many cycles. Toward the

east end of line 2, event C does show steep dips. It is possible that the steeply-dipping reflections on line 2 may represent a later thrust faulting (G. West, pers. commun.). If true, the steep fault is likely manifested by the apparent truncation of the shallow reflections seen at station 150 on line 5 (Fig. 4.26b). The later faulting has also been suggested by field geological observations (Bursnall, 1989). Reprocessing of the high-resolution seismic data acquired along line 2 may help to resolve this argument.

The high reflectivity of ILFZ observed along line 5 as well as line 2 raises an important question: why is the fault zone in the areas covered by lines 1, 6 and 8 not reflective? Four possible explanations are given by Wu et al. (1992): (1) inadequate processing; (2) poor ground conditions; (3) different types of fault rocks (cataclastic vs. mylonitic); (4) later faults having disrupted the fault zone. Reprocessing of lines 1 and 6 by Hajnal et al. (1991) shows no such high-reflectivity within the fault zone (Figs. 7.2, 7.3), indicating that the difference is not likely to be due to inadequate processing. This enigma may be resolved by combining the seismic data with other geophysical data. The residual Bouguer gravity map (Fig. 3.2) indicates that the ILFZ is best defined in the area covered by line 5 and so does the aeromagnetic map. These observations imply that the difference in the reflectivity is caused by the difference in the structure, suggesting that subsequent tectonic processes such as faulting (Bursnall, 1989) and magmatic injection (Nelson, 1991) may have disrupted the ILFZ in the areas covered by lines 1, 6 and 8. This scenario may predict that along most of the northern Chapleau block the fault zone is reflective as it appears to have been well preserved according to gravity (Fig. 3.2) and aeromagnetic data (West and Halls, 1991). Alternatively, the ILFZ might be of spoon-shaped geometry with its center located in the area covered by lines 2 and 5. The fault zone may

change to dominantly strike-slip character to the south as fault zone changes in strike. This alternative is supported by the measurements of Al_2O_3 contents of amphiboles across the ILFZ, which show a sharp contrast in the area covered by lines 2 and 5, and little difference in the area surveyed by lines 1 and 6 (Palmer and Barnett, 1992).

7.2 Midcrustal reflections

Perhaps the most continuous and prominent dipping feature imaged on line 5 is the north-northwest dipping reflections visible between 4 and 6 s TWT within the Abitibi greenstone belt (AGB) (Fig. 4.27b). The reflections tend to be flat-lying to the south-southeast and steepening downward to the north-northwest. There is some evidence that they may extend to the south end of line 5. Interestingly, a set of pronounced midcrustal reflections is also observed on the wide-angle reflection data from shotpoint G along refraction line GH (Figs. 6.1 and 6.3), progressively steepening downward to the west. The wide-angle reflections originate within the AGB, cross the ILFZ, and plunge under the KU with a lateral continuity of about 40 km. The two sets of reflections show a remarkably similar geometry and, moreover, their mid-point locations cut across each other (Fig. 6.2). These and their approximate correspondence in traveltime suggest that they originate from the same midcrustal reflector. The observation that the reflector has an apparent steeper dip along the south portion of line 5 running north-northwest than along refraction line GH running roughly west indicates that the reflector dips northwest.

Since this reflector is observed on line 5, one would expect to observe it on line 2, as line 2 is close to line 5 and overlaps with refraction line GH (Figs. 3.1, 3.2, 6.2). A small portion of it (E, Fig. 7.1) is indeed

observed on the east end of line 2 at about 4.5 s TWT (Geis et al., 1990; Green et al., 1990). Figure 6.2 might mislead one to think that the reflector would be seen along the whole section of line 2. The position of the reflector is more accurately given on the P wave velocity model (Fig. 6.5), as ray-tracing should produce results equivalent to migration. The length of reflector is reduced from 40 km on the NMO corrected section (Fig. 6.3) to 30 km after ray-tracing (Fig. 6.5).

Another interesting observation is that this bright reflector is overlain and underlain by a number of less prominent and discontinuous subparallel reflectors visible between 1 to 10 s TWT (Fig. 4.25). These reflectors together give the impression that significant portion of the crust of the AGB has been plunged under the KU. To be more confident, we should look at results from other reflection profiles. Lines 1 and 6, lying about 80 km southwest of line 5, also cross the ILFZ and have been reprocessed by Hajnal et al. (1991). Their results show no such single bright reflector under the AGB in the area covered by lines 1 and 6 (Figs. 7.2, 7.3). Rather, the whole crust, especially the upper crust of the AGB, is characterized by abundant north- or northwest-dipping subparallel reflections, which may extend beneath the KU through a considerable distance. All these reflections show a similar geometry to those on line 5. Hajnal et al. (1991) divide them into three groups from top to bottom: C, those occurring between 0.5 and 2 s, D, between 1 and 3 s and E, between 2.5 and 4.5 s TWT (Figs. 7.2, 7.3). Among them, E is the most prominent and has excellent lateral continuity (~15 km). It appears most likely that E is the lateral extension of the bright midcrustal reflector on line 5 (Z. Hajnal, pers. commun.), although shallower and thicker, while C corresponds to the shallow reflector seen between 1 to 2 s on line 5 (Fig. 4.25). The striking correlation among lines 1, 5 and 6

strongly suggests that the dominant structural grain of the AGB is dipping northwesterly and the same structure is distributed over a wide region under the ILFZ. Although no distinct reflector is readily apparent, line 8 exhibits similar seismic character, i.e. the entire crust of the AGB is dominated by northwest-dipping reflections (Wu and Mereu, 1991).

On the basis of these observations, we believe that the pronounced midcrustal reflector within the AGB demarcates the underthrusting of the Abitibi rocks. Alternatively, it may represent another deep crustal thrust with its surface projection further southeast of the ILFZ into the Abitibi, as its geometry resembles ramp-and-flat imbricate geometric configuration. This possibility is discarded as, at present, there is no evidence whatsoever for such large-scale crustal features. Putting together results from lines 1, 2, 3, 4, 5, 6 and 8, with the wide-angle reflection data, we are able to construct a more complete structural cross-section as shown in Fig. 7.4. On the northwest side, we note the overthrust of the KU along the northwest-dipping ILFZ and, on the southeast side, the underthrust of the Abitibi rocks beneath the KU. It is evident that the KU is a product of intraplate collision during the early Proterozoic, in agreement with Card (1990), who suggests that the whole Superior Province of the Canadian shield is the product of Archean plate convergence. One question arises from this section: what was the role of the underthrust in the formation of the KU? Hajnal et al. (1991) suggest that the pronounced northwest-dipping reflections represent subsidence of the Abitibi rocks as a means to balance the overloaded upper crust of the KU, implying that they played only a passive role in the formation of the KU. Although the surface part of the overthrust is well imaged on line 5, its expression on line 2 (Fig. 7.1) is by short and discontinuous reflections only. By contrast, the underthrust is well imaged

on lines 1, 5 and 6. The wide spread nature of the underthrust leads me to suspect that it is the underthrust along which the greater amount of displacement has taken place. Thus the uplift of the KU may be more related to the underthrusting of the AGB than the overthrusting of the KU. In plate tectonic terms, this may mean that the AGB was the active subducting element and the KU was a more passive obducted element, implying that the underthrusting of the AGB is primarily responsible for the emplacement of the KU.

This interpretation agrees with the observation that no large amount of detachment was detected under the KU on the seismic data, because most crustal shortening took place within the AGB. One could argue that later tectonic processes have disrupted the detachment. This argument may be dismissed by Bouguer gravity data (Fig. 3.2), which indicate that the KU has been well preserved, at least for the most part of the Chapleau block (Fig. 3.1). The origin of these midcrustal reflections is not certain due to the lack of surface control. Two explanations may be possible. First they were pre-existing before the KU was formed, probably from primary intrusive layering which occurred during the Archean time. Secondly, they originated from shearing due to the relative movements between rocks during the intraplate collision that formed the KU. Some combination of these two alternatives is preferable.

This model not only explains how the KU was formed but may also provide a strong constraint on the depth at which the KU was transported upward. It is quite likely that the northwest-dipping reflector corresponding to the ILFZ and the prominent midcrustal reflector were once connected at the same depth and then broken into two parts, with one obducted and another subducted as internal stress built up due to the lateral compression. If this is the case,

it suggests that the rocks of the KU were moved up from a depth of 12-15 km because the midcrustal reflector apparently flattens westward at 4 s (Figs. 4.27b and 6.3). This further indicates that the KU exposes Archean midcrustal rocks rather than the lower crust (Fountain et al., 1990; Wu and Mereu, 1990; Nelson, 1991).

It is well known that wide-angle reflections are sensitive to large-scale vertical or horizontal velocity changes with a resolution of a few kilometers, while near-vertical incident reflections are accurate in imaging the vertical fine structures of the crust with a resolution of a few hundred meters. That the midcrustal reflector is a thin layer across which velocity changes sharply, is manifested by the fact that it is well defined as a single strong reflector by both data sets. Ray-tracing modeling illustrates that positive velocity contrast across the layer is required in order to obtain large-amplitude wide-angle P wave reflections (Mereu et al., 1990c). However, the velocity contrast cannot be solely determined by fitting the amplitude ratio of the first to secondary arrivals, because the amplitude ratio is not very sensitive to the velocity contrast but rather to the velocity gradient near the surface. Clearly, the wide-angle reflection data not only confirm the existence of a northwest-dipping reflector imaged by the near-vertical reflection data to a much larger scale, but also provide useful constraints on the reflector's nature. The approximately overlapping of S- and P-wave wide-angle reflections implies that the rocks above the reflector possess an average Poisson's ratio of 0.25 (Fig. 6.6), further implying that there is no significant fluid trapped within the rocks.

7.3 Moho

Although line 5 has been extensively reprocessed, few deep reflections are

recognizable below 10 s TWT (Fig. 4.25). To make sure that this is not an artifact of seismic data processing, one should always go back to examine field data. Fig. 7.5 shows the two selected shot gathers, whose shallow parts are enlarged in Figs. 4.4 and 4.5. They are typical of line 5 in that virtually no reflection is recognizable below 10 s TWT (Fig. 7.6). The seismically transparent character of the lower crust cannot be due to poor source-surface coupling, because shallow or midcrustal reflections have been detected (Figs. 4.4, 4.5). One may question the penetrating capability of seismic energy. The fact that deep crustal reflections have been observed as late as 14 s TWT along lines 8, 9, and 10 (see chapters 8, 9), suggests that penetration is not a problem. Illustrated in Fig. 7.7 are amplitude decay curves, calculated by averaging a group of 20 traces of the two shot gathers shown in Fig. 7.5. It is evident that the energy continues to decay even at the end of recording, implying that penetration exceeds the Moho depths (~14 s or ~45 km for an average velocity of 6.5 km/s). On the basis of these observations, it can be concluded that the lack of the deep crustal reflection along line 5 is attributable to geological reality. The observation, that there is no indication whatsoever of the Moho, either on the raw data or processed data, is consistent with the results from the refraction data (Wu and Mereu, 1990), confirming that the Moho in the area is a wide transition zone rather than a first-order discontinuity (Fig. 7.3) (also see sections 9.4 and 10.4).

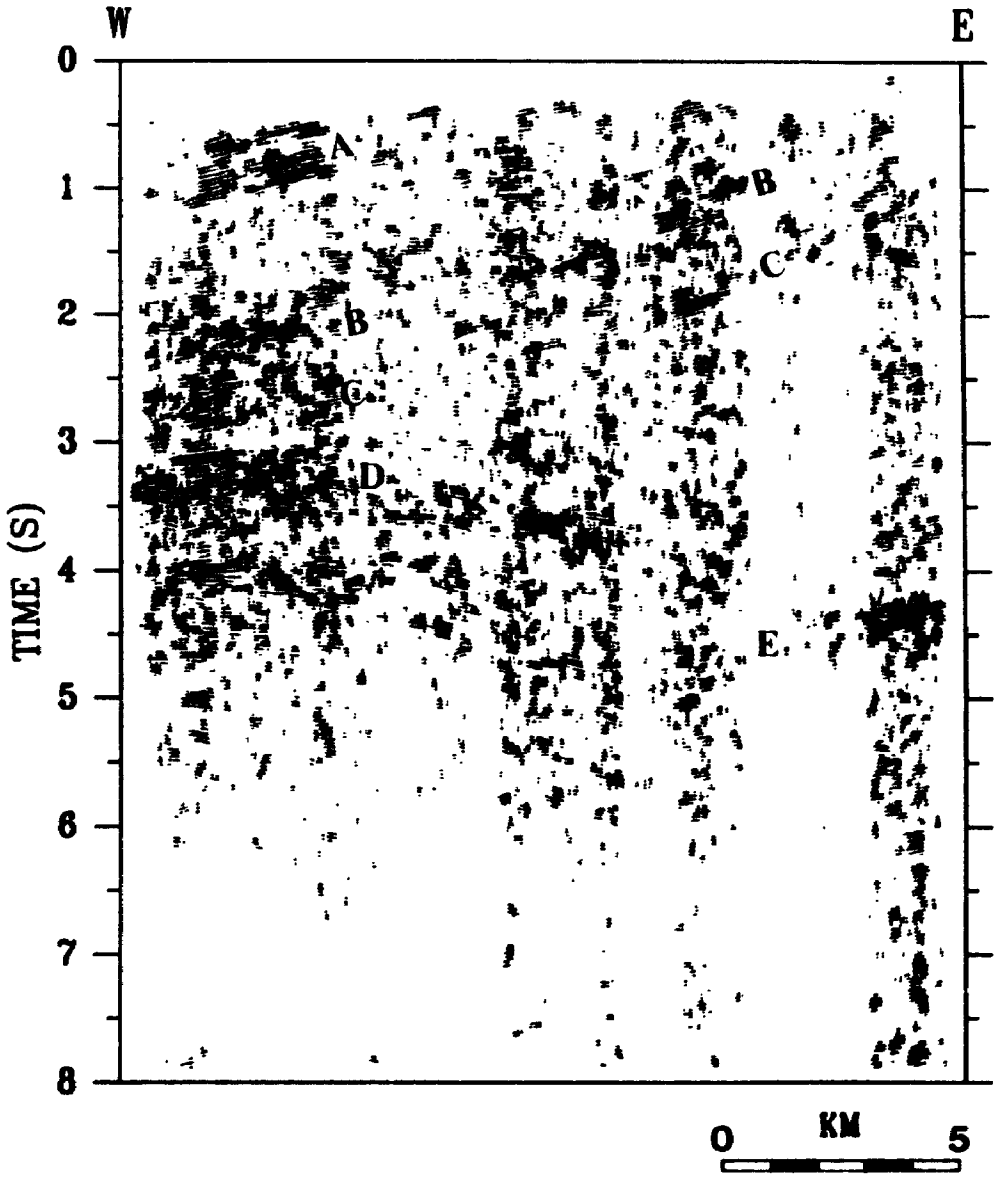

Fig. 7.1 The commercially processed section (see table 3.4) of line 2 (unmigrated, coherency-filtered), surveyed with high-resolution parameters (see table 3.3).

Fig. 7.2 The reprocessed section of line 1 (migrated) (after Hajnal et al., 1991).

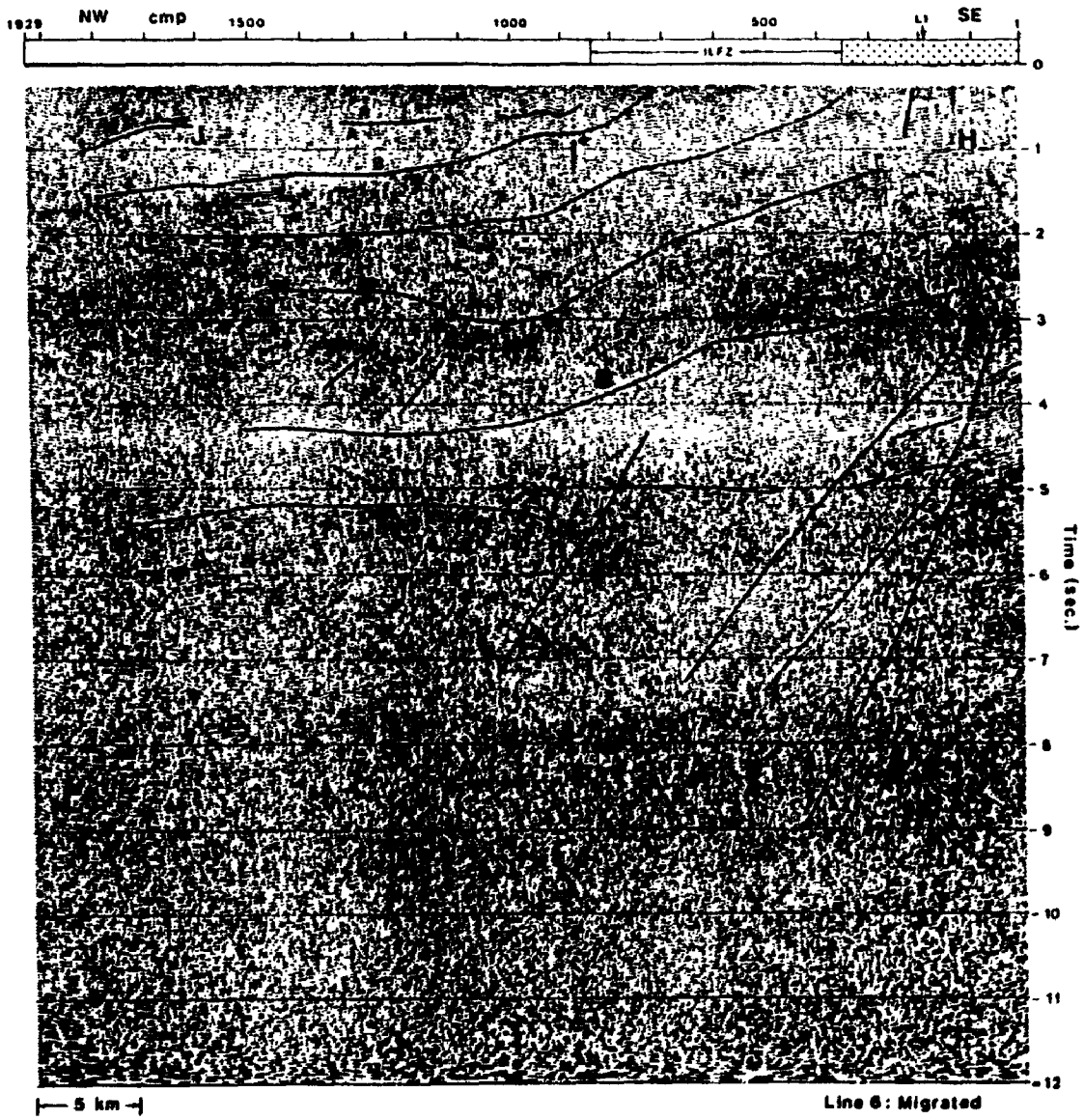

Fig. 7.3 The reprocessed section of line 6 (migrated) (after Hajnal et al., 1991).

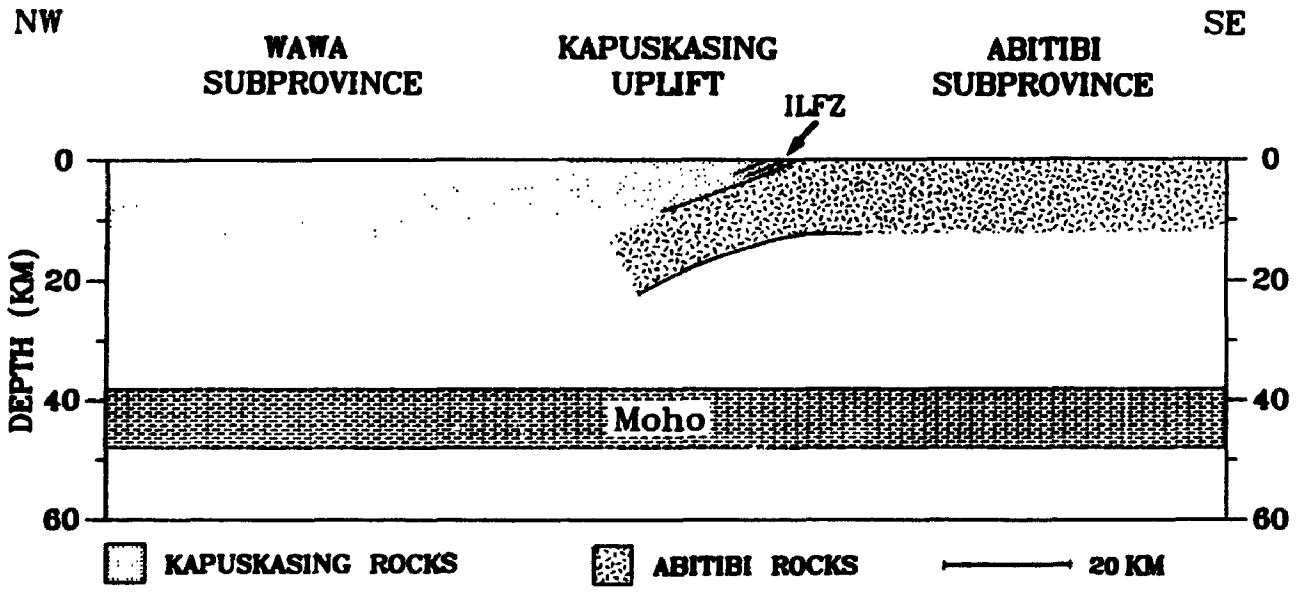

Fig. 7.4 A schematic cross-section showing the main features of the Kapuskasing Uplift (no exaggeration). This section is based on an integration of the near-vertical and wide-angle reflection data. The thin lines represent the band of north-dipping reflections, traceable to the surface trace of the Ivanhoe Lake fault zone (ILFZ). The heavy line represents the major midcrustal reflections. Note that the Moho is a wide-transition zone, and therefore is poorly constrained by seismic data.

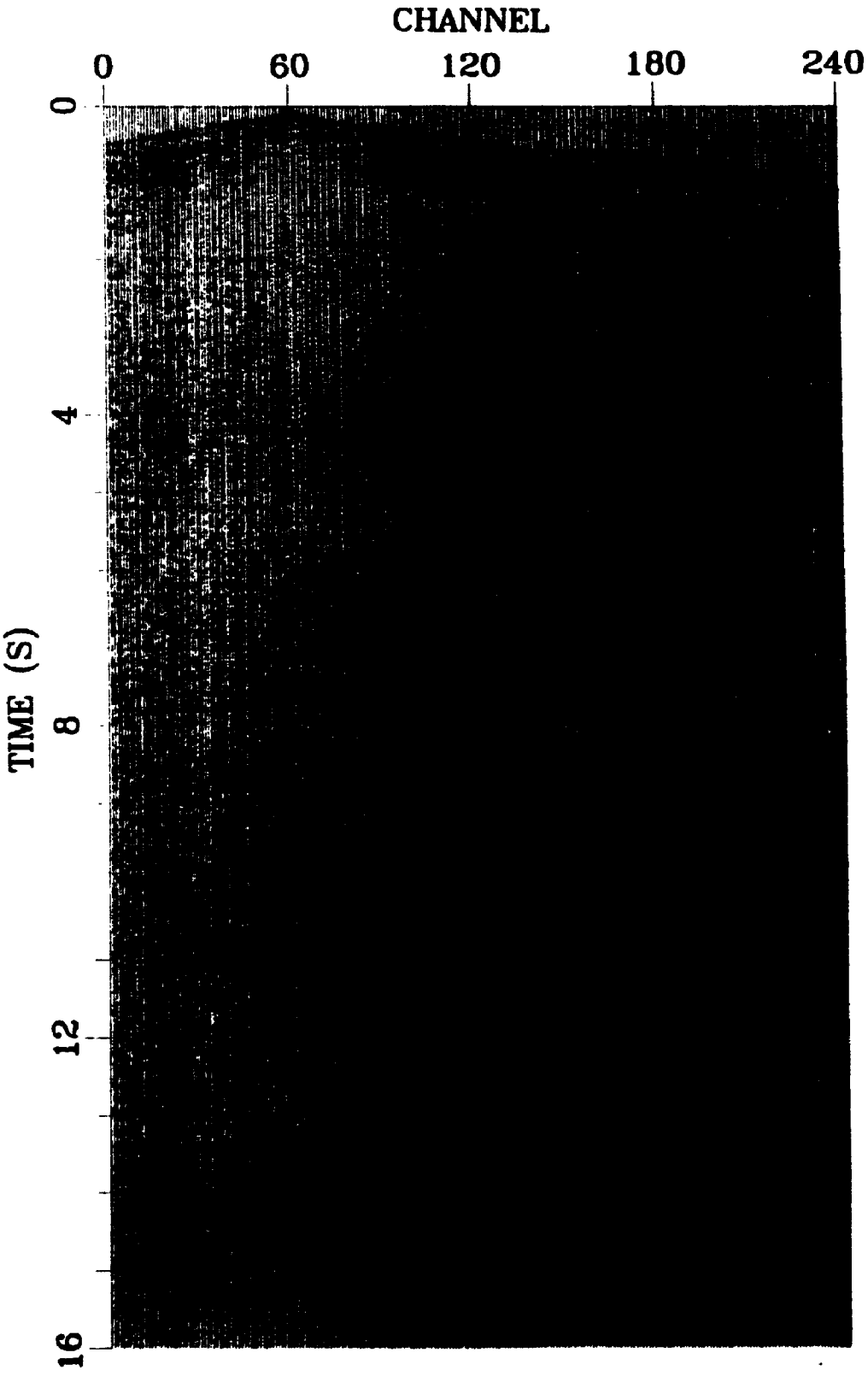

Fig. 7.5 a) field shot gather VP 219 with its shallow part shown enlarged in Fig. 4.4. The data were AGC-gained.

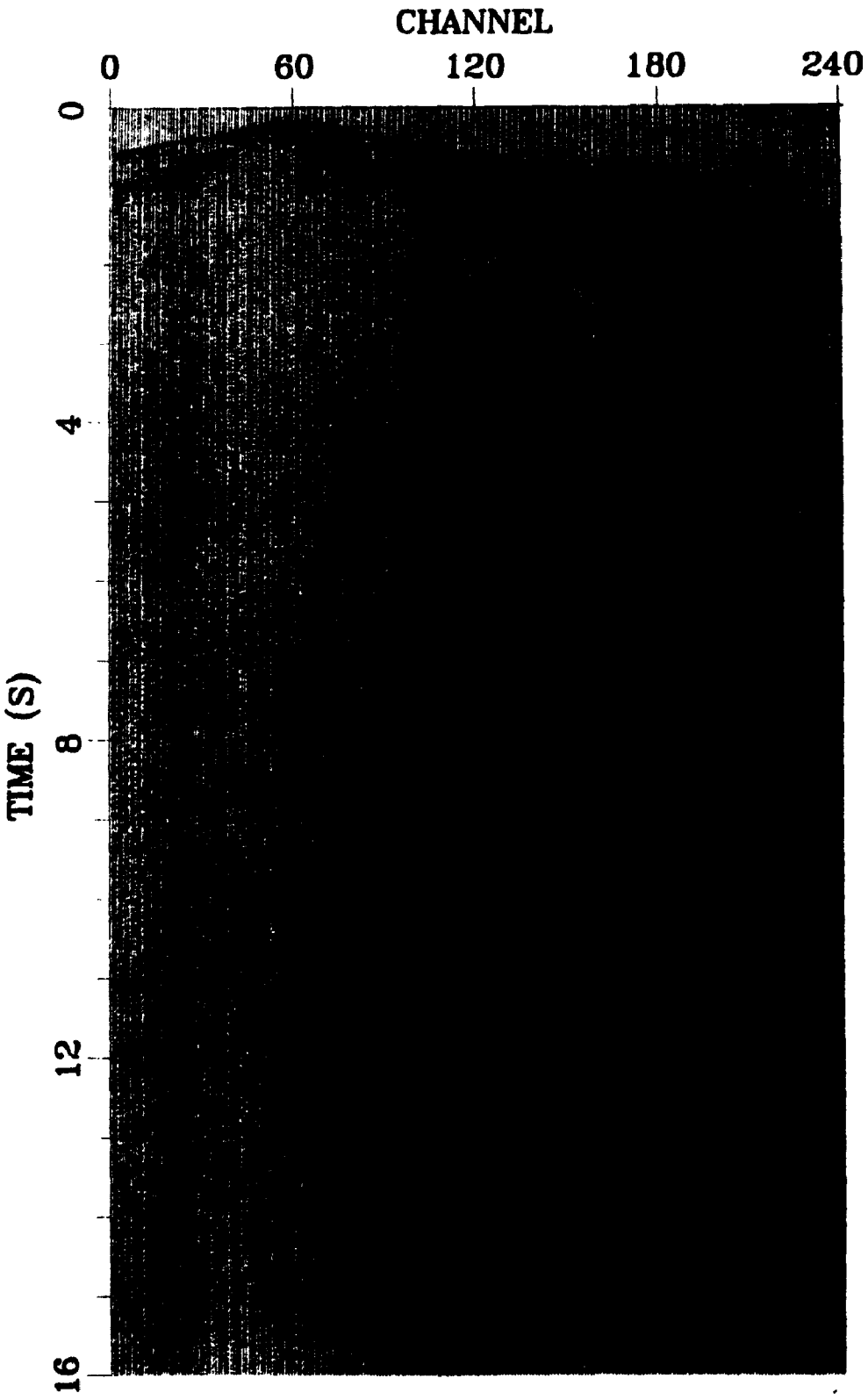

Fig. 7.5 b) field shot gather VP 387 with its shallow part shown enlarged in Fig. 4.5. The data were AGC-gained.

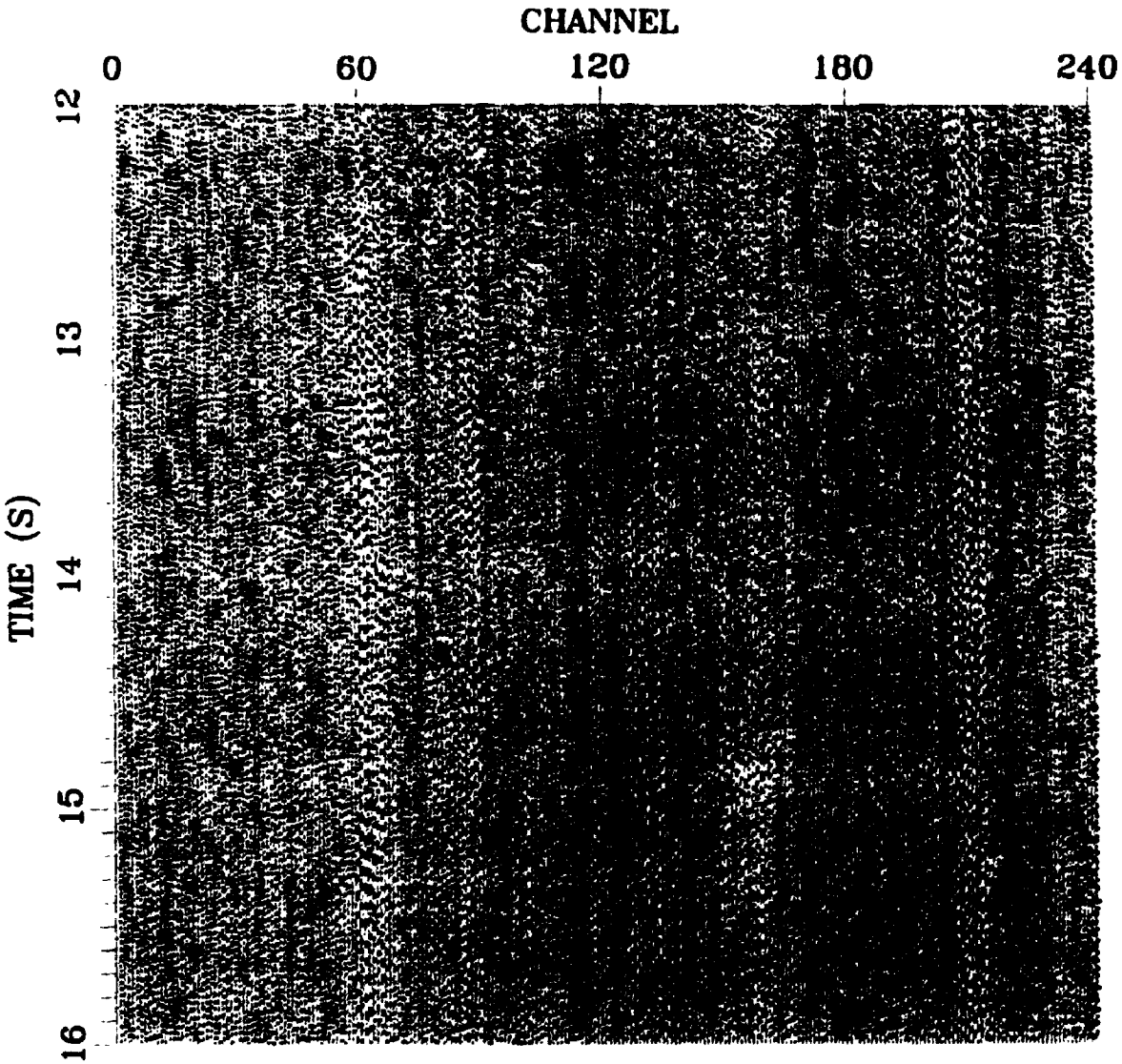

Fig. 7.6 a) Enlargement of the deep part of shot gather VP 219 (see Fig. 7.5a). The data were AGC-gained.

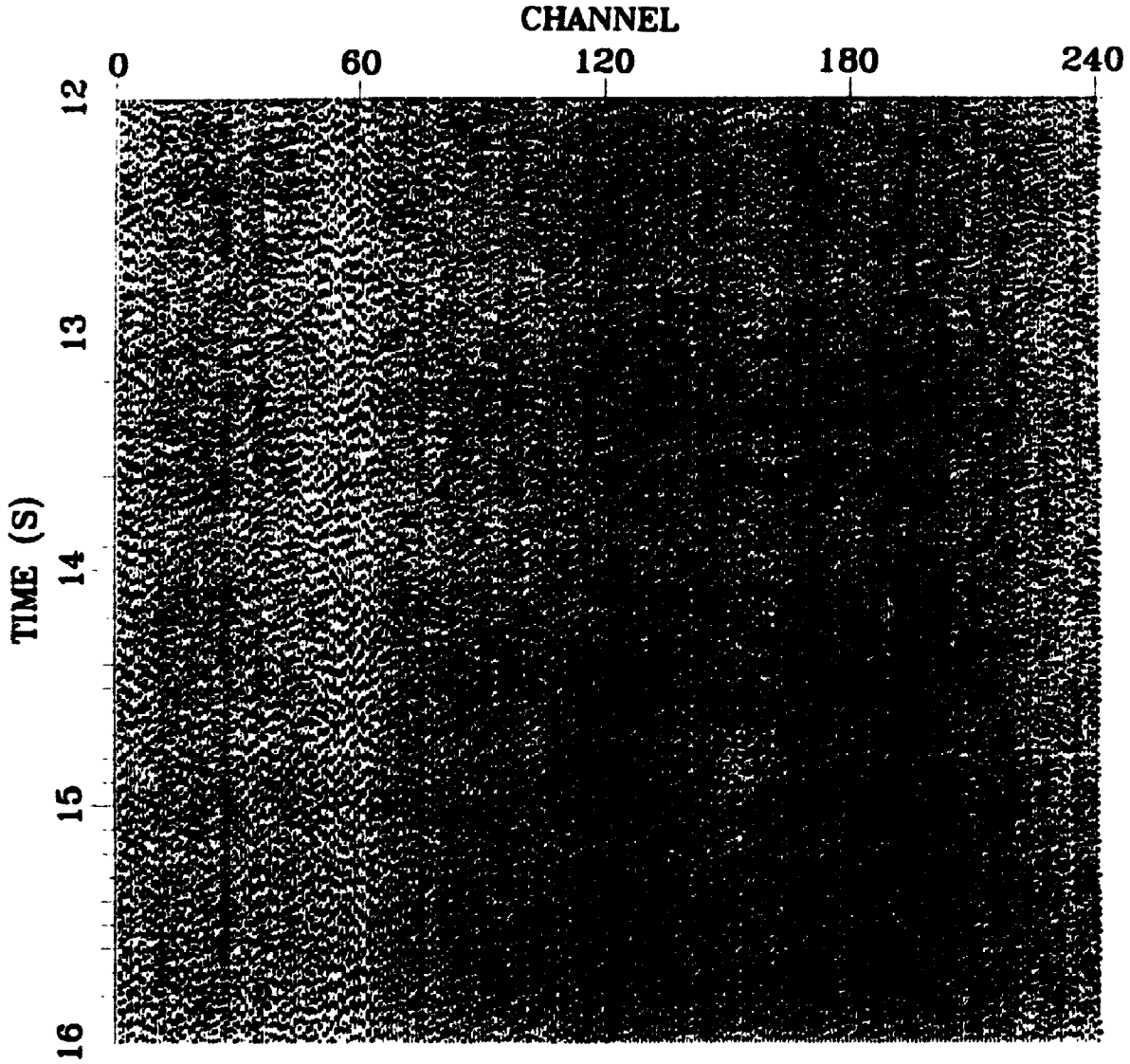

Fig. 7.6 b) Enlargement of the deep part of shot gather VP 387 (see Fig. 7.5b). The data were AGC-gained.

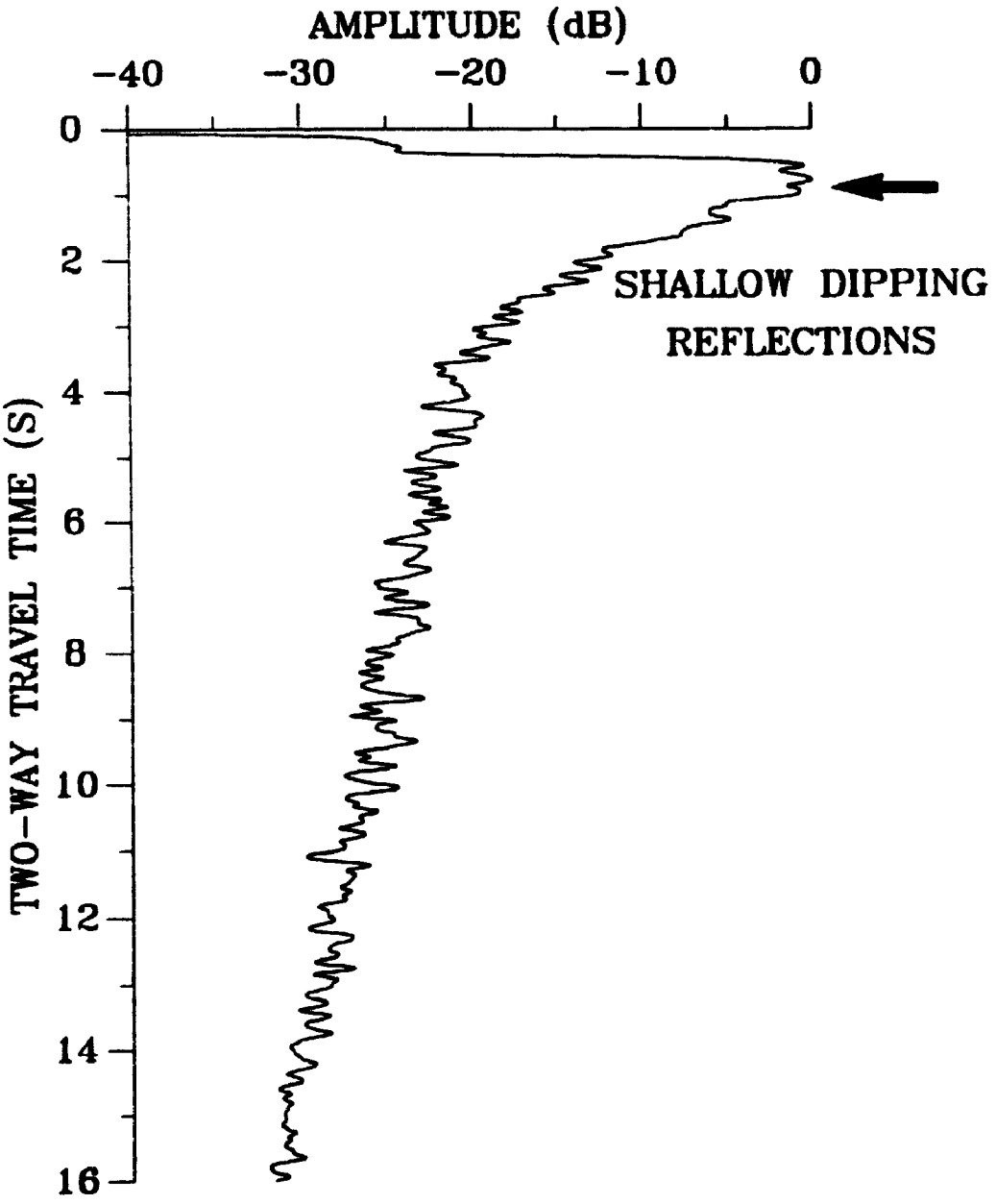

Fig. 7.7 a) Average amplitude decay curve determined from the first 20 channels of shot gather VP 219, where shallow dipping reflections are clearly observed (see Figs. 4.4 and 7.5a). No any gain was applied to the data.

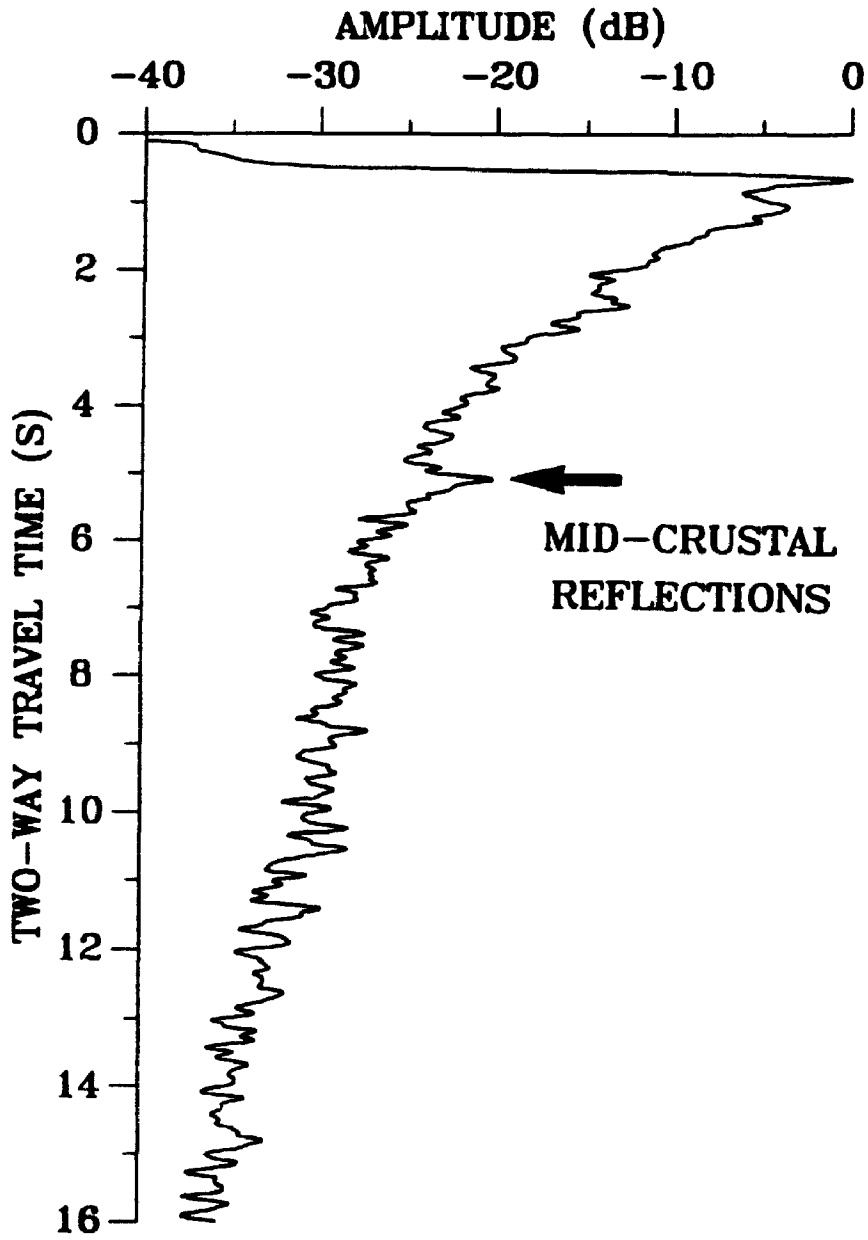

Fig. 7.7 b) Average amplitude decay curve determined from channels 101-120 of shot gather VP 387, where midcrustal reflections are clearly observed (see Figs. 4.5 and 7.5b). No any gain was applied to the data.

CHAPTER 8 INTERACTIVE PROCESSING OF REFLECTION LINE 9

8.1 Why process line 9

The significant improvement from the reprocessing of line 5 may well make one wonder whether all seismic reflection lines should be reprocessed, regardless of the relative quality of the commercially-processed seismic sections. To further test the credibility of the original processing, we choose line 9 as our second target following line 5, because line 9 was one of the best among all nine survey profiles in terms of the quality of the seismic sections. Geologically line 9 crosses a steep-dip normal fault, the Nansen Creek Fault (NCF) (Fig. 8.1). It is also hoped that reprocessing will provide a better image for the NCF.

8.2 Data Processing

The field data were first visually inspected to find out the data quality and to identify problems with the commercial processing. Two selected field shot gathers are given in Figs. 8.2 and 8.3. It is evident that the whole crust under line 9 is highly reflective. The seismic processing flow, developed during reprocessing line 5, was applied to line 9. In contrast to the commercial stacked section (Fig. 8.4), our final stacked section (Fig 8.5) brings out much more crustal reflections across the entire crust.

8.3 Results

Once again, our processing has greatly improved the seismic section of line 9, despite the fact that its original image was one of the best. The improvement can be seen across the whole section, in particular, the top three seconds of the section. The commercial section gives one the impression that the top two seconds were non-reflective. This seismic processing

artifact could be easily identified if one inspects the field data (Figs. 8.2a, 8.3a). It should be emphasized that both sections are plotted in the exact manner after the same coherency-filter is applied to both the commercial and reprocessed stacked data. To illustrate the contrast between the commercial and reprocessed sections more clearly, the top three seconds of the south portion of line 9, are shown enlarged in Fig. 8.6. Although the NCF was imaged on the commercial section at deep depths (Leclair et al., 1991), it cannot be traced to shallow depths. Therefore it is difficult to make direct correlation between the surface geology and the seismic images. With our enhanced seismic section, the NCF can be traced all the way from the deep crust (7 s TWT) to the surface (Fig. 8.5).

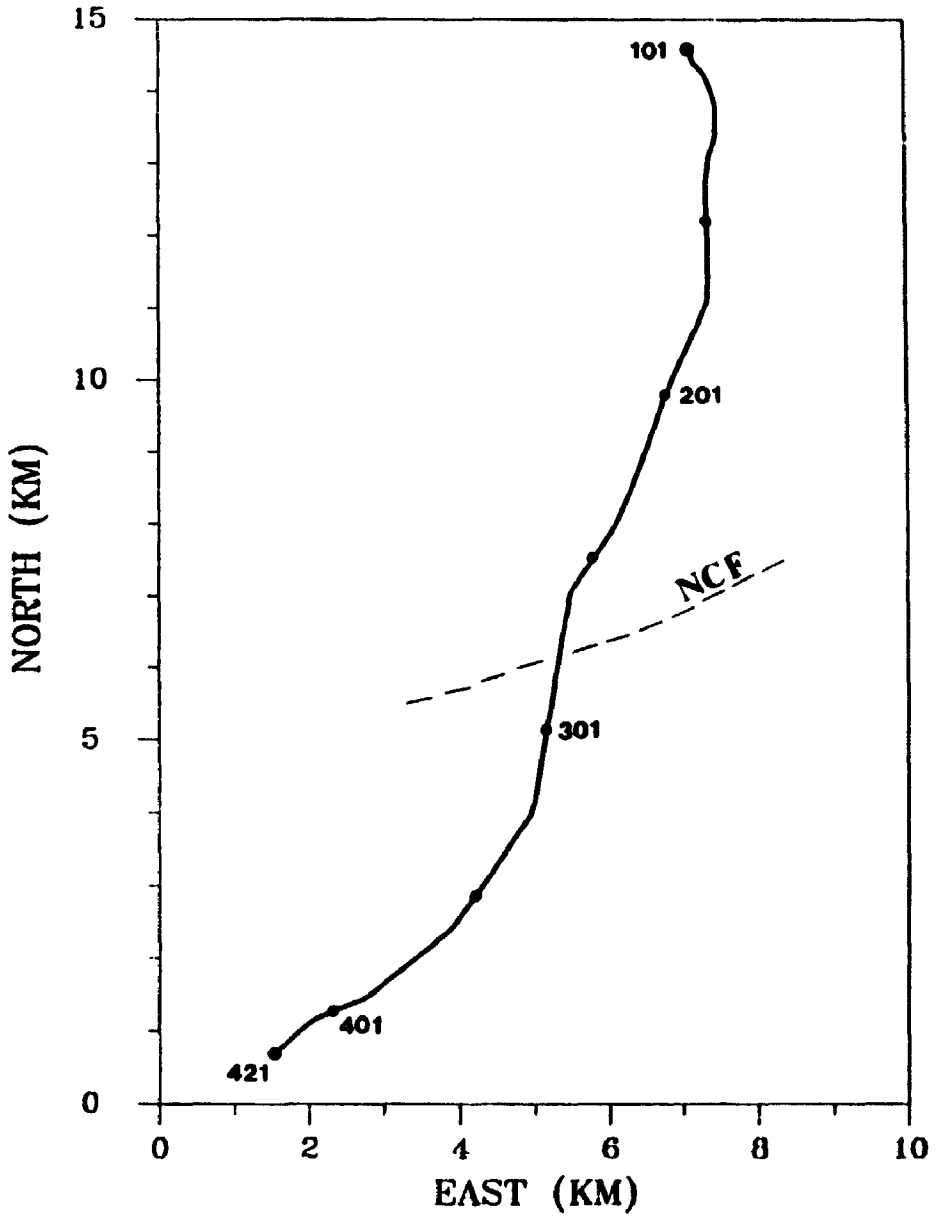

Fig. 8.1 Geometry of reflection line 9. NCF represents the Nansen Creek fault.

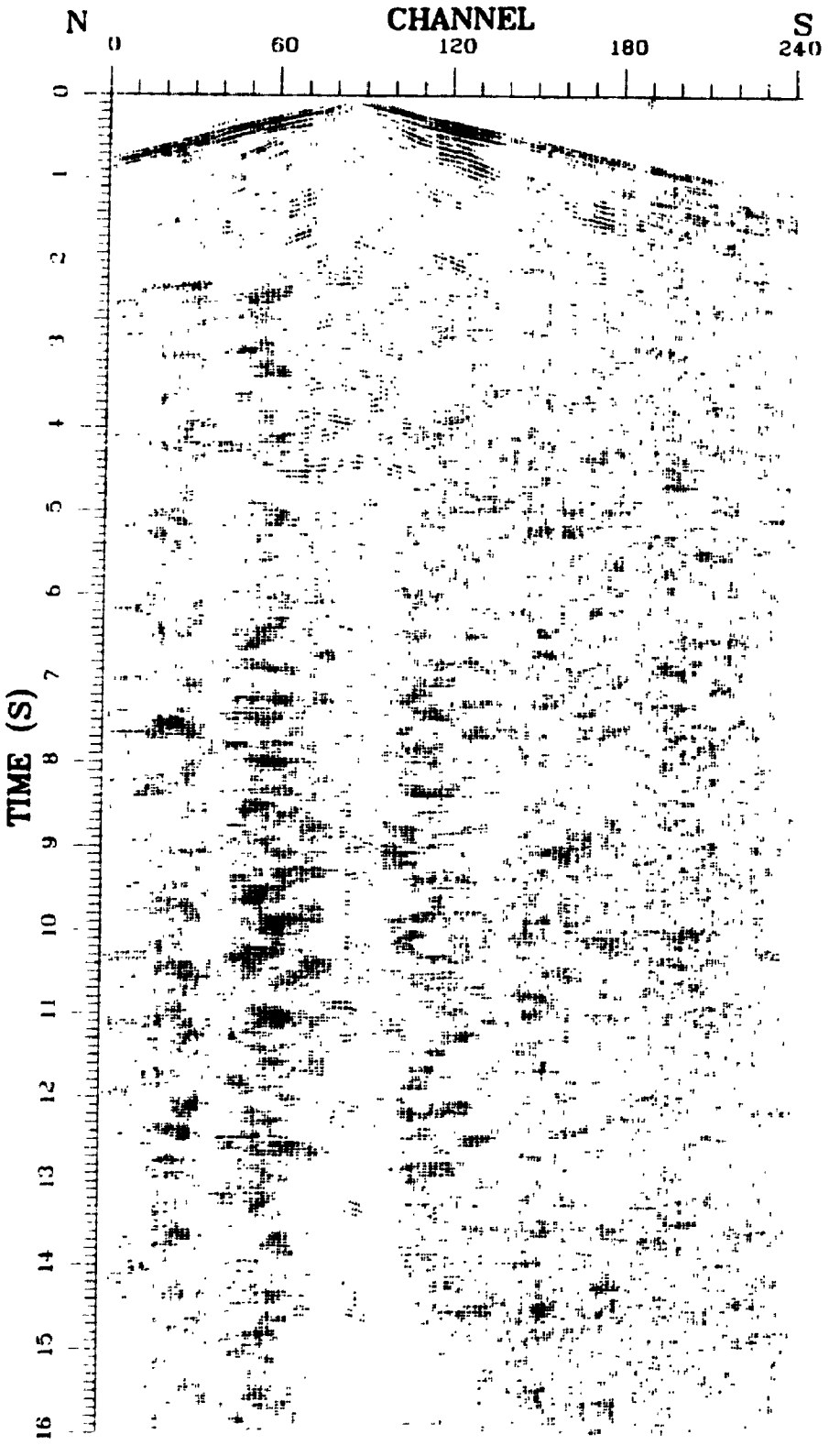

Fig. 8.2 a) Field shot gather VP 267 (coherency-filtered). The data were AGC-gained. The section was plotted with trace-normalization.

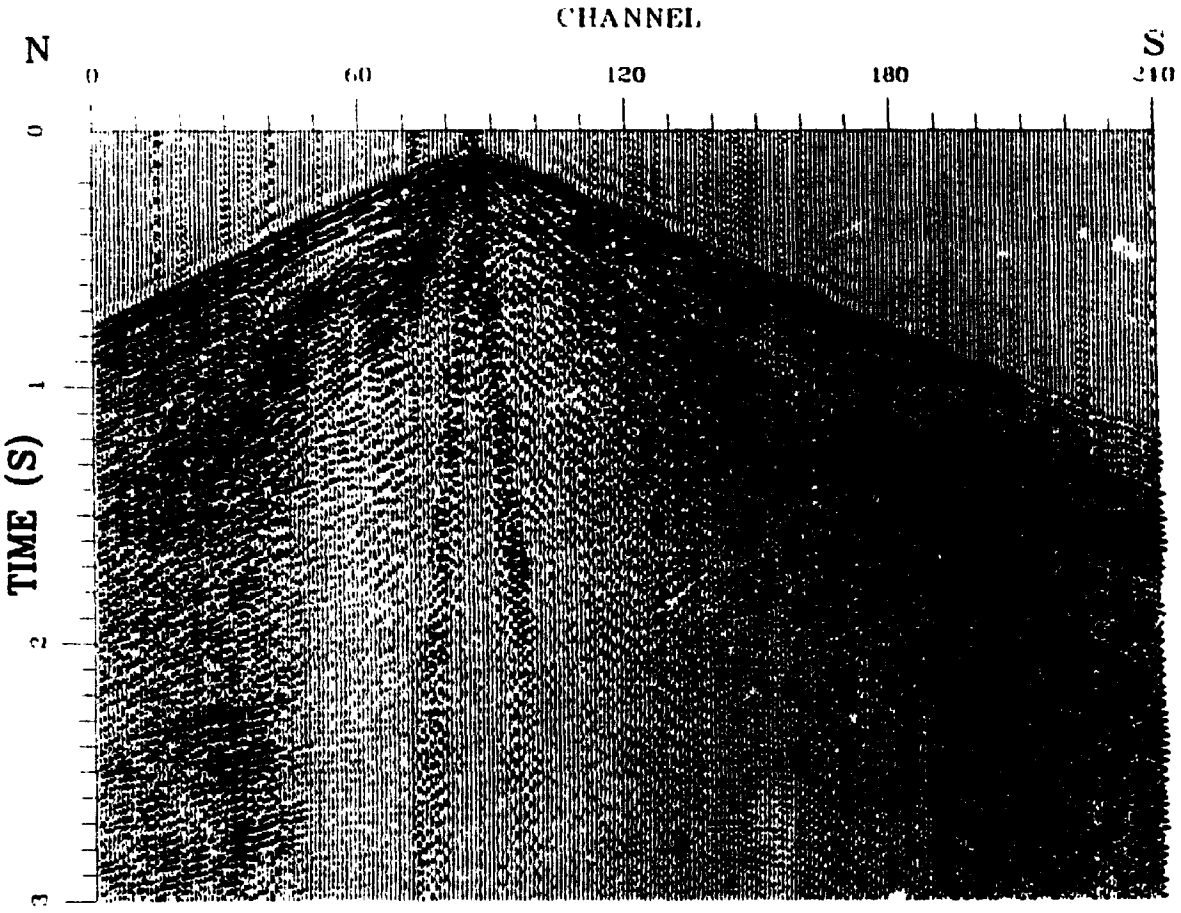

Fig. 8.2 b) Enlargement of the top three seconds of field gather VP 267. Note the shallow reflections between 1 and 2 s on two sides of the gather. No AGC gain was applied. The section was plotted with trace-normalization.

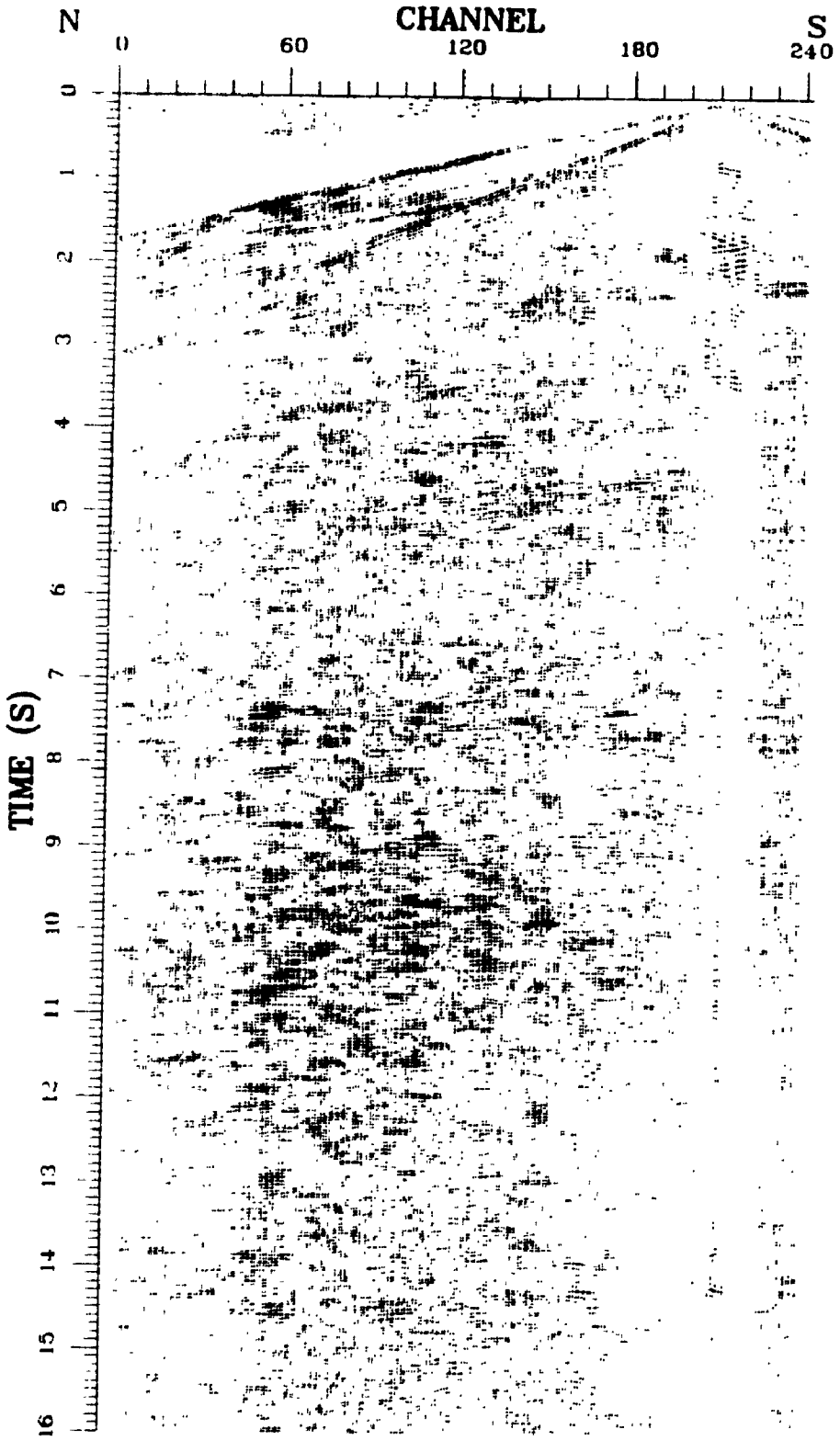

Fig. 8.3 a) Field shot gather VP 393 (coherency-filtered).The data were AGC-gained. The section was plotted with trace-normalization.

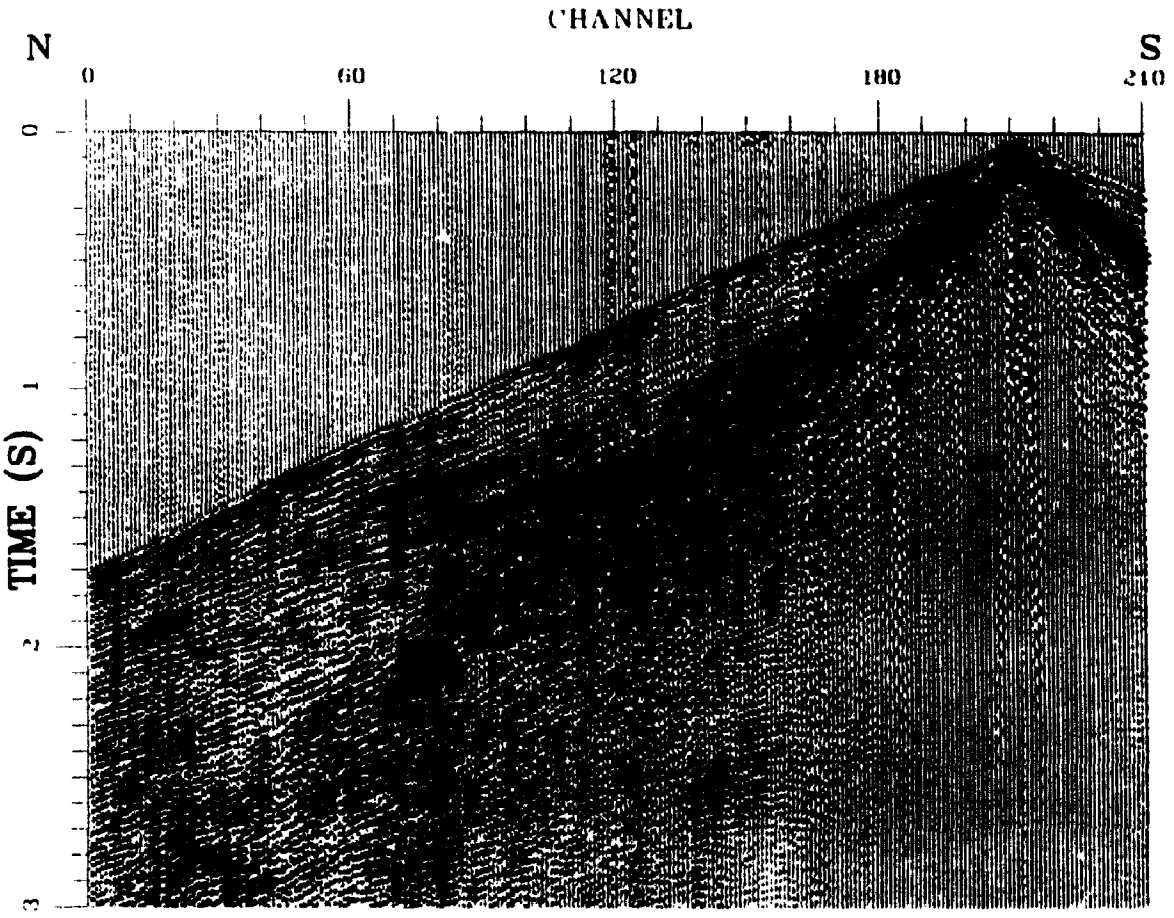

Fig. 8.3 b) Enlargement of the top three seconds of field gather VP 393. Note the shallow reflections seen on channels 60-180 between 1 and 2 s. No AGC gain was applied. The section was plotted with trace-normalization.

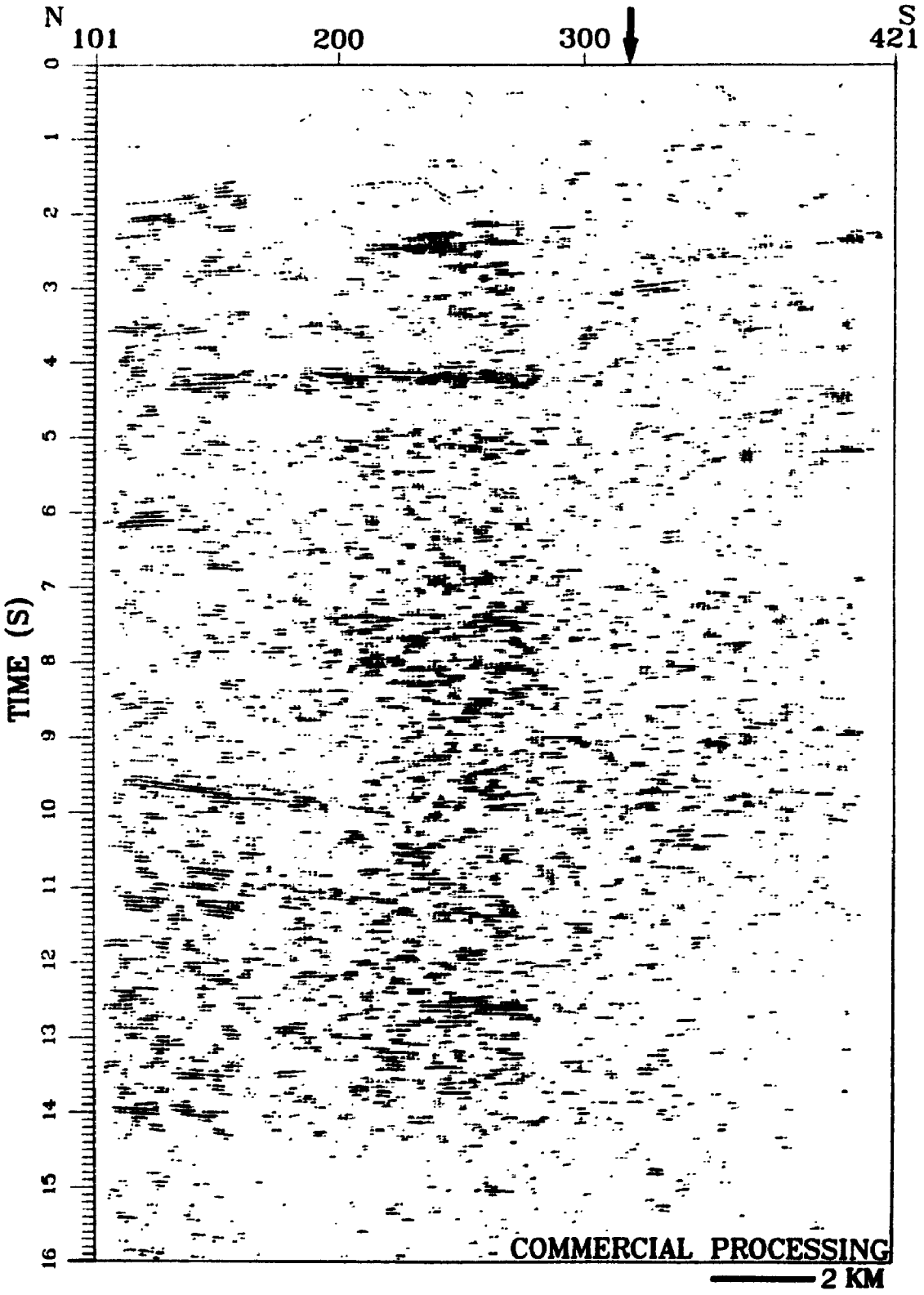

Fig. 8.4 The commercial seismic section of line 9 (coherency-filtered). The section is plotted 1:2 for an average velocity of 6 km/s. Station numbers are labelled at the top. The Nansen Creek fault is marked by arrow.

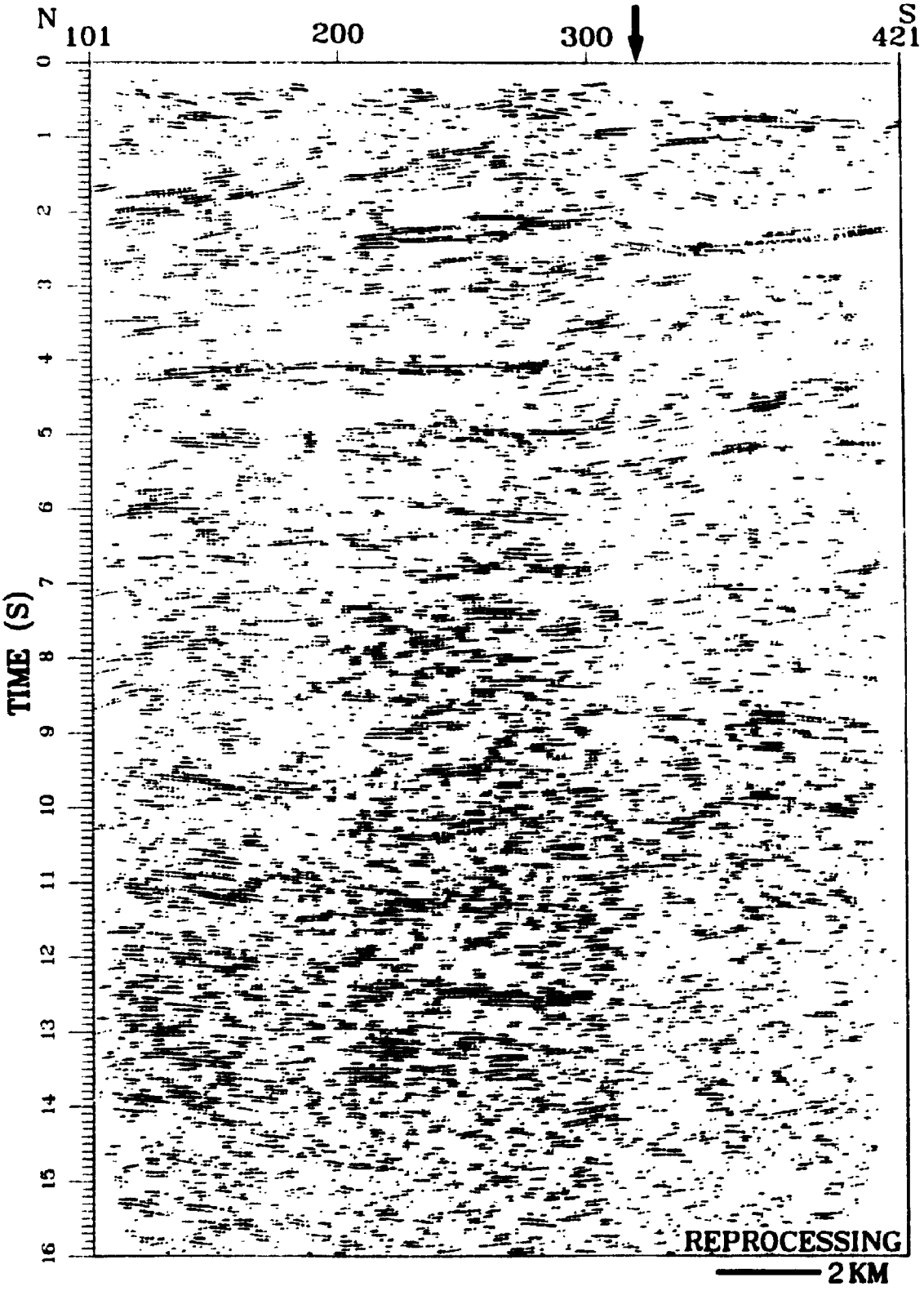

Fig. 8.5 The reprocessed seismic section of line 9 (coherency-filtered). The section is plotted 1:2 for an average velocity of 6 km/s. Station numbers are labelled at the top. The Nansen Creek fault is marked by arrow.

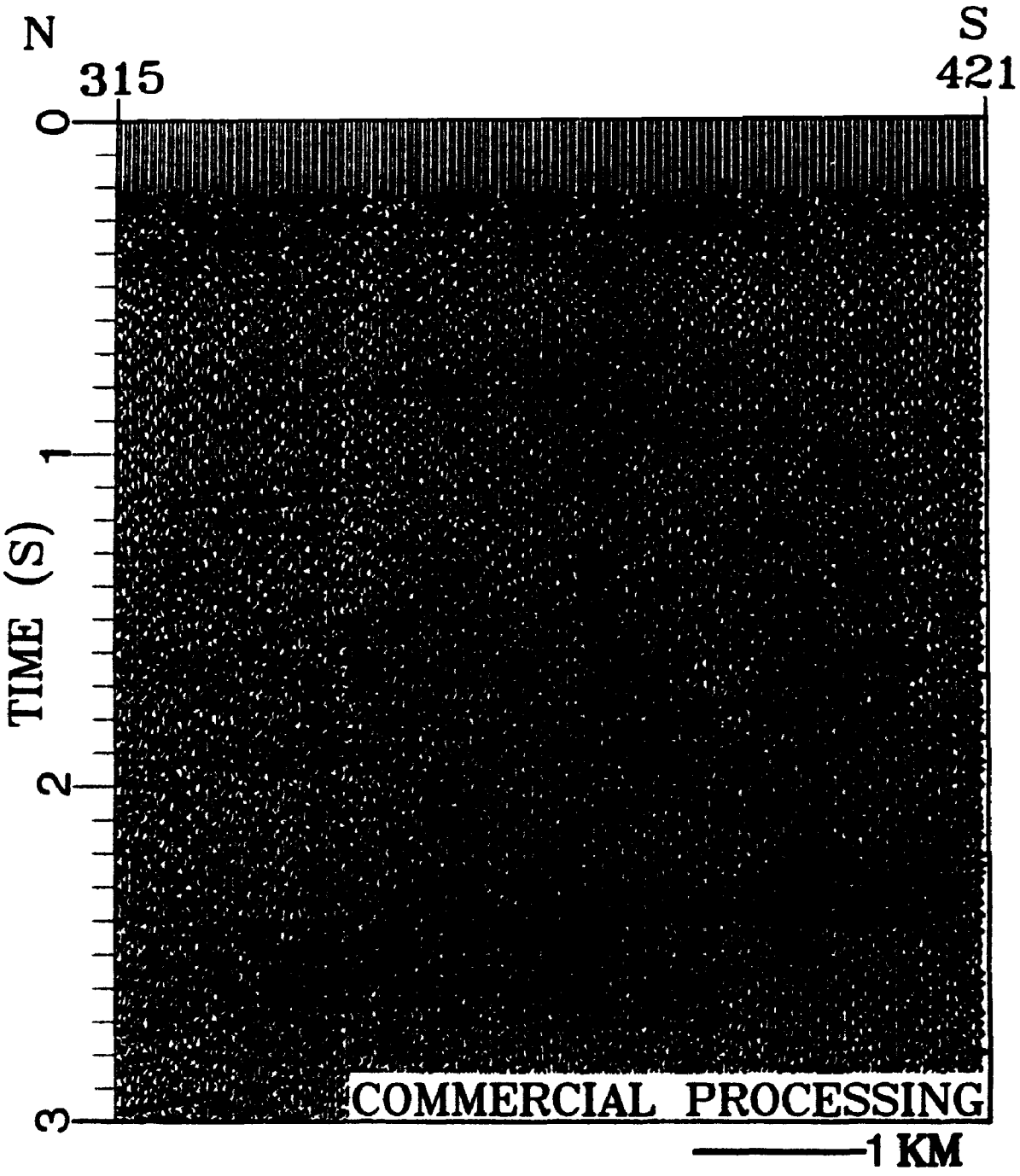

Fig. 8.6 a) The commercially processed section of the top south portion of line 9.

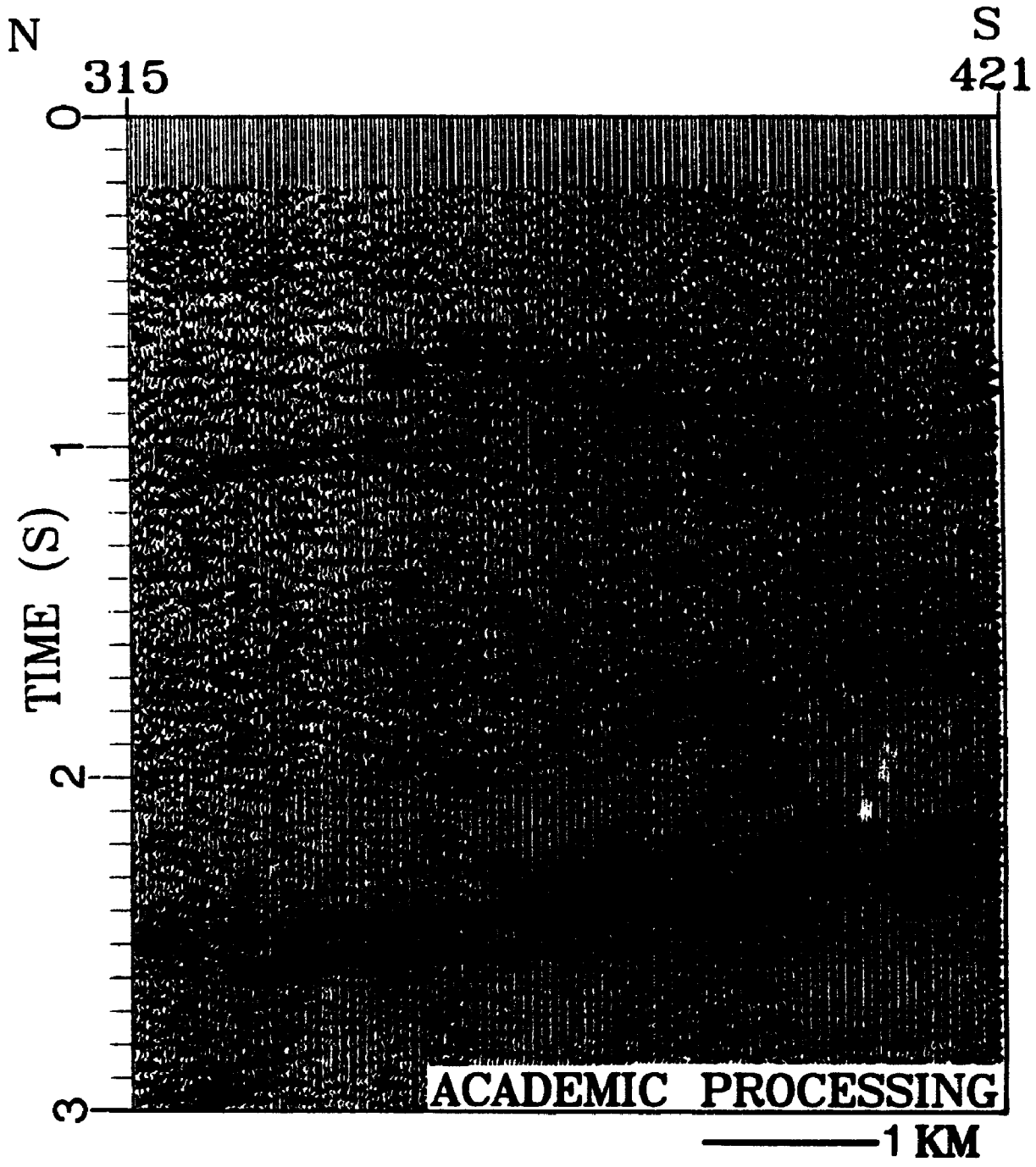

Fig. 8.6 b) The reprocessing section of the top south portion of line 9.

CHAPTER 9

SEISMIC REFLECTIVITY PATTERNS OF THE KAPUSKASING UPLIFT

9.1 Introduction

Over the past 20 years there has been a dramatic increase in the number of deep seismic reflection surveys conducted over the world (see for example, Barazangi and Brown, 1986a and b; Mereu et al., 1990a; Meissner et al., 1991). These studies have shown that the nature of the crust is exceedingly complex and that large differences in reflection pattern exist when different regions are compared with each other. An examination of these patterns and how they relate to tectonic processes such as extension and convergence has been the subject of numerous papers (Matthews and Cheadle, 1986; Brown, 1987; Mooney and Brocher, 1987; Smithson et al., 1987; Wever et al, 1987; and Meissner et al., 1990).

A consensus, which has emerged from these studies, is that a transparent upper crust overlying a reflective lower crust with the Moho clearly defined by layered reflections is a characteristic of young extensional terranes, while a reflective upper crust underlain by a transparent lower crust with the Moho poorly defined may be more characteristic of old shield areas. In this chapter it is shown that contrasting reflectivity patterns can also be seen between adjacent geological blocks in the Archean Canadian Shield and that there may not always be a simple relation between crustal reflectivity and crustal age.

The data employed here were obtained from the Kapuskasing deep seismic reflection survey and originally processed by an industry contractor (see chapter 3 for details). Ideally, reprocessed data should be used if available, as the commercial processing is inadequate. It should be mentioned

that part of this study was conducted by using the CYBER/DISCO batch processing system of the LSPF in Calgary (see chapter 3). This was done long before we started our processing work utilizing our SUN/ITA interactive processing system. Although reprocessing improves the quality of seismic sections dramatically, as demonstrated in chapters 4 and 8, the improvement is consistent across the whole section. Thus, it is believed that reprocessing will, in general, not change the overall reflectivity pattern. But in some cases, dramatic changes can result as is shown in chapter 4.

9.2 Methodology

In 1957 Dohr first introduced a statistical method to evaluate deep crustal reflection data. In his method the number of reflections observed at each time interval from the seismograms was counted and plotted against the corresponding travel time. This kind of plot presents the distribution of reflections with depth. This method was recently modified by Wever (1984) who measured the cumulative length of reflectors within a time interval from line drawing sections (drawn by hand according to the final stacked sections), normalized it by the length of the survey line, and plotted it against the travel time.

Since the data used in this analysis were acquired with the same parameters and originally processed with the same procedure, a modified version of Wever's method was adopted. First a coherency filter with a 100 ms time window and 32 ms increment was applied to all commerciallly stacked data to automatically extract coherent events, here treated as reflections (Fig. 9.1a). Then the number of reflections picked within each time interval for each common-middle-point (CMP) trace was added up along each segment or the whole section according to regional geology, normalized by the total number

of CMP traces and plotted against the travel time to form a histogram as shown in Fig. 9.1b. Theoretically, it would be better to have used migrated data, however these were not used here as it was felt that migrating artifacts contaminated the results (see Figs. 4.28, 4.29).

9.3 Results

The method described above was applied in the same manner to all the stacked data, excepting those from line 5 due to extremely poor quality of the commercially processed data. The main results are presented in Figs 9.1-9.6. The data can be divided into three groups according to the survey line locations: (1) lines 2, 3 ,4 and part of lines 1 and 6 are in the Chapleau block (CB) of the Kapuskasing structure; (2) south-east portions of lines 1, 6 and 8 are in the Abitibi greenstone belt (AGB); and (3) lines 9 and 10 are in the Val Rita block (VRB) of the Wawa greenstone belt (Fig. 3.1). Seismic reflections in the KU show a very complex pattern in which most reflectors are seen in the upper crust (Figs. 9.1-9.2). In general, shallow reflections can be related to surface rock outcrops (Percival et al., 1989). As the earth's crust is both laterally and vertically heterogeneous, it is doubtful that a histogram from one survey line would be representative of the entire survey region. Fig. 9.3 gives the overall reflection distribution in the CB, which is constructed by using all the data within the block (more than 6000 CMP traces). Statistically this is believed to represent the reflection signature of the CB, and hence the reflection signature of the Kapuskasing belt, as the CB is its most important part. The reflectivity changes resulting from the effects of source coupling and processing would be averaged out. Overall in the CB most of the reflections (67%) are concentrated in the first 6 s TWT. The lower crust and upper mantle are, for

the most part, transparent with no indication of the Moho.

One of the most striking aspects of the data is that across the Ivanhoe Lake fault zone (ILFZ) to the east, the crustal reflectivity shows a very significant increase as seen in Fig. 9.1. Similar observations are also shown along lines 6 and 8 (Figs. 9.2, 9.4). It is apparent that the ILFZ not only acts as a geological boundary separating the Kapuskasing belt from the AGB but also as a reflectivity boundary isolating the poor reflection zone (the KU) from the high reflection zone (the AGB). A similar phenomenon was reported from the BIRPS deep reflection surveys conducted around the Caledonian orogen (Brewer et al., 1983; and Peddy and Hobbs, 1987). It should be pointed out that the results from the reprocessing of line 5 do not support this observation.

In contrast to the CB, the entire crust in the survey region of the VRB is highly reflective (Figs. 9.5, 9.6). Near horizontal reflectors are predominant across the seismic sections. Moreover, they are strong and continuous. The rapid disappearance of the reflectors seen at 14 s TWT marks the reflection Moho (Brewer et al., 1983; and Klemperer et al., 1986), essentially a boundary contrasting the reflective lower crust with the seismically transparent upper mantle. This reflection Moho is in good agreement with the refraction Moho (see below).

9.4 Moho: Comparison of the Reflection and Refraction Data

Comparison of the near vertical reflection and long range refraction data displays some interesting features common to both methods. First of all, both data sets show the KU possessing a complex geological structure. Two refraction sections shot reversely along line CJ, the axis of the KU, are provided in Figs. 9.7a and 9.7b. Except for first arrivals, no other major

events such as the PmP, wide-angle reflection from the Moho, can be identified on the section. Pronounced coda energy is seen everywhere following the first arrival, implying that rocks in the KU are highly heterogeneous. Absence of the PmP reflections indicates that the Moho under the KU is a wide transition zone. These observations are consistent with those seen from the reflection data in the CB as described above. The Pn arrivals, refractions from the uppermost mantle, are clearly seen from shotpoint C but few from the reverse shotpoint J (Fig. 9.8). With limited Pn arrivals and with no PmP reflections, the depth to the Moho can not be constrained with much confidence. 2-D seismic ray-tracing modeling (Fig. 9.7c) indicates that the Moho under the KU is a wide transition zone (about 10 km thick).

Refraction line AE cuts through the VRB and the Groundhog River block in a direction almost perpendicular to the KU (Fig. 3.1). A refraction section shot at A along the line is presented in Fig. 9.9a. Large amplitude PmP reflections are prominent on the section between 120-180 km, implying that the Moho under the sampling points (middle points between the shot and stations) is a relatively sharp boundary. 2-D ray-tracing modeling (Fig. 9.9b) shows that the Moho under line AE varies in depth from 40-45 km (Wu, 1987). This is consistent with the reflection Moho beneath the VRB, defined as the base of the lower crustal reflecting zone at about 14 s TWT (Figs. 9.5, 9.6). This is equivalent to 42-45 km for an assumed average P velocity of 6.0-6.5 km/s. This agreement is consistent with the study by Mooney and Brocher (1987), who compare coincident reflection and refraction surveys worldwide and find that in many cases the reflection and refraction Mohos are the same. The marked contrast between refraction sections shot along lines CJ and AE is evident and further confirms the reflectivity differences between

the KU and VRB.

9.5 Discussion

The observed reflectivity patterns must owe their origins to the tectonic and geological processes which occurred in the historical development of the present day Shield. Geological studies such as those by Percival and Card (1983) show that the KU is distinguished from the adjacent Wawa, Abitibi, Quetico and Opatica belts by an abrupt increase in metamorphic grade and by broader positive gravity and aeromagnetic anomalies. The KU transects the east-west trends of the adjacent terranes, indicating that it was formed at a later stage in the Shield development. Using evidence from surface geology, geobarometric data and gravity modeling, Percival and Card (1983) interpreted the KU as an upthrust cross section of middle to lower Archean crust. Recent Analysis of high resolution seismic data resurveyed along line 2 by Geis et al. (1990) indicates that the KU is a thin thrust sheet traceable to a depth of 12 km. All these indicate that the Wawa and Abitibi belts are parts of a formerly continuous belt, now interrupted by the KU.

The reflectivity of these belts could originate from either layering due to ancient igneous intrusion or metasedimentary or metavolcanic layering. It is speculated that, since the Superior craton was established, both the Wawa and Abitibi belts have not been involved in any major tectonic process. Therefore, this layering including the Moho has been well preserved. The lack of reflections in the lower crust under the KU is interesting. It is possible that the large scale crustal compression from which the KU was formed, caused uplifting and near surface faulting in the upper crust where rocks are brittle. The upper crustal reflectivity could easily result from sheared mylonite zones (Smithson et al., 1986; Green et al., 1990; Wu et al., 1992).

The same compression force could have produced ductile flow in the lower crust. This flow in turn might have resulted in small scale fold or disrupted structures (Percival et al., 1989), which had the effect of scattering seismic energy and erasing both the near vertical and wide angle PmP reflections. This process destroyed the original geological layering and increased the thickness of the Moho transition zone.

In conclusion, we have demonstrated that the crustal reflectivity and the nature of the Moho in the Canadian Shield are highly variable from one tectonic block to another. This study may indicate that crustal age does not always have much control over crustal reflection behavior. The pattern once established tends to be well preserved and may well show a state in which the crust was left after its last major tectonic event.

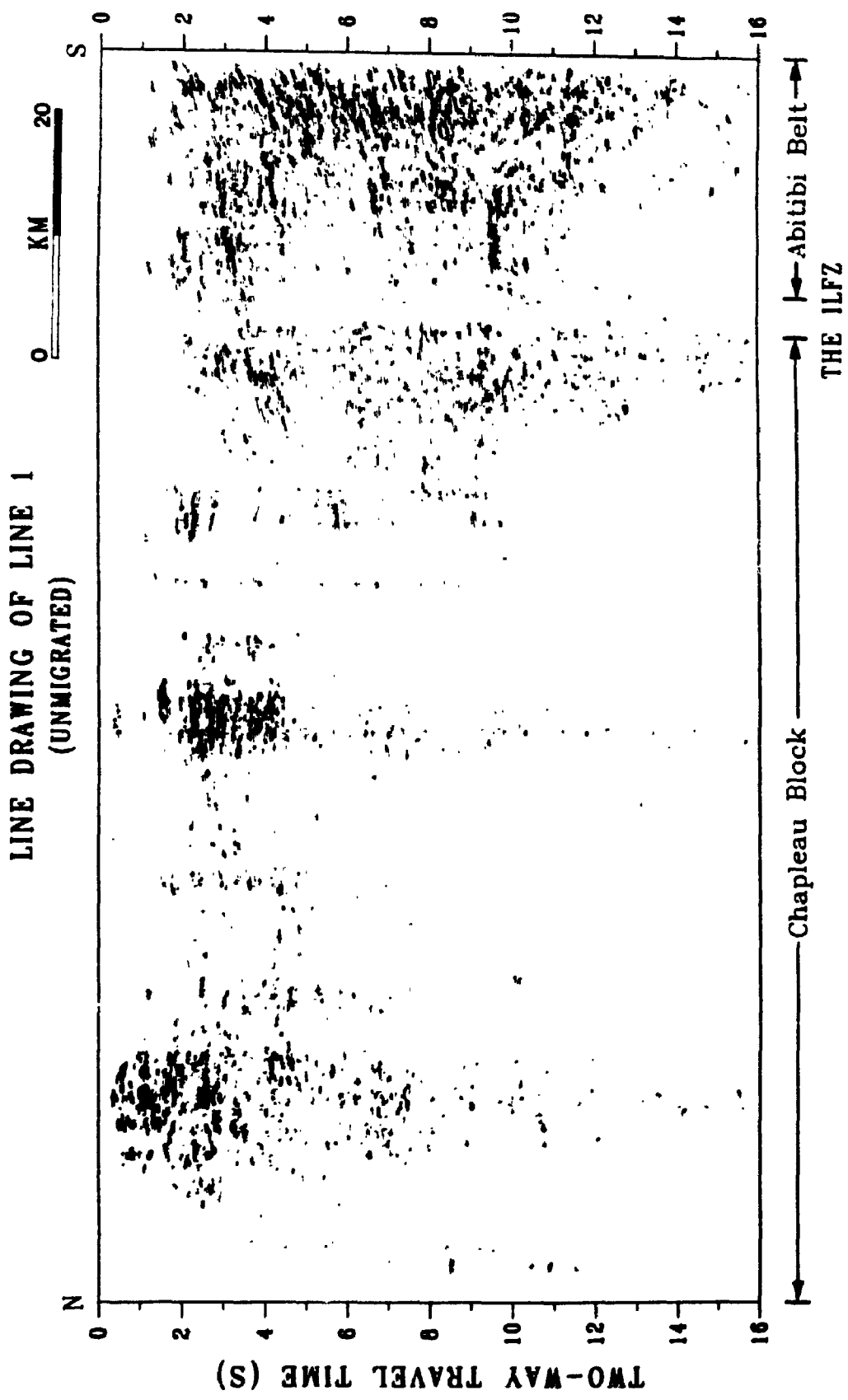

Fig. 9.1 a) Line drawing Of line 1.

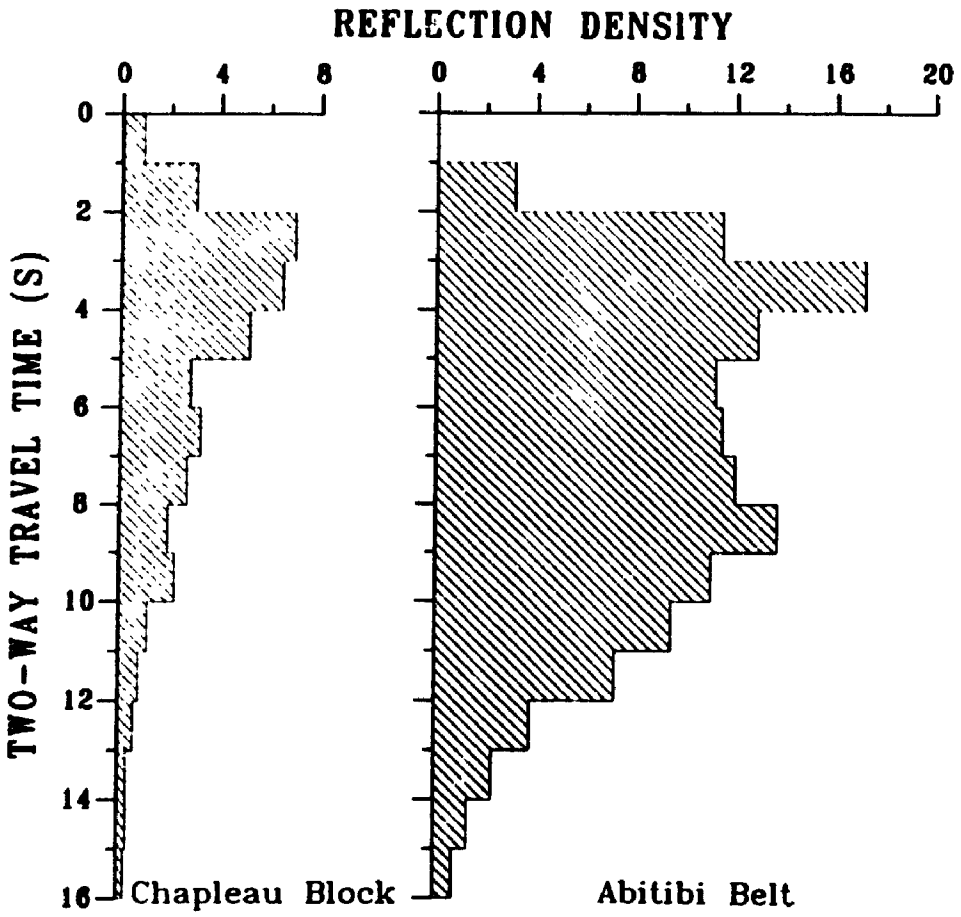

Fig. 9.1 b) corresponding segment reflectivity histograms.

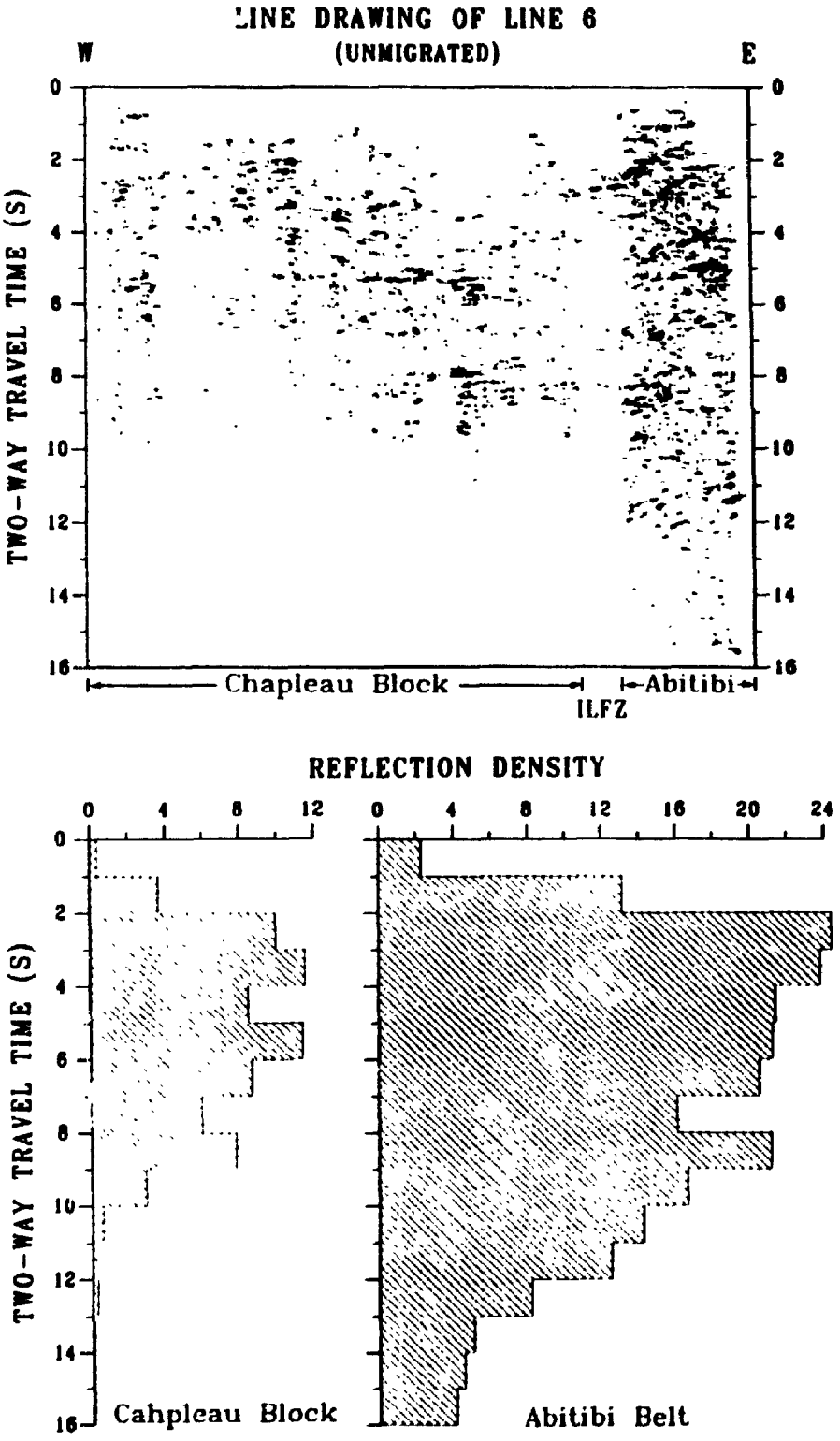

Fig. 9.2 Line drawing of line 6 and its segment reflectivity histograms.

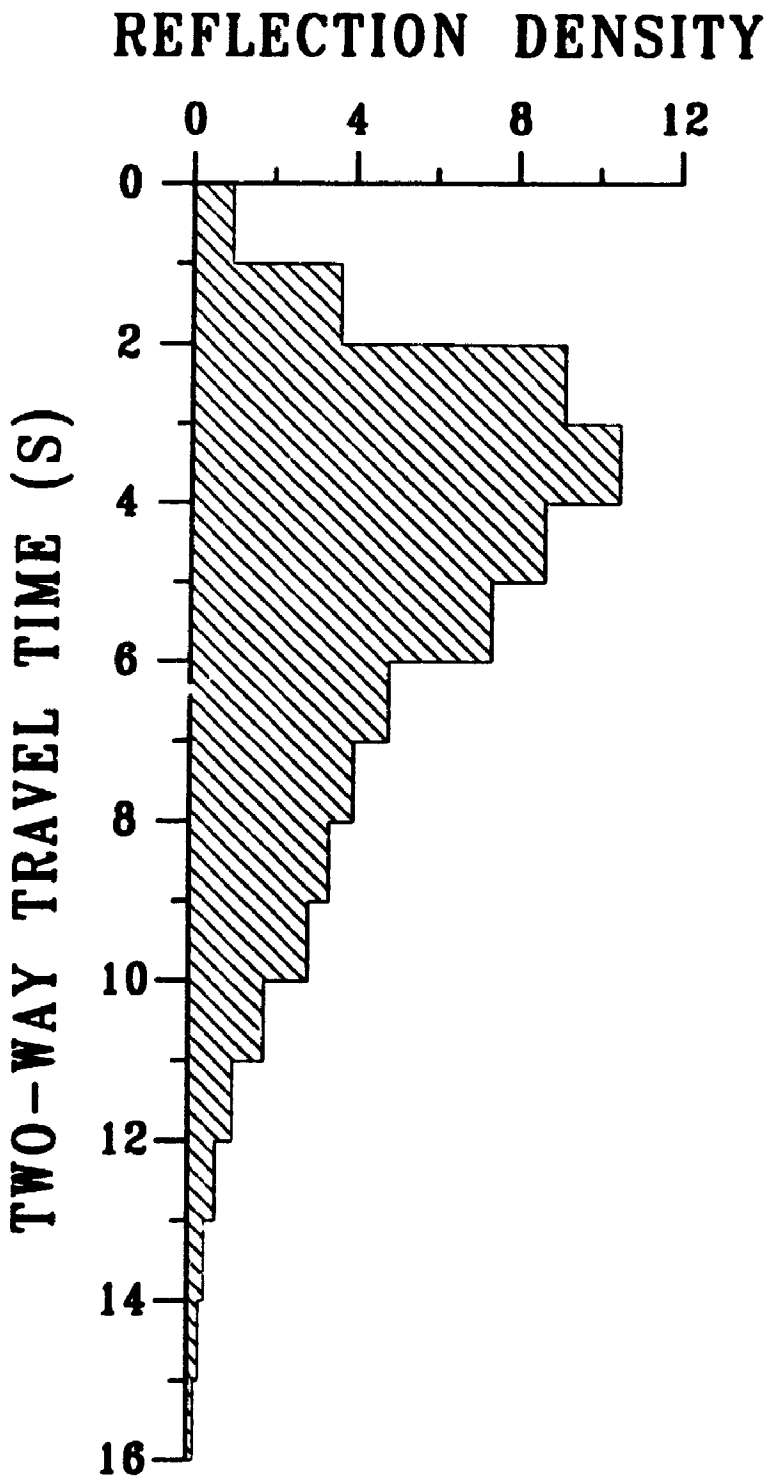

Fig. 9.3 The average reflection distribution for the Chapleau block of the Kapuskasing Uplift.

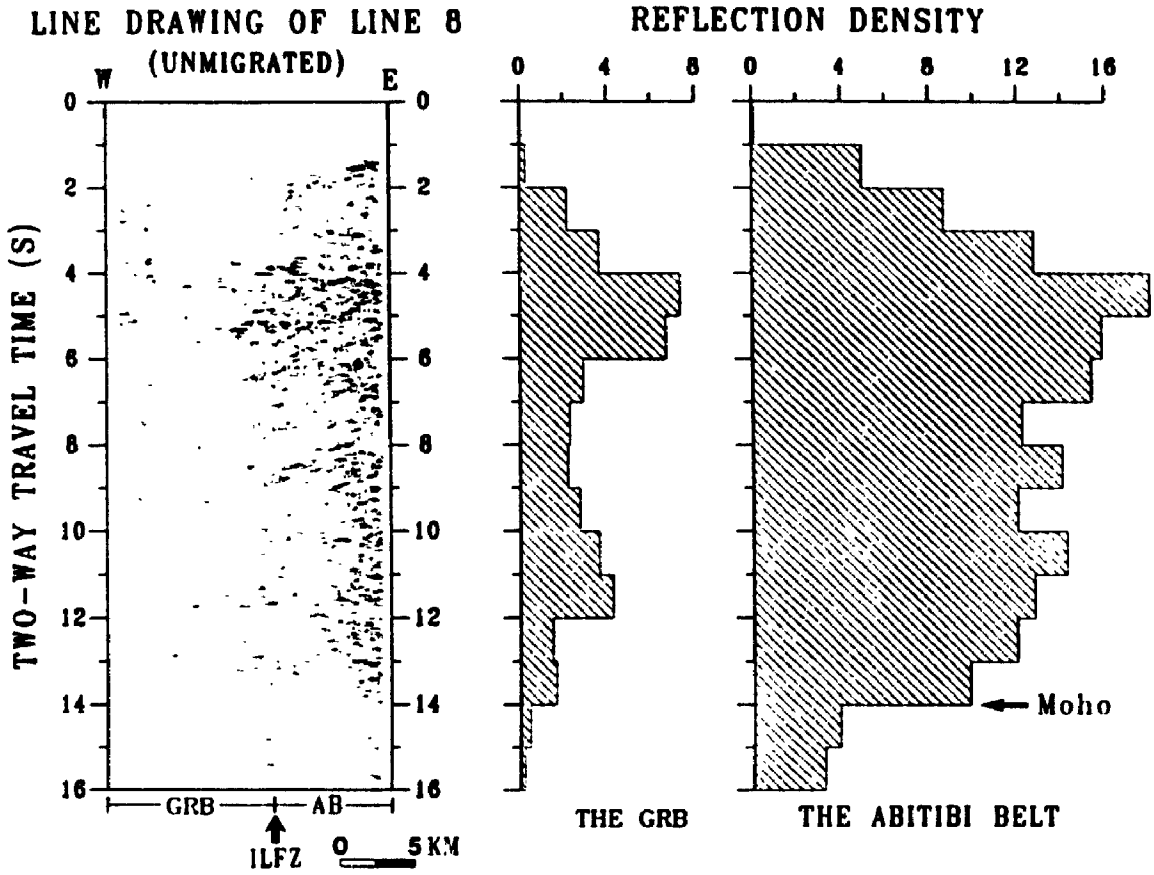

Fig. 9.4 Line drawing of line 8 and its reflectivity histograms.

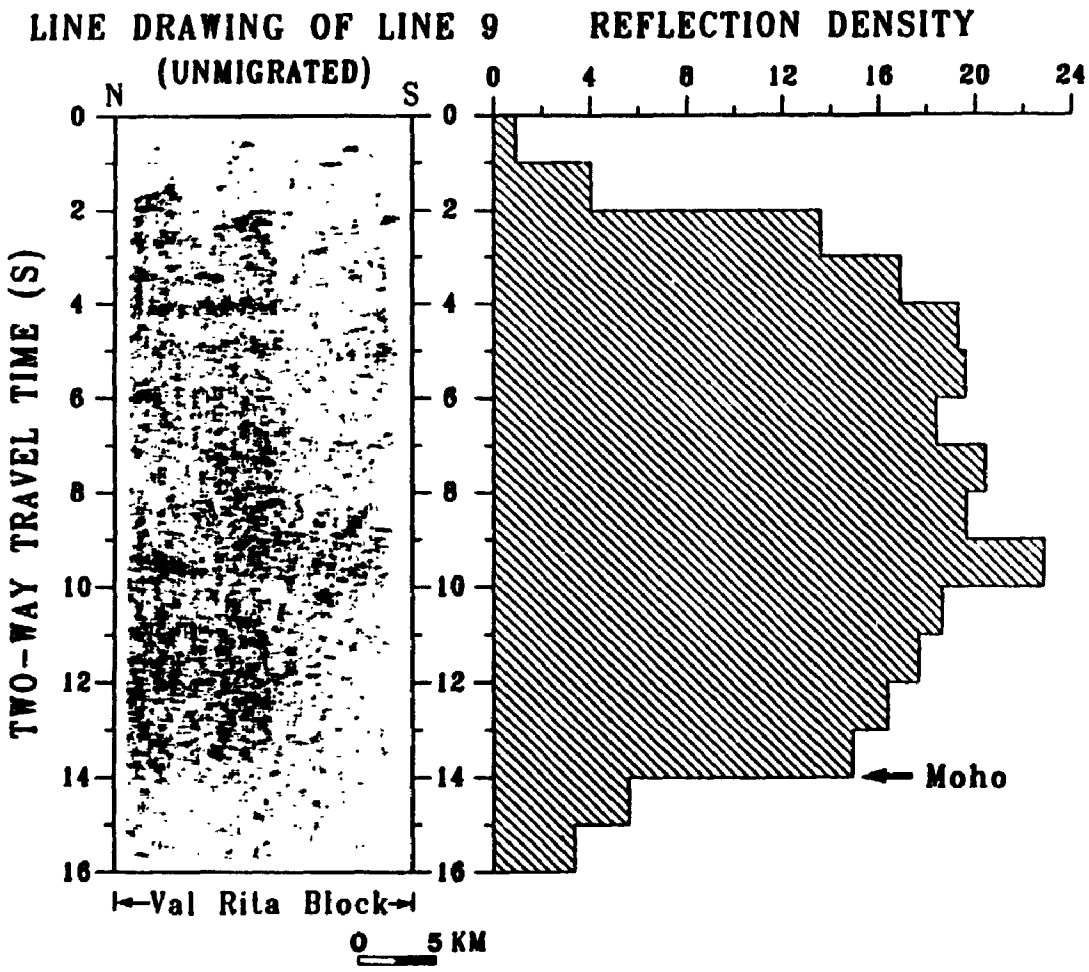

Fig. 9.5 Line drawing of line 9 and its reflectivity histogram.

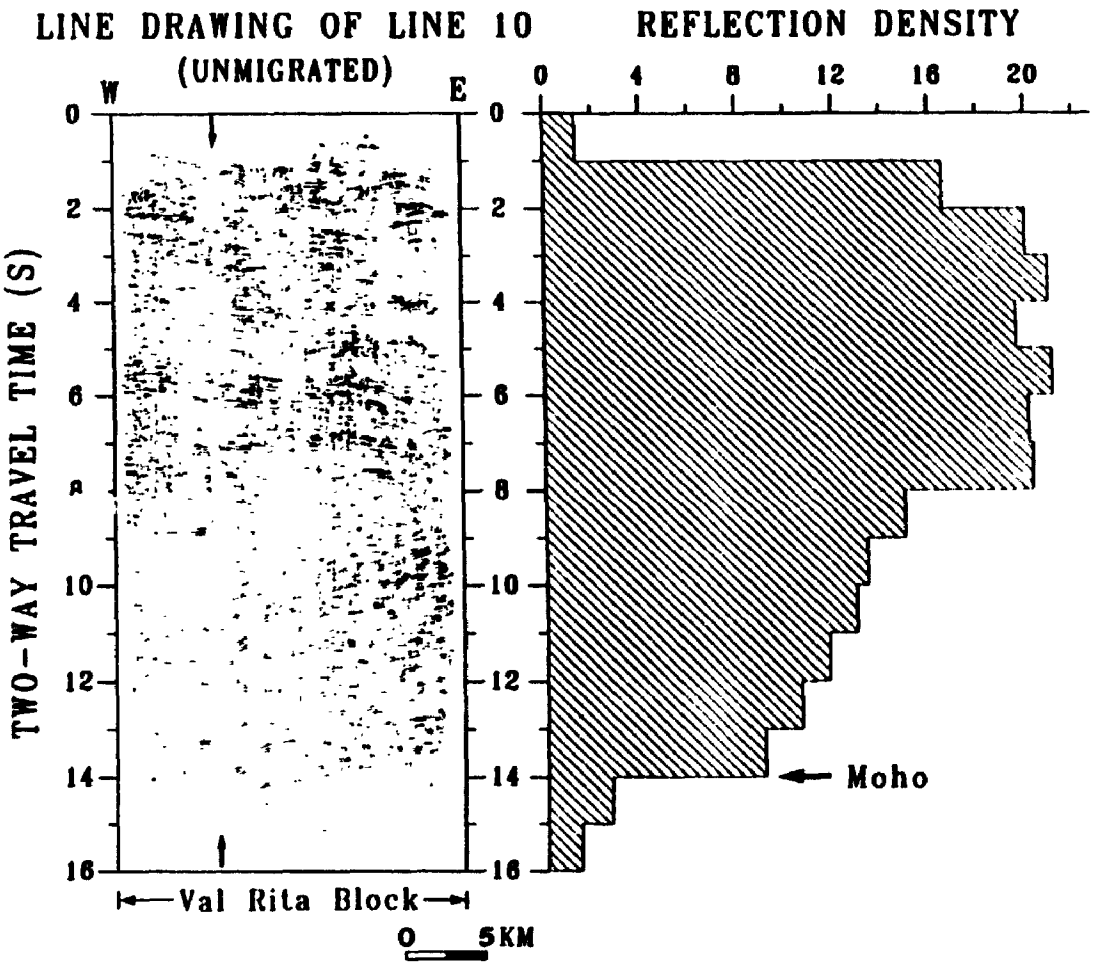

Fig. 9.6 Line drawing of line 10 and its reflectivity histogram.

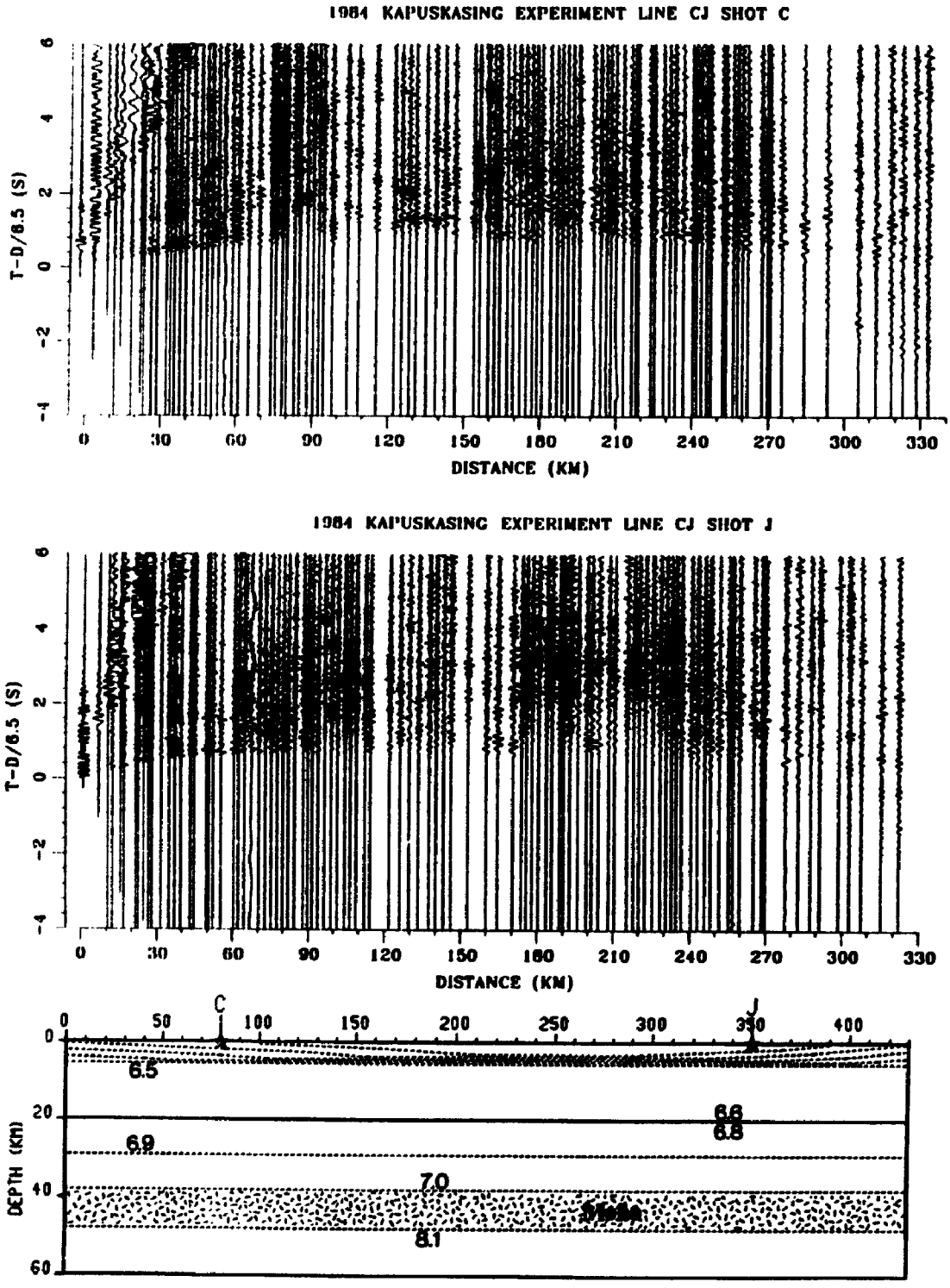

Fig. 9.7 a) Seismic refraction section shot at C along line CJ. b) Seismic refraction section shot at J along line CJ. c) 2-D P-wave velocity model along line CJ.

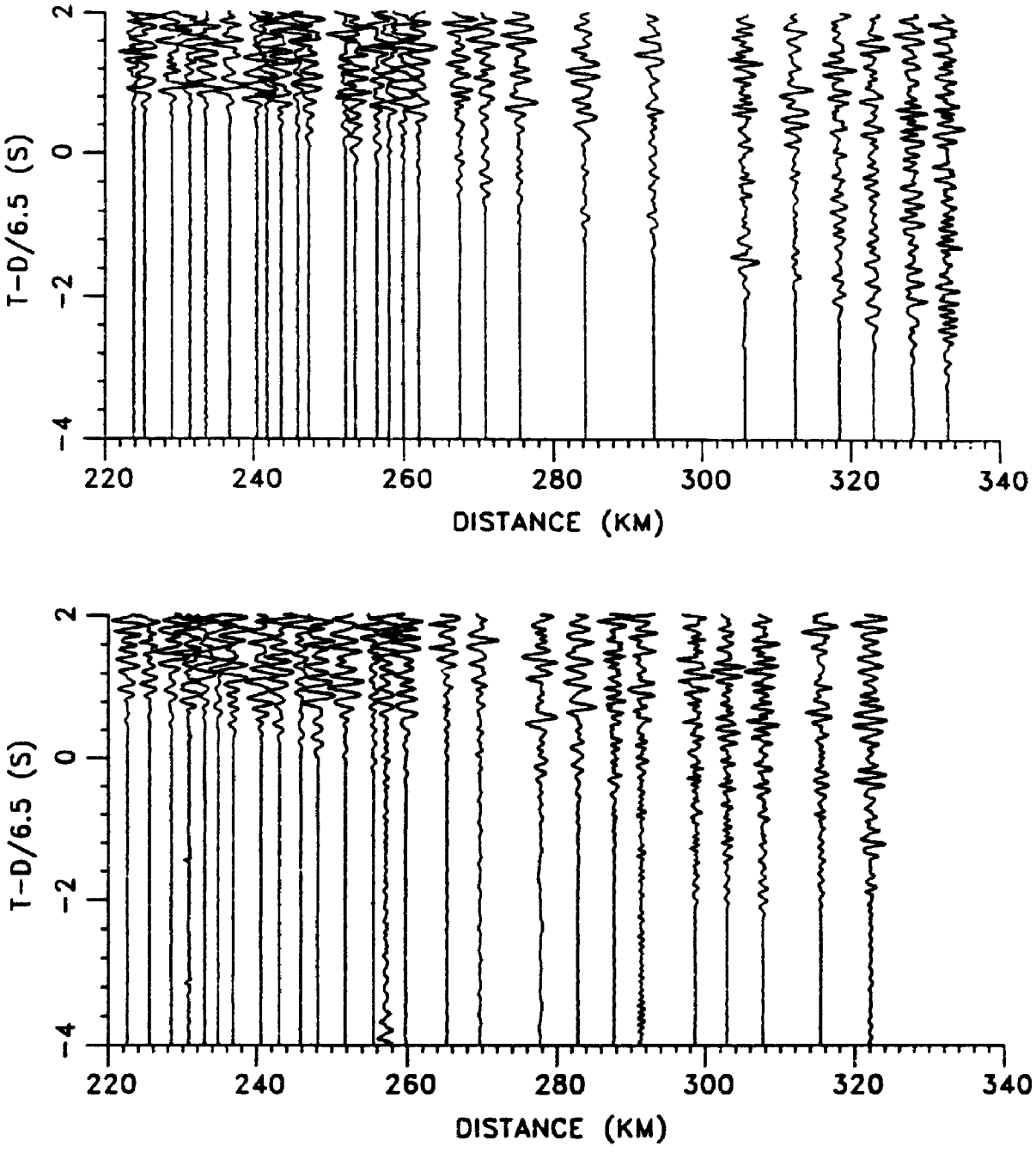

Fig. 9.8 Enlargement of Pn arrivals from shotpoints C (top) and J (bottom). Note that few Pn arrivals from shotpoint J can be identified with confidence.

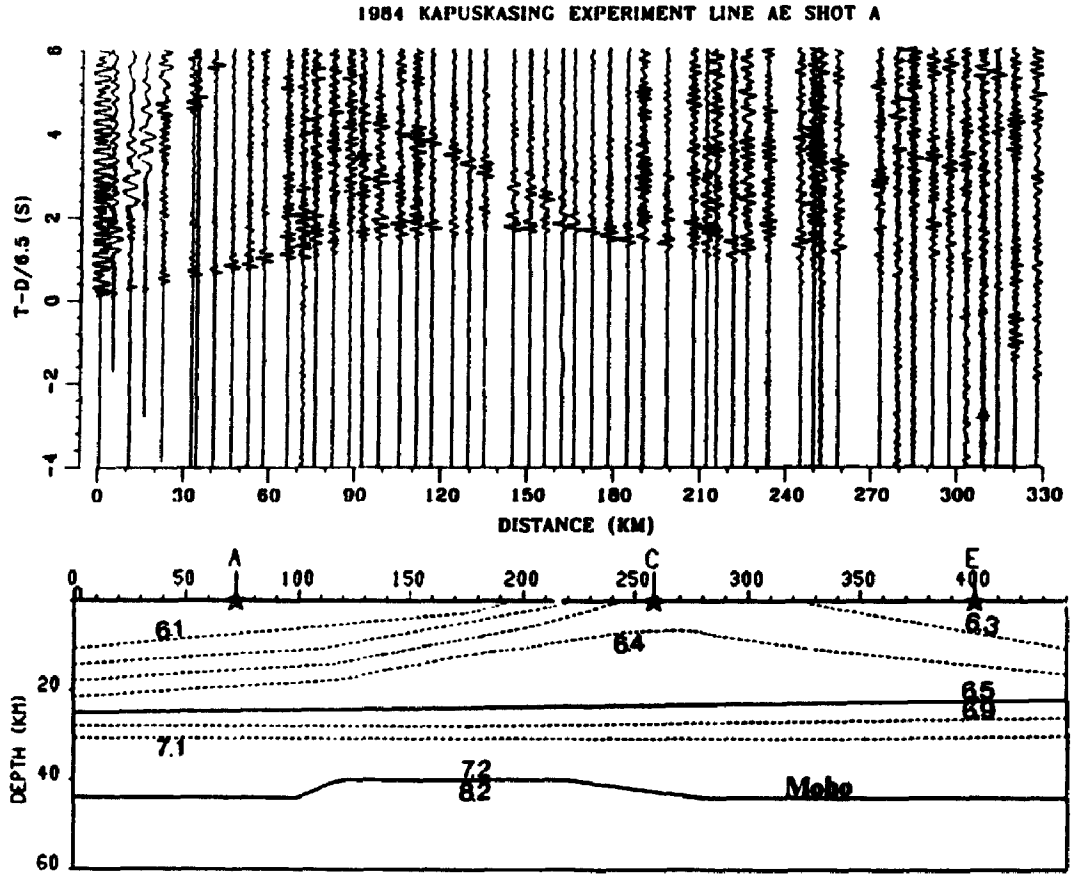

Fig. 9.9 a) Seismic refraction section shot at A along line AE. Note large amplitude PmP arrivals between 120-180 km. b) 2-D P-wave velocity model along line AE.

Chapter 10 DISCUSSION AND SUMMARY

10.1 Seismic Data Processing and Interpretation

Our processing has brought to life line 5, which was previously considered as uninterpretable and was therefore abandoned. It is worth mentioning that the acquisition of line 5 cost the Canadian taxpayers about $200,000 (estimated from LITHOPROBE Phase II Proposal). The processing also improved the seismic images of line 9 significantly, which was believed to be one of the best commercially processed. By processing two of the total of nine profiles, the worst and the best, from LITHOPROBE Kapuskasing deep seismic reflection survey, it is safe to say that the commercial processing is insufficient. Close examination of the field data shows that the data are, in general, of good quality in terms of signal-to-noise ratio. Strong shallow dipping reflections from the fault plane of Ivanhoe Lake fault zone are evident on the field shot gathers, but are not seen on the commercial section at all. Shallow dipping reflections are also observed on most of the field shot gathers from line 9. However, the commercial section gives the impression that the top two seconds of the section are non-reflective (Leclair et al., 1991).

Careful reprocessing is often rewarding. By carefully applying standard seismic data processing techniques such as first arrival muting, F-K filtering, refraction statics, and surface-consistent residual statics, one can improve seismic images significantly. Our tests indicate that the full data set should be used without mixing 2:1 in shot gather domain, as high fold is necessary for signal-to-noise enhancement. In addition, the stacking cancels dipping reflections. Our results further prove that seismic reflection profiling is a powerful tool in mapping subsurface geometries of

complex crustal structures in the Canadian Shield.

Since its formation in 1984, LITHOPROBE has always contracted seismic reflection data to professional seismic processing companies for processing. The interpretations are then made on the basis of commercially processed seismic sections. Although this approach guarantees quick outputs, it may not guarantee the quality of the outputs. Due to factors such as cost and time schedule involved, the seismic data were subjected only to basic processing techniques in the commercial processing. Many advanced processing techniques have not yet been applied to the data. On the other hand, special processing is often necessary to improve data quality because of a great diversity of surface conditions and the complexity of crust structures. Furthermore, this approach isolates interpretation from processing. It has been demonstrated that processing and interpretation are interdependent and should not be separated from each other (Brown, 1986; Johnson and Smithson, 1986). Our experience once again proves that a close link between processing and interpretation is essential and the credibility of an interpretation is very much dependent upon the processing applied. Without carefully examining the field data, the artifacts of seismic processing may be interpreted as geological features. For this reason, COCORP has processed its own seismic data in the first instance since the early 1980's. We recommend LITHOPROBE to consider a similar approach. At present, ten universities across Canada as well as Geological Survey of Canada have SUN workstations and ITA seismic processing software. In other words, LITHOPROBE has the capability to process its own seismic data. By choosing to do so, LITHOPROBE will have more money to support its members' research.

10.2 Is the Upper Crust Really Seismically Transparent?

The successful reprocessing raises an important question concerning crustal reflectivity studies: whether the seismically transparent upper crust, a common phenomenon seen on many seismic data sets worldwide (see chapter 9), is due to seismic data processing or geological reality. It has been argued that such upper crustal transparency, for the most part, if not all, is an artifact of seismic data acquisition and/or seismic data processing (Brown, 1987). An example showing how crustal reflectivity is closely related to seismic source is given by Valasek et al. (1991). While dynamite data show a non-reflective upper crust, Vibroseis data collected along the same profile suggest a highly reflective upper crust. Milkereit et al. (1991) also notice that high-frequency seismic source generates more crustal reflections than low-frequency one.

The reprocessing of lines 5 and 9 makes it irrefutable that seismic data processing certainly plays an important role in the apparent crustal reflectivity. According to the commercial processing, the top two seconds of the north part of line 5 are seismically transparent (Fig. 4.26a). In contrast, our processing shows that it is highly reflective (Fig. 4.26b), which is confirmed by field data analysis (Figs. 4.3a, 4.4, and 4.18). The same applies to line 9. Field data should be carefully examined repeatedly in the course of processing to eliminate processing artifacts. It is clear that some of the earlier observations of upper crustal transparency are an artifact of seismic data processing. The studies of crustal reflectivity and its relation to crustal tectonic history should be carried out with caution.

10.3 The Nature of the Kapuskasing Uplift

A wealth of new information on the subsurface structure of the Kapuskasing

Uplift has been revealed through reprocessing line 5, tomographic inversion of the multiple coverage first arrivals, and reanalysis of the wide-angle reflection data, providing important new insights into the nature and evolution of the Kapuskasing Uplift. Two main aspects of the reprocessed section of line 5 shed light on the nature of the KU. These are the bands of west-dipping shallow reflectors traceable to the surface trace of the Ivanhoe Lake fault zone (ILFZ) and the major midcrustal reflector within the Abitibi greenstone belt (AGB). While other interpretations may be possible, we interpret the shallow reflectors as the seismic image of the fault zone, because their location and shape reconcile very well with geological observations (J. Percival, pers. commun.). The 2-D tomographic image of the north part of line 5 indicates that these reflectors mark the boundary juxtaposing high-velocity against low-velocity rocks, providing additional and firm support for the interpretation. There is no doubt that high-velocity rocks above the reflectors are from the deep crust, corresponding to overthrusting of the Kapuskasing Uplift.

The dip angle of the ILFZ holds the key to understanding the nature and evolution of the KU, as it determines how much the crustal shortening associated with the uplift has been taken place with a given uplifting depth. As indicated by gravity data (Fig. 3.2), the north part of line 5 appears to cross the ILFZ perpendicularly. If so, the true dip of the fault may be determined on the migrated seismic section (Fig. 4.24b), which was plotted 1:1 for an average velocity of 6 km/s. A careful measurement indicates that on average, the ILFZ has a dip angle of ~20°, but steepens upward and may have a maximum dip of as much as 50° at the surface. This agrees well with the fact that the relative straightness of the ILFZ suggests that it is a fairly steep structure near the present surface, a suggestion supported by

the geological observations of Bursnall (1989). Although the seismic tomography cannot resolve the subsurface geometry of the ILFZ, it does indicate that the fault becomes steeper near the surface (Fig. 5.3). The ILFZ may dip consistently at this angle to ~12 km depth, based on the reprocessed section of line 5 and the high-resolution seismic section of line 2.

Although the fault was recognized long before as a major geological boundary separating the high-grade rocks of the KU from the low-grade rocks of the AGB to the east, its subsurface structure has been poorly known until now. By delineating its third-dimensional geometry, although limited by the survey line, the new seismic results substantiate the interpretation of Percival and Card (1983) that the ILFZ is a thrust fault.

The least expected yet most important finding is the pronounced northwest-dipping midcrustal reflector within the AGB, and plunging under the KU. In many ways, this reflector is more impressive than the shallow reflectors beneath the ILFZ. Of particular importance is the fact that this reflector appears also well imaged on lines 1 and 6 about 80 km southwest of line 5, indicating that the same crustal feature extends over a wide region along the ILFZ. This reflector most likely represents underthrusting of the Abitibi greenstone rocks beneath the KU, as currently there is no geological and/or geophysical evidence for other alternatives. If correct, the underthrust related to the thrust faulting, which created the KU, is defined, further supporting the model of Percival and Card (1983).

With the overthrust and underthrust mapped, it becomes obvious that the KU is a product of intraplate collision. Three possible tectonic mechanisms that account for the creation of the uplift have been proposed by Percival et al. (1989): (1) the Ivanhoe Lake detachment roots at an ancient plate boundary to the northwest; (2) convergence from the southeast caused

underthrusting of the Abitibi rocks beneath the KU; (3) brittle shortening of the upper crust was balanced by ductile flow in the lower crust. While Geis et al. (1990) prefer the first, Nelson (1991), on the other hand, supports the third. Given the new seismic results, we believe that the underthrusting of the Abitibi greenstone is primarily responsible for the emplacement of the KU. The nature of the KU seems best understood when viewed in terms of its interactions with the AGB.

The observation, that the upper crust of the AGB along lines 1 and 6 is dominated by north- or northwest-dipping subparallel reflections, was noticed by Percival et al. (1989) and Wu and Mereu (1991), and is more evident on the reprocessed seismic sections of lines 1 and 6 by Hajnal et al. (1991). This feature, however, was treated as a local structure for it was not identified on the commercially processed line 5. Although some indications for a midcrustal reflector in the area covered by refraction line GH and reflection line 2 were noticed before by a number of researchers (Wu, 1987; Boland and Ellis, 1989; Geis et al., 1990; Green et al., 1990), their broad lateral extent and tectonic significance are only now being recognized. For the last decade, it has been thought that the structure of the KU is similar to that of the Wind River thrust (Percival and Card, 1983; Cook, 1985; Percival and Mcgrath, 1986; Geis et al., 1990). The revelation of the extensive underthrusting of the Abitibi rocks beneath the KU clearly indicates that they are different, as no underthrusting was detected there. Much emphasis in the earlier interpretations has been placed on evidence for the overthrusting of the KU, but little on the dipping reflections within the AGB.

10.4 Is there a Thick Crustal Root under the Kapuskasing Uplift?

It has been suggested that a crustal root may be present beneath the

Kapuskasing Uplift in order to isostatically compensate the dense granulites in the upper crust (Percival and Card, 1983). On the basis of the results of trial-and-error forward modeling of the low-resolution seismic refraction data, Boland and Ellis (1989) have claimed that the crust is about 10 km thicker beneath the Kapuskasing Uplift than in the surrounding areas. Since then, the crustal root has been widely cited in the literature. As one of a few people who have analyzed both seismic refraction and reflection data sets, we have been constantly looking at seismic evidence for such a thicker crust. As discussed in sections 7.3 and 9.4, the seismic reflection data show no indication whatsoever of the Moho reflections. This agrees well with the seismic refraction data (Fig. 8.5), as no wide-angle reflections from the Moho are observed along the axis of the uplift, corroborating that the Moho beneath the KU is a wide transition zone rather than a sharp boundary separating the crust from the upper mantle. Without the Moho reflections, we have to rely on Pn arrivals, the refracted energy from the Moho, to determine the crustal thickness beneath the KU. If so, line CJ, running along the axis of the KU, is in the best position to define the crustal thickness. Displayed in Fig. 9.8 is the enlargement of the Pn arrivals from shotpoints C and J. Some good Pn arrivals (~20) are observed from shotpoint C but with a few from shotpoint J (Wu and Mereu, 1991). It is impossible to constrain the crustal thickness with these very limited Pn arrivals because of very coarse ray coverage. This problem is excellently illustrated by White and Boland (1992), who have carried a tomographic inversion of first arrivals from the seismic refraction profile GH (Fig. 3.1) and compared their results with those of Boland and Ellis (1989). Their resolution tests show that the first arrivals can constrain the velocity model to a depth of no more than 2.5 km for the east part of line GH (0 to ~80 km from shotpoint G), and less than 10 km for

the west part. At greater depths resolution decreases rapidly and the final velocity model is heavily dependent on the starting models. In contrast, the trial-and-error forward modeling analysis mapped a high-velocity anomaly (6.6 km/s) along line GH that extends to ~20 km depth with a dip of 15 ± 2° (Boland and Ellis, 1989). It appears that the trial-and-error forward modeling is apt to be influenced by geological models.

While the seismic refraction data might indicate a crustal root beneath the KU, as suggested by Boland and Ellis (1989), it should be kept in mind that there has been no conclusive evidence from both seismic refraction and reflection data for it. It is of great interest to note that our new crustal model (Fig. 7.3) does not require a crustal root to compensate the dense upper crustal rocks, because the overload upper crust could have been balanced by the subsidence of the less dense Abitibi rocks (Hajnal et al., 1991; Wu and Mereu, 1992). In other words, underthrusting of the Abitibi rocks might not only be primarily responsible for the creation of the uplift, but also act as a means to balance the overload

10.5 Recommendations for Future Work

More reflection profiles across the Ivanhoe Lake fault zone are needed north of line 5 in order to provide 3-D seismic image of the fault and resolve the debate on shallow against steep faulting.

The reprocessed seismic section of line 5 provides the best image of the Ivanhoe Lake fault zone, at least for the time being. The west-dipping seismic reflections can be followed upward right to the surface trace of the fault zone. Therefore, we strongly recommend that the Canadian Continental Drilling Program consider drilling its first deep borehole at this site. This site is definitely superior to the middle of line 2, the previously proposed

site, for investigating the subsurface geology of the fault zone and for determining the origin of shallow reflections.

APPENDIX A SEISMIC PROCESSING TECHNIQUES

In this appendix, some standard seismic processing techniques used in our processing are briefly examined. Detailed descriptions can be found in many seismic exploration textbooks such as those by Dobrin and Savit (1988) and Yilmaz (1987).

1 Amplitude Recovery

Raw seismic data show a very marked decrease in amplitude with time (Figs. 4.2, 4.3, 4.4). Such data are known as 'geophone amplitude' data and contain the various attenuation effects at work on the seismic pulse as it passes through the earth. Divergence (geometrical spreading according to the inverse square law), absorption by anelastic propagation (As the seismic pulse travels through the earth, seismic energy is converted into heat through anelastic movement of rock particles), scattering from small heterogeneities, and transmission losses are believed to be the main causes. There are two general types of amplitude compensation: automatic gain control (AGC), commonly used for structural mapping, and relative, true amplitude gain preservation, usually used for lithologic or stratigraphic studies. AGC attempts to make amplitudes similar for all offsets, for all times, and for all midpoints. A typical method of calculating the gain to be applied is to calculate the median or average amplitude within sliding windows down the trace, and then to calculate the multipliers needed to equalize the median values in all the windows. the multipliers are normally smoothed over time and then applied. A separate gain function is calculated and applied for each trace.

2 Static Corrections

To optimize the overall quality of seismic sections and to obtain a correct

structural interpretation, it is necessary to correct reflection times for near-surface irregularities. Surface elevation and weathered layer are two main sources of such irregularities. If not allowed for, static shifts caused by such irregularities will degrade the seismic section severely, as seismic reflections will not line up properly after NMO correction.

ELEVATION STATICS: The correction for Elevation difference can be made simply by subtracting (or adding) the time required for the seismic wave to travel the vertical distance between a reference elevation and that of the earth's surface at the point in question. A refraction-type estimation of the near-surface velocity is usually used for the correction.

REFRACTION STATICS: The weathered layer just below the surface consists of unconsolidated rock or soil materials. Its low velocity causes a significant time delay in the arrival of the desired deeper reflections. The first events to arrive at each station on a reflection profile have traveled either directly through the weathered layer or by refraction along the top of the high-velocity zone just below the weathered layer. Using the travel times of the first arrivals, one can calculate the delay time for each station. Slope/Intercept, Plus-Minus, Delay Time, and Time-Term methods are commonly used for calculating refraction static corrections. The Plus-Minus method is adopted by the ITA.

RESIDUAL STATICS: The real earth is much more complicated than theoretical models. For example, the velocity can vary both laterally and vertically within a single layer due to changing lithology. The thickness of weathered layer may change rapidly. Therefore, elevation and refraction static corrections do not provide a complete solution. By taking advantage of the data redundancy inherent in the CMP method of shooting, one can refine estimates of static corrections. Trim or correlation statics and surface-

consistent residual statics methods are normally used to calculate residual statics. The former assumes that by aligning the reflections within a single CMP gather after NMO correction, one can account for subtle errors in elevation and refraction static corrections. The latter assigns a constant statics to each station on a reflection profile. The stack-power optimization algorithm of Ronen and Claerbout (1985) is adopted by the ITA to calculate surface consistent residual statics. It is assumed that statics shifts can be estimated by maximizing the stack power.

3 F-K FILTERING

F-K filtering distinguishes signal from noise based on their different apparent velocities, since events that dip in the T-X domain can be separated in the F-K domain by their dips (Fig. 4.18b). Coherent linear noise, such as ground-roll, can be eliminated in the F-K domain with ease. Although F-K filtering is commonly used in seismic data processing, it must be used with care to avoid possible processing artifacts. F-K filtering works on events sufficiently sampled in space. Occasionally, coherent noise is spatially aliased.

4 Velocity Spectra

A CMP gather is repeatedly NMO-corrected and stacked using a range of constant velocity values. And resultant stack traces are displayed side by side on a plane of velocity versus two-way=traveltime (Fig. 4.22c). This is called the velocity spectra, which is commonly used in velocity analysis. A stacking velocity function may be picked from velocity spectra.

5 Migration

Stacked sections truly represent geological structures only when the

reflectors are horizontal. Seismic migration is the process that moves dipping reflections from its common-midpoint position to its true subsurface location. The dip angle of the reflector is greater than that observed in the stacked section. The length of the reflector is shorter that that observed in the stacked section. Three major techniques of migration are commonly used in seismic data processing. They are Kirchhoff, finite-difference, and frequency domain migration. Each has its advantages and disadvantages, but generally produces similar results. Kirchhoff migration performs well when dips are large, but performs poorly with a low signal-to-noise ratio. Finite-difference migration works well with a low signal-to-noise ratio, but cannot handle steep dip properly and is very time-consuming. Frequency domain migration is based on the two-dimensional Fourier transform. The advantages of this method include fast computing time, good performance under low signal-to-noise conditions, and excellent performance for steep dip. A serious disadvantage is that the method breaks down in presence of wide lateral velocity variations. This method was used in our processing for its fast time computing.

The ITA Jobdecks

Two ITA jobdecks are provided below. The first One performs amplitude recovery (module *AGC*), elevation (module *DATM*) and refraction static (module *SFT2*) corrections. Refraction statics are calculated by module *REFSTAT* and is stored in a file called *line5.ref*. The second implements F-K filtering (module *FKS2*). F-K filters are interactively designed using the graphical program *FKSURG* and is saved in a file called *line5.fkp*. See the ITA manual for details.

JOBDECK 1

```
open   1 1 'line5.data'
seft   1 1 0.0 16.0 0.004
open   2 2 'line5_1.dat

osft   'line5.ref'              !Open and read refraction statics file

bsec   299
getr   1 0
agc    2 1.0                    !Apply AGC gain
datm   400 5500                 !Apply elevation corrections
sft2                            !Apply refraction statics
putr   2 0
esec

clos   1 1
clos   2 2
end
```

JOBDECK 2

```
open   1 1 'line5_1.dat'
seft   1 1 0.0 16.0 0.004
open   2 2 'line5_2.dat'

ofks   line5.fkp                !Open and read F-K filtering information

bsec   299
getr   1 0
fks2   10 55 1 10 0 0           !Apply F-K filtering
putr   2 0
esec

clos   1 1
clos   2 2
end
```

APPENDIX B INTERACTIVE FIRST ARRIVAL PICKING

In conventional data processing, refraction static corrections are required to reduce the effects of weathered layer (see appendix A). To make refraction static corrections, a large number of first arrivals have to be picked, which is usually a very time-consuming task. The SUN/ITA system provides software tools to carry out this task with relative ease. As one of the first Lithoprobe users, I have spent a lot of time to figure out a procedure for the first arrival picking. In this appendix, a simple procedure, developed during this study, is briefly described. It should be mentioned that the updated manual for INSIGHT/1 package provides much better description for first arrival picking than two years ago, when I began learning to use the package.

There are two modules within INSIGHT/1 package, **vaq** and **vaq2**, to implement the interactive first arrival picking. **vaq2** is recommended by ITA. In the new version of INSIGHT/1, INSIGHT_912, **vaq** is phased out. Therefore, only **vaq2** is discussed here. To initiate **vaq2**, type *vaq2* and hit return. After giving the name of the input datafile, choosing a proper time range for display (such as 0 to 1.5 or 2 s) and scaling (**ENER** seems working better than **AGC**), two image planes will be displayed on the SUN graphics screen, **Kill Screen** and **Pick Screen**. The **Kill Screen** is the first image displayed, which consists of a shot gather upon which trace edits may be performed. The **Pick Screen** is the second image plane displayed, which consists of a shot gather upon which first arrival picking may be performed. Most of the time spent on first arrival picking goes towards creating these two displays. Although trace editing may not be necessary in some cases, the model always displays the two planes. All the following description is applied to the **Pick Screen** only.

The interactive first arrival picking requires two steps of preparation: a

definition step to set the picking parameters and a macro construction step to set the picking sequence.

Definition Step

This step determines a set of picking parameters which will produce reliable first arrival picks.

1) Manually pick first arrivals for a shot gather, usually the first one, by utilizing mouse buttons (see the ITA manual for details).

2) Tune first arrival picks to highest amplitude of wavelet by selecting the **turn** option from the VAQUICK2 GRAPHICS MENU.

3) Reject anomalous first arrival picks by selecting the **fix** option from the VAQUICK2 GRAPHICS MENU.

4) Store the first arrival characteristics by selecting the **lear** option from the VAQUICK2 GRAPHICS MENU.

5) Copy the first arrival picks into temporary memory by selecting the **load** option from the VAQUICK2 GRAPHICS MENU.

Macro Construction Step

At this point, a macro can be constructed to automate the pick of first arrivals, using the derived set of picking parameters.

1) Select the macro option from the VAQUICK2 GRAPHICS MENU.

2) Within the MACR SUB-MENU, select options from the right side menu and insert them in the macro template on the left side of the screen. The following macro appears working well for the Lithoprobe vibroseis data:

COPY	copy previous picks to screen
TURN	turn picks to highest amplitude of wavelet
FIX	reject spurious first arrival picks
PICK	pause at Pick Screen to allow manual pick editing
LOAD	save current picks into temporary memory
NEXT	advance to next shot gather

Once the macro is set up, one may start automated picking by first toggling **on** and then **start** options at the bottom of the screen within the MACRO SUB-MENU. To stop the macro at any time, press the **STOP** button on the keyboard.

The reason to use the previous picks as initial picks for the current shot gather is that the two shot gathers are acquired only 50 m apart and there is not much difference in travel time between them. If signal-to-noise ratio is relatively high, the procedure shall work well. Using this technique, one may expect to determine the first arrival times of 12,000 traces (i.e. 50 shotgathers, each with 240 channels) within one hour.

APPENDIX C COHERENCY-FILTERING WITHIN THE SUN/ITA Environment

The goal of seismic reflection profiling is to produce a seismic section which is similar to the geological cross-section. To present a seismic section, one is often confronted with a challenge of displaying a large amount of seismic data on a small piece of paper. Coherency-filtering is frequently applied to stacked seismic data to select highly coherent events and to eliminate the background noise. After coherency-filtering, the stacked data is highly compressed and can be plotted with relatively ease. At present, the INSIGHT/1 package does not provide any module to do post-stack coherency-filtering. However, the INSIGHT/1 does have a module called *'SLCW'* to conduct pre-stack coherency-filtering, which works on shot gathers or common-midpoint (CMP) gathers only. It performs a local slant-stack transformation, with semblance weighting, in order to enhance signal-to-noise ratio. By tuning the transformation parameters, incoherent and linearly coherent noise can be attenuated or completely eliminated (for details, see the ITA manual). After many tests, I have discovered that with small modifications on trace header of the stacked data, one can utilize this module to do post-stack coherency-filtering.

For the ITA-formatted data, each trace consists of a header of 64 words (or points) followed by floating point data points. The acquisition and processing information is stored in the trace header. The first 13 words of the trace header are:

WORD	TYPE	INFORMATION
1	Integer	Original trace sequential number when put on disk
2	Integer	Original file number
3	Integer	CMP number
4	Integer	Used for sorting/channel number
5	Integer	Used for sorting/shotpoint after stack
6	Integer	Trace use: 0 = dead; .ne. 0 = not dead
7	Integer	Number of points/trace
8	Integer	Sampling interval in microseconds
9	Integer	Trace start time in milliseconds
10	Integer	Trace end time in milliseconds
11	Integer	Contains trace number and unit number
12	Integer	Number of trace within records
13	Integer	Trace number within record

All traces within each shot gather belong to the same file and is numbered sequentially, as they consist of a single record. While every trace within a stacked data set has a different file number and is in wild disorder, as each trace is a single record, a summation of a whole CMP gather. In order to apply *SLCW* module to the stacked data, one should modify the words 1, 2, 12, and 13 of the trace header of the stacked traces so that the stacked data can be treated as a shot gather. The modifications can be achieved using one of the utility routines within the INSIGHT/1, called *UTILITY*. The details of the modifications are given as follows:

1) To initiate *UTILITY*, type **util**. Then, enter the filename of the stacked data set which is to be modified.

2) Position the mouse arrow to the **Edit Headers** option and CLICK the LEFT mouse button. A prompt will be displayed looking like **edit>**.

3) Type **mod** for modification. It allows the user to modify the trace header according to a specified word. By giving a trace window, increment, word, word type, new values and running increment. The user is prompted:

enter trace window and increment to modify:

Enter the first and last trace number and trace increment. For example, if the stacked data set consists of 1500 traces, one should type: **1, 1500, 1,**

and return. The user is prompted:

enter a word to modify (1-64). enter "0" to exit

Type **1**, or **2**, or **12**, or **13**, and return. The user is prompted:

enter type of word (1 - integer, 2 - real, 3 - double, 4 - hex):

Type **1** and return. The user is prompted:

enter new value and running increment:

For word 1, one should type **1** for new value and **1** for running increment to make sure that all stacked traces are sequentially numbered. For word 2, one may input **1** and **0** to unify file number, so that the module *SLCW* will treat the stacked data as a shot gather. For word 12, one should enter number of trace within the data set for new value and **0** for increment. Finally for word 13, one may give 1 and 1.

After these modifications, one can go ahead to apply coherency-filtering to the stacked data using *SLCW*. The ITA manual provides an example to show the usage of the module. It should be pointed out that the above procedure has been developed within the INSIGHT/1 version 904 environment and does not work within the INSIGHT/1 updated version 912 environment for unknown reasons. The difference between the two versions has been reported to the ITA and so far nothing has been done yet. Fortunately, the updated version has a module, called *NODIO*, which is capable to convert the new ITA-formatted data to its old format. One can switch back to the version 904 by typing **use904** and to the version 912 by typing **use912** on our SUN workstation.

APPENDIX D THE UWO PRINTER-PLOTTER PROGRAM

In this appendix, a brief description on how to plot a seismic section from the SUN/ITA system utilizing the UWO printer-plotter program is provided. Two major steps are involved.

Data Rasterizing:

The user runs a computer program, residing on the SUN workstation, to create a condensed plot file, using a plot table from the PLTAB file. A typical plot table is shown below:

```
        PLTAB ---     FOR PRINTER-PLOTTER PROGRAM "PSSMFPF".
NSETT    PLOT TABLE FOR PSSMFPF
 999
 ------------------------------------------------------------------------
 ------------------------------------------------------------------------
 1    UNIX Test Set
      FILEIN----fault.dat
      FILEOUT---cdfault.dat
      FILETAB---tab001
   DBGN    DEND    DPI    TBGN    TEND    TPI    AMIN    API    AMPLIM
   0.0      6.0     1.0     0.0     2.0     0.5     0.0    15.0     0.0
   AZBGN    AZEND    AZPI  SR  NORM    DFACT    REDV  XG  HTITLE
   236.0    321.0     4.0  250.0    1      0.0     0.0    1.0     0.6
   ISEGY   ISHADE  IUP  IDST   IANGTRC   IDUMDST   DSTART  DINC
      2        1     3     1       0          0        1.0      1.0
    TITLE
      'THE SEISMIC IMAGE OF THE IVANOE LAKE FAULT ZONE'
    XTITLE
      'DISTANCE (KM)'
    YTITLE
      'TWO-WAY-TRAVELTIME (S)'
      THTX     AHTX    IDECX    DSTBL       KX
      .400     .300      -1     1.000       10
      THTT     AHTT    IDECT    TMBL        KT
      .400     .300       1     1.000       10
    IDOTPIH IDOTPIV  PWIDTH    PLEN    NPINH    NPINV     NBIT
       180      180  16.000 240.000       24       24        7
     P1CMD    'PRINTER COMMAND 1)
        '<27><64><27><51><24>'
     P2CMD    (PRINTER COMMAND 2)
        '<27><42><39>'
     P3CMD    (PRINTER COMMAND 3)
        '<27><64>'
 ------------------------------------------------------------------------
```

Here, FILEIN is the name of input data file to be plotted. FILEOUT is the name of output condensed data file. And FILETAB is the name of table file, which contains detailed information on all the seismic traces to be plotted. Details on the plot table definitions are given in *PC Printer-Plotter Program User's Guide* by B. Dunn, R. F. Mereu, and J. Brunet. To initiate the computer program on the SUN workstation, type **/user/local/pssmfpf.**

Plotting Data:

After the plot data file is created on the SUN workstation, the user can log into the SUN/ITA system through a PC computer, to which a dot matrix printer is attached. First, set working directory properly. Second, exit from the SUN/ITA system by pressing **Alt+X**. Now the use is back to C drive. Third, type **ssplot sun**. The user is prompted:

Main Menu

1 Connect to Host

2 Enter Plot Menu

3 Return to DOS

Selection >>

Press 2. The user is prompted:

Plot Menu

1 Plot Only - Single Strike

2 Plot Only - Double Strike

3 Plot and Save - Single Strike

4 Plot and Save - Double Strike

5 Save Only

6 Return to Main Menu

Selection >>

Press 1 or 2. The user is prompted:

Name of Condensed File

Type FILEOUT. Waiting for a couple of seconds, the printer starts to print the seismic section.

The whole process usually takes about 10 minutes depending on the size of the plot data. However, in order to produce a good seismic section, one has to play around with some plotting parameters, such as DPI, TPI, API, AMPLIM, and NORM. This is a very time-consuming task. Unfortunately, there is no short-cut to take. One should write down the set of parameters as soon as he or she obtains a good section.

REFERENCES

Armstrong, R.L., 1981. Radiogenic isotopes: the case for crustal recycling on a near-steady state no-continent-growth Earth, *Philosophical Transactions of the Royal Society*, London, series A, **301**, 443-472

Bailey, R.C., Craven, J.A., Macnae, J., and Polzer, B., 1989. Imaging deep fluids in Archean crust, *Nature*, **340**, 136-138.

Barazangi, M., and Brown, L. (eds.), 1986a. Reflection Seismology: A Global Perspective, *AGU Geodyn. Ser.*, **13**.

Barazangi, M., and Brown, L. (eds.), 1986b. Reflection Seismology: The Continental Crust, *AGU Geodyn. Ser.*, **14**.

Bennett, G., Brown, D.D., George, P.T., and Leahy, E.J., 1967. Operation Kapuskasing, *Miscellaneous Paper 10, Ontario Department of Mines*, 1-98.

Bennett, G., 1969. Geology of the Belford-Strachan area, District of Cochrane; Ontario Department of Mines, *Geological Report*, **78**, 30p.

Bishop, T.N., Bube, K.P., Culter, R.T., Langan, R.T., Love, R.L., Resnick, J.R., Shuey, R.T., Spindler, D.A., and Wyld, H.W., 1985. Tomographic determination of velocity and depth in laterally varying media, *Geophysics*, **50**, 903-923.

Boland, A.V., and Ellis, R.M., 1989. Velocity structure of the Kapuskasing uplift, Northern Ontario, from seismic refraction experiment studies, *J. geophys. Res.*, **94**, 7189-7204.

Boland, A.V., and Ellis, R.M., 1991. A geophysical model for the Kapuskasing uplift from seismic and gravity studies, *Can. J. Earth Sci.*, **28**, 342-354.

Bording, R.P., Gersztenkorn, A., Lines, L.R., Scales, J.A., and Treitel, S., 1987. Applications of seismic travel-time tomography, *Geophys. J. R. astr. Soc.*, **90**, 285-303.

Brewer J.A., Matthews, D.H., Warner M.R., Hall, J., Smythe,D.K., and Whittington, R.J., 1983. BIRPS deep seismic reflection studies of British Caledonides, *Nature*, **305**, 206-210

Brown, L.D., 1987. Lower continental crust: variations mapped by COCORP deep seismic profiling, *Ann. Geophys.*, **5b**, 325-330

Burke, K., and Dewey, J.F., 1973. Plume-generated triple junction: key indicators in applying plate tectonics to old rocks, *J. Geol.*, **81**, 406-433.

Bursnall, J.T., 1989. Structural sequence from the southeastern part of the Kapuskasing structural zone in the vicinity of Ivanhoe Lake, Ontario, in: Current research, *Geol. Surv. Can.*, **89-1C**, 405-411.

Card, K.D., 1990. A review of the Superior Province of the Canadian Shield, a product of Archean accretion, *Precambrian Research*, **48**, 99-156.

Cassell, B.R., 1982. A method for calculating synthetic seismograms in laterally varying media, *Geophys. J. R. astr. Soc.*, **69**, 339-354.

Christensen, N.I., and Szymanski, D.L., 1988. Origin of reflections from the Brevard fault zone, *J. Geophys. Res.*, **93**, 1087-1102.

Clowes, R.M., 1984. Phase 1: LITHOPROBE - A coordinated national geoscience project, *Geoscience Canada*, **11**, 122-126.

Cook, F.A., 1985. Geometry of the Kapuskasing structure from a Lithoprobe pilot reflection survey, *Geology*, **13**, 36?-371.

Coward, M.P., and Fairhead, J.D., 1980. Gravity and structural evidence for the deep structure of the Limpopo belt, Southern Africa, *Tectonophysics*, **68**, 31-34.

Dewey, J.F., and Windley, B.F., 1981. Growth and differentiation of the continental crust, *Philosophical Transactions of the Royal Society*. London, series A, **301**, 189-206.

Dines, K., and Lytle, R.J., 1979. Computerized geophysical tomography, *Proc. IEEE*, **67**, 1067-1073.

Dobrin, M.B., and Savit, C.H., 1988. Introduction To Geophysical Prospecting (fourth edition), McGraw-Hill Book Company, New York.

Dohr, G., 1957. Zur reflexionsseismischen Enfrassung sehr tiefer Unstetigkeisflächen, *Erdöl undo kohle*, **10**, 278-281.

Dohr, G., and Fuchs, K., 1967. Statistical evaluation of deep crustal reflections in Germany, *Geophysics*, **32**, 951-967.

El-Isa, Z., Mechie, J., and Prodehl, C., 1987. Shear velocity structure of Jordan from explosion seismic data, *Geophys. J. R. astr. Soc.*, **90**, 265-281.

Fountain, D.M., and Salisbury, M.H., 1981. Exposed cross-sections through the continental crust: implications for crustal structure, petrology and evolution, *Earth planet. Sci. Lett.*, **56**, 263-277.

Fountain, D.M., and Salisbury, M.H. (eds.), 1990. *Exposed Cross-Sections of the Continental Crust*, Kluwer Academic Publishers, Dordrecht, 662p.

Fountain, D.M., Salisbury, M.H., and Percival, J., 1990. Seismic Structure of the Continental Crust Based on Rock Velocity Measurements From the Kapuskasing Uplift, *J. geophys. Res.*, **95**, 1167-1186.

Garland, G.D., 1950. Interpretation of gravimetric and magnetic anomalies on traverses in the Canadian Shield in Northern Ontario, *Publications of Dominion Observatory*, Ottawa, **16-1**, 57p.

Gaucher, E.H., 1966. Elsas-Kapuskasing-Moosonee magnetic and gravity highs, in: Report of activities, *Geol. Surv. Can.*, **66-1**, 189-191.

Geis, W.T., Cook, F.A., Green, A.G., Milkereit, B., Percival, J.A., and West,

G.F., 1990. Thin thrust sheet formation of the Kapuskasing structural zone revealed by Lithoprobe seismic reflection data, *Geology*, **18**, 513-516.

Gibb, R.A., 1978. A gravity survey of James Bay and its bearing on the Kapuskasing Gneiss Belt, Ontario, *Tectonophysics*, **45**, 7-13.

Goodings, C.R., and Brookfield, M.E., 1992. Proterozoic transcurrent movements along the Kapuskasing lineament (Superior Province, Canada) and their relationship to surrounding structures, *Earth Sci. Rev.*, **32**, 147-185.

Green, A., Milkereit, B., Percival, J., Davidson, A., Parrish, R., Cook, F., Geis, W., Cannon, W., Hutchinson, D., West, G., and Clowes, R., 1990. Origin of deep crustal reflections: results from seismic profiling across high-grade metamorphic terranes in Canada, *Tectonophysics*, **173**, 627-638

Halls, H.C., and Palmer, H.C., 1990. The tectonic relationship of two Early Proterozoic dyke swarms to the Kapuskasing Structural Zone: a paleomagnetic and petrographic study, *Can. J. Earth. Sci.*, **27**, 87-103.

Hajnal, Z., Scott, D., Pandit, B.I., and Reilko[illegible], B., 1991. Improved interpretation of Kapuskasing crustal reflection data by selection of the most effective reprocessing sequences, in: R. Meissner, L. Brown, H. Dürbaum, W. Franke, K. Fuchs, and F. Seifert (eds.), Continental Lithosphere: Deep Seismic Reflections, *AGU geodyn. Ser.*, **22**, 417-433.

Hamilton, D.A., 1991. Two-dimensional tomographical tweaking of the GLIMPCE data set across the Midcontinent Rift Zone, *M.Sc thesis*, University of Western Ontario, London, Canada.

Hawman, R.B., Colburn, R.H., Walker, D.A., and Smithson, S.B., 1990. Processing and inversion of refraction and wide-angle reflection data from the 1986 Nevada PASSCAL Experiment, *J. geophys. Res.*, **95**, 4657-4691.

Holbrook, W.S., Gajewski, D., Drammer, A., and Prodehl, C., 1988. Interpretation of wide-angle compressional and shear wave data in southwest Germany: Poisson's ratio and petrological implications, *J. geophys. Res.*, **93**, 12081-12106.

Hurich, C.A., Smithson, S.B., Fountain, D.M., and Humphreys, M.C., 1985. Seismic evidence of mylonite reflectivity and deep structure in the Kettle dome metamorphic core complex, Washington. *Geology*, **13**, 577-590.

Innes, M.J.S., 1951. Some Structural Features of the Canadian Shield as Revealed by Gravity Anomalies, *Ph.D Thesis*, University of Toronto, Canada.

Innes, M.J.S., 1960. Gravity and isostasy in northern Ontario and Manitoba, *Publications of the Dominion Observatory*, Ottawa, **21**, 261-338.

Innes, M.J.S., Goodacre, A.K., Weber, J.R., and McConnell, R.K., 1967. Structural Implications of the gravity field in Hudson Bay and vicinity, *Can. J. Earth. Sci*, **4**, 977-993.

Johnson, R. A., and Smithson, S.B., 1986. Interpretive processing of crustal seismic reflection data: examples from Laramie Range COCORP data, in: M.

Barazangi and L.D. Brown (eds.), Reflection Seismology: A Global Perspective, *AGU geodyn. Ser.*, **13**, 197-208.

Junger, A., 1951. Deep basement reflections in Big Horn County, Montana, *Geophysics*, **16**, 499-505.

Kanasewich, E.R., Clowes, R.M., and McCloughan, C.H., 1969. A buried Precambrian rift in Western Canada, *Tectonophysics*, **8**, 513-527.

Klemperer, S.L., Hauge, T.A., Hauser, E.C., Oliver, J.E., and Potter, C.J., 1986. The Moho in the northern Basin and Range province, Nevada, along the COCORP 40°N seismic reflection transect, *Geol. Soc. Am. Bull.*, **97**, 603-618.

Kurtz, R.D., Macnae, J.D., and West, G.F., 1989. A controlled source, time-domain electromagnetic survey over an upthrust section of Archean crust in the Kapuskasing Structural Zone, *Geophy. J. Int.*, **99**, 195-203.

Leclair, A.D., and Nagerl, P., 1988. Geology of the Chapleau, Groundhog River and Val Rita blocks, Kapuskasing area, Ontario, in: Current Research, *Geol. Surv. Can.*, **88-1C**, 83-91.

Leclair, A.D., Percival, J.A., Milkereit, B., Green, A.G., and West, G.F., 1991. Seismic-reflection profiles across major faults of the central Kapuskasing Uplift, *Geol. Assoc. Can. Abstr.*, **16**, A73.

Levin, F.K., 1971. Apparent velocity from dipping interface reflectors, *Geophysics*, **36**, 510-516.

Lewchuk, M.T., and Symons, D.T.A, 1990. Paleomagnetism of the Clay-Howells complex: constraints on Proterozoic motion in the Kapuskasing structural Zone, Superior Province, Canada, *Tectonophysics*, **172**, 67-75.

MacLaren, A.S., 1968. Aeromagnetic interpretation, in: A Preliminary Study of the Moose Rever Belt, Northern Ontario, *Geol. Surv. Can.*, **67-38**, 7-11.

Mareschal, M., 1990. Electrical conductivity: The story of an elusive parameter, and how it possibly related to the Kapuskasing uplift, in: M.H. Salisbury and D.M. Fountain (eds.), *Exposed Cross-Sections of the Continental Crust*, Kluwer Academic Publishers, Dordrecht, 453-468.

Matthews, D.H., and Cheadle, M.J., 1986. Deep reflections from the Caledonides and Vaiscides west of Britain and comparison with the Himalayas. In: Reflection Seismology: A Global Perspective, *AGU Geodyn. Ser.*, **13**, 5-20.

Meissner, R., Wever, Th., and Sadowiak, P., 1990. Reflectivity patterns in the Variscan mountain belts and adjacent areas: an attempt for a pattern recognition and correlation to tectonic units, *Tectonophysics*, **173**, 361-378.

Meissner, R., Brown, L., Dürbaum, H., Franke, W., Fuchs, K., and Seifert, F., (eds.), 1991. Continental Lithosphere: Deep Seismic Reflections, *AGU geodyn. Ser.*, **22**.

Mereu, R.F., 1990. An interpretation of CCSS data set I using the triangular

block model method, in: A.G. Green (ed.), Studies of laterally heterogeneous structures using seismic refraction and reflection data, *Geol. Sur. Can.*, **89-13**, 53-63.

Mereu, R.F., Mueller, St., and Fountain, D. (eds.), 1990a. The Lower Crust: Properties and Processes, *AGU Monograph*, **51**.

Mereu, R.F., Dunn, B., and Brunet, J., 1990b. An efficient method for sending a large seismic section from a mainframe computer to a dot matrix printer located at a remote site, *Tectonophysics*, **173**, 155-161.

Mereu, R.F., Epili, D., and Green, A.G., 1990c. Pg shingles: preliminary results from the onshore GLIMPCE refraction experiment, *Tectonophysics*, **173**, 617-626.

Milkereit, B., Percival, J.A., White, D., Green, A.G., and Salisbury, M.H., 1991. Seismic reflectors in high-grade metamorphic rocks of the Kapuskasing uplift: results of preliminary drill site surveys, in: R. Meissner, L. Brown, H. Dürbaum, W. Franke, K. Fuchs, and F. Seifert (eds.), Continental Lithosphere: Deep Seismic Reflections, *AGU geodyn. Ser.*, **22**, 39-45.

Mooney, W.D., and Brocher, T.M., 1987. Coincident Seismic Reflection/Refraction Studies of the Continental Lithosphere: A Global Review, *Reviews of Geophysics*, **25**, 723-742.

Moorbath, S., and Taylor, P.N., 1981. Isotopic evidence for continental growth in the Precambrian, in: A. Kröner (ed.), *Precambrian Plate Tectonics*, Elsevier, Amsterdam, 491-526.

Nelson, K.D., 1991. A unified view of craton evolution motivated by recent deep seismic reflection and refraction results, *Geophys. J. Int.*, **105**, 25-35.

Nisbet, E.G., 1987. The Young Earth: An introduction to Archaean geology, Allen and Unwin Publisher.

Northey, R.C., and West, G.F., 1985. The Kapuskasing structural zone seismic refraction experiment, *DSS Contract Rep. OST84-00060 06ST, 23235-3-1478*, 117p, the University of Toronto.

Oliver, J., Dobrin, M., Kaufman, S., Meyer, R., and Phinney, R., 1976. Continuous seismic reflection profiling of the deep basement, Hardeman County, Texas, *Geol. Soc. Amer. Bull.*, **87**, 1537-1546.

Palmer, H.C., and Barnett, R.L., 1992. Amphibole and plagioclase chemistry in two Proterozoic dyke swarms and its relation to the uplift history of the Kapuskasing Structural Zone, *Can. J. Earth Sci*, in press.

Peddy, C.P., and Hobbs, R.W., 1987. Lower crustal reflectivity of the continental margin southwest of Britain, *Ann. Geophys.*, **5b**, 331-338.

Percival, J.A., and Card, K.D., 1983. Archean crust as revealed in the Kapuskasing uplift, Superior province, Canada. *Geology*, **11**, 323-326.

Percival, J.A., and Card, K.D., 1985. Structure and evolution of the Archean Crust in Central Superior Province, Canada, In: Evolution of Archean

Supracrustal Sequences, *Geol. Assoc. Can. Spec. Pap.* , **28**, 179-192.

Percival, J.A., 1985. The Kapuskasing structure in the Kapuskasing-Fraserdale area, Ontario, in: Current Research, *Geol. Surv. Can.*, **85-1A**, 1-5.

Percival, J.A., and McGrath, P.H., 1986. Deep crustal structure and tectonic history of the Northern Kapuskasing uplift of Ontario: an integrated petrological-geophysical study, *Tectonics*, **5**, 553-572.

Percival, J.A., Green, A.G., Milkereit, B., Cook, F.A., Geis, W.T., and West, G.F., 1989. Seismic reflection profiles across deep continental crust exposed in the Kapuskasing uplift structure, *Nature*, **342**, 416-420.

Percival, J.A., Shaw, D.M., Milkereit, B., White, D.J., Jones, A.G., Salisbury, M.H., Bursnall, J.T., Moser, D.E., Green, A.G., Thurston, P.C., Bailey, R.C., and Mareschal, M., 1991. A Closer Look at Deep Crustal Reflections, *EOS*, **72**, 337-341.

Raase, P., Raith, M., Ackermand, D., and Lal, R.K., 1986. Progressive metamorphism of mafic rocks rocks from greenschist to granulite facies in the Dharwar craton of South India, *J. Geol.*, **94**, 261-282.

Robertson, G., 1963. Intrabasement Reflections in Southwestern Alberta, *Geophysics*, **28**, 910-915.

Ronen, J., and Claerbout, J. F., 1985. Surface-consistent residual statics estimation by stack-power maximization, *Geophysics*, **50**, 2759-2767.

Smithson, S.B., Brewer, J., Kaufman, S., Oliver, J., and Hurich, C., 1978. Nature of the Wind River thrust, Wyoming, from COCORP deep-reflection data and from gravity data, *Geology*, **6**, 648-652.

Smithson, S.B., Johnson, R.A., and Hurich, C.A., 1986. Crustal reflections and crustal structure. In: Reflection Seismology: The Continental Crust. *AGU Geodyn. Ser.*, **14**, 21-32.

Smithson, S.B., Johnson, R.A., Hurich, C.A., Valasek. P.A., and Branch, C., 1987. Deep crustal structure and genesis from contrasting reflection patterns: an integrated approach, *Geophys. J. R. astr. Soc.*, **89**, 67-72.

Thurston, P.C., Siragusa, G.M., and Sage, R.P., 1977. Geology of the Chapleau Area, Districts of Algoma, Sudbury, and Cochrane; Ontario Division of Mines, *Geoscience Report*, **157**, 293p.

Valasek, P., Mueller, St., Frei, W., and Holliger, K., 1991. Results of NFP 20 seismic reflection profiling along the Alpine section of the European Geotraverse (EGT), *Geophys. J. Int.*, **105**, 85-102

Warner, M., 1987. Migration - why doesn't work for deep continental data? *Geophys. J. R. astr. Soc.*, **89**, 21-26.

Watson, J., 1980. The origin and history of the Kapuskasing structural zone, Ontario, Canada, *Can. J. Earth. Sci.*, **17**, 866-875.

West, G.F., and Halls, H.C., 1991. Aeromagnetic survey of the Ivanhoe Lake fault

zone, LITHOPROBE KSZ Transect, *Geol. Assoc. Can. Abstr.*, **16**, A131

West, G.F., and Ernst, R.E., 1991. Evidence from aeromagnetics on the configuration of Matachewan dykes and the tectonic evolution of the Kapuskasing Structural Zone, Ontario, Canada. *Can. J. Earth. Sci.*, **28**, 1797-1811.

Wever, Th., 1984. Häufigkeitsstatistik von Steilwinkelreflxionen aus Gebieten der kontinentalen Kruste und ihre Anwendung auf die Analyse der kontinentalen Krustenstrukturen, Diploma thesis, Christian-Albrechts Universität, kiel.

Wever, Th., Trappe, H., and Meissner, R., 1987. Possible relations between crustal reflectivity, crustal age, heat flow, and the viscosity of the continents. *Ann. Geophys.*, **5b**, 255-266.

White, D.J., 1989. Two-dimensional seismic refraction tomography, *Geophys. J.*, **97**, 223-245.

White, D.J., and Boland, A.V., 1992. A comparison of forward modeling and inversion of seismic first arrivals over the Kapuskasing Uplift, *Bull. Seism. Soc. Am.*, **82**, 304-322.

Wilson, H.D.B., and Brisbin, W.C., 1965. Mid-North American ridge structure, *Geol. Soc. Amer. Spec. Pap.*, **76**, 186-187.

Wilson, J.T., 1968. Comparison of the Hudson Bay arc with some other features, in: C.S. Beals and D.A. Shenstone (eds.), *Science, History and Hudson Bay*, Dep. Energy Mines Res., Ottawa, 1015-1033.

Woods, D.V., and Allard, M., 1986. Reconnaissance electromagnetic induction study of the Kapuskasing structural zone: Implications for lower crustal conductivity, *Phys. Earth Planet. Int.*, **42**, 135-142.

Wu, J., 1987. The analysis of the data of the 1984 Kapuskasing seismic experiment. *M.Sc thesis*, University of Western Ontario, London, Canada.

Wu, J., and Mereu, R.F., 1990. The nature of the Kapuskasing structural zone: results from the 1984 seismic refraction experiment, in: M.H. Salisbury and D.M. Fountain (eds.), *Exposed Cross-Sections of the Continental Crust*, Kluwer Academic Publishers, Dordrecht, 563-586.

Wu, J., and Mereu, R.F., 1991. Seismic reflectivity patterns of the Kapuskasing structural zone, in: R. Meissner, L. Brown, H. Dürbaum, W. Franke, K. Fuchs, and F. Seifert (eds.), Continental Lithosphere: Deep Seismic Reflections, *AGU geodyn. Ser.*, **22**, 47-52.

Wu, J., Mereu, R.F., and Percival, J.A., 1992. Seismic image of the Ivanhoe Lake fault zone in the Kapuskasing uplift of the Canadian shield, *Geophys. Res. Lett.*, **19**, 353-356.

Wu, J., and Mereu, R.F., 1992. Crustal Structure of the Kapuskasing Uplift from LITHOPROBE Near-vertical/Wide-angle Seismic Reflection Data, *J. Geophys. Res.*, in press.

Yilmaz, Ö., 1987. Seismic data processing, *Soc. Explor. Geophys.*, Tulsa.

PAPERS PUBLISHED IN SCIENTIFIC JOURNALS

Wu, J., and Mereu, R.F., 1992. Crustal Structure of the Kapuskasing Uplift from LITHOPROBE Near-vertical/Wide-angle Seismic Reflection Data, *Journal of Geophysical Research*, in press.

Wu, J., Mereu, R.F., and Percival, J.A., 1992. Seismic image of the Ivanhoe Lake fault zone in the Kapuskasing uplift of the Canadian shield, *Geophysical Research Letters*, **19**, 353-356.

Wu, J., and Mereu, R.F., 1991. Seismic reflectivity patterns of the Kapuskasing structural zone, in: R. Meissner, L. Brown, H. Dürbaum, W. Franke, K. Fuchs, and F. Seifert (eds.), Continental Lithosphere: Deep Seismic Reflections, *AGU geodyn. Ser.*, **22**, 47-52.

Wu, J., and Mereu, R.F., The nature of the Kapuskasing structural zone: results from the 1984 seismic refraction experiment, in: M.H. Salisbury and D.M. Fountain (eds.), *Exposed Cross-Sections of the Continental Crust*, Kluwer Academic Publishers, Dordrecht, 563-586, 1990.

Mereu, R.F., Baerg, J., and Wu, J., The complexity of the continental lower crust and Moho from PmP data: Results from COCRUST experiments. In: R.F. Mereu, St. Mueller, and D.M. Fountain (eds.), Lower Crust: Properties and Processes, *AGU. Monograph, 51*, 102-119, 1989.

PAPERS PRESENTED AT SCIENTIFIC MEETINGS

Wu, J., and Mereu, R.F., Crustal Structure of the Kapuskasing Uplift from LITHOPROBE Near-vertical/Wide-angle Seismic Reflection Data (Invited). American Geophysical Union/Canadian Geophysical Union Joint Spring Meeting, Montreal, May, 1992.

Wu, J., and Mereu, R.F., 1992. Seismic imaging of the Ivanhoe Lake fault zone in the central Canadian shield. Canadian Society of Exploration Geophysicists Annual Meeting, Calgray, May, 1992.

Wu, J., and Mereu, R.F., Seismic imaging of the Ivanhoe Lake cataclastic zone, LITHOPROBE KSZ workshop III, Toronto, April, 1991.

Wu, J., and Mereu, R.F., Seismic reflectivity patterns of the Kapuskasing structural zone. The Fourth International Symposium on Deep Seismic Reflection Profiling of the Continental Lithosphere. Bayreuth, Federal Republic of Germany, September, 1990.

Wu, J., and Mereu, R.F., A combined P-S wave and gravity interpretation of the data from the Kapuskasing refraction experiment. Geological Association of Canada/Canadian Geophysical Union Annual Meeting, Montreal, May, 1989.

Wu, J., and Mereu, R.F., A P-S wave seismic-gravity inversion of the Kapuskasing structural zone. LITHOPROBE KSZ Workshop II, Toronto, November, 1989.

Mereu, R.F., and Wu, J., Crustal structure of the Kapuskasing Uplift: results from the 1984 Kapuskasing seismic refraction survey, NATO Advanced Study Institute Program on "Exposed Cross Section of the Continental Crust", Killarney, Ontario, September, 1988.

Wu, J., and Mereu, R.F., Crustal models of the Kapuskasing structural zone: results from the 1984 seismic refraction experiment. Canadian Geophysical Union Annual Meeting, Saskatoon, May, 1988.

Wu, J., and Mereu, R.F., Crustal models of the Kapuskasing structural zone: results from the 1984 seismic refraction experiment. LITHOPROBE KSZ Workshop I, Toronto, February, 1988.

Epili, D., Mereu, R.F., Cox, T.P., and Wu, J., The GLIMPCE seismic experiment: ON-shore refraction and wide-angle reflection observations from profiles across the Great Lake. XIX General Assembly, IUGG, Vancouver, August, 1987.

Mereu, R.F., and Wu, J., The complexity of the Lower Crust and Moho from PmP Data: Results from COCRUST and Lithoprobe Experiments. XIX General Assembly, IUGG, Vancouver, August, 1987.

Wu, J., and Mereu, R.F., Analysis of the Results of the Kapuskasing Seismic Experiment. American Geophysical Union Spring Meeting, Baltimore, May, 1987.